The Synthesis and Study of Novel Squaramide Scaffolds: From Sensors to Soft Materials.

A thesis submitted to the National University of Ireland in fulfilment of the requirements for the degree of

Masters of Science

By

Anthony A. Abogunrin, B.Sc.

Department of Chemistry,

Maynooth University,

Maynooth, Co. Kildare,

Ireland.

October 2017

Research Supervisor: Dr. Robert Elmes

Head of Department: Dr. Jennifer McManus

Table of Contents

Declaration

I hereby certify that this thesis has not been submitted before, in whole or in part, to this or any university for any degree and is, except where otherwise stated, the original work of the author.

Signed:_____Date:_____

Maynooth University

To my family, James, Bolajoko, Jade, Catherine, Felix, Cecelia and James Jnr.

Thanks for everything.

Acknowledgements

First of all, I would like to thank my supervisor Dr. Robert Elmes for entrusting this project to me, and his endless enthusiasm, support, advice, encouragement and generosity with his time over the past two years. Without you none of this would have been possible so Rob, my role model, thank you so much!! I really could not have asked for a better supervisor. I would also like to thank the Maynooth Chemistry Department for providing the funding to complete my research at Maynooth.

To all members of the Elmes research group, Xiang, Nan and Michelle – thanks for the nice chat and laughs that kept me sane in the laboratory. Especially Xiang, my partner in crime and my day one lab partner – and to the newest member of the group, Luke – good luck with your research and I'm 100% sure you'll be okay, because you've got a very caring and enthusiastic supervisor to looks after you.

Thanks to all the academic and technical staff in the department, to, Ollie, Barbara, and Walter for their help, advice and mass spec samples. A special thanks to our lab mother, Ria for a caring attitude and supports towards everyone in the lab and especially towards me. Very special thanks to Dr. Ken Maddock for giving up a few long days to help me with the variable temperature NMR experiments. Thanks also to Donna and Carol for being so helpful with everything I ever needed.

Special thanks are also due to Neol, thank you for fixing my laptop during my time writing my thesis and everything I ever broke I the lab and also for organising the Halloween party decorations.

Thanks to all the postgrads, past and present, for making my time in the chemistry department a very memorable and enjoyable experience. Thanks to my write up room buddies, Xiang, Jessica, Jack and Sam, for the chats, craic and banter. To the rest of the postgrads I haven't mentioned, Gama, Harlie, Muhib, Mark K., Amanda, Mark G., Lucy, Carloine, Mathew and Stephen, thanks for your friendship and best of luck with your research.

I need to thanks all my friends who have made sure that chemistry hasn't entirely taken over my life over the past two years. Thanks to Thabani, Harry, Danny, Alex, Moses, Prince, Leon and Dafe without whom my life would have been extraordinarily boring. Special thanks to my housemate and friend, Cian, for the proof-reading my thesis and for bring me packed lunches and diner during my time in the study room, I really owe you one Bro!!!

I would like to thank my family, especially my Mum and Dad for their financial, emotional and moral support. Thank you so much for always being there for me, I would never forget your kindness.

Finally, I would like to thank myself for never giving up despite the struggles having to work three different jobs during my post graduate studies.

"Goals on the road to achievement cannot be achieved without self-discipline and consistency."

Denzel Washington

Abstract

This thesis entitled 'The Synthesis and Study of Novel Squaramide Scaffolds: From Sensors to Soft Materials' is divided in 6 Chapters. Chapter 1, squaramide based receptors as potential anion sensors, gives a brief introduction into the history of anion recognition and the significant role anions play in biology and in the environment. A range of relevant examples of anion receptors and sensors from the literature are also given. This Chapter concludes with the aims of the research conducted in Chapter 2.

In Chapter 2, a set of novel squaramide based anion receptors are described. The synthesis of each receptor is discussed in addition to their photophysical and anion binding properties.

Chapter 3, squaramide based low molecular weight gelators (LMWGs), gives a concise background into the field of gels, from their formation and classification to their characteristics. It also gives a brief introduction on the topic of supramolecular gels with some relevant examples from the literature. This Chapter concludes with the aims of the research conducted in Chapter 4.

In Chapter 4, a series of novel squaramides potential low molecular weight oragano-gelators (LMWOGs) are described. The synthesis of each new compound is discussed, in addition to preliminary gelation tests.

In Chapter 5, an overall conclusion of the entire preceding chapter is given.

Finally, in Chapter 6, general experimental procedures are outlined and the synthesis and characterisation of each of the compounds is given. Subsequently, literature references are provided and are followed by the Appendix which provides spectroscopic, titration data and photographic images to support work described in the main text.

Abbreviations

1D	1-dimensional
2D	2-dimensional
3D	3-dimensional
AcO^-	acetate ($CH_3CO_2^-$) anion
Au	Gold
$CHCl_3$	chloroform
Cl^-	chloride anion
conc.	concentration
d	doublet
dd	doublet of doublets
δ	chemical shift
DCM	dichloromethane
DMF	N, N-dimethylformamide
DMSO	dimethylsulfoxide
ε	molar extinction coefficient
eq.	equivalents
ESI	electrospray ionisation
Et_3N	triethylamine
Et_2O	diethyl ether
EtOH	ethanol
EWG	electron withdrawing group

F^-	fluoride anion
FTIR	Fourier transform infrared
HRMS	high resolution mass spectroscopy
Hrs	hours
Hz	hertz
ICT	internal charge transfer
I	insoluble
IR	infrared
J	coupling constant (expressed in Hz)
KOH	potassium hydroxide
λ	wavelength
Pet.Ether	petroleum ether
PO_4^{3-}	phosphate anion
PG	partial gel
PS	partially soluble
LMW	low molecular weight
LMWGs	low molecular weight gelators
LMWOGs	low molecular weight organogelators
m	multiplet
MeCN	acetonitrile
MeOH	methanol
m.g.c	minimum gelator concentration

mins	minutes
m/z	mass to charge ratio
nm	nanometre
NMR	nuclear magnetic resonance
OP	opaque gel
PET	photoinduced electron transfer
ppm	parts per million
q	quartet
s	singlet
S	soluble
SANS	small angle neutron scattering
SAXS	small angle X-ray scattering
SEM	scanning electron microscopy
SO_4^{2-}	sulphate anion
t	triplet
TBA (salt)	tetrabutylammonium salt
TEM	transmission electron microscopy
TFA	trifluoroacetic acid
TG	transparent gel
UV/Vis	ultraviolet/visible
XRD	X-ray diffraction

Chapter 1 - Squaramide Based Receptors as Potential Anion Sensors

1.1 Introduction

The recognition of anions is a broad field of supramolecular chemistry.[1] Several hosts incorporating functional groups such as ureas, pyrroles, indoles, amides and sulfonamides have been shown to successfully complex a range of anionic guests via hydrogen bonding.[2-6] Generally, these receptor molecules are designed with some degree of pre-organisation, resulting in a cleft-like structure.[7, 8]

The catalytic activity of most organocatalysts involves groups such as those listed above *via* hydrogen bonding to highly anionic or negative intermediate.[9-15] The major objective of receptor design is the molecular recognition of anions, giving rise to the potential application of molecular receptors for anion recognition.[16, 17]

This review Chapter will present a review of the areas of anion recognition giving a brief history, some key findings and more recent developments.

1.2 Why Anions?

Anions play a crucial role in biology and industrial processes and hence their recognition and detection has gained considerable research attention.[18-20] For example, chloride is essential in biological systems and is involved in a variety cellular and physiological function, such as in regulating membrane potentials.[21] Misregulation of chloride concentrations is associated with a number of diseases, including cystic fibrosis.[22] Cyanide is also a well-recognised anion, for its extremely high physiological toxicity and its presence as an environmental pollutant due to widespread use in photography, gold mining and petrochemical industry.[23] Bromide is found in saliva, serum and urine of living organisms.[24] Bromide deficiency results in hyperthyroidism which inhibits growth, fertility and life expectancy. However, excess bromide leads to bromide toxicity "bromism" which results in skin eruption.[25, 26] Fluoride ions are important for oral care and are present in toothpastes.[27, 28] Fluoride ions help to maintain healthy bone structure in the human body.[29] However, excess of fluoride intake results in skeletal fluorosis, a disease which causes stiffness, pain and calcification of bones in the body.[30] Phosphate is an essential component of many important biomolecules like ATP (energy production), DNA (genetic information), Haemoglobin (oxygen carrier) and RNA (protein synthesis).[31] Phosphate has crucial role in bone and teeth development,[32] signal transduction and energy storage in biological systems.[33] Excess use of phosphate and nitrate anions lead to eutrophication of lakes and waterways.[34] Sulfate is a prominent troublesome species in the nuclear wastes that can interfere in their treatment processes.[35, 36] Therefore, the development of novel receptors for monitoring of these anions in various physiological and environmental samples is extremely important and has become an active area of research. As outlined above there is a variety of anionic species that carry out diverse functions in both biological process and the environment.

The design of selective and sensitive anion receptors is extremely important but also challenging task[18]. Anions are generally larger than cations and therefore have lower charge to radius ratio.[37] Under acidic conditions, anions may become sensitive to pH and become protonated, thus losing their charge. Solvent effects can also play a major role in controlling binding strength and selectivity. Some

solvents can form H-bonds to anions and an anion receptor must compete with the solvent for the binding site. Anions also possess a wide range geometries, resulting in a high degree of pre-organisation being required for effective anion receptor design. Halides such as bromide (Br^-), chloride (Cl^-), fluoride (F^-) and iodide (I^-) are spherical in shape while linear anions include cyanide (CN^-) and hydroxide (OH^-). Nitrate (NO_3^{2-}) and Carbonate (CO_3^{2-}) ions are trigonal planar in nature whereas dihydrogen phosphate ($H_2PO_4^{3-}$), phosphate (PO_4^{3-}) and sulfate (SO_4^{3-}) are tetrahedral anions. Examples of Y-shaped anions include; acetate (AcO^-) and benzoate (BzO^-) (Figure 1.1).

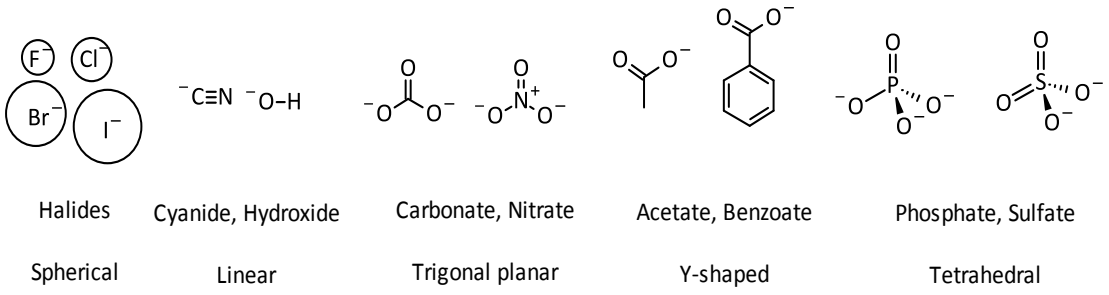

Figure 1.1: *Different types of anion shapes showing examples of spherical, linear, trigonal planar, tetrahedral and Y-shaped anion.*

Given these variations and the complex nature of anion recognition, a number of approaches have been pursued. The following section will outline the development of the field of anion recognition and summarise some of the recent advances in the area.

1.3 Anion Recognition

The slow developing field of anion receptor chemistry began in the late 1960s by Shriver and Biallas[38] and by Park and Simmons.[39] However, Park and Simmons discovered that deprotonated bicyclic katapinands could encapsulate halide ions as a result of hydrogen-bonding interactions (Figure 1.2),[39] a finding that heralds the field of anion coordination chemistry.[40] Until approximately 30 years ago, the

coordination of anions was relatively unexplored even with the development of the first synthetic receptor by Park and Simmons in 1968.[39]

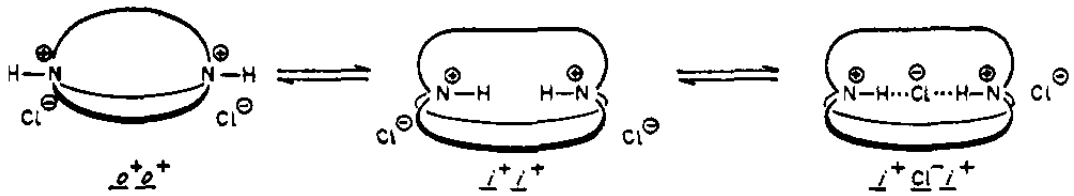

Figure 1.2: *Katapinate diammonium salts with complexed and free chloride anion.*[39]

In the mid-1970s, Lehn and co-workers also reported macrotricyclic hosts, which could encapsulate halides.[41] Coordination of anions has become an important area of supramolecular chemistry due to potential applications in the fields of biology, the environment and chemical processes.[18, 39] Anion coordination chemistry was originally concerned with the design and synthesis of simple uncharged receptors which could complex anions in an organic environment,[42] However, the focus has recently shifted towards the selective anion binding in aqueous solvent conditions,[43] selective sensing of significant biological anions *in vivo*,[44] anion transport across cell membranes,[21] detection of anionic pollutants at very low levels,[45] and extraction and transport of specific anions against Hofmeister bias from aqueous to organic conditions.[46]

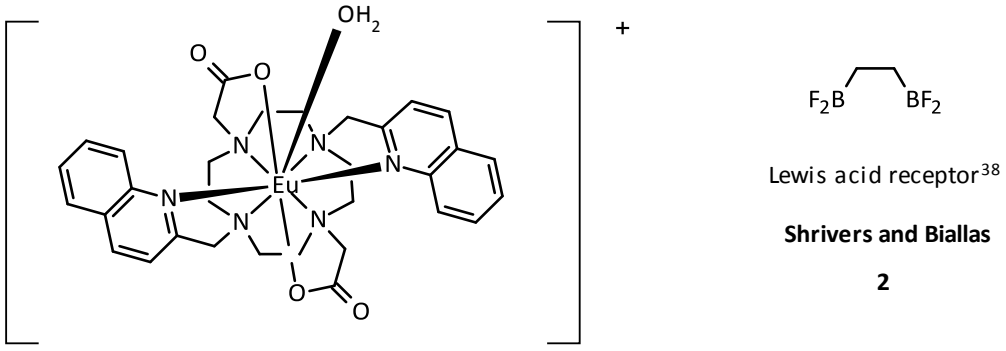

Metal-anion complex[47]

Butler

1

Lewis acid receptor[38]

Shrivers and Biallas

2

Figure 1.3: *Receptor capable of binding anionic guest via metal anion complexation*[47] *and an example of a Lewis acid receptor.*[38]

Receptors may complex anionic guest through metal-anion complexation[47-50] (Figure 1.3) and strong electrostatic interactions.[51] Complexation of receptors to anionic guest could also occur via weaker but more directional interactions such as π-anion,[52] Lewis acid-base,[38, 53] hydrophobic effects or hydrogen bonding (H-bonding),[19, 54, 55] the most common being through hydrogen bonding.[18, 56] Given the subject matter of this thesis the following sections will concentrate on anion receptors based on hydrogen bonding interactions.

Hydrogen bonds are directional, which allows for the possibility of designing receptors with specific shapes that are capable of differentiating between anionic guests with different geometries or hydrogen-bonding requirements in non-polar solvents.[37] Several H-bonds can be incorporated into a supramolecular structure to form a cleft with convergent H-bonding groups, able to cooperatively bind anions. Some neutral anion receptors bearing groups such as pyrrole,[3, 57, 58] indole,[4, 59] amide,[60] sulphonamide,[6] squaramide,[61, 62] urea and thiourea[4, 63-66] groups as H-bond donors have been reported to effectively bind anions (Figure 1.4).

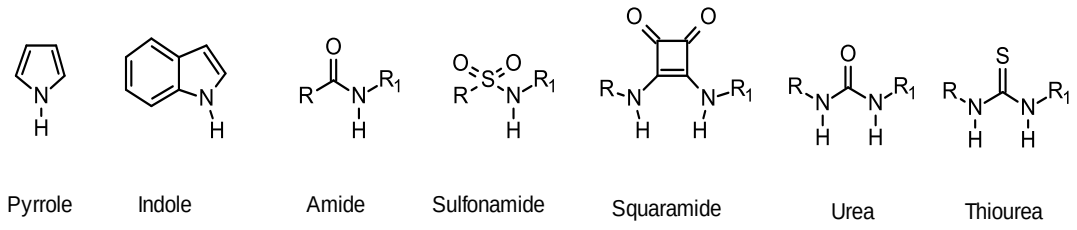

Figure 1.4: *Some functional groups capable of H-bonding to anions.*

However, secondary amides are generally used in anion receptors as they act as efficient H-bond donors.[67] Secondary amides can also act as H-bond acceptors which promotes intra-molecular H-bonding, self-association and disruption to anion binding. However, they have been found to effectively bind anions,[68] neutral molecules such as dicarboxylic acids[69] and barbiturates.[70] Pyrrole and indole based receptors can only act as H-bond donors, thus intramolecular H-bond formation which can inhibit anion binding is not possible (Figure 1.4). Sulfonamide moieties have been shown to be effective anion receptors due to their highly acidic H-bond donating groups (Figure 1.4).[71] Squaramide moieties have also been reported to bind halides and oxyanions with high binding strength.[61] Ureas and thioureas are

commonly known to be efficient anion receptors, due to their possession of two N-H groups which can bind a single acceptor atom such as a halide anion resulting in the formation of a six-membered chelate ring or can also bind two adjacent oxygen atoms of an oxyanion resulting in the formation of an eight-membered ring system. The most important challenge of anion recognition is to develop synthetic receptors for binding of particular anions selectively in highly competitive solvents. The next sub-sections will provide a general overview of anion binding including a consideration of the design of simple anion receptors and comparison of their anion complexation abilities. Due to the large number of examples in the literature, this is not intended to be an exhaustive list but a summary of some of the more important examples and those pertinent to the subject of this thesis.

1.4 Indole Based Amide/Urea Receptors for Anion Binding

Indoles and indole-based receptors are a modern feature of anion coordination chemistry.[56] In 2007, Pfeffer *et al*. developed indole receptors which also incorporated amide, urea and thiourea groups and ^{1}H NMR spectroscopic titrations with several anions were conducted, monitoring all four N-H groups of the receptors **3-5** (Figure 1.5).[4] Deprotonation of the indole N-H and urea N-H groups occurred with F^- for **3-5**. Receptors **3** and **4** were shown to possess strong AcO^- binding and weaker Cl^- and Br^- through the urea groups with only minor binding observed to the indole and amide N-H groups. However, in the case of the larger receptor **5** with AcO^-, the amide and indole bound the anion strongly upon the addition of 1 equivalent of anion. At which point the large size could accommodate independent anion binding at these sites. K_a values of approximately 7,900 M^{-1} in DMSO-$_{d6}$ were obtained for **5** with both AcO^- and $H_2PO_4^-$ lower values were obtained for Cl^- binding.

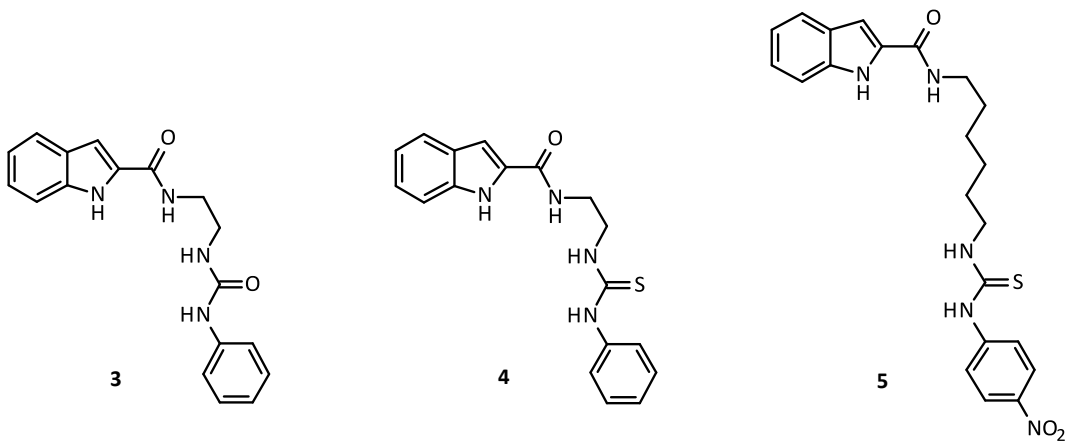

Figure 1.5: *Structure of Indole based urea and thiourea receptors studied by Pfeffer et al. in 2007.*[4]

Bates *et al.* developed a series of functionalised indoles with *bis*-amides attached and ureas in a similar cleft arrangement to an isophthalamide and found they strongly bound to AcO^- in wet DMSO (Figure 1.6).[72] The amide functionalised indoles bound anions more weakly compared to the urea analogues whereas the thiourea derivative gave lower K_a values due to steric effects with the sulfur (S) atom inhibiting the approach of anions.

6: R = C_4H_9, R^1 = C_4H_9
7: R = Ph, R^1 = Ph
8: R = $PhCH_2$, R^1 = Ph

9: X = O, R = C_4H_9, R^1 = C_4H_9
10: X = O, R = Ph, R^1 = Ph
11: X = S, R = Ph, R^1 = Ph

Figure 1.6: *Indole receptors developed by Bates et al. in 2007.*[72]

Furthermore, after recognising the minor role played by the amide at the 2-position in the coordination of anions evaluated in the indole receptors **6-11** (Figure 1.6). Caltagirone *et al*. synthesised 1,3-diindolylurea and 1,3-diindolylthiourea based receptors (Figure 1.7).[59] The urea receptors showed a high affinity for oxoanions and a particular selectivity for $H_2PO_4^-$ in DMSO-$_{d6}$ ($K_a > 10^4$ M^{-1} in presence of 0.5% H_2O for oxyanions; 4790 M^{-1} in 10% H_2O for $H_2PO_4^-$). X-ray crystallography showed

that the diindolylurea **12** was bound to BzO^- through four H-bonds incorporating all N-H groups (Figure 1.7). However, due to the steric effects from the large S atom, significantly lower K_a values were observed for thioureas.

(a) **(b)**

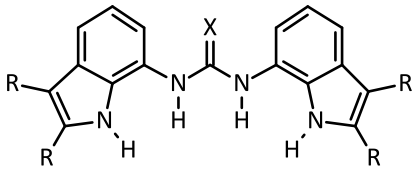

12: R = Me, X = O
13: R = H, X = O
14: R = Me, X = S
15: R = H, X = S

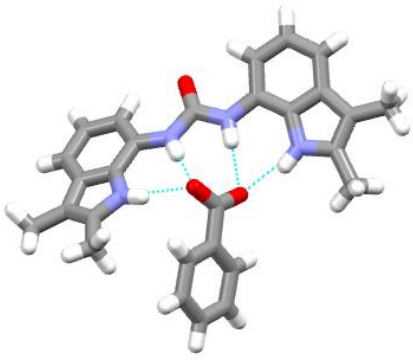

Figure 1.7 (a): *Structure of diindolylureas and diindolylthioureas binding to benzoate developed by Caltagirone et al. in 2008.*[59] ***(b):*** *Top view of X-ray crystal structure of tetrabutylammonium benzoate complex of compound* ***12****.*[59]

Furthermore, Caltagirone and co-workers later synthesised bis-2-amidoindole receptors of varying acidity coupled through 1,5-diaminopentane or 1,3-phenylenediamine groups (Figure 1.8).[73] ^{1}H NMR spectroscopic titrations in DMSO-$_{d6}$/0.5% H_2O preferentially bound oxoanions, in particular $H_2PO_4^-$. Caltagirone *et* al. reported the formation of a 1:2 receptor:dihydrogen phosphate complex in solution with receptor **19** and in the solid state with receptor **16** evidence by X-ray crystallography (Figure 1.9).[73] These results suggest a potentially useful strategy for complexing oxyanions containing both hydrogen bond donors and acceptors.

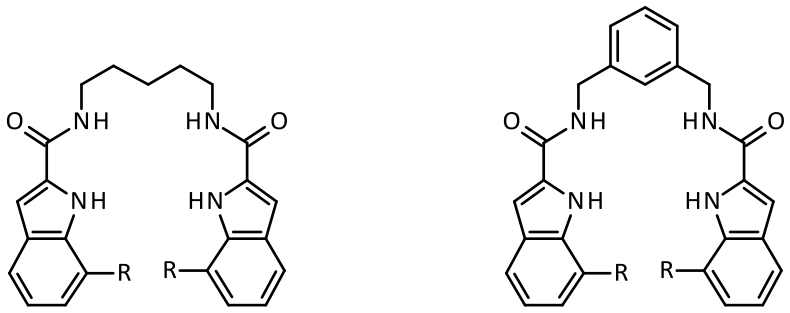

16: R = H
17: R = NO_2

18: R = H
19: R = NO_2

Figure 1.8: *Structure of 2-amidoindole receptors studied by Caltagirone and co-workers in 2009.*[73]

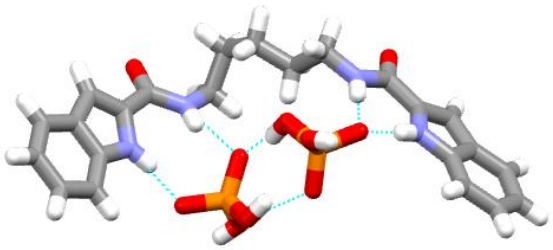

Figure 1.9: *Receptor **16** binding a dihydrogen phosphate dimer in the solid state.*[73]

1.5 Sulfonamide Based Anion Receptors

In 2008, Caltagirone *et al*. reported urea receptors containing sulphonamide groups (Figure 1.10).[74] Anion binding was monitored via ^{1}H NMR spectroscopy in CD_3CN and upon addition of Cl^-, 1:1 complexes were formed with K_a values of 7550 M^{-1} and $>10^4$ M^{-1} for **20** and **21** respectively. Upon addition 1 equivalent of AcO^- or 2 equivalents of F^- the urea N-H resonance shifted downfield. It subsequently migrated upfield with further additions, due to decomplexation effects and deprotonation of the acidic sulfonamide N-H group.

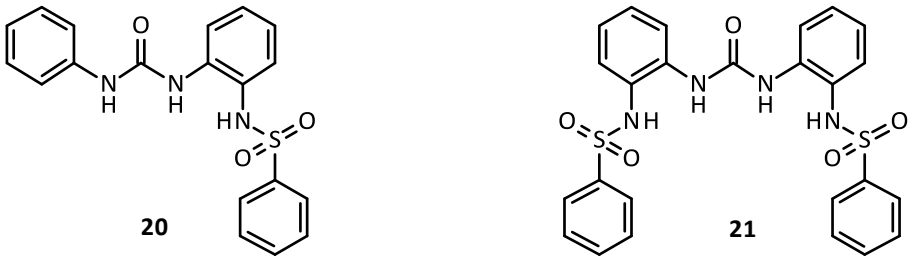

Figure 1.10: *Structure of ureas containing sulfonamide groups observed to bind anions and which become deprotonated upon addition of further equivalents of basic anions.*[74]

Huggins *et al*. developed pyrrole sulfonamide based receptors **22-25** (Figure 1.11).[6] Anion binding titration studies carried out in dry $CDCl_3$ showed 1:1 receptor:anion binding of **22-25** with a range of anions with K_a values up to 1768 M^{-1}. The sulfonamide N-H signals migrated further downfield compared to the pyrrole N-H protons. Further molecular modelling and ^1H NMR spectroscopic studies confirmed that no change in conformation occurred upon anion binding.

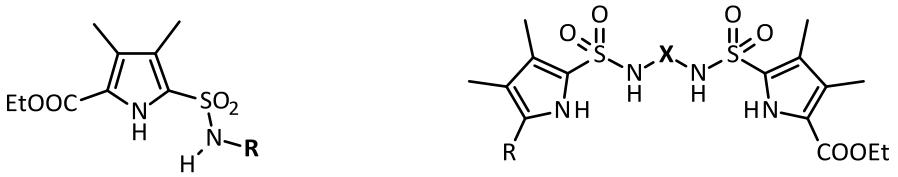

22: R = C_6H_5
23: R = C_4H_9

24: X = $(CH_2)_2$
25: X = $(CH_2)_4$

Figure 1.11: *Structure of pyrrole sulfonamide receptors developed by Huggins et al. in 2009.*[6]

1.6 Urea and Thiourea Based Anion Receptors

Ureas and thioureas are attractive scaffolds for the design of anion receptors. They both contain two N-H fragments which can bind a single anion e.g. a halide anion or two adjacent oxygen atoms of an oxyanion.[19, 75] Ureas and thioureas are the most widely employed hydrogen bond donor groups in anion receptor systems, due to their facile synthesis and easily tunable N-H acidity.[76] In 1992, Smith and co.

workers reported a urea receptor **26** which was capable of binding anions such as carboxylates, phosphonates and sulfates (Figure 1.12).[77] Kelly and Kim also developed a urea based receptor **27** which was capable of binding phosphonate and sulfate anions (Figure 1.12).[78]

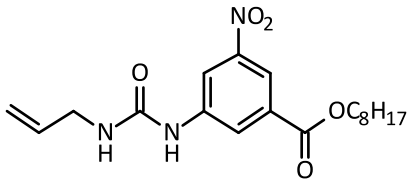

Smith and co-workers

26

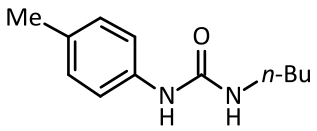

Kelly and Kim

27

Figure 1.12: *Structure of urea based receptors studied by Smith et al.[77] and Kelly and Kim.[78]*

Gunnlaugsson *et al.* developed naphthalimide thiourea based receptors **28** and **29** which were reported to bind anions such as AcO^-, F^- and $H_2PO_4^-$ in aqueous solution with an accompanying colour change (Figure 1.13).[79] K_a values of approximately $10^4 – 10^5$ M^{-1} for AcO^-, F^- and $H_2PO_4^-$ were observed with stronger binding for **29** than **28**. Deprotonation was observed in the presence of F^- accompanied by colour changes which could not be reversed upon addition of water or ethanol. UV titrations in DMSO were consistent with anion complexation which required the syn orientation. X-ray crystallography also showed that the thiourea protons existed in the anti-conformation to carbonyl carbon with intermolecular interaction between adjacent molecules (Figure 1.13).[79]

In 2005, Brooks *et al*. reported enhanced anion binding constants from receptors containing bis-urea groups linked by a 1,2-phenylenediamine spacer compared to non-urea based receptors **30** and **31** (Figure 1.14).[80] ^1H NMR spectroscopic titrations in DMSO-$_{d6}$/0.5% water showed that the bis-urea receptor **32** was selective for carboxylate anions with K_a values of 3210 M^{-1} and 1330 M^{-1} for AcO^- and BzO^- respectively compared with 100 – 200 M^{-1} for non-urea based receptors **30** and **31**.

(a) **(b)**

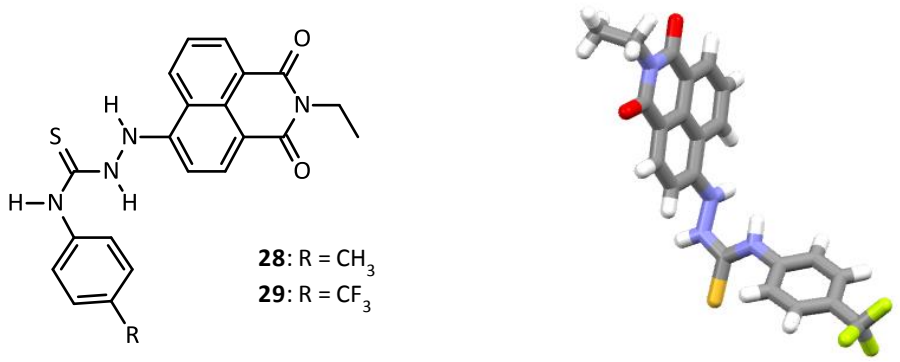

Figure 1.13 *(**a**): Structure of naphthalimide thiourea based receptors developed by Gunnlaugsson et al.*[79] *(**b**): X-ray crystal structure of **28**.*[79]

Significantly improved K_a values were obtained using a 4,5-dichloro-substituted central ring and a nitro group at the 2-position of the urea N-aryl rings **34** (Figure 1.14).[80, 81] Bis-thiourea based receptor **34** produced significantly lower K_a values, due to the large S atom changing the shape of the binding site which prevents binding to the outer N-H groups. X-ray crystallography showed that receptor **32** binds anions through four H-bonds (Figure 1.15).[80, 81]

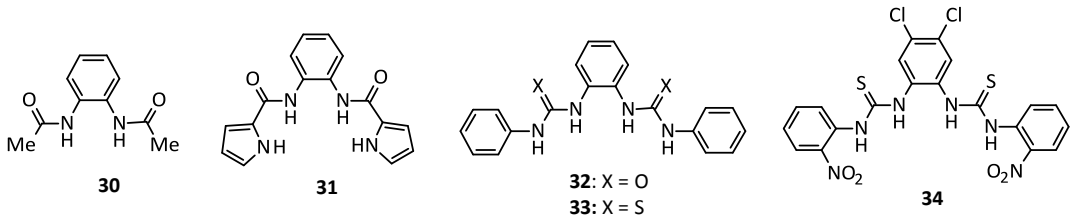

Figure 1.14: *Structure of urea and thiourea based receptors studied by Brooks et al.*[80, 81]

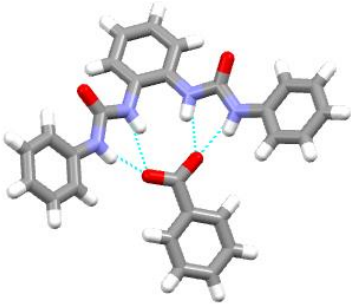

Figure 1.15: *The benzoate complex of receptor* ***32*** *showing the formation of four hydrogen bonds between the receptor and the carboxylate anion in the solid state.*[80, 81]

1.7 Squaramide Based Anion Receptors

Squaramides are four-membered ring systems derived from squaric acid which can form up to four H-bonds. Its carbonyl groups may act as H-bond acceptors while its N-H groups may act as H-bond donors. The physical properties of squaramides and their complexes with anions and cations have been discussed in several papers.[82-85] It was recognised that secondary squaramides offer the potential to hydrogen bond to acceptors, donors and to mixed acceptor-donor groups (Figure 1.16).[84]

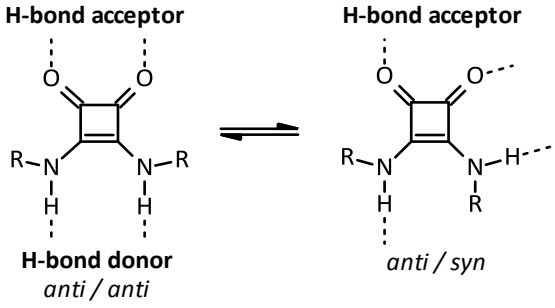

Figure 1.16: *Hydrogen bonding donor ability of squaramides.*[84]

The strong hydrogen bond donor ability of the squaramide functional group has been exploited in the design of anion receptors,[83, 86-90] catalysts,[91, 92] and self-complementary recognition motifs.[93] The squaramide group possesses remarkable hydrogen bonding donor and acceptor abilities and theoretical studies showed its

tendency to increase the aromaticity of the four-membered ring upon binding.[82, 94] This important feature along with directional hydrogen bond donor ability in the extended conformation make this structural motif a useful building block in the design of various synthetic receptors that have applications in the supramolecular chemistry field. Squaramides have found application in numerous contexts: they have been used as scaffolds for crystal engineering,[95] as linkers for bioconjugation[96] and as emerging pharmacophores in medicinal chemistry.[97-101]

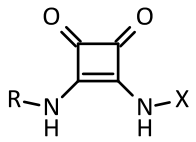

35: R, X = ^{t}Bu
36: R, X = Bu
37: R = Bn, X = $CH_2CH_2NMe_2$

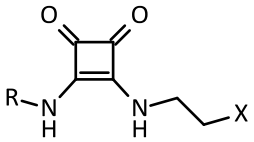

38: R = Bn, X = NMe_3+

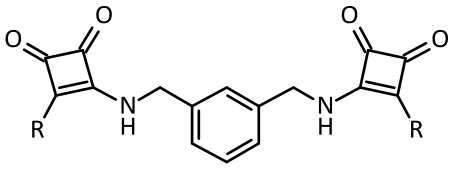

39: R = NHC_6H_{11}
40: R = NHBn
41: R = $NHCH_2CH_2NMe_2$
42: R = $NHCH_2CH_2NMe_3$+

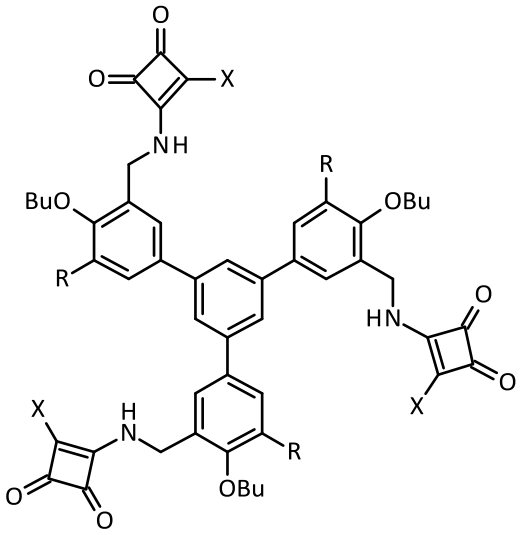

43: R = nPr, X = NHBn

Figure 1.17: *Structure of squaramide based receptors studied by Prohens et al.*[83]

In 1998, Prohens *et al*. studied the H-bonding capability of squaramide based receptors **35-43** (Figure 1.17).[83] Upon the addition of tetramethylammonium (TMA) AcO^- solution to squaramide based receptors receptors **35-38**, characteristic shifts of both squaramidic and methylenic protons were observed. Neutral receptors **35-37** showed moderate to good K_a values whereas the positively charged receptor **38** produce an eight to ten fold increase in binding.[83] Prohens *et al*. reported that

receptors **39-42** are appropriated for binding dicarboxylates derived from glutaric or glutaconic diacids.[83]

In pure DMSO the K_a values of the complexes formed between the bis-tetrabutylammonium (TBA) glutarate and receptors **39-42** are too large (>10^4 M^{-1}) to be measured by NMR spectroscopy. However, the addition of water lowered the K_a values into a measurable range. Prohens *et al*. also reported an increase in binding constant for receptor **43** compared to receptors **39-42**, which was due to the presence of an extra squaramide unit in receptor **43**.[83]

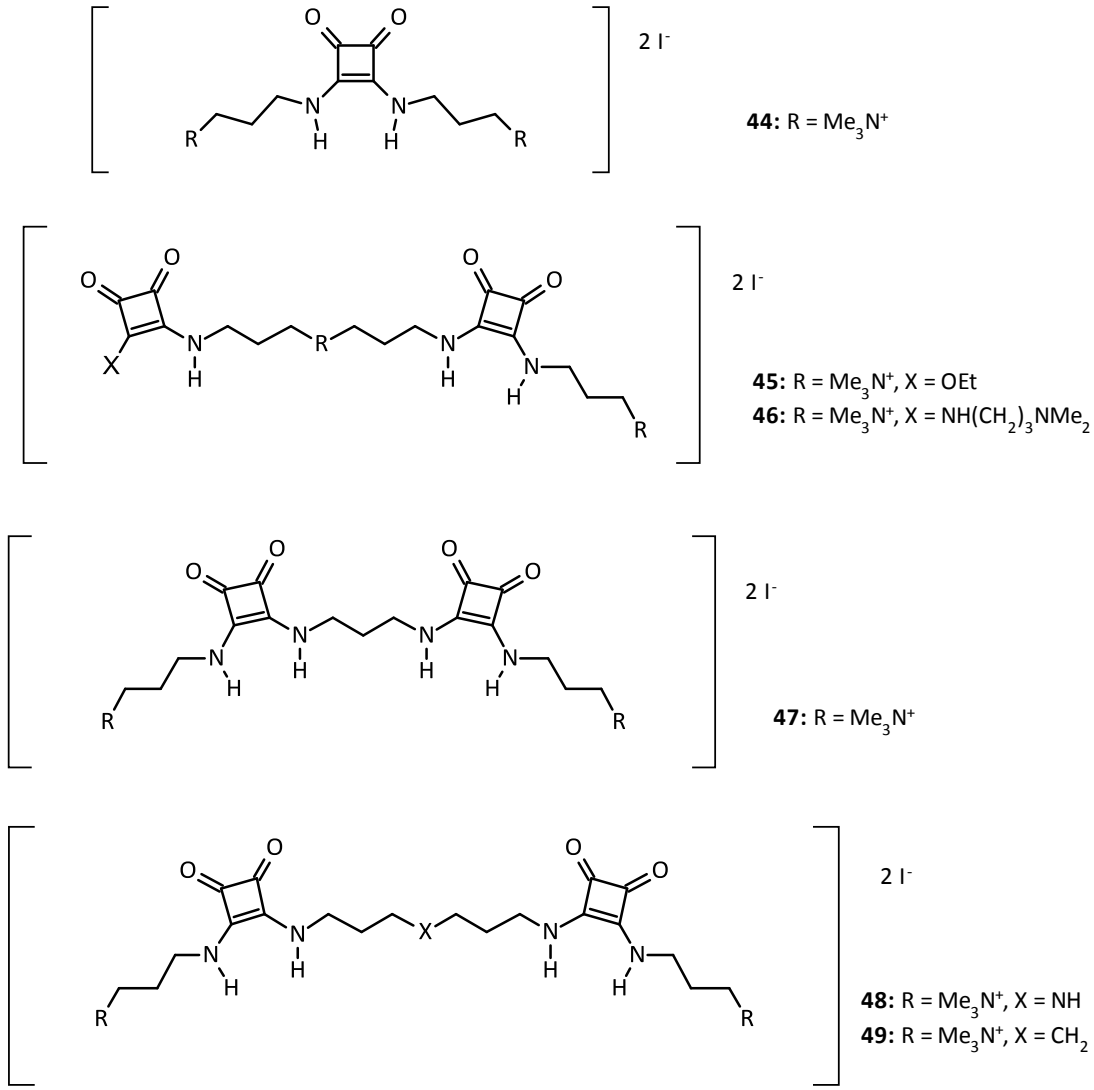

Figure 1.18: *Positively charged squaramide receptors developed by Costa and co-workers.*[87]

Costa and co-workers conducted a thermodynamic study probing the implications of binding of squaramides to carboxylates.[102] It was observed that binding was exothermic in DMSO and chloroform.[102] Whereas in methanol, the association was endothermic and driven by entropy due to the breakage of solvent interactions and release of solvent molecules to the bulk phase.[102] Costa *et al*. later reported a range of positively charged SO_4^{2-} selective squaramide receptors **44-49** which could bind SO_4^{2-} and $H_2PO_4^-$ in ethanol / water mixtures (Figure 1.18).[87]

Furthermore, Ramalingam *et al.* developed squaramide molecules bearing carbonyl groups which could effectively open and close the anion binding cleft due to intramolecular interactions and application which was designed with anion transport in mind (Figure 1.19).[90] In non-polar solvents, no Cl^- binding was observed due to intramolecular H-bonding. In polar solvents, H-bonding was disrupted, resulting in a conformational change to occur and Cl^- binding to proceed.

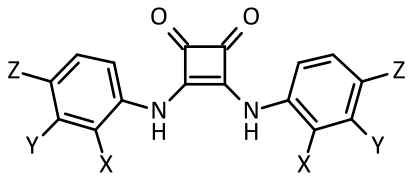

50: X = COPh, Y = H, Z = H
51: X = COPh, Y = H, Z = Cl
52: X = H, Y = COPh, Z = H

Figure 1.19: *Squaramide based receptors studied by Ramalingam and co-workers.*[90]

There was no Cl^- binding of **50** and **51** observed in $CHCl_3$ whereas in CH_3CN, both receptors bound anion with a 5-fold increase observed in K_a value for **51** over **50** as a result of chloro-substitution. The meta-isomer **52** of the non-chlorinated receptor **50** bound anions in both polar and non-polar solvents with higher K_a values reported due to the lack of steric hindrance effects in receptor **52** compared to receptors **50** and **51**.

In 2010, Al-Sayah and Branda studied a thiourea **53** and a squaramide **54** bipyridine containing receptor for binding AcO^- in a variety of solvents (Figure 1.20).[103] In 1:1

$CD_3CN:CDCl_3$, thiourea **53** yielded a K_a value of 5790 M^{-1} while the squaramide **54** bound AcO^- with a K_a value of 7390 M^{-1}.

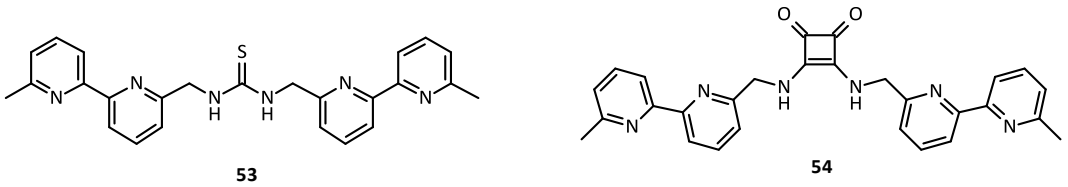

Figure 1.20: *Structure of thiourea and squaramide based receptors developed by Al-Sayah and Branda.*[103]

Amendola *et al*. compared the anion binding properties of the urea based receptor **55** possessing an electron withdrawing NO_2 group with a similar squaramide receptor **56** (Figure 1.21).[61, 104] 1:1 complexes were reported in all cases through UV/Vis and ^{1}H NMR spectroscopy. According to the squaramide based receptor **56**, H-bond interactions involved the N-H and also the closely located aryl C-H groups resulting in a total of four H-bonds.

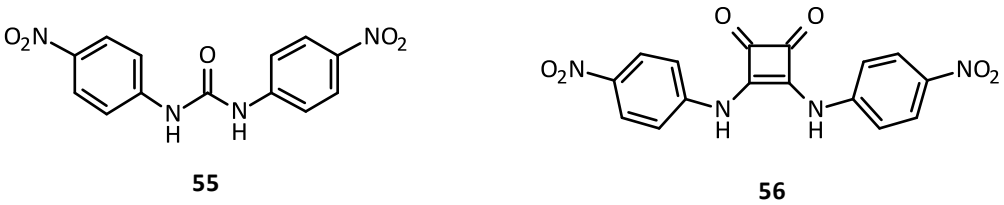

Figure 1.21: *Structure of urea and corresponding squaramide based receptors studied by Amendola et al.*[61]

Squaramide receptor **56** complexes containing halides as guests were approximately 1 to 2 orders of magnitude more stable than urea based receptor **55.** Both receptors **55** and **56** complexes of the same guest possessed approximately equal K_a values for oxyanions. For the most basic anions such as AcO^- and F^- complexed with receptor **56**, 1:1 H-bonding complexes were originally formed followed by N-H deprotonation. However, deprotonation did not occur for receptor **55** with AcO^-, due to its lower acidity. Amendola *et al*. concluded that squaramide based receptor **56** was a more efficient halide receptor while both receptors **55** and **56** possessed similar tendencies towards oxyanions.

Rostami *et al*. reported a new synthetic procedure for the preparation of squaramide receptors and examined an acidic 4-nitroaniline derived squaramide **57** (Figure 1.22) for its anion binding properties through UV/Vis spectroscopy.[62] Significant differences in UV spectra of **57** were observed in CH_3CN compared to DMSO, which was due to deprotonation of one of the squaramide NH groups in DMSO without the addition of a base.[62]

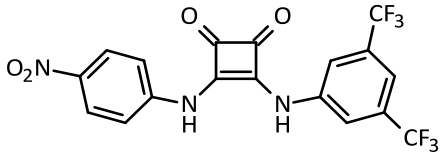

57

Figure 1.22: *Squaramide based receptor **57** which undergoes proton transfer events reported by Rostami et al.*[62]

The deprotonation was more evident with increasing dilution. It was proposed that the H-bond accepting ability of DMSO promoted this equilibrium process which became unfavoured at higher concentrations of **57** due to self-association. Addition of basic anions such as AcO^- and $H_2PO_4^-$ to a solution of **57** in DMSO did not impart in any spectral changes.[62] However, addition of TBA fluoride induced deprotonation of the second squaramide NH group with an accompanying colour change.[62] In acetonitrile, **57** existed in its neutral state with deprotonation induced upon addition of F^-, AcO^-, $H_2PO_4^-$, and p-toluenesulfonate. Interestingly, receptor **57** was observed to reprotonate upon addition of excess TBA tosylate following initial deprotonation.[62] This effect was reported to be due to the formation of a stable double H-bonded complex which was more stable than the protonated form of DMSO.[62]

Amendola and co-workers later conducted a thermodynamic study to compare the anion binding properties of urea **58**, squaramide **59**, and sulfonamide **60-62** based receptors using spectrophometric, isothermal titration calorimetry (ITC) and ^1H NMR titrations in CH_3CN (Figure 1.23).[104] The results showed that all receptors **58-62** formed 1:1 H-bond complexes to Br^- and Cl^- with **59** producing the strongest binding.[104] Receptors **58** and **59** formed extremely strong binding complexes with

AcO^- while proton transfer effects were evident in the titration of sulfonamide receptors **60-62** with AcO^-.[104] Potentiometric studies of receptors **59-62** showed that the pK_a values of **59**, **60**, **61** and **62** were 10.9, 8.3, 8.3 and 4.3 respectively.[104] These results highlighted the enhanced acidity of **62** which was due the stabilising effect of the *meta*-NO_2 groups on the negative charge formed through deprotonation.[104] However a pK_a value for **58** could not be calculated as this receptor did not deprotonate.[104]

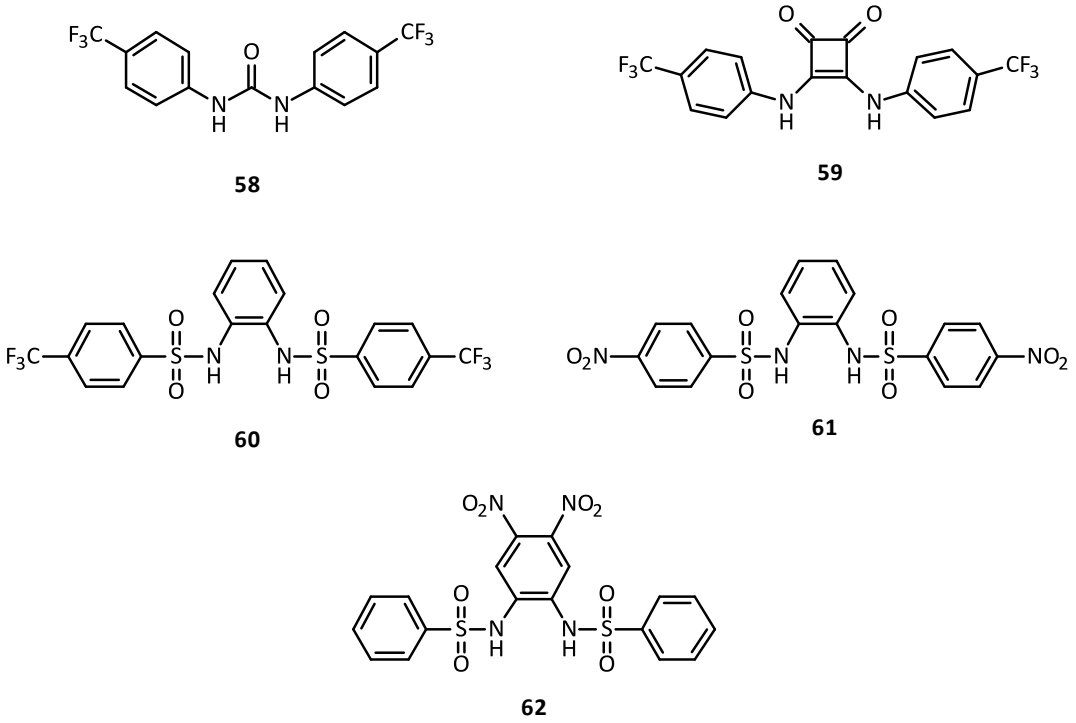

Figure 1.23: *Receptors studied by Amendola and co-workers.*[104]

In 2014, Gaeta *et al*. developed squaramidocalix[4]arene based receptors **63** and **64** (Figure 1.24), in which two squaramide moieties were attached to the upper rim of the calix[4]arene scaffold.[105] Spherical anions such as Cl^- and Br^- were found to induce dimerization of receptors **63** and **64**, thus forming 2:1 calixarene-anion complexes as demonstrated by Job plots and electrospray ionization mass spectrometry (ESI-MS) data.[105] However, the binding and dimerization with trigonal-planar anions such as BzO^- and NO_3^- was only observed for receptor **64**. Gaeta reported this behaviour to be due to an intramolecular H-bond in receptor **64** that favours binding with trigonal-planar anions via one squaramide moiety.[105]

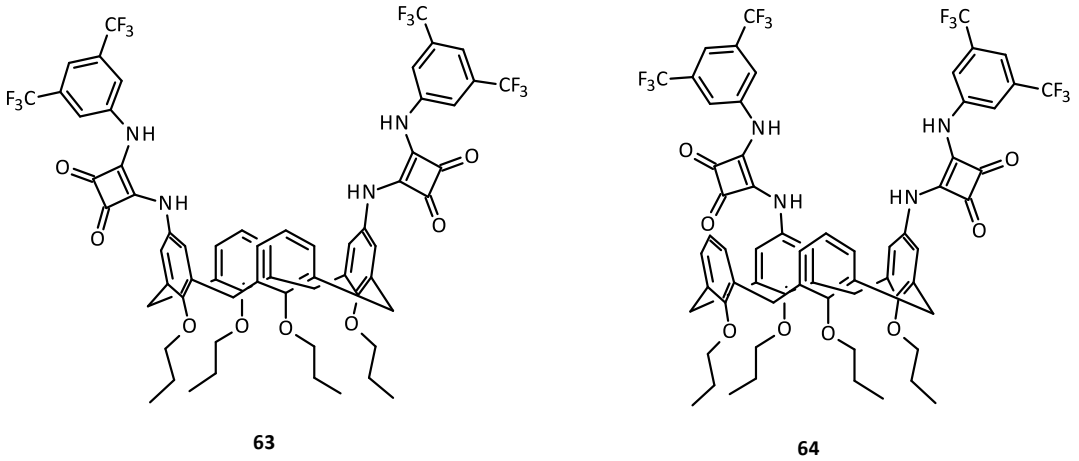

Figure 1.24: *Structure of squaramidocalix[4]arene based receptors developed by Gaeta et al.*[105]

Elmes and co-workers studied the anion binding and spectroscopic sensing properties of squaramide-based anion receptors **65-68** (Figure 1.25), which showed the highly unusual behaviour of deprotonation by the relatively weakly basic Cl^- anion in DMSO.[106] Titration of **65-67** with Cl^- led to dramatic changes in the colour of the solution and quenching of the excimer emission at 530 nm.

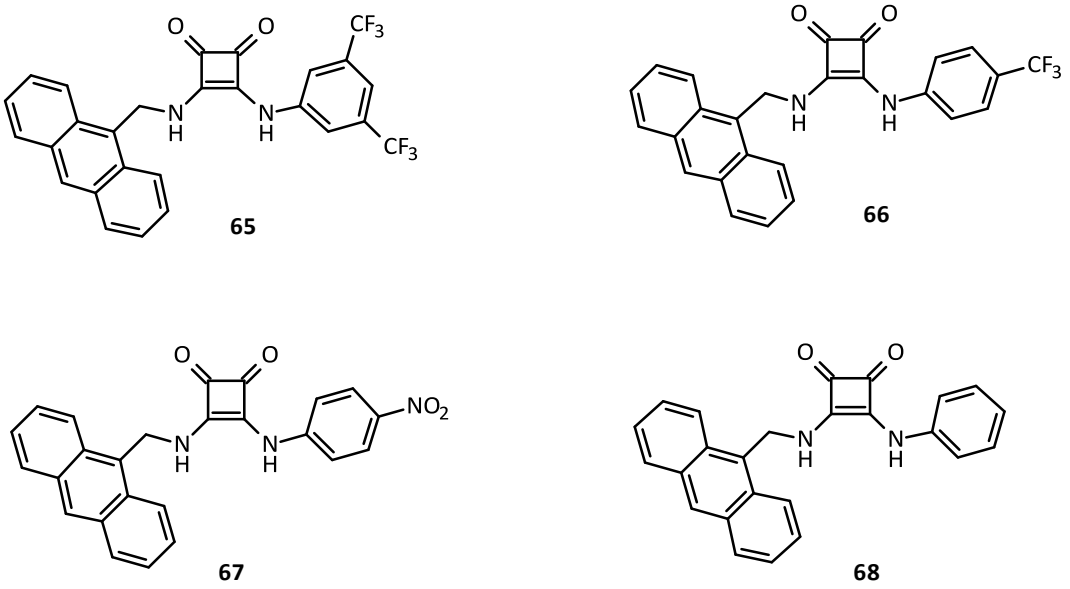

Figure 1.25: *Squaramide based fluorescent anion sensors developed by Elmes et al.*[106]

On the basis of the disappearance of the NH ^{1}H NMR resonances and colour changes induced by high concentrations of chloride, Elmes *et al*. proposed that

receptors **65-67** could be deprotonated by Cl^- at high concentrations, whereas H-bonding to Cl^- occurred at low Cl^- concentrations.[106] However, deprotonation was not observed with less basic anions (Br^-, I^-, and NO_3^-) or with the less acidic squaramide **68** in the presence of Cl^-. X-ray analysis revealed that receptor **65** forms a 1:1 (receptor/anion) complex with Cl^-, where the encapsulated anion is bound by two H-bonding interactions with both available squaramide NH groups (Figure 1.26).[106]

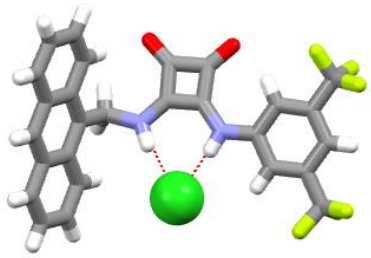

Figure 1.26: *Single crystal X-ray structure of the chloride complex of receptor* ***65****.*[106]

Elmes *et al*. later developed a series of thiosquaramides[107] **69-72** and oxothiosquaramide[108] **73** receptors that function as pH-dependent anion transporters (Figure 1.27). Titration binding studies with TBA Cl^- by ^1H NMR spectroscopy in DMSO-d_6/0.5% H_2O, fitted to a 1:1 binding model, derived the K_a of thiosquaramides **69-72** (60–400 M^{-1}) and oxothiosquaramide **73** (470 M^{-1}).[107, 108] The pH-dependent Cl^- anion- transport activities were determined by using POPC liposomal Cl^-/NO_3^- exchange assay and monitored by chloride-ISE in phosphate buffer at pH 7.2 and citrate buffer at pH 4.0. Receptors **69**, **70**, and **73** were significantly more active at pH 4.0 than at pH 7.2.[107, 108] However, thiosquaramides receptors **71** and **72** were inactive in both neutral and acidic media because lipophilicities were too high. pH-Spectrophotometric titration studies in CH_3CN/H_2O (9:1, v/v) demonstrated that the NH H-bond donors of receptors **69**, **70**, and **73** were much more acidic than the respective analogous oxosquaramides.[107, 108] The derived pKa values of receptors **69**, **70** and **73** were 7.3, 5.3 and 6.6 respectively. This result provided evidence that these receptors were mainly deprotonated as

negatively charged species at neutral pH, hence transport activities were enhanced at pH 4.0 with the receptors in the neutral state.[107, 108]

A

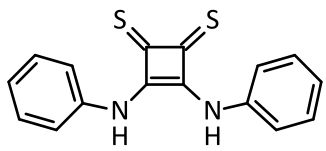

69

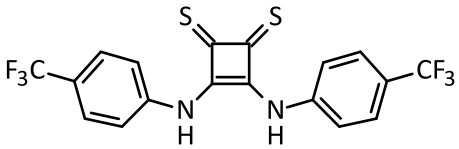

70

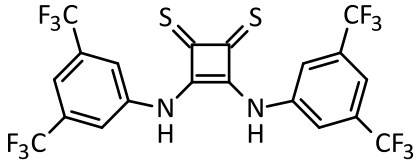

71

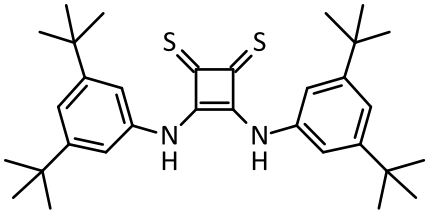

72

B

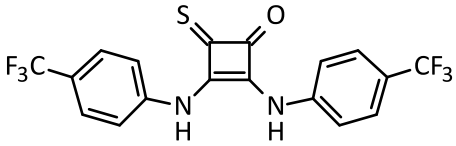

73

C

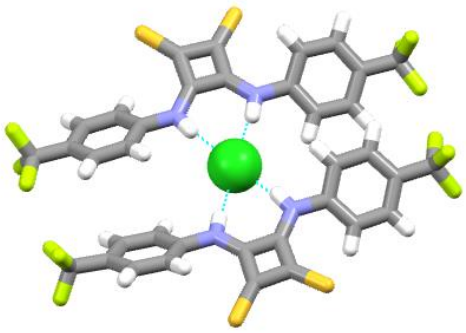

Figure 1.27: (A) *Structure of thiosquaramides receptors* ***69-72****.*[107] ***(B)*** *Structure of oxothiosquaramide receptor* ***73*** *studied by Elmes et al.*[108] ***(C)*** *X-ray crystal structure of thiosquaramide receptor* ***70*** *with TMA chloride.*[107]

1.8 Conclusion

This chapter gave a detailed insight on the significant role anions play in biology and in the environment. It also gave a brief introduction into how these anions can be

selectively recognised by anion receptors *via* H-bonding. The design, synthesis and spectroscopic anion binding studies of our novel squaramide based fluorescent receptors will be discussed in the next chapter.

Chapter 2 - Synthesis and Spectroscopic Anion Binding Studies of Potential Novel Squaramide Based Receptors

2.1 Introduction

Squaramides have found application in a number of areas of chemical research from their use for bioconjugation[109] to emerging pharmacophores in medicinal chemistry.[110] The strong hydrogen bond donor ability of the squaramide functional group has also recently been exploited in supramolecular chemistry for the design of anion receptors,[62] self-complementary molecular recognition motifs,[93] and catalysis.[111]

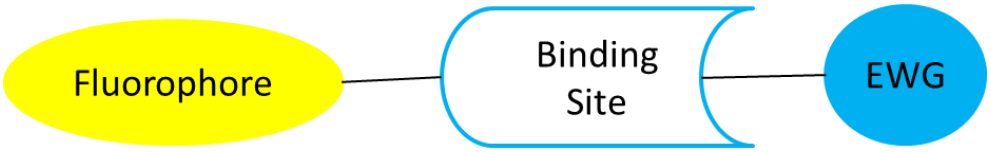

Figure 2.1: *Schematic representation of potential squaramide based anion receptors.*

Research in the Elmes group has centered on the development of napthalimide based fluorescent anion receptors and sensors, (Figure. 2.1), with potential uses in numerous biomedical and environmental applications.[106, 112] In particular, we have focused on receptors capable of selectively recognising sulfate due to its major role as a ground water contaminant in mining associated water pollution and in proposed radioactive waste-treatment processes.[113] In any case, binding of anions to receptors via H-bonding can lead to favourable applications in environmental chemistry and potential applications as emerging pharmacophores in medicinal chemistry.[101, 106] With this in mind, the overall aim of the work presented in this Chapter is to identify the potential of compounds **85 - 88** as fluorescent receptors and also as possible anion sensors (Figure 2.2).

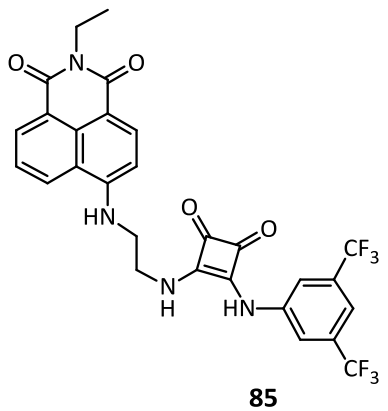

85

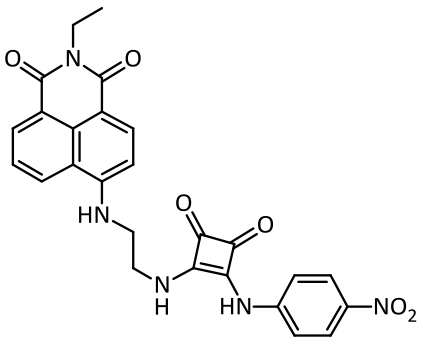

86

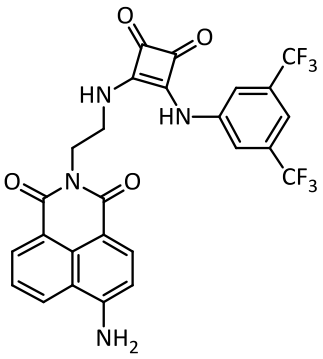

87

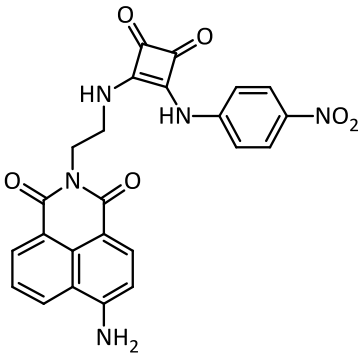

88

Figure 2.2: *Structure of target squaramide based fluorescent anion receptors* ***85 - 88****.*

2.2 Design Requirements

The design of the novel receptors will be based on four different requirements which include; the binding site, the signalling unit, the electron withdrawing group (EWG) and the position of the binding site.

2.2.1 The Binding Site

In the design of our novel receptors, we foresaw that the remarkable hydrogen bonding donor ability of the squaramide motif could be utilised. The four membered ring conjugated diamines derived from squaric acids, have the capacity for selectively binding to different H-bond acceptors through their acidic N-H groups (Figure 2.3). Therefore due to this reason, we decided to exploit the strong

hydrogen bond donor ability of the squaramide motif in the design of our novel receptors.

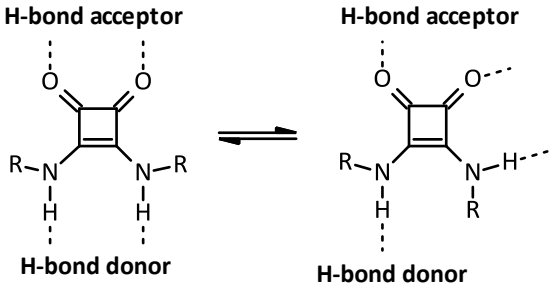

Figure 2.3: *Hydrogen bonding donor ability of squaramides.*[84]

2.2.2 The Signalling Unit

In the design of our novel receptors, we foresaw that the set of known photophysical properties provided by the naphthalimide fluorophore could be used to monitor the anion binding process of our novel receptors. The naphthalimide structure has found application in many areas of chemistry, ascribed to its unique photophysical properties.[114-117] Its absorption and fluorescence emission spectra lie within the UV/Vis regions and the various photophysical properties can be adjusted through rational structural design.[118] The electron donating amine and the electron withdrawing imide of the 4-amino-1,8-naphthalimide results in a 'push – pull' based, internal charge transfer (ICT) (Figure 2.4).[118] The ICT character, gives rise to a large excited-state dipole and, in turn, broad absorption and emission bands centred at 450 and 550 nm respectively when recorded in water.[118] The potential of the highly versatile 4-amino-1,8-naphthalimide signalling unit that absorbs and emit at long wavelengths was employed for as the signalling unit for the anion sensing of our novel receptors.

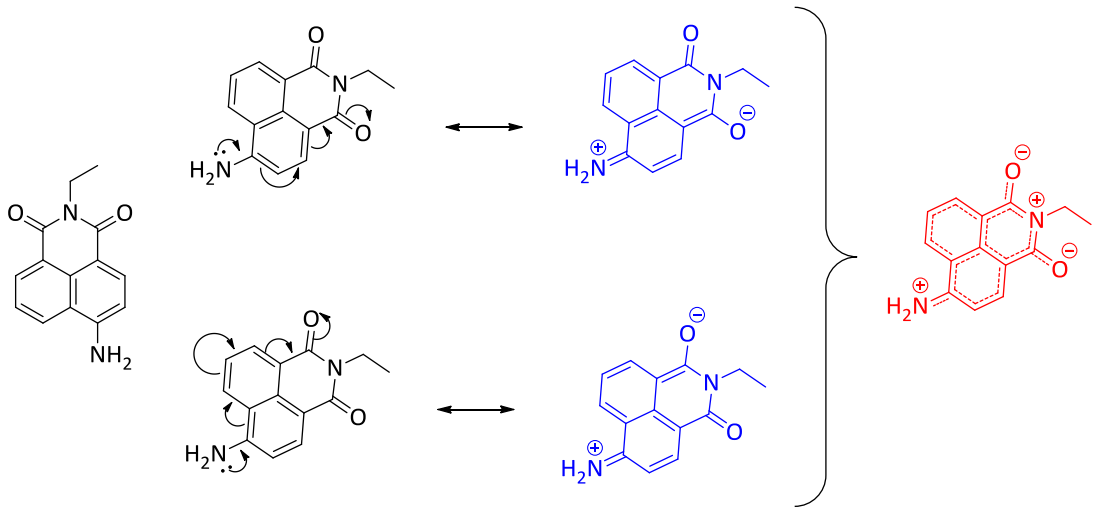

Figure 2.4: *Structure of 4-amino-1,8-naphthalimide and the schematic representation of the ICT excited state within the 4-amino-1,8-naphthalimide fluorophore caused by a 'push – pull' action.*[118]

2.2.3 The Electron Withdrawing Group (EWG)

It was anticipated that the presence of electron-withdrawing groups (EWG) would increase the acidity and the H-bonding capability of the N-H hydrogen bond donor of the squaramide motif, as has been previously seen with receptors **57, 59, 65** and **67**.[62, 65, 67, 104] Therefore, it was also predicted that the presence of EWG could improve the anion binding affinities towards our novel receptors. The electron-withdrawing abilities of the trifluoromethyl and nitro substituents were explored for this purpose (Figure 2.5).

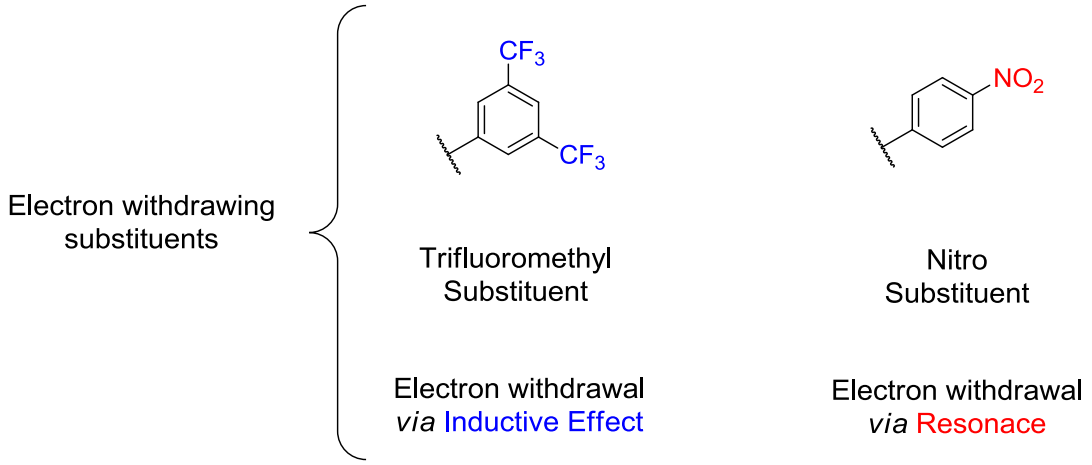

Figure 2.5: *Schematic representation of the EWG employed for the receptor design.*

2.2.3 The Binding Site Position

In the design of our novel receptors, we varied the position of our binding site by attaching the binding site to either the top or the bottom of the signalling unit as shown in Figure 2.6. The position of the binding site was altered from the bottom to the top of the signalling unit in order to observe any changes in the binding affinity of our novel receptors.

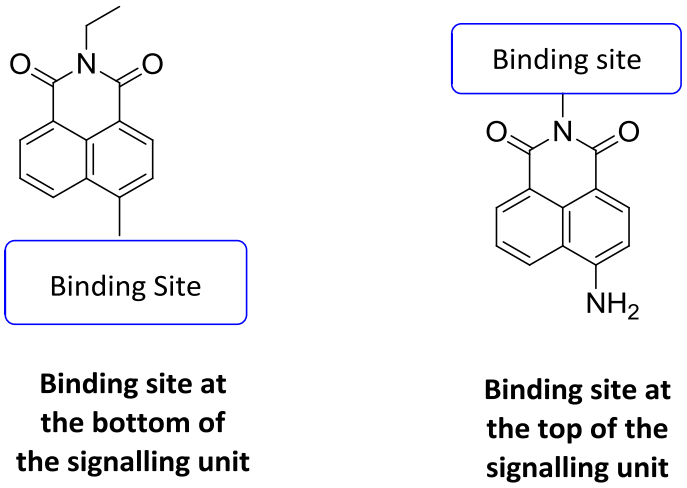

Figure 2.6: *Schematic representation of the binding site postion (Top or Bottom) on the signalling unit for the receptor design.*

In the following chapter, the description of the synthesis and characterisation of each of the compounds **85 - 88** will be given. This will be followed by a discussion of the photophysical properties of each compound and their anion binding behaviour which may be established using a range of different spectroscopic techniques.

2.3 Synthesis

The target compounds **85 - 88** were prepared from commercially available starting materials. All target and intermediates compounds were fully characterised using ^{1}H NMR, ^{13}C NMR, infrared spectroscopy and high resolution mass spectroscopy.

2.3.1 Synthesis of Novel Compounds 85 and 86

The synthesis of compound **85** was achieved using intermediates **75** and **79** in the synthetic pathway of **85** as outlined in Scheme 2.4. Firstly, intermediate **75** was synthesised as outlined in Scheme 2.1, by stirring a solution of 3,5-bis(trifluoromethyl)aniline in EtOH with a solution of diethyl squarate **74** and zinc triflate to ensure that **74** was electrophilic enough prior to nucleophilic attack by bis(trifluoromethyl)aniline **i**n EtOH. Removal of solvent by filtration yielded the desired product **75** as an off-white amorphous solid in 79% yield.

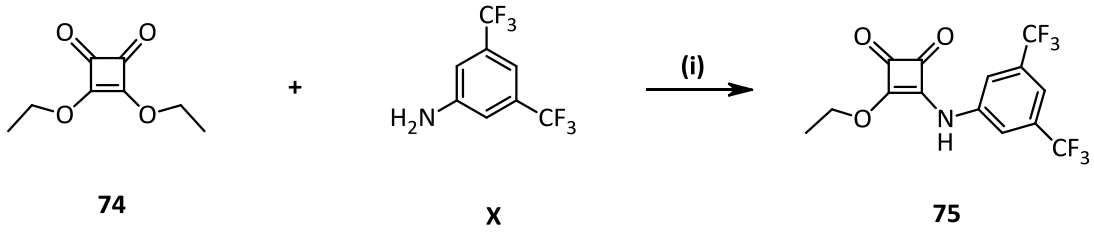

74 **X** **75**

***Scheme 2.1**: Synthetic pathway to **75 (i)** Zn(OTf)$_2$, EtOH.*

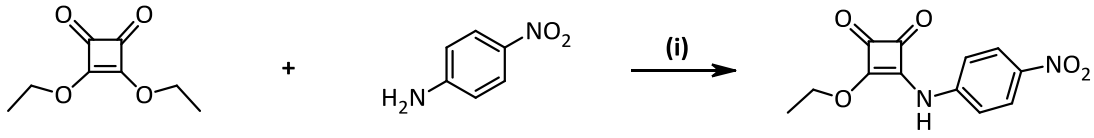

74 **Y** **76**

***Scheme 2.2**: Synthetic pathway to **76 (i)** Zn(OTf)$_2$, EtOH*

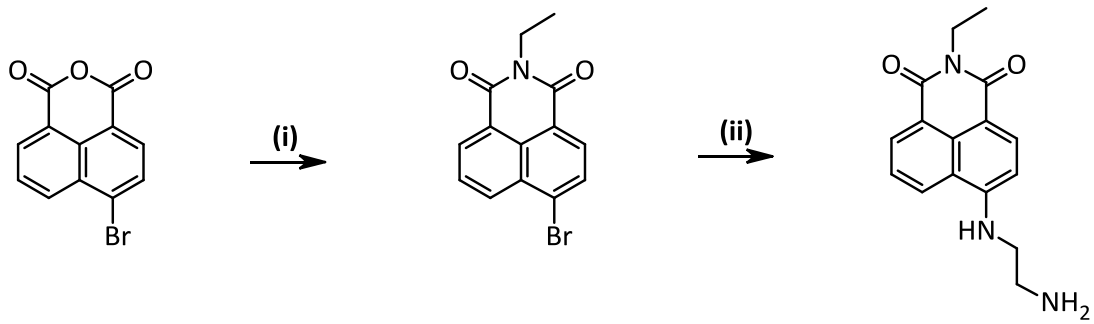

77 **78** **79**

Scheme 2.3*: Synthetic pathway to* ***79*** ***(i)*** *Ethylamine, EtOH, reflux;* ***(ii)*** *Ethylenediamine.*

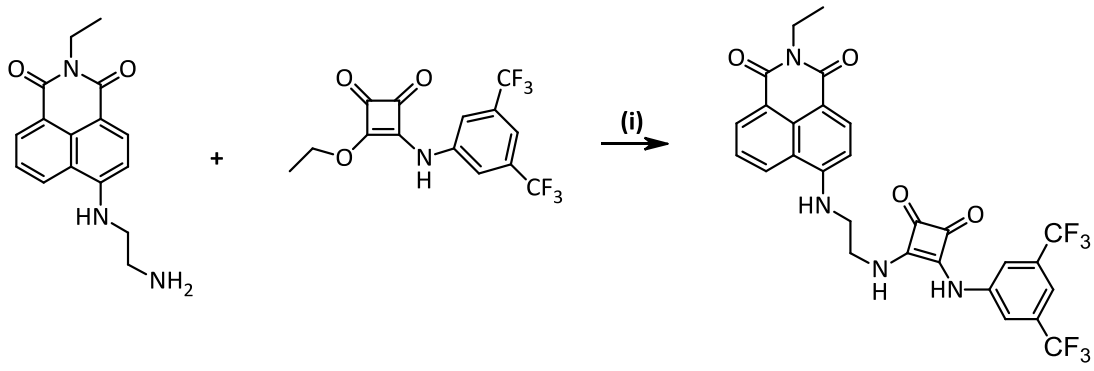

79 **75** **85**

Scheme 2.4*: Synthetic pathway to* ***85 (i)*** Et_3N*, EtOH.*

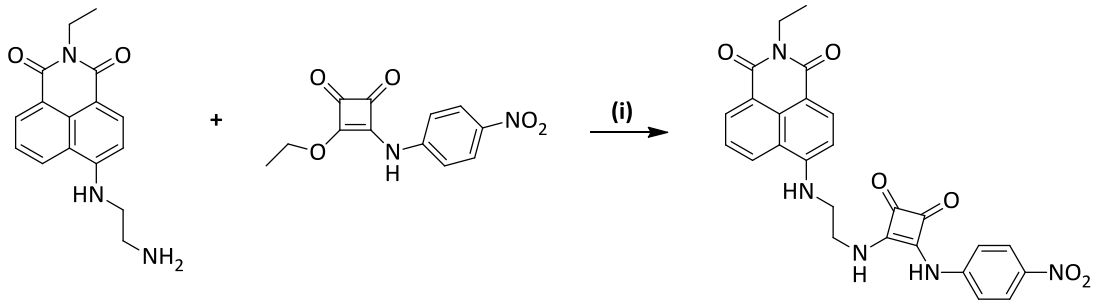

79 **76** **86**

Scheme 2.5*: Synthetic pathway to* ***86 (i)*** Et_3N*, EtOH.*

Intermediate **79** was synthesised according to Scheme 2.2, by direct amination of **78** using ethylenediamine at room temperature to yield **79** as a yellow amorphous solid in 80% yield. Finally, receptor **85** was synthesised as outlined in Scheme 2.4, *via* the nucleophilic addition of intermediates **75** to **79** in Et_3N and EtOH to yield receptor **85** as a yellow amorphous solid in 78% yield. The same procedure was applied to synthesis of compound **86** using intermediate **76** instead of intermediate **75** as outlined in Scheme 2.5. Compound **86** was obtained as an orange amorphous solid in 73% yield. Novel receptors **85** and **86** were fully characterised by ^{1}H NMR, ^{13}C NMR, HRMS and IR spectroscopy. The ^{1}H NMR spectrum of **85** at 293 K is shown in Figure 2.7.

The ^{1}H NMR spectrum of **85** and **86** at 293 K in DMSO-*d6* could not be accurately assigned due to peak broadening observed in both the ^{1}H NMR spectrum of **85** and **86** at 293 K in DMSO-*d6*. This observation was proposed to be ascribed to a self-association interaction between the receptor molecules. Therefore, the ^{1}H NMR analysis of **85** and **86** at 343 K was considered to aid in the accurate characterisation of **85** and **86** in DMSO-*d6*.

(A)

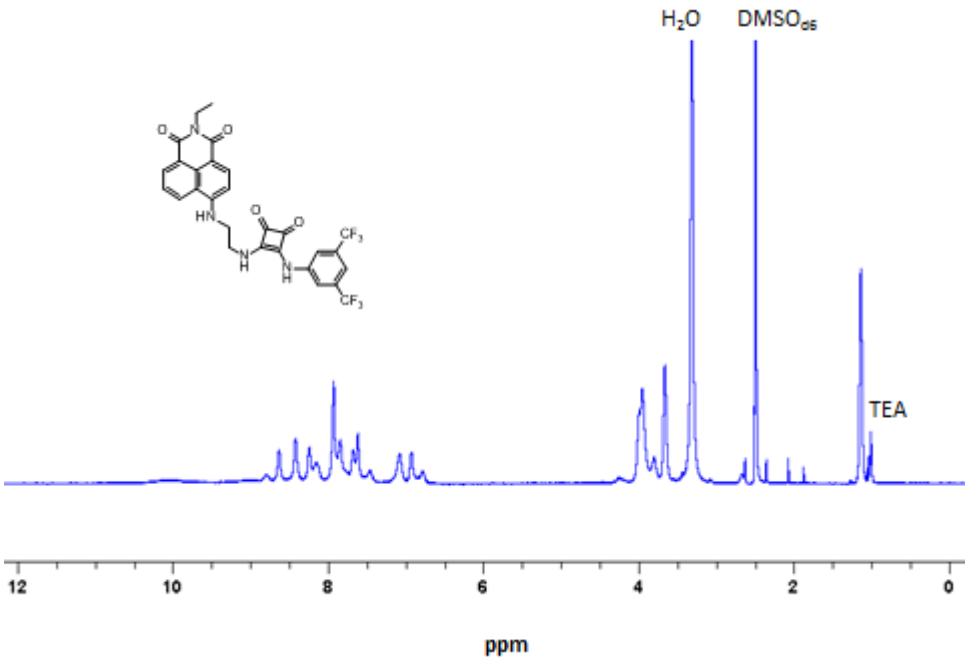

(B)

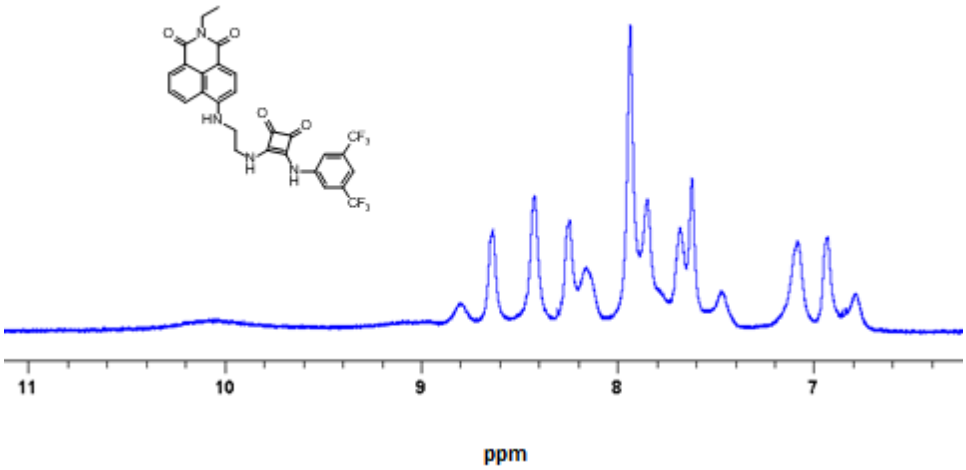

Figure 2.7: (A) *The ^{1}H NMR spectrum of compound **85** at 293 K (500.13 MHz, DMSO-$_{d6}$).* ***(B)*** *The zoomed in ^{1}H NMR spectrum of the aromatic region of compound **85** at 293 K (500.13 MHz, DMSO-$_{d6}$).*

As shown in Figure 2.8, the ^{1}H NMR spectrum of receptor **85** at 343 K resulted in sharper peaks of all the signals observed for compound **85** at room temperature. The ^{1}H NMR peaks were assigned using 2-D C-H and H-H COSY analysis, the results of which correlated to the expected number of protons, integration and chemical shifts were appropriate. Resonances corresponding to both the 1,8-naphthalimide and the trifluomethyl aromatic moieties are evident, in addition to those for the squaramide anion binding site. Successful formation of compound **85** was also evident from accurate mass spectrometry, where **85** displayed a peak at 591.1439 corresponding to the [M + H] ion (-3.8 ppm).

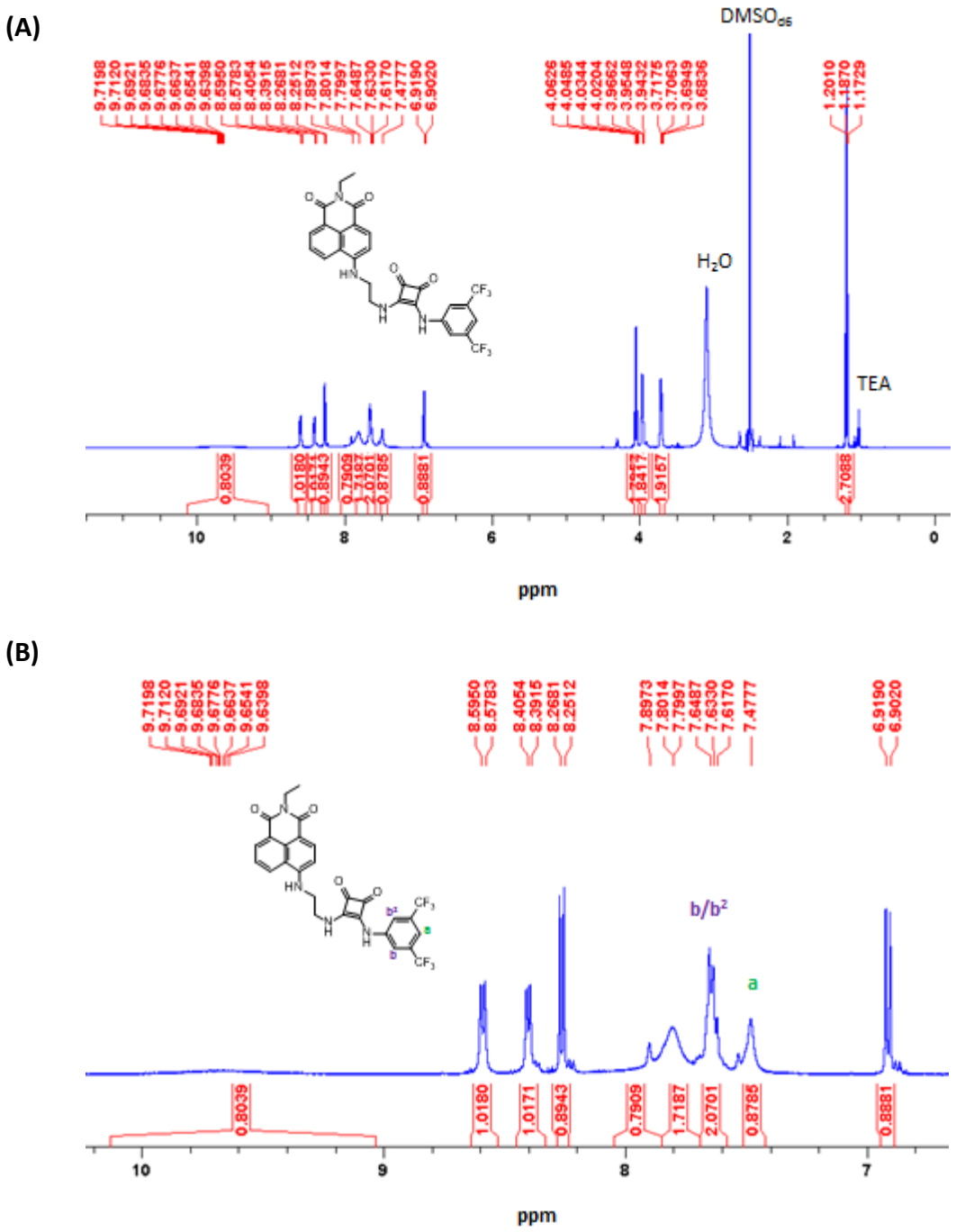

Figure 2.8: (A) *The ^{1}H NMR spectrum of compound **85** at 343 K (500.13 MHz, DMSO-$_{d6}$).* ***(B)*** *The zoomed in ^{1}H NMR spectrum of the aromatic region of compound **85** at 343 K (500.13 MHz, DMSO-$_{d6}$).*

2.3.2 Synthesis of Novel Compounds 87 and 88

An alternative synthetic strategy was utilised in the synthesis of compounds **87** and **88**, in which the binding site is attached to the top position of the signalling unit. The synthesis of compounds **87** was achieved using intermediates **75** and **84** in the synthetic pathway of **87** as outlined in Scheme 2.7. Firstly, intermediate **75** was synthesised as outlined in Scheme 2.1. Intermediate **84** was synthesised according to Scheme 2.6, by direct amination of **80** using Boc-protected ethylenediamine (tert-butyl(2-aminoethyl)carbamate) **81** in EtOH by heating under microwave reaction conditions (1 hour at 110°C, 1 mbar, 300 Watts). The extraction the organic layer with de-ionised H_2O, followed by the removal of the solvent under reduced pressure, yielded the desired product **82** as a peach amorphous solid in 76% yield.

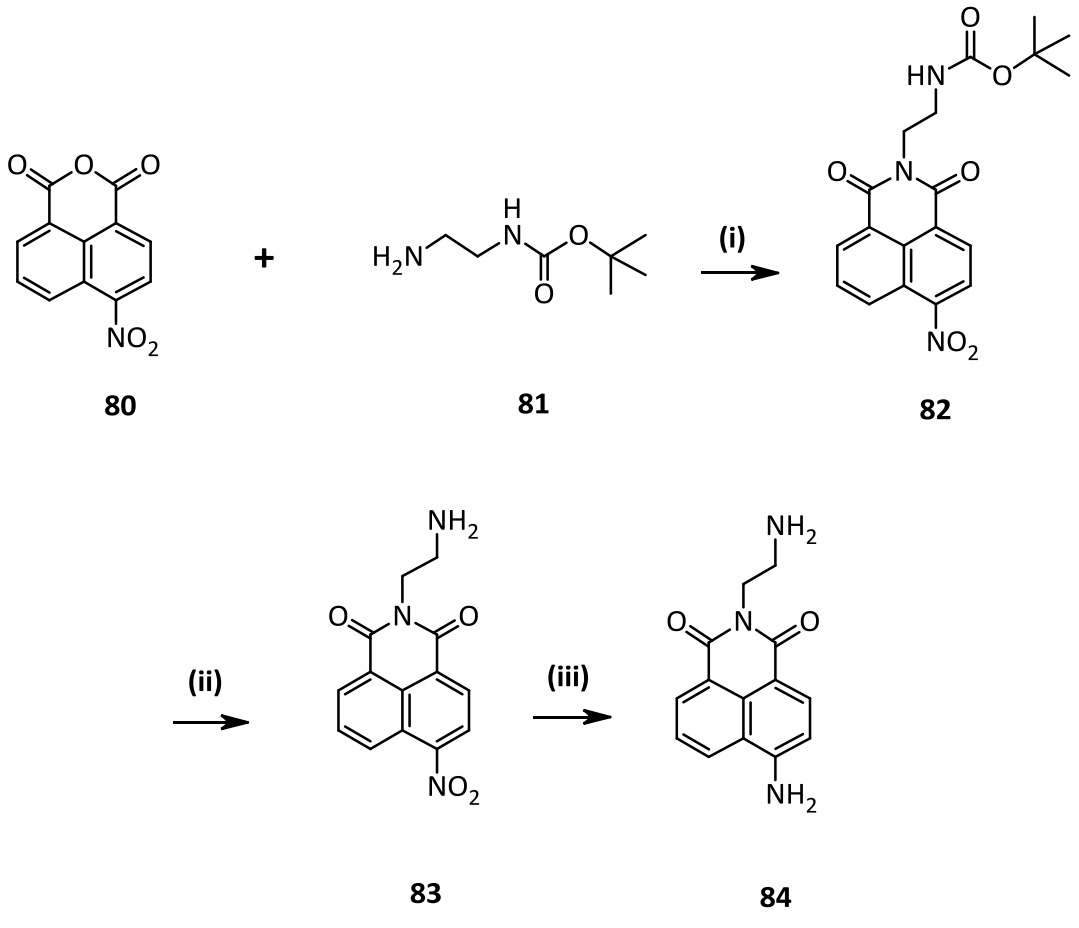

80 **81** **82**

83 **84**

***Scheme 2.6**: Synthetic pathway to **84** **(i)** EtOH, Microwave (1 hour at 110°C, 1 mbar, 300 Watts); **(ii)** TFA:DCM, (50:50) **(iii)** Pd/H_2, MeOH.*

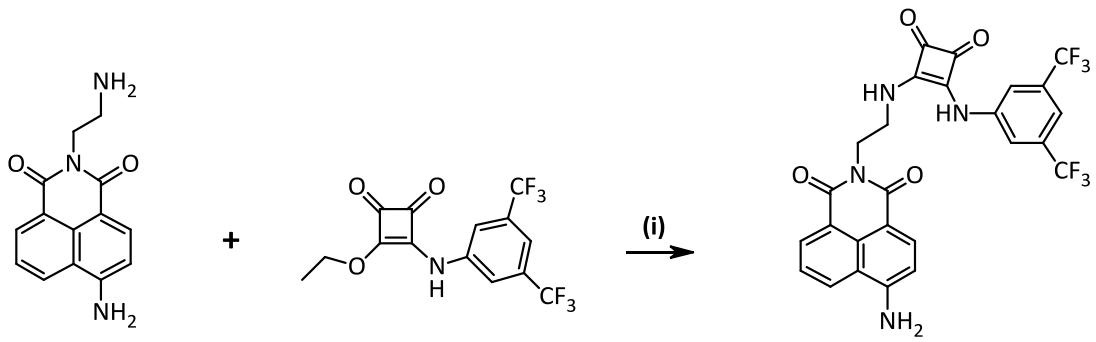

84 **75** **87**

Scheme 2.7*: Synthetic pathway to* ***87 (i)*** Et_3N*, EtOH.*

The de-protection of **82** in a mixture of TFA : DCM (50 : 50) yielded **83** as a beige amorphous solid in 93% yield. Reduction of the nitro group of **83** using Pd/H_2 in MeOH, gave the pure diamine **84** as a mustard solid in 75% yield. Finally, compound **87** was synthesised as outlined in Scheme 2.6, *via* the nucleophilic addition of intermediates **75** and **84** in Et_3N and EtOH to yield receptor **87** as an olive green solid in 56% yield. The same procedure was applied to synthesis of compound **88** using intermediate **76** instead of intermediate **75** as outlined in Scheme 2.2. Receptor **88** was obtained as an orange solid in 67% yield. Novel compounds **87** and **88** were fully characterised by ^{1}H NMR, ^{13}C NMR, HRMS and IR spectroscopy. The ^{1}H NMR spectrum of **87** at 293 K is shown in Figure 2.9.

Analogous to compound **85** and **86,** the ^{1}H NMR spectra of **87** and **88** at 293 K in DMSO-*d6* could not be accurately characterised due to peak broadening observed in both the ^{1}H NMR spectra of **87** and **88** at 293 K in DMSO-*d6.* This observation was also predicted to be due to self-association interaction between the receptor molecules. Therefore, similar to compounds **85** and **86**, the ^{1}H NMR analysis of **87** and **88** at 343 K was considered to aid in the accurate characterisation of **87** and **88** in DMSO-*d6.* As shown in Figure 2.10, the ^{1}H NMR spectrum of compound **87** at 343 K also resulted in sharper peaks of all the signals observed for compound **87** at room temperature. The ^{1}H NMR peaks were assigned using 2-D C-H and H-H COSY analysis, the results of which correlated to the expected number of protons, integration and chemical shifts were appropriate. Resonances corresponding to

both the 1,8-naphthalimide and the trifluomethyl aromatic moieties are evident, in addition to those for the squaramide anion binding site. Successful formation of receptor **87** was also evident from accurate mass spectrometry, where **87** displayed a peak at 565.1231 corresponding to the [M + H] ion (4.31 ppm).

(A)

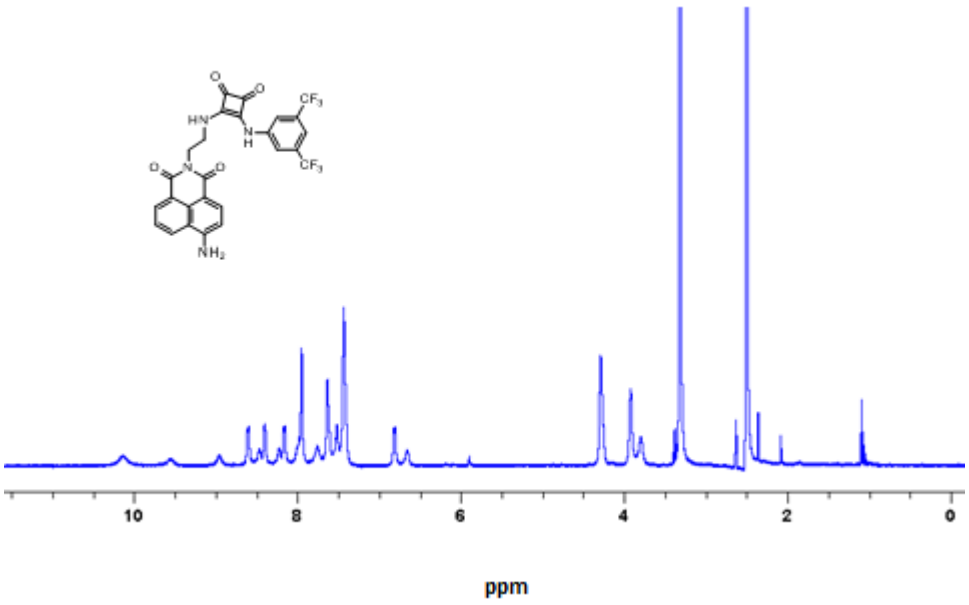

(B)

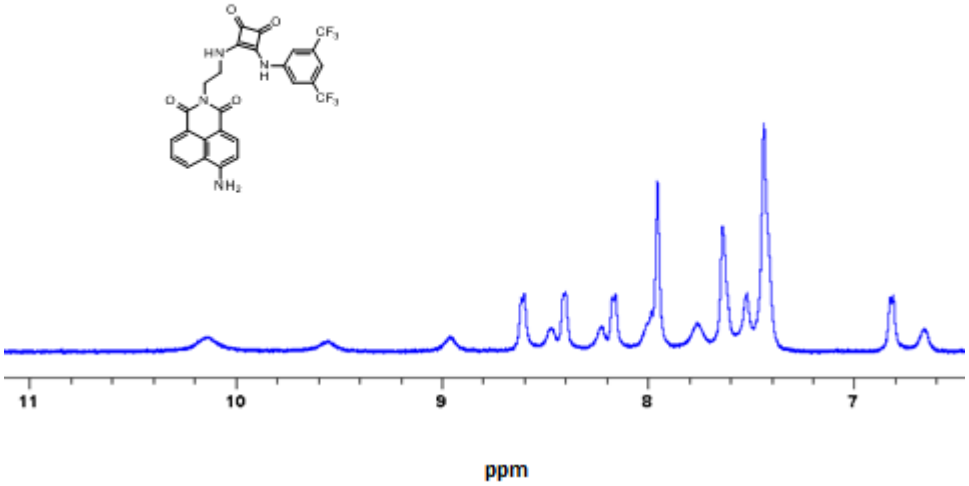

Figure 2.9: (A) *The ^{1}H NMR spectrum of compound **87** at 293 K (500.13 MHz, DMSO-$_{d6}$).* ***(B)*** *The zoomed in ^{1}H NMR spectrum of the aromatic region of receptor **87** at 293 K (500.13 MHz, DMSO-$_{d6}$).*

(A)

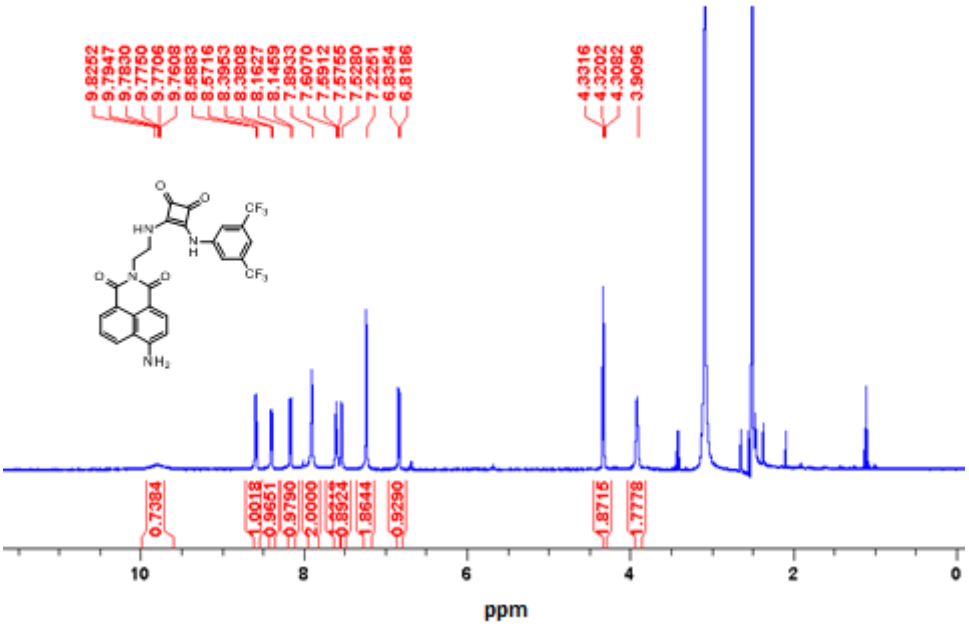

(B)

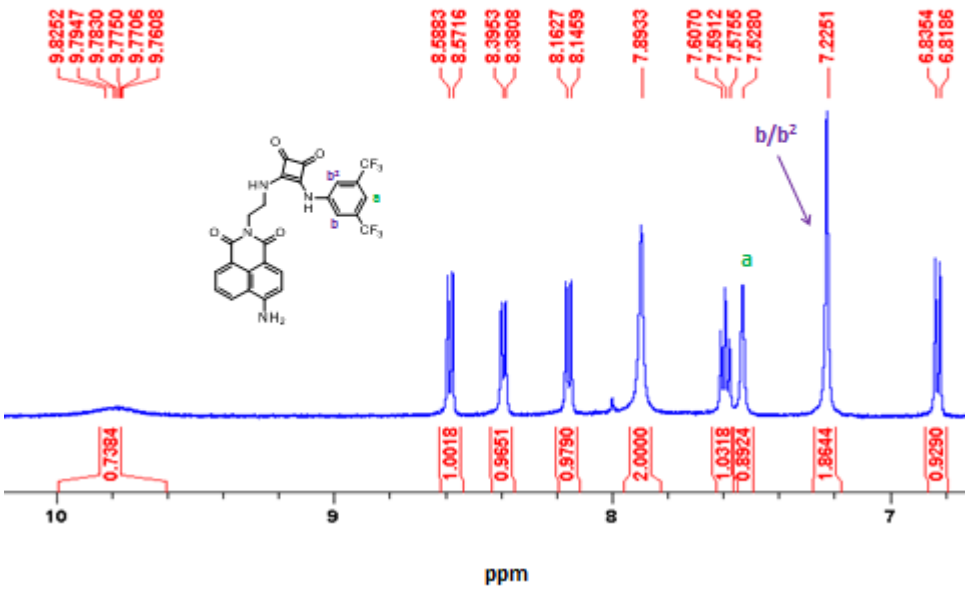

Figure 2.10: (A) *The ^{1}H NMR spectrum of compound* ***87*** *at 343 K (500.13 MHz, DMSO-$_{d6}$).* ***(B)*** *The zoomed in ^{1}H NMR spectrum of the aromatic region of receptor* ***87*** *at 343 K (500.13 MHz, DMSO-$_{d6}$).*

In summary, the position of the binding site (bottom or top) to the signalling unit did not hinder the successful synthesis of compounds **85 – 88**. The analysis of the ^{1}H NMR spectra at 343 K of compounds **85 – 88** in DMSO-$_{d6}$ resulted in better

resolution which was attributed to peak sharpening of the characteristic peaks of compound **85 – 88** at 293 K. However, the ^{1}H NMR spectra of compounds **85 – 88** in DMSO-$_{d6}$ could not be accurately assigned at 293 K due peak broadening of the characteristic peaks of compounds **85 – 88**. This observation was proposed to be attributed to self-association interaction between the potential receptor molecules of **85 – 88**. With this in mind, potential self-association ability of compounds **85 – 88** will be investigated next via scanning electron microscopy (SEM).

2.4 Scanning Electron Microscopy (SEM)

The potential self-association ability of compounds **85 – 88** was investigated using SEM analysis. Interesting patterns were observed in the SEM images of compound **85, 86, 87** and **88** as shown in Figures 2.11, 2.12, 2.13 and 2.14 respectively. These unique patterns further confirms our prediction of self-association interaction between compounds **85 – 88** molecules from the ^{1}H NMR broadened spectra of **85 - 88** at 293 K in DMSO-$_{d6}$.

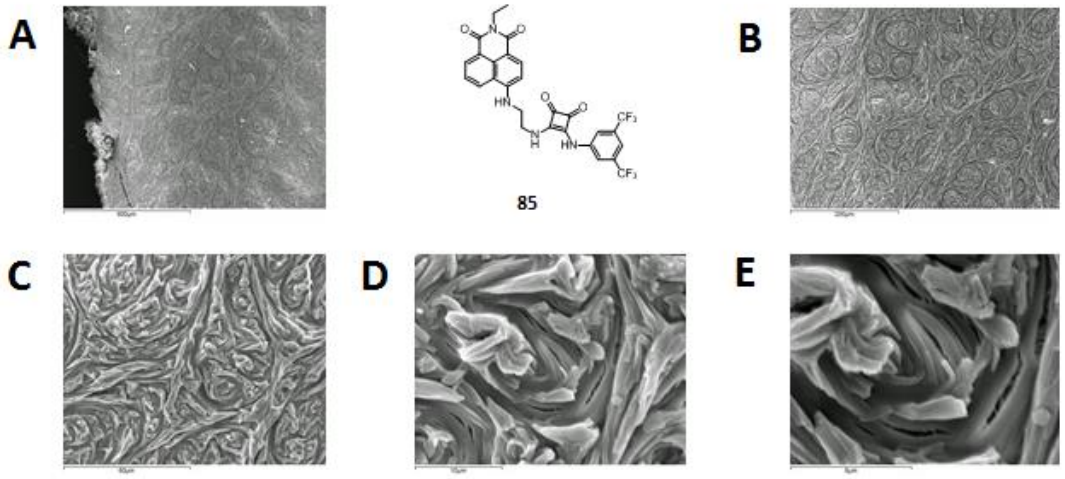

***Figure 2.11**: Scanning electron microscopy (SEM) images of compound **85** spotted with Au, **(A):** Mag x 100; **(B):** Mag x 200; **(C):** Mag x 1000; **(D):** Mag x 4000; **(E):** Mag x 7000.*

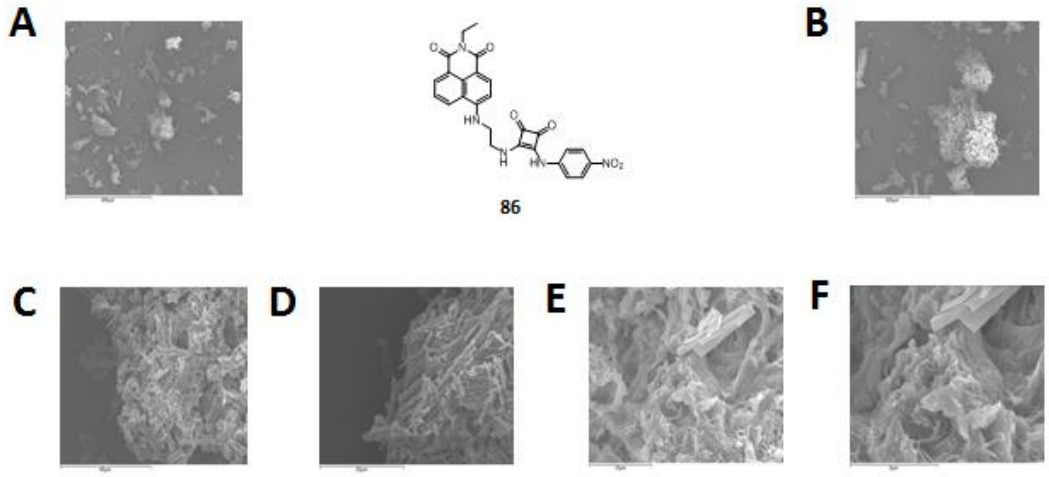

***Figure 2.12**: Scanning electron microscopy (SEM) images of compound **86** spotted with Au, **(A):** Mag x 100; **(B):** Mag x 250; **(C):** Mag x 1000; **(D):** Mag x 1800; **(E):** Mag x 4000; **(F):** Mag x 7000.*

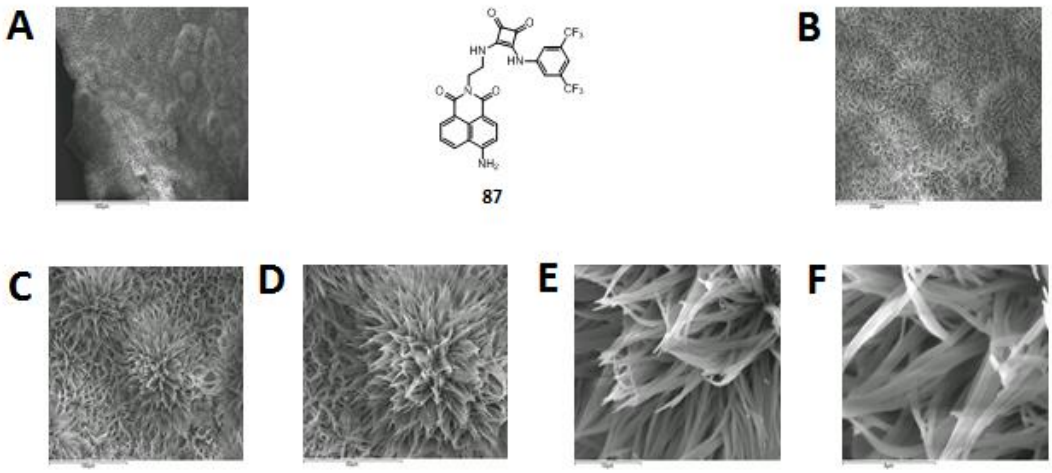

***Figure 2.13**: Scanning electron microscopy (SEM) images of compound **87** spotted with Au, **(A):** Mag x 100; **(B):** Mag x 250; **(C):** Mag x 500; **(D):** Mag x 1000; **(E):** Mag x 4000; **(F):** Mag x 7000.*

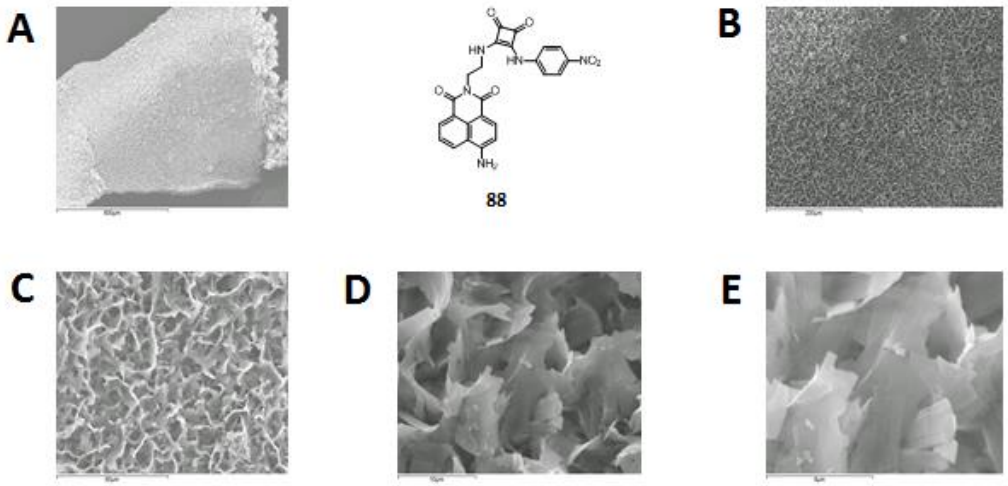

***Figure 2.14**: Scanning electron microscopy (SEM) images of compound **88** spotted with Au, **(A):** Mag x 100; **(B):** Mag x 250; **(C):** Mag x 1000; **(D):** Mag x 4000; **(E):** Mag x 7000.*

In summary, ^{1}H NMR analysis at 293 K in DMSO-$_{d6}$ and SEM analysis revealed the presence of self-association interaction between the molecules of potential receptors **85 – 88**. However, upon increasing the temperature, it was observed that molecules of potential receptors **85 – 88** self-dissociates from each other. This was supported by the increase in resolution and the sharpening of characteristic peaks in the ^{1}H NMR spectra of compounds **85 – 88** at 343 K in DMSO-$_{d6.}$ The photophysical characterisation of compounds **85 – 88** will be discussed next.

2.5 Photophysical Characterisation

Characterisation of the photophysics of novel compounds **85 – 88** was undertaken in order to fully understand their photophysical behaviour necessary to monitor the interaction of such systems with anions.

2.5.1 Photophysical Characterisation of Novel Compound 85

The UV/Vis absorption spectrum of compound **85** in DMSO (0 – 57 µM) is shown in Figure 2.15. Three different absorption maxima are shown in the UV/Vis absorption spectrum at 280 nm, 340 nm and 445 nm with extinction coefficient values of 32642 M^{-1}, 19559 M^{-1} and 15439 M^{-1} respectively as shown in Table 2.1. The

intense band at 280 nm is attributed to π - π^* transition with the naphthalimide fluorophore. The less intense bands at 340 nm and 445 nm are attributed to the internal charge transfer (ICT), which is a well documented feature of the naphthalimide fluorophore.

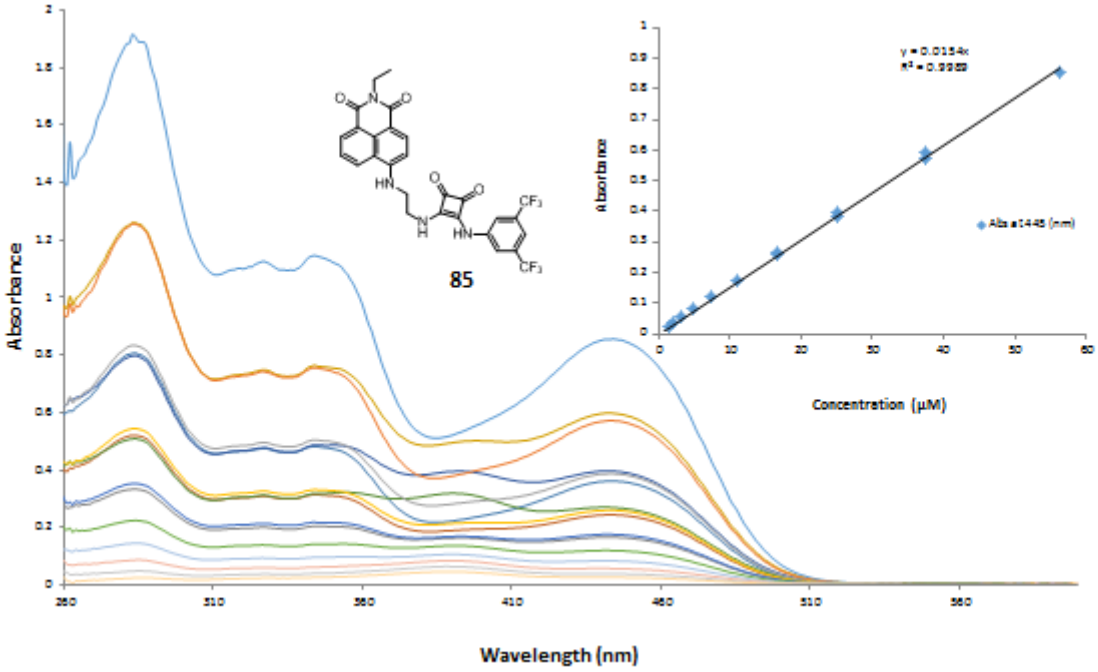

***Figure 2.15**: Changes in UV/Visible spectra upon increasing concentration of **85** in DMSO* (0 – 57 µM). ***Inset:** Plot of absorbance at 445 nm as a function of increasing concentration of **85**.*

2.5.2 Photophysical Characterisation of Novel Compound 86

The UV/Vis absorption spectrum of compound **86** in DMSO (0 – 67 µM) is shown in Figure 2.16. Two different absorption maxima are shown in the UV/Vis absorption spectrum at 280 nm and 420 nm with extinction coefficient values of 34375 M^{-1} and 29899 M^{-1} respectively as shown in Table 2.1. The intense band at 280 nm is attributed to π - π^* transition with the naphthalimide fluorophore. The band at 420 nm is attributed to the internal charge transfer (ICT) within the naphthalimide fluorophore.

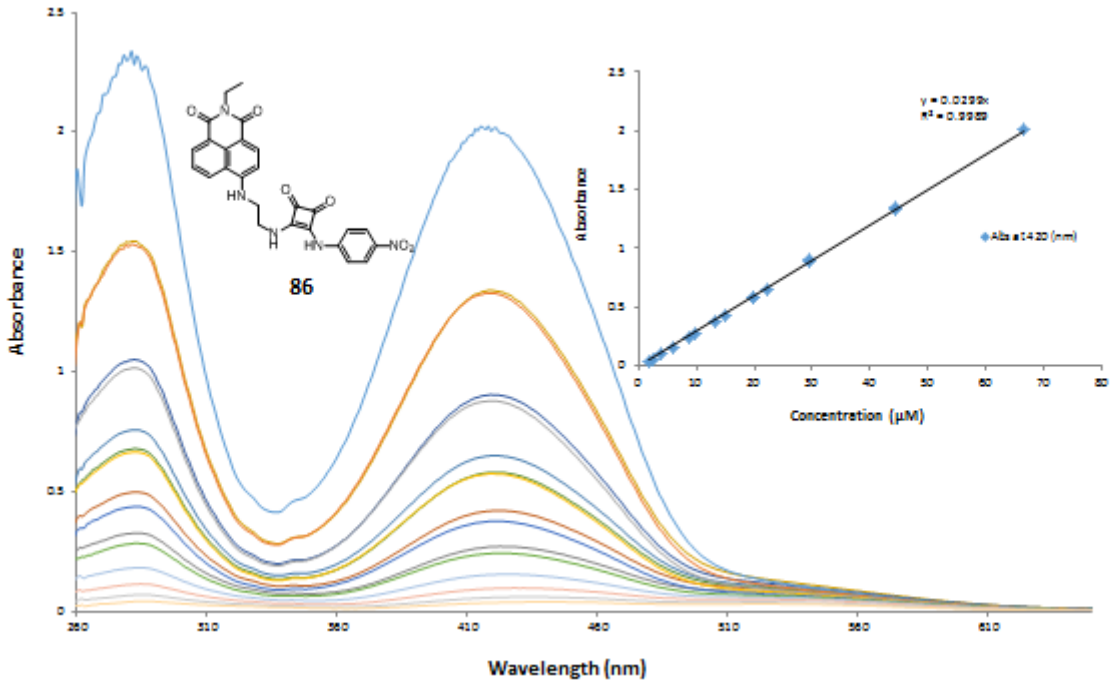

***Figure 2.16**: Changes in UV/Visible spectra upon increasing concentration of **86** in DMSO* (0 – 67 µM). ***Inset:** Plot of absorbance at 420 nm as a function of increasing concentration of **86**.*

2.5.3 Photophysical Characterisation of Novel Compound 87

The UV/Vis absorption spectrum of compound **87** in DMSO (0 – 60 µM) is shown in Figure 2.17. Three different absorption maxima are shown in the UV/Vis absorption spectrum at 280 nm, 340 nm and 445 nm with extinction coefficient values of 34785 M^{-1}, 20405 M^{-1} and 13717 M^{-1} respectively as shown in Table 2.1. The intense band at 280 nm is attributed to π - π^* transition with the naphthalimide fluorophore.[118] The less intense bands at 340 nm and 445 nm is nm is attributed to the internal charge transfer (ICT) within the naphthalimide fluorophore.

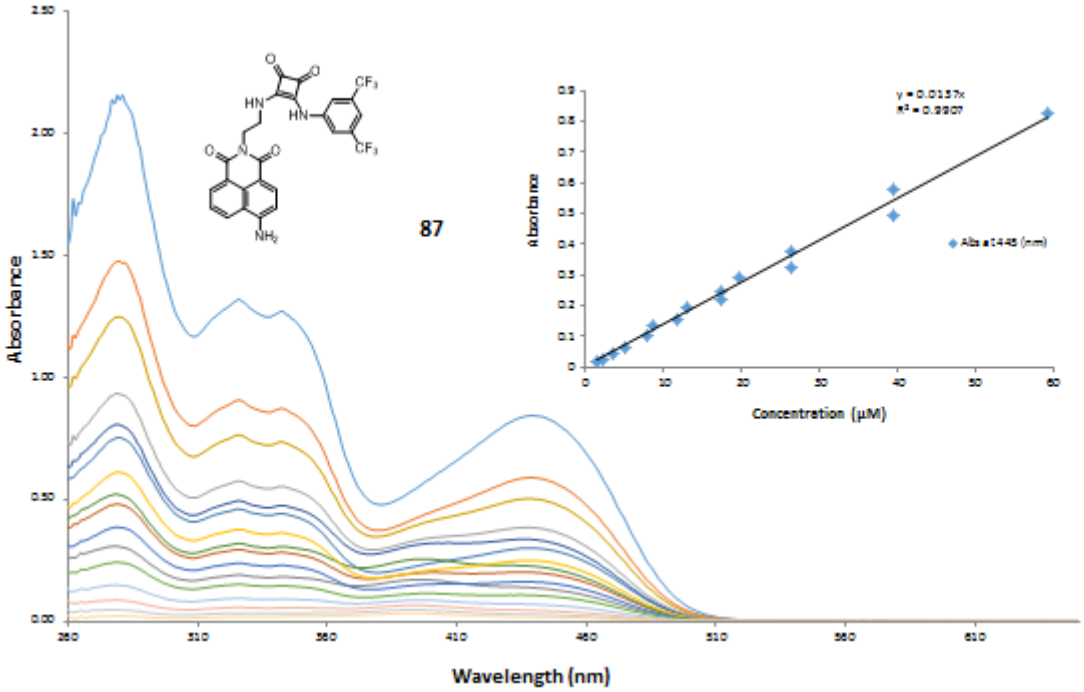

***Figure 2.17**: Changes in UV/Visible spectra upon increasing concentration of **87** in DMSO* (0 – 60 µM). ***Inset:** Plot of absorbance at 445 nm as a function of increasing concentration of **87**.*

2.5.4 Photophysical Characterisation of Novel Compound 88

The UV/Vis absorption spectrum of compound **88** in DMSO (0 – 70 µM) is shown in Figure 2.18. Two different absorption maxima are shown in the UV/Vis absorption spectrum at 280 nm and 420 nm with extinction coefficient values of 35187 M^{-1} and 27410 M^{-1} respectively as shown in Table 2.1. The intense band at 280 nm is attributed to π - π^* transition with the naphthalimide fluorophore. The band at 420 nm is attributed to the internal charge transfer (ICT) within the naphthalimide fluorophore. A third absorption maxima at 545 nm attributed to the naphthalimide π – π stacking band was also observed in the UV/Vis absorption spectrum of compound **88**.[79, 118, 119] However, the naphthalimide π – π stacking band at 545 nm does not obey the Beer-Lambert law which further suggests the presence of a self-association interaction within the molecules in compound **88**. A summary of the absorption properties of potential anion receptors **85 - 88** as well as their molar absorptivities is given in Table 2.1.

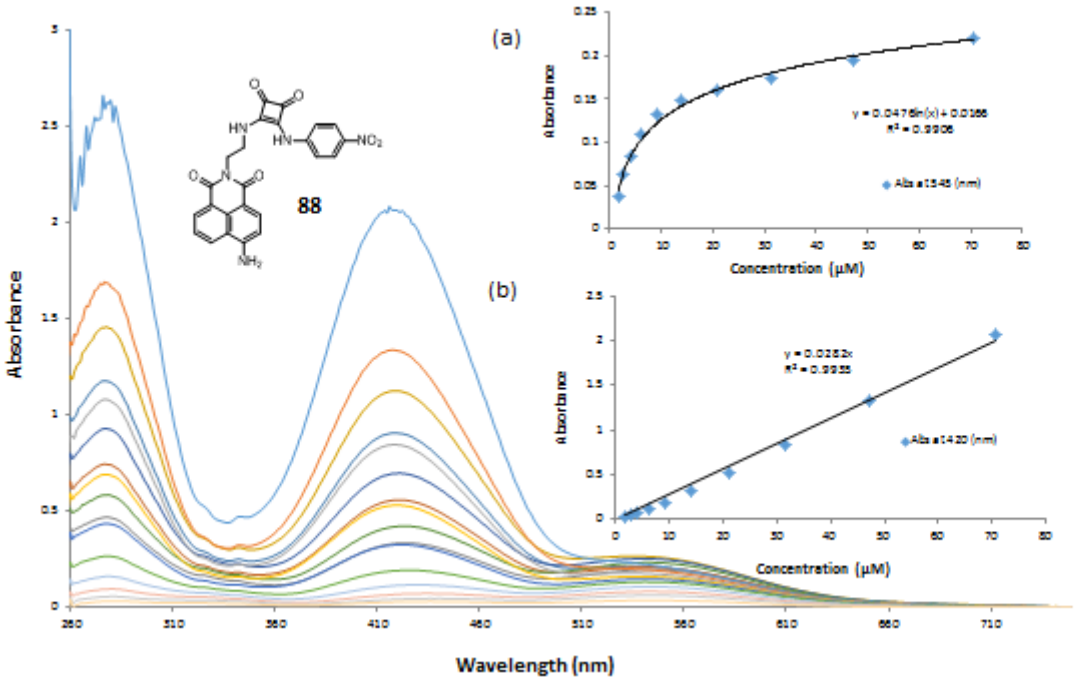

***Figure 2.18**: Changes in UV/Visible spectra upon increasing concentration of **88** in DMSO* (0 – 70 μM). ***Inset:** Plots of absorbance at (a) 545 nm and (b) 420 nm as a function of increasing concentration of **88**.*

***Table 2.1:** Absorption properties of potential anion receptors **85, 86, 87** and **88** in DMSO*

Receptor	λ_{max} (nm) [ε(M^{-1} cm^{-1}) in DMSO (3mL)		
	π - π^*		ICT
85	**280 [32642]**	**340 [19559]**	**445 [15439]**
86	**280 [34375]**	**-**	**420 [29899]**
87	**280 [34785]**	**340 [20405]**	**445 [13717]**
88	**280 [35187]**	**-**	**420 [27410]**

In summary, **85 – 88** display varied and potentially useful photphysical properties in DMSO. They possess multiple absorption bands which are expected to be sensitive to their environment and, thus, are expected to change upon intraction with anions. Furthermore, receptor **85** and **87** are more emissive in DMSO solution and as such it is anticipated that, the interruption of the quenching process upon anion binding may lead to a switch on and switch off effect being exhibited. This

behaviour is in contrast to compounds **86** and **88** which are less emissive in DMSO solution. The nature of the interactions of compounds **85 - 88** with anions will be dicussed in the following sections and will form the basis of this study of a novel set of flourescent receptors for targeting anions.

2.6 Anion Binding Studies

It has been observed that squaramides exhibit significantly higher H-bonding abilities compared to their urea and thiourea analogues[82, 94] and that this results in superior anion binding affinities.[61, 104, 106, 112] Hence, spectroscopic titrations of receptor **85 – 88** with different anions were carried out to investigate the nature and binding affinity of these receptors with anions. These results are presented and discussed in the following sections.

2.6.1 Spectroscopic Titrations of Novel Compounds 85 – 88

2.6.1.1 UV/Vis Absorption Titrations of Novel Compounds 85 – 88 with Anions (AcO^-, Cl^-, F^-, PO_4^{3-} and SO_4^{2-}) in DMSO

The interaction of **85 – 88** with anions was firstly examined using UV/Vis spectroscopy. The titrations were performed by additions of aliquots of the putative anionic guest (AcO^-, Cl^-, F^-, PO_4^{3-}, SO_4^{2-}) as the tetrabutylammonium (TBA) salt solutions (20 mM made up in 1.199×10^{-5} M solutions of the receptors in DMSO) to a 1.199×10^{-5} M solution of the receptor in DMSO. Typically, up to 70 equivalents of the salts were added. The changes in the UV bands upon anion addition were monitored for each receptor. All titration experiments were run in duplicate and where contrasting results were obtained triplicate experiments were conducted. The overall changes in the ground state of **88** with TBA sulphate are shown in Figure 2.20., with those of **85, 86** and **87** shown in the Appendix.

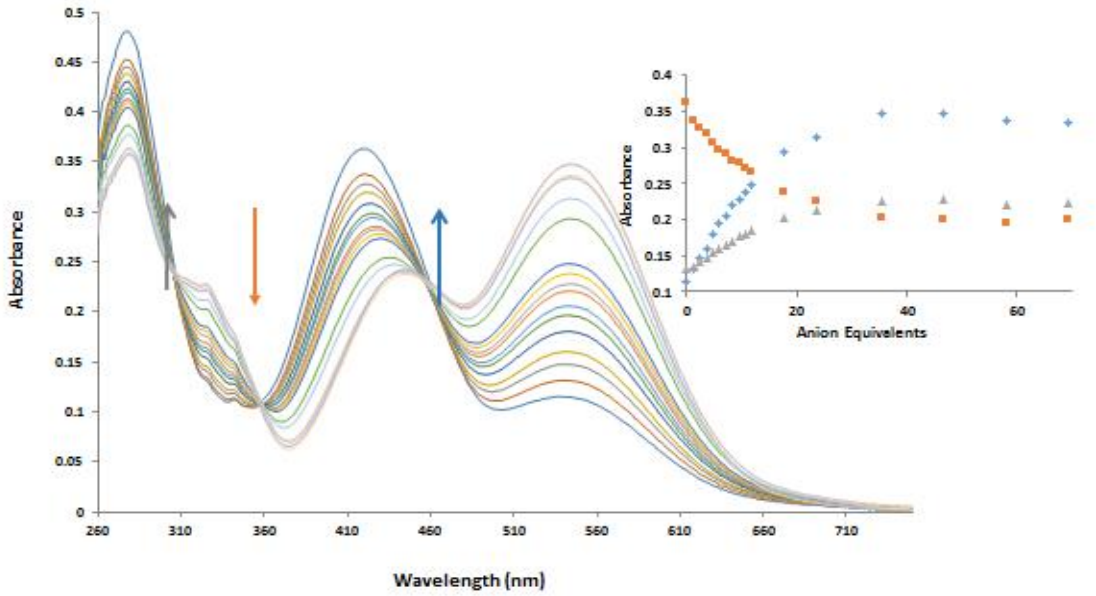

***Figure 2.20**: Changes in the UV/Visible spectrum of **88** (11.9 µM) with increasing TBA sulphate equivalents in DMSO (0 - 70 eqs). **Inset:** Plot of the change in absorbance at 420 nm (orange), 325 nm (grey) and 545 nm (blue) as a function of increasing TBA sulphate equivalents.*

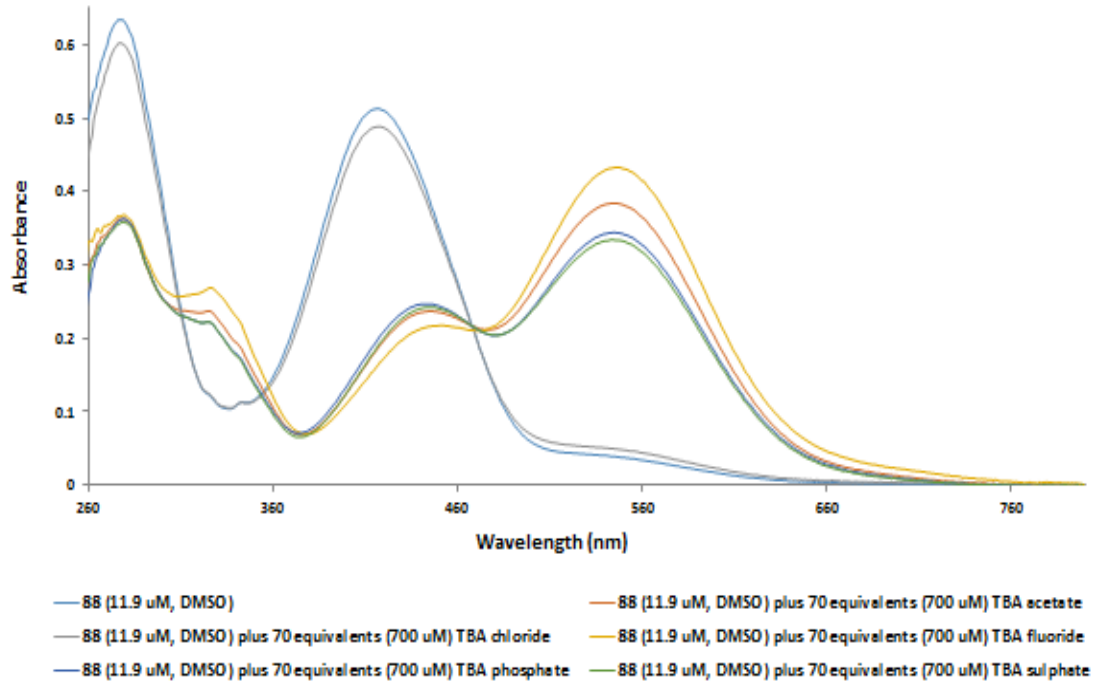

***Figure 2.21:** Changes in the UV/Visible spectrum of **88** (11.9 µM, DMSO) with 70 equivalents (700 µM) of different solution of anions as TBA salts in DMSO (AcO^-, Cl^-, F^-, PO_4^{3-} and SO_4^{2-}).*

(A)

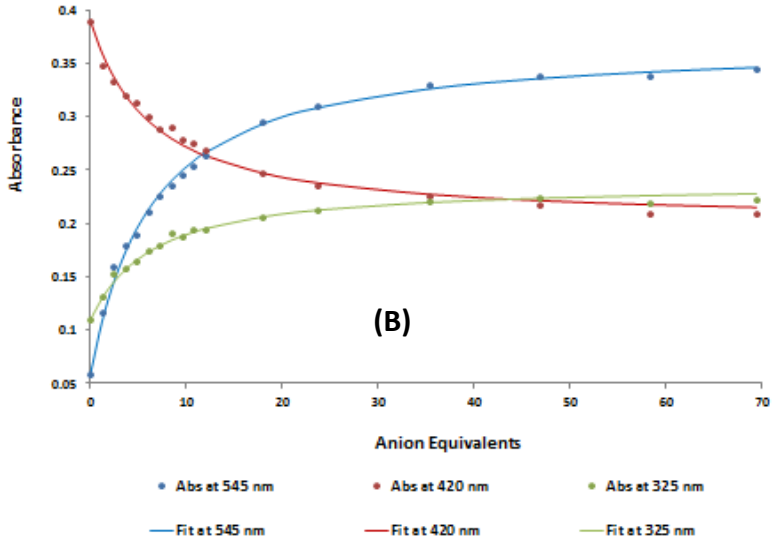

(B)

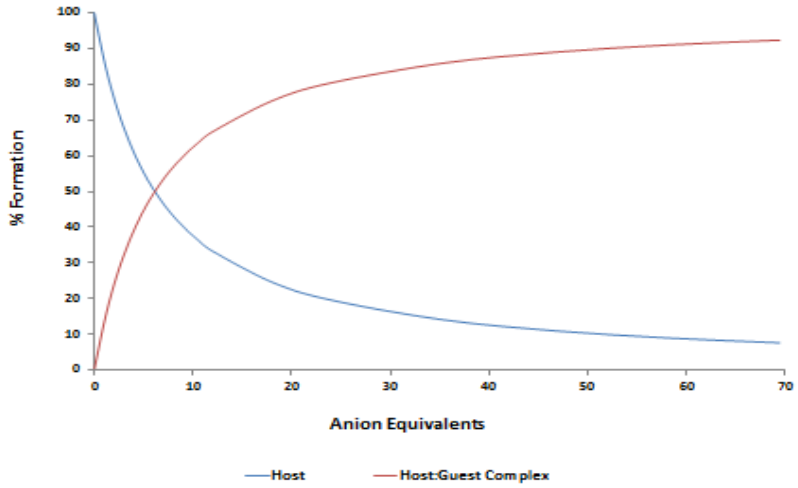

***Figure 2.22**: **(A)** Bind fit graph of UV titration of **88** (11.9 µM, DMSO) with increasing TBA sulphate equivalents in DMSO (0 - 70 eqs). **(B)** The speciation distribution diagram derived from the fitting of the changes in the absorption titration of **88** (11.9 µM, DMSO) with TBA sulphate in DMSO (0 - 70 eqs), showing the formation of a 1 : 1 binding isotherm for **88** with TBA sulphate.*

Upon titration of receptors **85 – 88** with Cl^- very minor changes were seen in the absorprtion spectra of **85 – 88** suggesting that little interaction with Cl^- is occuring at the squaramide. In contrast, much more significant changes were seen absorprtion spectra of **85 – 88** upon addition of AcO^-, F^-, PO_4^{3-} and SO_4^{2-}. The

absorption spectra of **88** changed significantly upon incremental addition of SO_4^{2-} with an increase in absorption of its band at 545 nm being observed and a concomitant decrease in the band at 280 nm and 420 nm also resulting in an isobestic point at 460 nm. Similar changes were observed in the absorption spectra of **88** upon incremental addition of AcO^-, F^- and PO_4^{3-} as shown in Figure 2.21. These results suggest the occurrence of a deprotonation event at the squaramide binding site, upon the incremental addition of AcO^-, F^-, PO_4^{3-} and SO_4^{2-}. The data from the UV/Vis absorption titrations were next analysed in order to obtain a binding affinity for the anions of interest. To determine association constants K_a, for the receptor-anion complexes, global analysis of the absorbance data was carried out using the open access BindFit software program[120] as shown in Figure 2.22. A representative plot of absorbance vs concentration for **88** is shown as an inset in Figure 2.20 and a summary of the results obtained from the global analysis of the absorbance data of receptors-anion complexes of **85 – 88** are detailed in Table 2.2.

*Table 2.2: Summary of the anion association constants K_a (M^{-1}) of receptors **85 – 88** in DMSO acoording to the UV anion titration data.*

Receptor	K_a of receptors with anions [M^{-1} (% error)]				
	AcO^-	Cl^-	F^-	PO_4^{3-}	SO_4^{2-}
85	–[a]	–[b]	–[a]	**3.6×10^4 (10.4 %)**	**4.6×10^3 (15.8 %)**
86	–[a]	–[b]	–[a]	**4.5×10^4 (23.1 %)**	**1.2×10^4 (17.4 %)**
87	–[a]	–[b]	–[a]	**2.0×10^4 (8.1 %)**	**1.2×10^4 (15.3 %)**
88	–[a]	–[b]	–[a]	**1.7×10^4 (3.7 %)**	**1.7×10^4 (3.7 %)**

[a] The changes observed were associated with deprotonation of receptors **85 – 88**, therefore the association constant K_a (M^{-1}) was not determined. [b] The changes observed in the UV data prevented accurate determination of the association constant because Cl^- does not cause deprotonation of receptors **85 – 88**.

2.6.1.2 Fluorescence Emission Titrations of Novel Compounds 85 – 88 with Anions (AcO^-, Cl^-, F^-, PO_4^{3-} and SO_4^{2-}) in DMSO

The interaction of **85 – 88** with anions was also examined using fluorescence spectroscopy. The titrations were performed by additions of aliquots of the putative anionic guest (AcO^-, Cl^-, F^-, PO_4^{3-}, SO_4^{2-}) as the tetrabutylammonium (TBA) salt solutions (20 mM made up in 1.199×10^{-5} M solutions of the receptors in DMSO) to a 1.199×10^{-5} M solution of the receptor in DMSO. Typically, up to 70 equivalents of the salts were added. The changes in the emission intensity upon anion addition were monitored for each receptor. All titration experiments were run in duplicate and where contrasting results were obtained triplicate experiments were conducted. The overall changes in the emission spectra of **85** with TBA sulphate are shown in Figure 2.23., with those of **85, 86** and **87** shown in the Appendix.

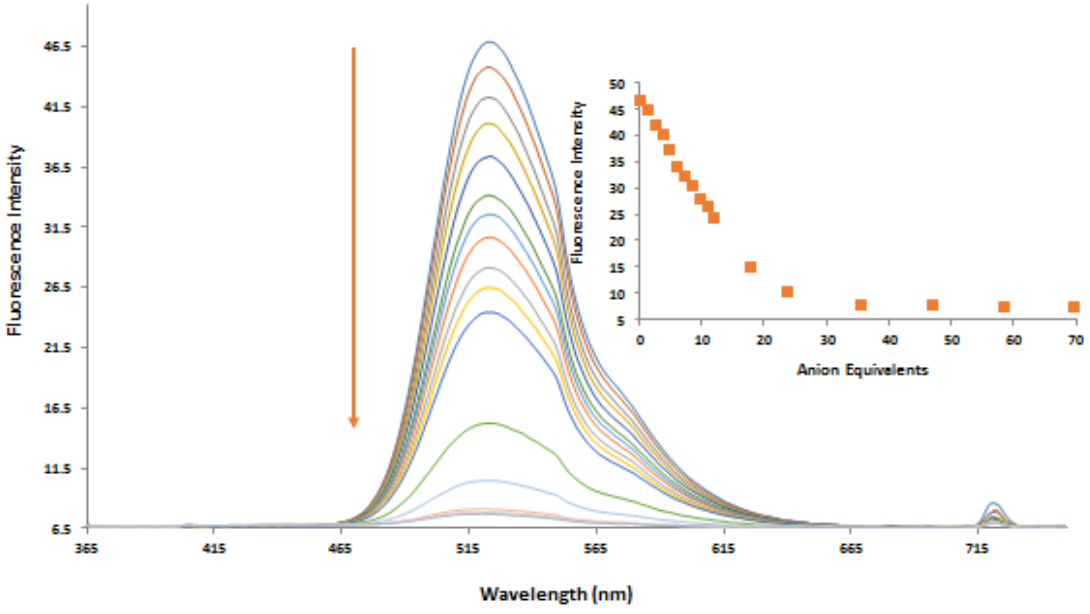

Figure 2.23: *Changes in the fluoresence emmission spectrum of* ***85*** *(11.9 μM) at* λ_{ex} *360 nm with increasing TBA acetate equivalents in DMSO (0 – 70 eqs).* ***Inset:*** *Plot of emission intensity at 522 nm as a function of TBA acetate equivalents.*

Minor changes were observed in the emission spectra of **85 – 88** upon titration with Cl^-. Titration with AcO^-, F^-, PO_4^{3-} and SO_4^{2-}, however, led to much more significant changes as shown in Figure 2.23 for titration of SO_4^{2-} with **85**, where fluorescence

quenching was observed. The observed emission centred at 360 nm was significantly "switched off" by the presence of AcO^-, F^-, PO_4^{3-} and SO_4^{2-} ions. A similar effect was observed for **87** at an emission centred at 355 nm. However, a smaller emission decrease was exhibited for receptor **86** and **88** emission centred at 430 nm and 460 nm respectively. Furthermore, the decrease in fluorescence of **85** upon incremental addition of SO_4^{2-}, also suggests the possible occurrence of some deprotonation events.

2.6.2 ^{1}H NMR Spectroscopic Studies of Novel Compounds 85 – 88 with Anions (AcO^-, Cl^-, F^-, PO_4^{3-} and SO_4^{2-}) in DMSO-*d6*.

^{1}H NMR titrations were conducted in order to further investigate the anion binding behaviour of **85 – 88**. ^{1}H NMR spectroscopic investigations of receptors **85 – 88** in DMSO-$_{d6}$ (2.5×10^{-3} M) with putative anionic guest (AcO^-, Cl^-, F^-, PO_4^{3-}, SO_4^{2-}) as the TBA salt solutions (200 mM made up in 2.5×10^{-3} M solutions of the receptors in DMSO-$_{d6}$) was performed, to understand the mechanism of the host – guest interactions. Figure 2.24 (a) shows the changes observed in the ^{1}H NMR spectrum of **85** upon the addition of 20 equivalents of anions as TBA salts in a DMSO-*d*$_6$ solution of **85** (AcO^-, Cl^-, F^-, PO_4^{3-}, SO_4^{2-}). Dramatic, changes were observed in the ^{1}H NMR spectra of **85 - 88** upon the addition of 20 equivalents of AcO^-, F^-, PO_4^{3-} and SO_4^{2-} in a DMSO-*d*$_6$ solution of **85 - 88**, addition of these anions (AcO^-, F^-, PO_4^{3-} and SO_4^{2-}) led to the disappearance of the NH signal (H_a) as shown in Figure 2.24 (a) for **85**. Stark colour changes of the solutions of **85** and **87** were observed upon the addition of F^- under "naked eye" and UV illumination, although the addition of AcO^-, PO_4^{3-} and SO_4^{2-} only led to major colour changes under UV illumination as shown in Figure 2.25 (a) and (b) for receptor **85**. However, the solutions of **86** and **88** only showed stark colour changes under "naked eye", upon the addition of AcO^-, Cl^-, F^-, PO_4^{3-} and SO_4^{2-}, but no colour changes under UV illumination was observed. This was ascribed to the non-fluorescent nature of the receptors **86** and **88** with the nitro aryl substistuent. The disappearance of NH signal (H_a) in ^{1}H NMR spectra of **85 – 88** and the stark colour changes upon the addition of AcO^-, F^-, PO_4^{3-} and SO_4^{2-} suggests that deprotonation event is responsible for the colour changes and NH signal loss as observed with the addition of AcO^-, F^-, PO_4^{3-} and SO_4^{2-} to **85 – 88.** We

further confirmed this deprotonation behavior by the presence of bifluoride (HF_2^-) in the ^{1}H NMR spectrum of **85 – 88** upon the addition of F^- as shown Figure 2.24 (b) for receptor **85**.[121, 122]

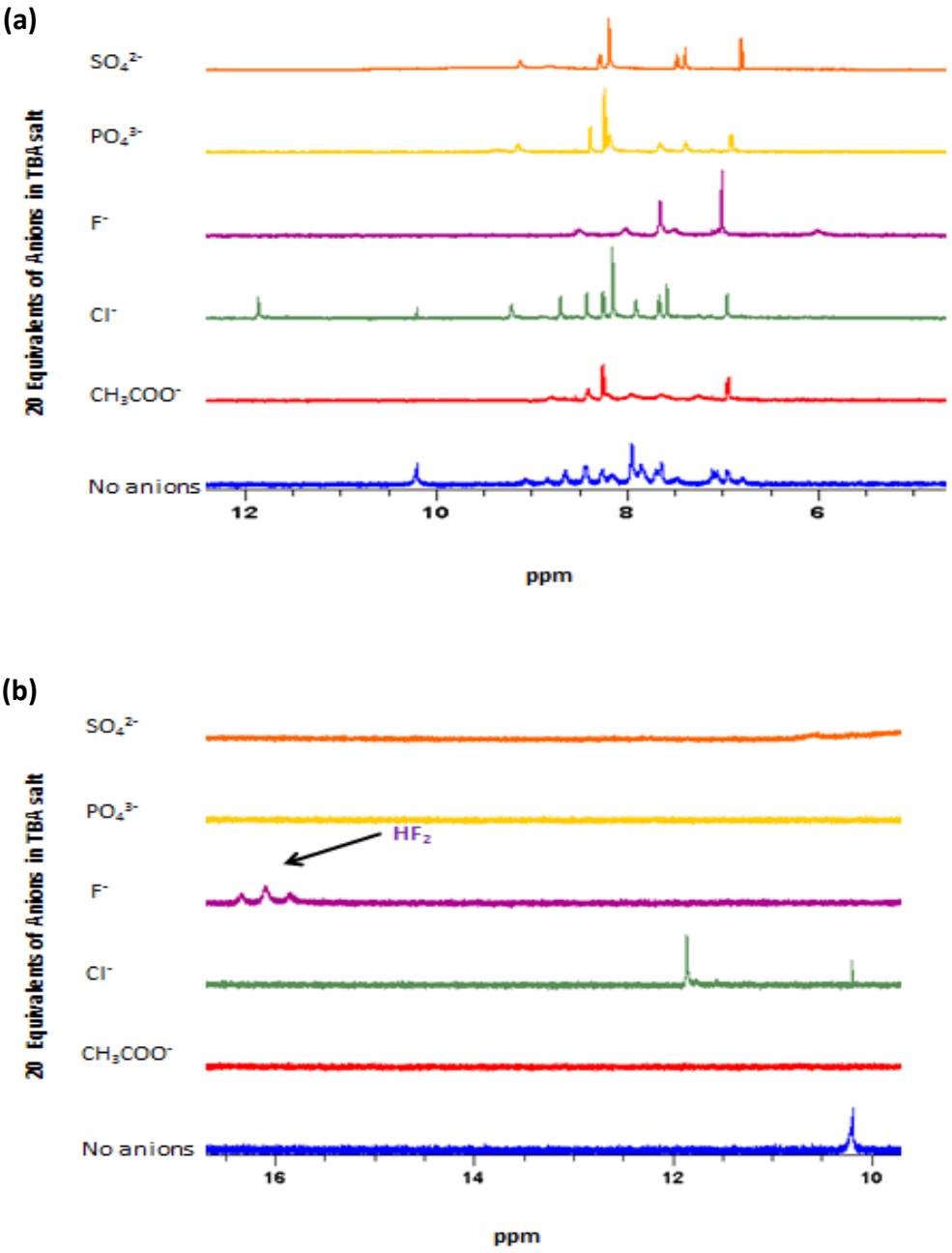

Figure 2.24: *Changes in the ^{1}H NMR spectrum of **85** (2.5×10^{-3} M) upon the addition of 20 eqvivalents of anions as TBA salts in a DMSO-d_6 solution of **85** (AcO^-, Cl^-, F^-, PO_4^{3-} and SO_4^{2-}). **(a)**: Aromatic region of **85**. **(b)**: Formation of HF_2 upon the addition of 20 equivalents TBA fluoride to **85** in DMSO-$_{d6}$.[121, 122] The differing spectroscopic response of compound **85** upon the addition of 20 eqvivalents of anions as TBA salts in a DMSO-d_6 solution of **85** (AcO^-, Cl^-, F^-, PO_4^{3-} and SO_4^{2-}).*

Moreover, interesting changes were observed in the ^{1}H NMR spectra of **85 - 88** upon the addition of 20 eqvivalents of Cl^- in a DMSO-d_6 solution of **85 – 88**. The addition of Cl^- led to the dramatic downfield shift of the NH signal (H_a) from 10.3 ppm to 11.8 ppm as shown in Figure 2.24 (a) for **85**. Subtle colour changes from yellow to bright yellow of the solutions of **85** and **87** were observed upon the addition of Cl^- under UV illumination, as shown in Figure 2.25 (a) and (b) for receptor **85**. The dramatic downfield shift of the NH signal (H_a) in the ^{1}H NMR spectra of **85 – 88** and the subtle colour change from yellow to bright yellow, upon the addition of Cl^- to **85** and **87** suggests a binding interaction between Cl^- and novel receptors **85 – 88**. To further investigate the binding interaction of Cl^- with receptors **85 – 88**, ^{1}H NMR spectroscopic titrations of **85 – 88** with TBACl was conducted.

(a)

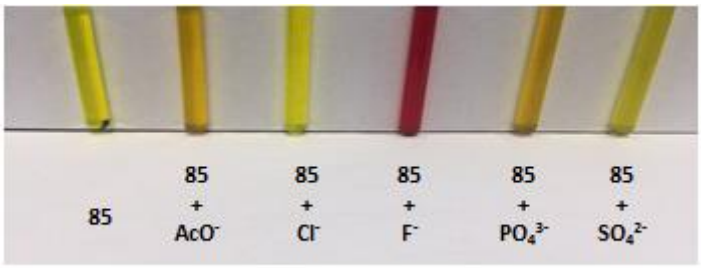

(b)

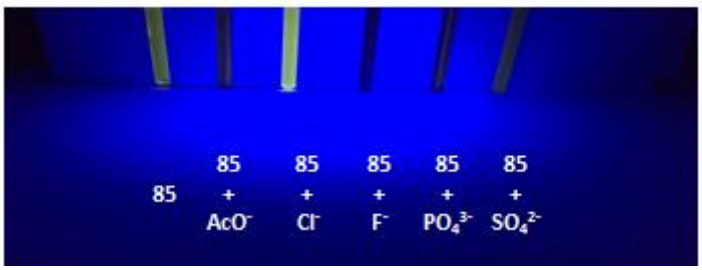

Figure 2.25: *Changes in the appearance of a sample of* ***85*** *(2.5 × 10^{-3} M) upon the addition 20 eqvivalents of anions as TBA salts in a DMSO-d_6 solution of* ***85*** *(AcO^-, Cl^-, F^-, PO_4^{3-} and SO_4^{2-}). **(a)** With the naked eye and **(b)** Under UV illumination.*

2.6.2.1 ^{1}H NMR Spectroscopic Titration of 85 – 88 with TBACl in DMSO-$_{d6}$

We performed ^{1}H NMR spectroscopic investigations in DMSO-d_6 with each of the receptors **85 – 88** to establish the stoichiometry of their anion complexes with Cl^-,

while gaining an understanding of host–guest interaction. Similarly, we sought to investigate the effect of the electron-withdrawing trifluoromethyl and nitro substituents on receptors **85 – 88**. ^{1}H NMR titrations of receptors **85 – 88** with Cl^- were performed by additions of aliquots of the putative anionic guest as TBACl in a DMSO-d_6 solution of **85 – 88** (20 equivalents) to a 2.5 × 10^{-3} M solution of the receptor in DMSO- d_6. The data obtained from these titrations were plotted as cumulative changes in chemical shifts (Δδ) against the equivalents of Cl^- anions added and the resulting data were analyzed using the open access BindFit software program as previously described.[120]

(a)

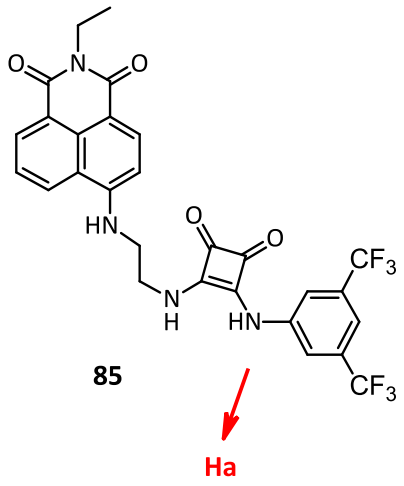

85

(b)

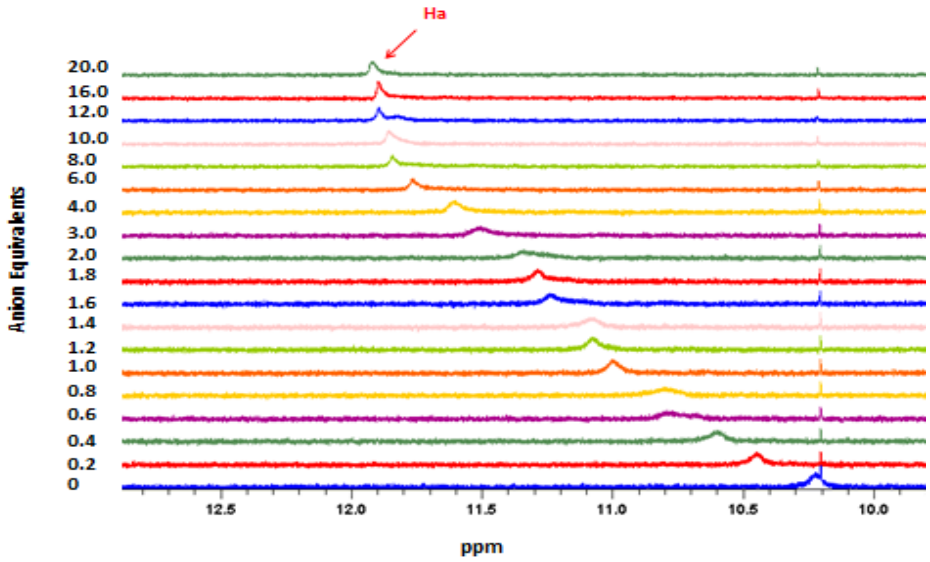

***Figure 2.26**: **(a)**: Structure of **85** showing the NH proton as Ha. **(b)**: Changes in the ^{1}H NMR spectrum (Ha proton) of **85** (2.5 × 10^{-3} M) upon the addition 0 - 20 eqvivalents of anions as TBA chloride in a DMSO-d_6 solution of **85**.*

(a)

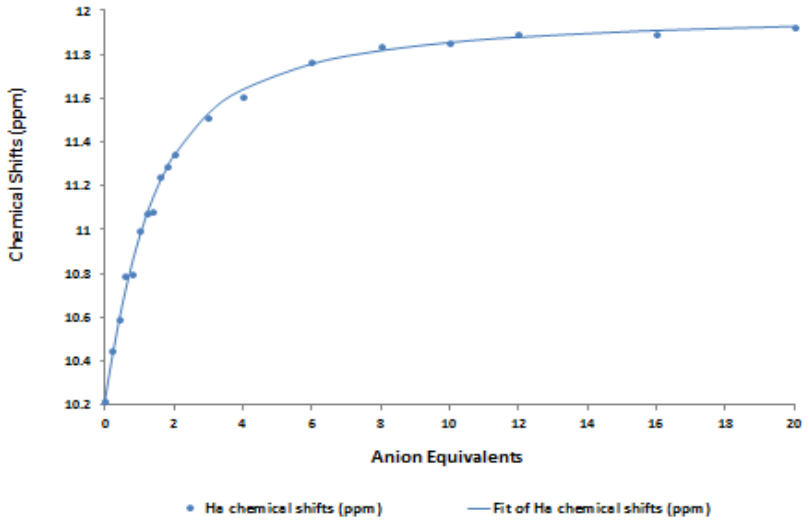

(b)

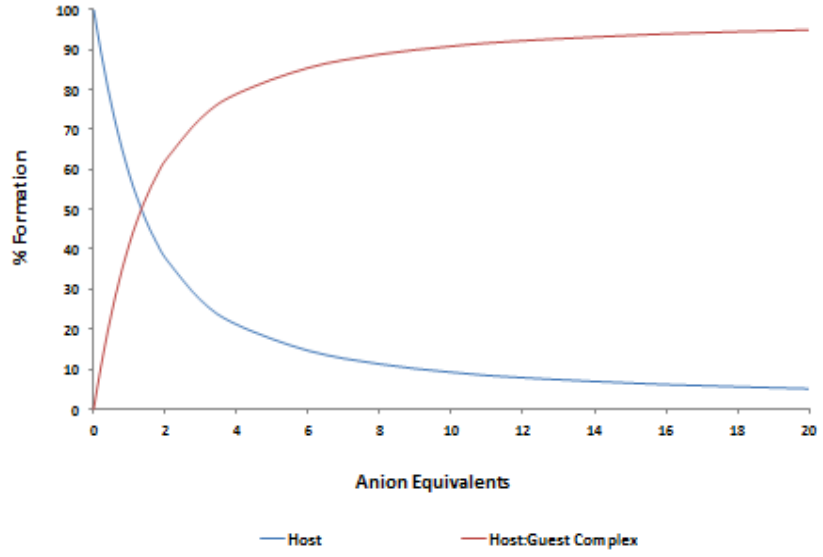

***Figure 2.27**: **(a)**: Bind fit graph of the chemical shift of Ha proton (ppm) of **85** (2.5 × 10^{-3} M, DMSO-$_{d6}$) with increasing TBA chloride equivalents in a DMSO-d_6 solution of **85** (0 - 70 eqs). **(b)**: The speciation distribution diagram derived from the fitting of the changes in the chemical shift of Ha proton (ppm) of **85** (2.5 × 10^{-3} M, DMSO-$_{d6}$) with TBA chloride (0 - 70 eqs), showing the formation of a 1 : 1 binding isotherm for **85** with TBA chloride.*

Figure 2.26 (b) shows the changes observed in the ^{1}H NMR spectrum of **85** upon the addition of Cl^- (20 equiv.). A gradual downfield shift of the NH signal (H_a) from 10.2 ppm to 11.8 ppm in the ^{1}H NMR spectrum **85** was observed upon the increasing concentration of Cl^-. These changes together with the subtle colour changes of these compounds observed upon the addition of Cl^-, clearly support a classical H-bonding interaction between Cl and the NH protons (H_a) of the receptors at low Cl^- concentrations (Figure 2.28).

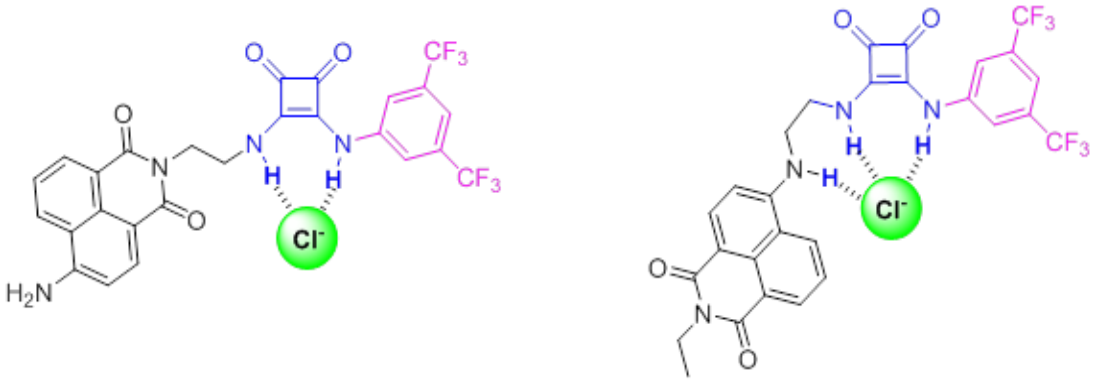

Figure 2.28: Possible chloride binding modes for receptors **85** and **87** based on UV/Vis, fluorescence and ^{1}H NMR titration studies.

The changes observed in the ^{1}H NMR spectra of receptors **85 – 88** upon the addition of TBACl showed that the NH (Ha) signals associated with the squaramide NHs were significantly shifted downfield. Unepectedly however, the NO_2 substituted receptors **86** and **88** did not exhibit an increase in fluorescence and showed lower binding affinities for Cl^- than both **85** and **87** respectively. Morever, while CF_3 substituted receptors **85** and **87** showed higher affinities for Cl^- than their NO_2 substituted counterparts **86** and **88**, **87** showed a slightly lower affinities for Cl^- than **86**. The association constants (K_a) of **85 – 88** in DMSO-$_{d6}$ (determined by BindFit) with Cl^- are summarised in Table 2.3 and the number of the electron withdrawing substituents on the squaramide unit results in higher affinities for Cl^-.

*Table 2.3: Summary of the chloride association constants K_a (M^{-1}) of receptors **85 – 88** in DMSO-$_{d6}$ at 273 K according to the ^{1}H NMR titration Cl^- data*

Receptor	K_a (M^{-1})	% Error
85	**488.62**	**6.3 %**
86	**273.65**	**4.1 %**
87	**221.26**	**9.1 %**
88	**114.80**	**5.9 %**

The relative position of the squaramide group with the electron withdrawing group attached on the receptor also play a major role in the strength of the association constant with Cl^-. As seen in **85**, where the squaramide motif was placed at the bottom of the naphthalimide fluorophore resulted in a higher affinity for Cl^- compared to **87** where the squaramide motif was placed at the top of the naphthalimide fluorophore. A similar trend was also observed for the NO_2 substituted counterparts **86** and **88**. On all occasions a good fit to a 1:1 binding isotherm was observed for receptor **85** as shown in Figure 2.27., with those of **86, 87** and **88** shown in the Appendix while Figure 2.29 shows a combination of bind fit graph of the ^{1}H NMR spectrum (chemical shift of Ha proton (ppm)) of **85, 86, 87** and **88** with increasing Cl^- equivalents in DMSO-$_{d6}$.

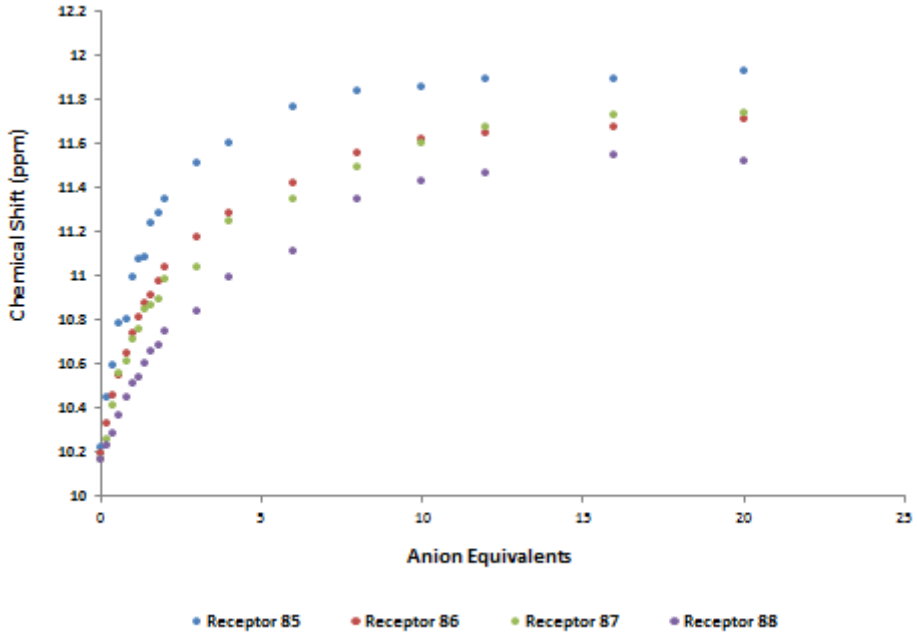

Figure 2.29*: *(a)*:** *Combination of bind fit graph of the ^{1}H NMR spectrum (chemical shift of Ha proton (ppm)) of* ***85, 86, 87 *and* ***88*** *(2.5 × 10^{-3} M, DMSO-$_{d6}$) with increasing TBA chloride equivalents in a DMSO-d_6 solution of* ***85 – 86****.*

2.7 Conclusion and Future work

In this Chapter, we have successfully developed four novel anion receptors **85 – 88**. These novel receptors have been shown by ^{1}H NMR analysis and SEM analysis to self-associate at room temperature and self-dissociate at higher temperatures (343 K). According to the photophysical properties of receptors **85 – 88** in DMSO, receptor **85** and **87** have proved to be more emissive in DMSO solution compared to receptors **86** and **88** which are less emissive in DMSO solution. Furthermore, the addition of anions (AcO^-, F^-, PO_4^{3-} and SO_4^{2-}) as their TBA salts led to deprotonation events within receptors **85 – 88**, this event was evident by UV/Vis titration, fluorescence titration and ^{1}H NMR spectroscopic analysis. However the receptors were shown to be selective towards Cl^- *via* classical H-bonding interaction between the binding site and Cl^-, resulting in a subtle colour change. The position of the binding site (top or bottom) on the signalling unit was observed to play a major role in the affinity towards Cl^- binding, these was ascribed to the number of H-bonding

available in the binding pocket. This was further by a good 1:1 binding isotherm observed for **85, 86, 87** and **88** with a K_a value of 488.62, 273.65, 221.26 and 114.80 M^{-1} respectively. In conclusion, **85** is the most selective receptor towards Cl^- binding with **88** being the least selective.

Future perspectives of this work will look to further evaluate the SEM images of novel anion receptors **85 – 88**, in order to further understand the unique morphologies of our novel receptors.

Chapter 3 - Squaramide Based Low Molecular Weight Gelators (LMWGs)

3.1 Introduction

In recent years, the study of gels derived from low molecular weight gelators have gain immense attention due to their ability to serve as media for a range of applications.[123-127]

This review Chapter will present a review of the areas of supramolecular gel, especially low molecular weight gelators (LMWGs), giving a brief introduction into the definition, formation, classification and characteristic of a gel. This Chapter will also elaborate on some key findings and more recent developments.

3.2 What is a Gel?

Gels are stiff, flexible, soft, solid materials present in our everyday life. From commercial products such as shampoo, hair gel, toothpaste to other cosmetics, as well as soft contact lenses and lubricating grease (Figure 3.1).

Figure 3.1: *Examples of gels present in our everyday life.*

In general, gels have a solid-like appearance and do not flow, being predominantly liquid in composition. Gels have found applications in fields as diverse as food, cosmetics, materials science and petroleum industries, and have potential applications in lithography,[128] catalysis[129, 130] and drug delivery.[131-135] Despite the fact that gels are common in nature and are frequently encountered in our everyday life, a precise definition was still unknown, until Flory in 1974.

Flory defined a gel as a two component colloidal dispersion exhibiting a continuous microscopic structure with macroscopic dimensions, which is permanent on time scale of analytic experiments, and that is solid-like in its rheology behaviour below certain stress limit, despite of being mostly liquid.[136] The colloidal dispersion causes an increase in the viscosity in the liquid medium by forming a matrix which entraps

the liquid. This allows the system to attain a semi-solid consistency in-between the liquid and solid state. However, not all gel systems are colloidal in nature, gels consist of a solid 3D matrix which is constructed by the crosslinking of polymeric strands of macro-molecules by physical or chemical forces, in the presence of bulk gas or liquid phases.[137] The viscoelastic solid-like appearance of a gel is a result of the entrapment and adhesion of the bulk gas or liquid phase (solvent) in the surface area of the solid 3D elastic matrix of the gelator molecules through surface tension and capillary forces.[138] The following section will give a brief introduction on how gels are formed.

3.3 Gels Formation

In analogy to proteins the fibrous network of gels can be divided into primary, secondary and tertiary structures (Figure 3.2).[139-141] The primary structure (angstrom to nanometer scale) derives from the anisotropic aggregation of gelator molecules in 1D or 2D structures. The primary rod like aggregates is determined by molecular level recognition in which their characteristics depend on the influence of the ratio of cross-sectional areas of hydrocarbon chain, polarity of the solvent and the different moieties of the gelator.

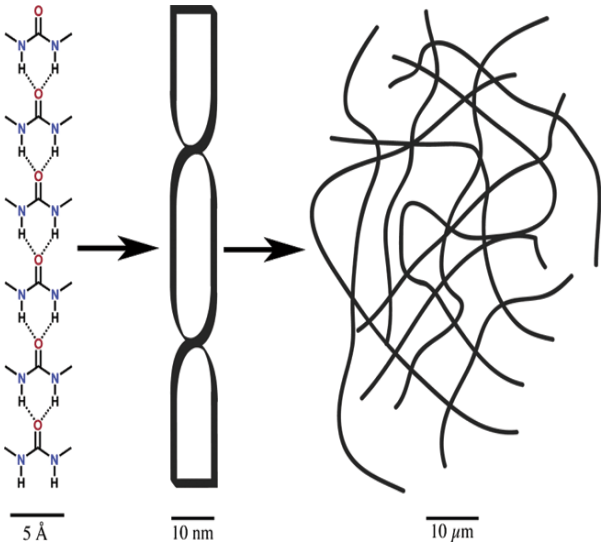

Figure 3.2: *The primary, secondary and tertiary structures of a self-assembled urea based LMWG.*[141]

Furthermore, these primary structures self-assemble to form aggregates (nano- to micro-meter scale) that may acquire several morphologies such as vesicles, sheets, micelles, ribbons or fibres, and is directly influenced by the molecular structure (Figure 3.2). Finally, the transition from secondary to tertiary (micro- to milli-meter scale) depends on the strength and type of interactions between the individual aggregates (Figure 3.2). However, the important factors affecting the gelation process includes the nature and polarity of the solvent, temperature and the molecular shape of gelator. The following section will give a brief introduction on how gels are classified based on their origin, constitution, the type of cross-linking that creates their 3D network.

3.4 Classification of Gels

Gels may be classified according to their origin, constitution, the type of cross-linking that creates their 3D network and the solvent they are surrounded by (Figure 3.3). Regarding the solvent, gels may be formed in water (hydrogel), in an organic solvent (organogel) or in air (aero or xerogel). The non-covalent interactions required to promote gelation are dependent on the solvent. Gelation in organogels is mostly achieved by dipolar interactions such as H-bonding and metal coordination whereas gelation in hydrogels is often due to the solvophobic effect.[142] Gels can be further subdivided into chemical gels and physical gels, depending on the strength and type of interactions that assist in self-assembly. In chemical gels, the formation the 3D network occurs *via* covalent crosslinking of its components which most cases usually results in the formation of crosslinked polymer gels.

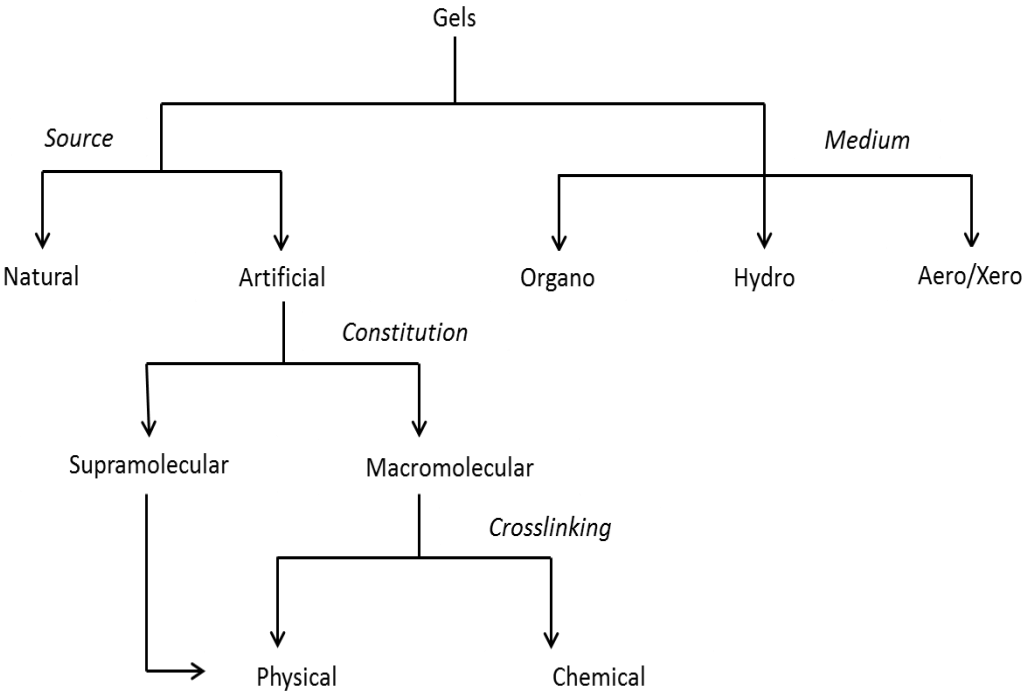

Figure 3.3: *Classification of gels.*

However, the self-assembly process of physical gels is promoted *via* non-covalent interactions such as van der Waals, dipole-dipole, π-π stacking, charge transfer, H-bonding, and metal coordination interactions. The majority of the natural occurring gelators are macromolecular and they form gels by physical cross-linking usually *via* H-bonding.[143] However, gels derived from synthetic compounds can be further subdivided depending on their constitution (macromolecular or molecular). Furthermore, gels formed by strong chemical bonds are thermally irreversible, whereas gels formed by weak non-covalent interactions are thermoreversible.[144, 145] With respect to this thesis, it is important to define supramolecular gels, which are nanostructured soft materials formed by anisotropic aggregation of low-molecular weight (LMW) molecules into 1D structures, that further self-assemble into 3D fibrillar networks that percolate the solvent and supramolecular polymer gels which are due to the physical aggregation of polymer chains.[146, 147] The following section will give a brief insight into how a gel can be quantified and characterised using various techniques.

3.5 Characterisation of Gels

The thermoreversibility of gels formed by the heating and cooling method allows for the identification of characteristic temperatures related to self-assembly and disassembly processes. The characteristic viscosity points of a gel, such as the temperature at which the gel is formed (T_{gel}) and the temperature at which the gel loses its structural integrity (T_{sol}) may be identified by visual inspection techniques such as bubble motion, dropping ball technique and the common inverted test tube method. The temperatures, T_{gel} and T_{sol} are dependent on the nature of the solvent, structure of the gel and the total concentration of the gelator. The minimum gelator concentration (m.g.c) which is defined as the minimum amount of gelator required to achieve the formation of a gel network capable of entrapping a specific solvent, may also be determined by the visual inspection techniques mentioned above. The m.g.c is the result of the concentration of the material required for the 3D network formation (C_{agg}) and the concentration of gelator molecules that remain in solution (C_{sol}). C_{sol} may be determined by ^{1}H NMR spectroscopy, using a concentric tube with an internal reference of know concentration.[148]

Furthermore, another important characteristic of a gel is related with its mechanical stability, which can be determined by rheology. Rheology is the study of deformation and flow of matter under the influence of applied stress. In rheological experiments, the gel is subjected to an oscillatory stress, and the response of the material is measured in terms of elastic storage modulus (G', the contribution of the elastic) and elastic loss modulus (G'', the contribution of the viscous). Rheology gives an insight on the relaxation and lifetime of the non-covalent bonds between gelator molecules. This allows the differentiation between hard gels (where, G' >> G'' at all frequencies) and soft gels (where, G' > G'' at high frequencies and G'< G'' at low frequencies). The gel point, which is defined as the point at which G' starts to exceed G'', may also be determined by rheology.[149, 150] Rheology studies may also be complemented with microscopy techniques such as scanning electron microscopy (SEM) or transmission electron microscopy (TEM) in order to relate the viscoelastic properties of the gel with the morphology of the fibre network. Crystallographic techniques such as small angle X-ray scattering (SAXS) and small

angle neutron scattering (SANS) may give an insight on the size, morphology and supramolecular arrangement of the fibres present in a gel.[151] However, the use of SAXS and SANS is limited due to the presence of defects on the fibres and the difficulty of obtaining a crystal. Therefore, powder X-ray diffraction (XRD) of lyophilised gels is commonly used to obtain information on the structure of the gel and organisation of fibres. Fourier transform infrared (FTIR), Raman and NMR spectroscopy also provide information on the supramolecular arrangement of the gel *via* the study of H-bonding interactions. However, in the gel phase very broad ^{1}H NMR signals are obtained due to the large correlation time of the assemblies and the very short transversal relaxation times (T_2).[152] The next section will give a brief introduction on supramolecular gels and especially gels derived from low molecular weight gelators (LMWGs).

3.6 Supramolecular Gels

Low molecular weight gelators (LMWGs) are molecules with molar mass less than 3000 Da and are capable of gelling in organic solvents (organogels) or in water (hydrogels). Although LMWGs discovered in the early nineteenth century,[153] it is only recently that they have become a focused area of supramolecular chemistry. Organogels are formed by assembly of low molecular weight organogelators (LMWOGs) into entangled 3D networks through weak intermolecular forces such as H-bonding, van der Waals, metal coordination, π-π stacking, solvophobic forces and van der Waals interactions in which solvent molecules are efficiently entrapped and immobilised.[154-157] However, these weak intermolecular forces can easily be manipulated by external stimuli such as pH,[158] anions,[159-161] redox agents,[162] electric or magnetic fields,[163, 164] light[165, 166] and sound,[167] which allows for the tuning of the physical properties of the gel. Gelation by LMWOGs is thermally reversible, a sample can be heated above and cooled below the gel transition temperature, T_{gel} (the sol ↔ gel transition temperature), many times to transform a gel into a sol and the back into a gel unless there is thermal decomposition. The general thermorevesibility of LMWOGs is one of the features that separate them from most polymer gelators.[137, 144]

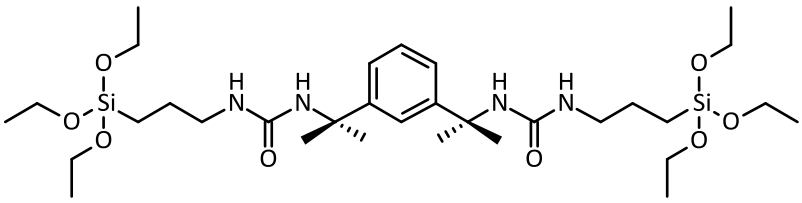

Polymer based organogelator[168]

Steed and co-workers

89

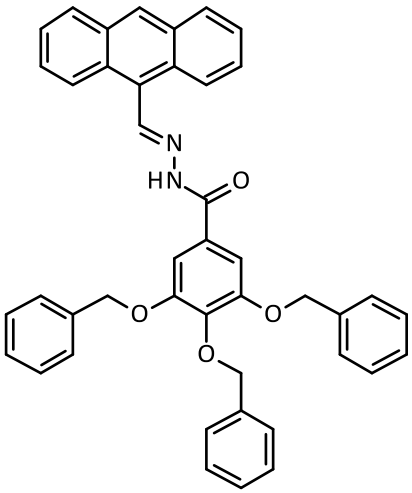

Low molecular weight fluoroscent organogel[169]

Prasad and co-workers

90

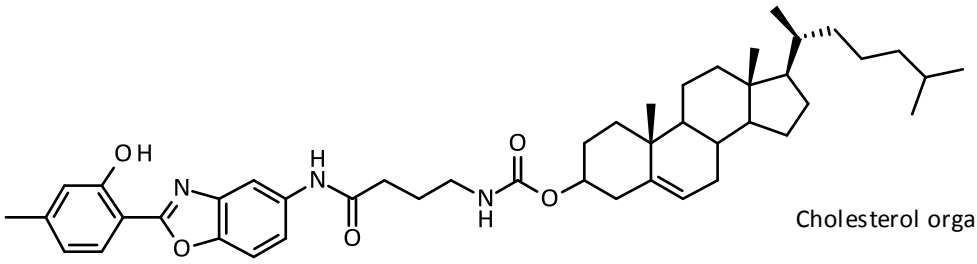

Cholesterol organogelator[170]

Lee and co-workers

91

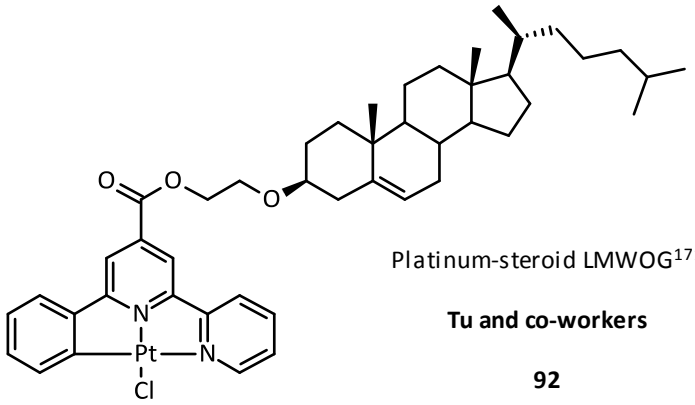

Platinum-steroid LMWOG[171]

Tu and co-workers

92

Figure 3.4: *Some examples of LMWOGs* ***1 - 4****.*[168-171]

LMWOGs which are able to gel organic liquids, generally do not display hydrogelling[141] capability and *vice-versa*. LMWOGs have attracted growing attention particularly in the field of supramolecular chemistry.[172] These recent attractions are due to the reversible nature of the interactions between the gelator molecules, the wide range of solvents that can be gelled and the possibility of adjusting the gel's behaviour by introducing responsive or switching functionality either as part of the gelator itself or by an external chemical stimulus such as change in pH, or addition of molecules or ions that interact with the gel.[173]. In LMWOGs, directional H-bonding and dipolar interactions tend to dominate the gel self-assembly process. Compounds like amides and ureas are particularly effective LWMGs because of their ability to form a primary structure comprising infinite H-bonded tapes in 1D while interacting laterally by much weaker bonds such as van der Waals interactions.[174] LMWOGs as illustrated in (Figure 3.4) can be polymer based, metal based, synthetic cholesterol based, some organogels have also been reported to be fluorescent.[168-171]

As discussed in chapter one, amide and urea units not only constitute ideal anion binding sites, but also act as useful motifs for supramolecular architectures *via* intra- or inter- molecular H-bonding and self-assembly interactions. The following section will give a range of examples of amide, urea and squaramide based LMWGs.

3.7 Amide based LMWGs

Amide N-H units are well known anion binding sites due to polarisation *via* π-conjugation with the neighbouring carbonyl moiety. Webb and co-workers developed an alkyl-substitued pyromellite tetraamide based LMWOG **93** (Figure 3.5) that gels non-polar organic solvents such as hexane, toluene, diethyl ether and cyclohexane due to the H-bonding interactions between the gelators.[159] LMWOG **93** binds to anions added as tetrabutylammonium (TBA) salts through conformation changes of its amide units in dilute solutions. The cyclohexane gel of **93** is transformed into a solution by the addition of 0.25 eq of TBA salts (Cl^-, Br^-, I^-, AcO^- and NO_3^-). This is due to the weaker association between the gelator molecules which is caused by the interaction with the anion at the H-bonding N-H sites.[159]

Webb and co-workers reported that upon the addition of TBA salts as solid on the gel surface, the transformation from gel to solution takes from minutes to seconds, depending on the affinity of **93** to the anions salts (Cl^- > AcO^- > Br^- > NO_3^- > I^-). However, inorganic salts such as NaI do not produce such a transition to the solution state.[159]

(A)

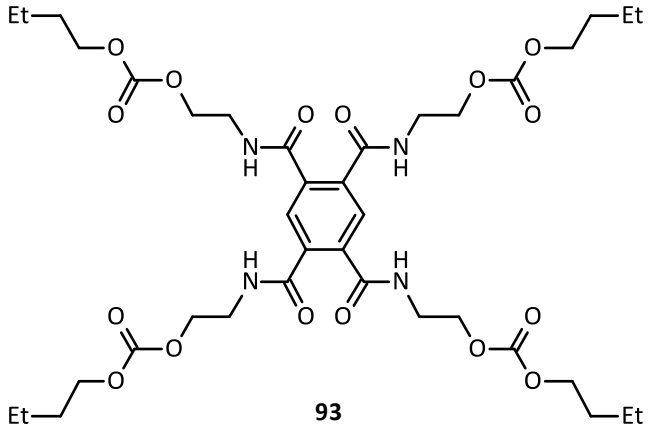

93

(B)

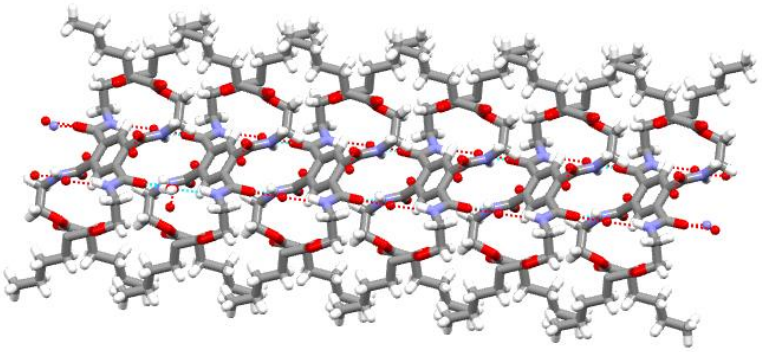

Figure 3.5: (A) *Structure of gelator* ***93*** *developed by Webb and co-workers.*[159] ***(B)*** *X-ray crystal structure of gelator* ***93*** *showing the formation of 1-D columnar stacks via intermolecular H-bonding network.*[159]

Džolić *et al*. studied the gelation properties of anthraquinone based oxalamide gelators **94** and **95** (Figure 3.6).[175] Gelator **94** was reported to possess excellent gelation properties toward alcohols and aromatic solvents. However, gelator **95** only affords precipitates and was incapable of forming gels with any of the tested solvents. This result suggests that the position of amide-substituents significantly

influences the gelation abilities.[175] According to Džolić *et al*., molecular modelling showed that the minimised conformation of gelator **94** contains a strong intramolecular H-bond which is formed between the anthraquinone bound N-H and the vicinal anthraquinone carbonyl oxygen leading to planarization with the first oxalamide unit. However, such H-bonding was not achieved for gelator **95** which makes the N-H more available for H-bonding with PO_4^{3-} and AcO^- oxygens.[175]

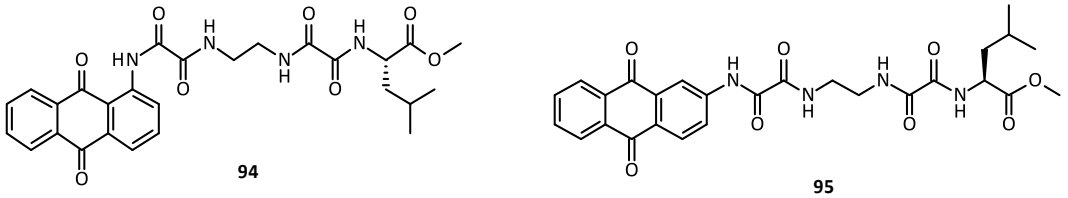

Figure 3.6: *Structure of gelator **94** and **95** studied by Džolić et al.*[175]

3.8 Urea Based LMWGs

Ureas are attractive scaffolds for the design of LMWGs due to the urea α-tape motif which allows urea based LMWGs to undergo self-assembly (Figure 3.7).[176]

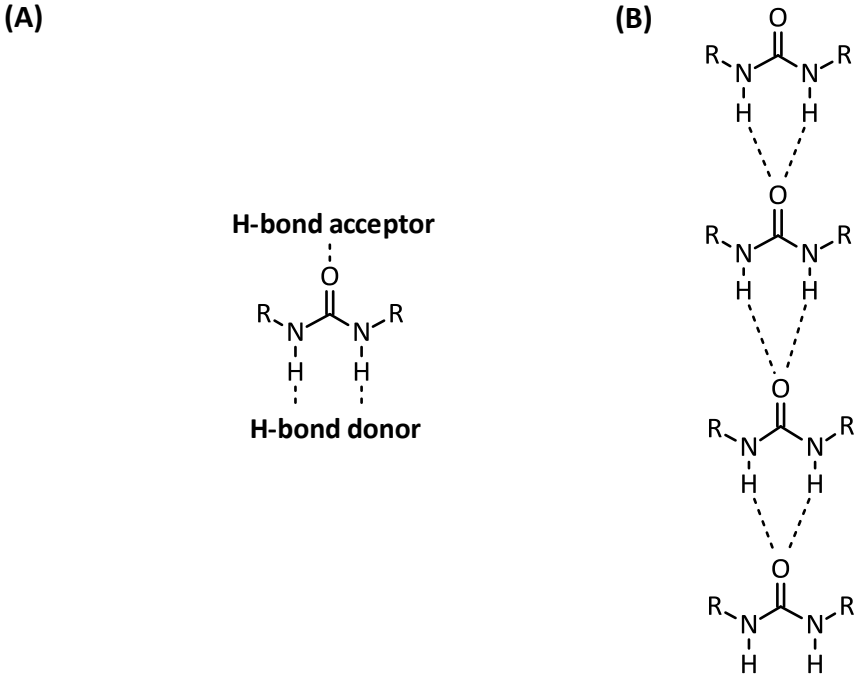

Figure 3.7: ***(A)*** *Hydrogen bond donor and acceptor abilities of urea.* ***(B)*** *Urea hydrogen bonding via the urea α-tape motif.*[176]

This key supramolecular interaction that results from urea self–association to form a 6-membered hydrogen bonded ring based on two donors and one carbonyl acceptor has been used extensively in supramolecular self-assembly.[177]

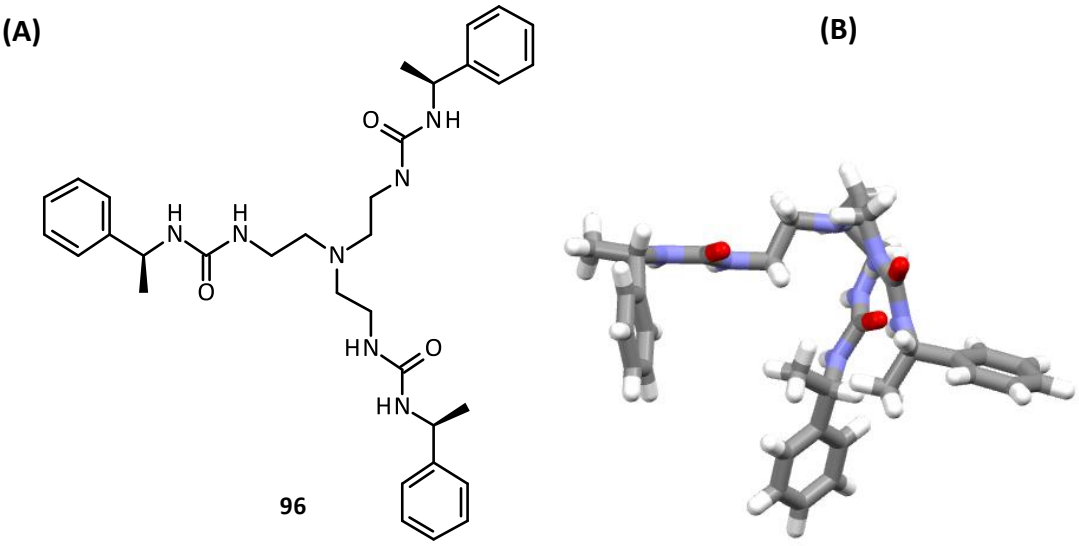

Figure 3.8: (A) *Structure of organogelator 96 developed by Steed and co-workers.*[178] ***(B)*** *X-ray crystal structure of gelator 96.*[178]

Steed *et al*. developed a chiral tris-urea organogelator **96** (Figure 3.8) that exhibits Cl^- affinity in DMSO and gels aqueous DMSO and aqueous methanol.[178] Addition of TBACl to the gel impedes the gelation process, decreases the amount of solvents included in the gel, and thus results in the formation of both gel and crystals.[178] X-ray crystallography analysis revealed that the crystals formed in the absence of Cl^- salts comprised only the gelator molecules bound through intramolecular and intermolecular hydrogen bonding between the urea units.[178]

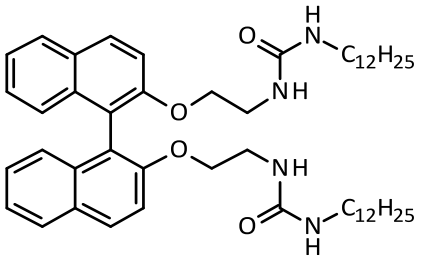

97

Figure 3.9: *Structure of urea-substituted binaphthalene* ***97*** *based LMWG developed by Wang et al.*[179]

Wang *et al*. synthesised a urea-substituted binaphthalene based LMWG **97** (Figure 3.9), which gives transparent supramolecular gels from cyclohexane through H-bonding and π-π stacking interaction.[179] Upon the addition of one equivalent of TBAF, Wang *et al*. observed an interference of the H-bonding between the gelator molecules to afford a solution.[179] However, no significant absorption spectral changes caused by F^- binding have been observed as a result of the σ-bond connection between the H-bonding amide units and the chromophore binaphthyl unit. Yang *et al.* synthesised bis-urea functionalised naphthalene organogelators **98 - 100** (Figure 3.10), which use cooperative H-bonding and π-π stacking interaction to form emissive supramolecular gels from various solvents[156].

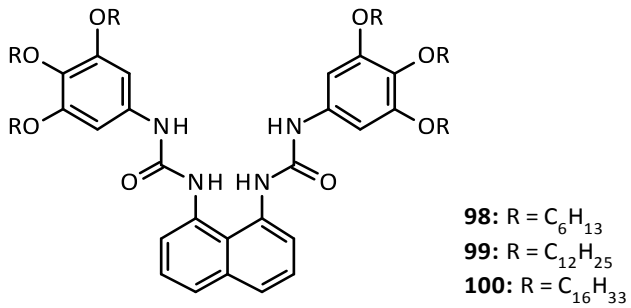

Figure 3.10: *Structure of bis-urea functionalised naphthalene organogelators* ***98-100*** *designed and developed by Yang et al.*[156]

The gel-sol transition of the system, as well as the fluorescent emission were both reported to be reversibly controlled by a change of temperature or upon the alternating addition of F^- and H^+. The gels are decomposed to solution by F^- addition and are re-formed by H^+ addition. However, the reformed gels exhibit emission behaviour and organised structures unlike those of the original gels. Yang *et al.* reported the influence of F^- on the fluorescence and gel-sol processes to be due to the dissociation of intermolecular H-bonds by bonding of F^- with the urea groups of the gelator.[156] Yamanaka and co-workers developed a C_3-symmetric tris-urea based gelator **101** (Figure 3.11) which is capable of forming opaque supramolecular gels from acetone by sonication.[180] However, cooling the thermally dissolved acetone solution results in precipitation and no gel formation. Compound **101** gels in a variety of polar organic solvents such as THF, methanol and diethylphthalate but

forms no gels from non-polar solvents such as toluene, hexane and dichloromethane.

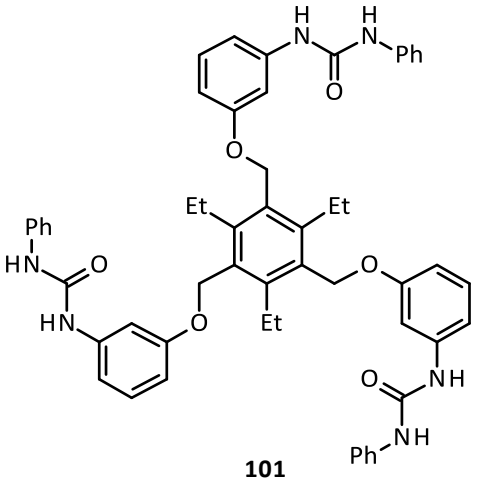

101

Figure 3.11: *Structure a tris-urea based gelator* ***101*** *developed by Yamanaka and co-workers.*[180]

According to IR measurements, H-bonding at the urea unit is reported to be a crucial factor for gel formation.[180] This was also supported by the gelation behaviours of the derivatives lacking these interaction sites. Yamanaka and co-workers, reported gel state recovery upon the addition of $BF_3{\cdot}OEt_2$ to the F^- mediated solution state.[180] Acetone gel was also reported to transform to solution upon the addition of TBAF and TBACl. Furthermore, the addition of $ZnBr_2$ to the solutions mediated by F^-, Cl^-, Br^-, I^- and AcO^- also affords supramolecular gels.[180]

In 2008, Steed *et al*. developed seven alkyl-bridged bisurea compounds of type **102** (n = 2-8) (Figure 3.13), which form gels if the number of methylene units is even (n=2, 4, 6, 8) and no gels if odd (n= 3, 5, 7) from CH_3CN, $CHCl_3$, MeOH, toluene and solvents mixture such as DMSO/H_2O and MeOH/H_2O.[181]

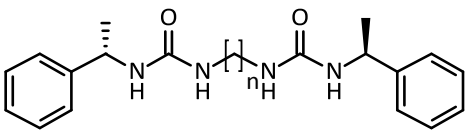

102 (n = 2-8)

Figure 3.12: *Structure of gelator compounds* ***102*** *with n = 2-8.*[181]

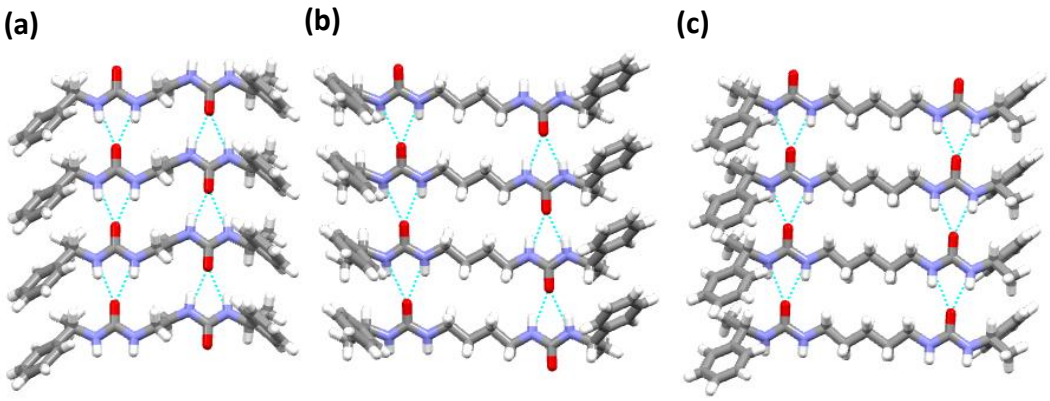

Figure 3.13: *Crystal packing diagrams showing the urea tape motif of compounds* ***102*** *with n = 2* ***(a)****, 4* ***(b)****, 5* ***(c).***[181]

This observation was reported to be correlated with the orientation of the urea units as interaction sites which is also confirmed justified *via* X-ray crystallography analysis.[181] In 2013, Wu and co-workers designed an anthracene gelator **103** based on cyclic urea unit to produce molecular gels in various solvents (Figure 3.14).[182] Interestingly, the resulting gel **103**/DMSO provides fascinating potential in TBAF discrimination via both colour and fluorescent alternation with high selectivity and sensitivity. The gel-to-sol transformation is reversible by the alternative addition of F^- and methanol.[182]

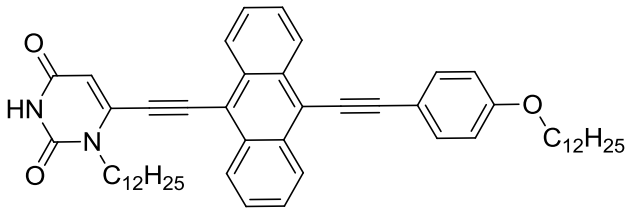

103

Figure 3.14: *Structure of organogelator* ***103*** *developed by Wu and co-workers.*[182]

3.9 Squaramide Based LMWGs

As seen in chapter 1, squaramides are four membered ring conjugated diamines derived from squaric acids, with the capacity for selectively binding to different H-bond acceptors through their acidic N-H groups (Figure 1.16).[110] Analogous to ureas as discussed in section 3.7, squaramides are interesting scaffolds for the design of LMWGs due to their enhanced hydrogen bond donor-acceptor ability (Figure 3.15). Disecondary squaramides and squaramic acids are extremely advantageous scaffolds for LMWGs assembly, because they can establish synergic H-bonding/aromaticity relationships that control the outcome of the aggregation process.[183]

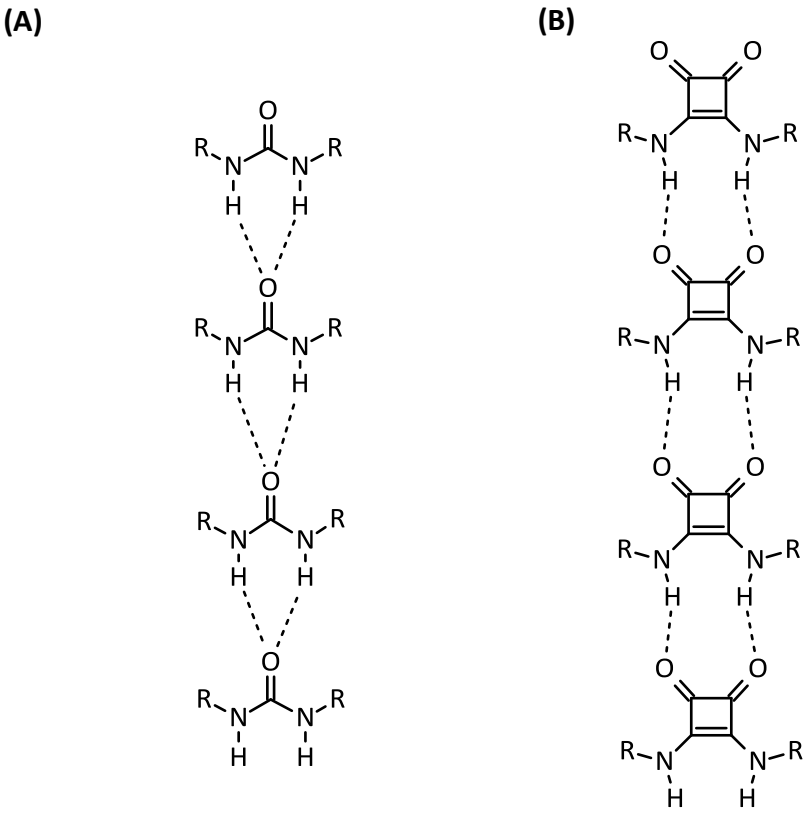

Figure 3.15: (A) *Urea hydrogen bonding via the urea α-tape motif.* ***(B)*** *Squaramide hydrogen bonding via the urea α-tape motif.*

However, despite the increasing number of squaramide based compounds in literature, the study of their self-assembly properties in solution for the synthesis of soft functional materials (gels) has remained mostly unexplored.[184] Diaz *et al*. reported the self-assembly properties of squaramide based supramolecular

LMWOGs **104 - 113** (Figure 3.16).[185] Compound **104** showed an unusual selectivity to form stable gels in a number of alcoholic solvents (alcogels), with the exception of acetone due to the keto-enol equilibrium of acetone. However, no gelation tendency was reported for compounds **105 - 113**, which suggests the existence of unique molecular interactions and a hydrophobic/hydrophilic balance that supports the self-assembly of compound **104** in alcohols.[185]

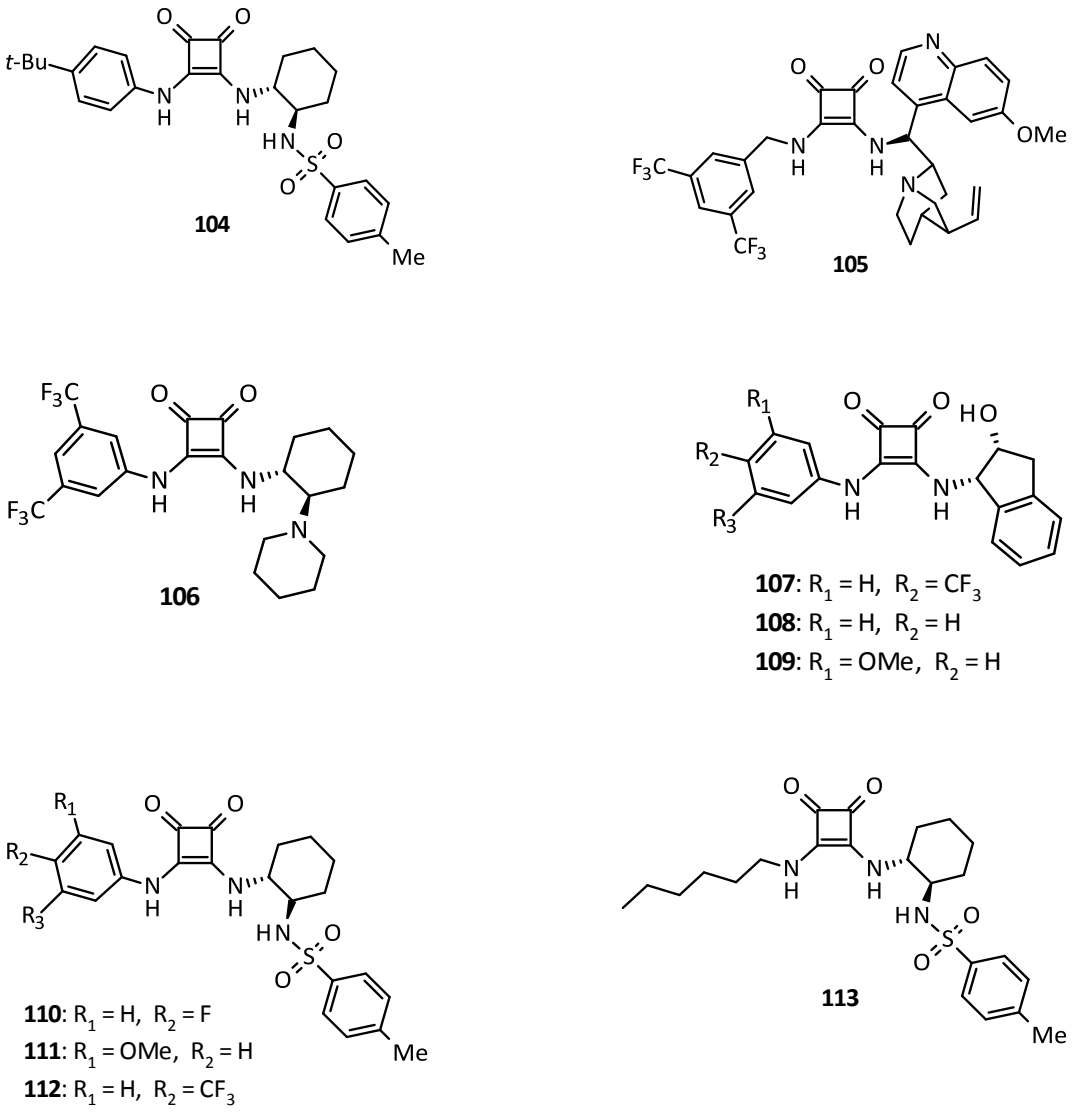

Figure 3.16: *Structure of squaramide based supramolecular LMWOGs* ***104 - 113*** *studied by Diaz et al.*[185]

According to UV-vis analysis of compound **104**, the sol-to-gel transition did not show a shift of the absorption maximum, suggesting that the aggregation mode of

compound **104** in solution is similar to in the gel phase. Furthermore, the comparison of the FTIR spectrum of solid compound **104** with those of the xerogels and compound **104** in solution only revealed a slight alteration with small frequency shifts to lower wavelengths for characteristic peaks.[185] Diaz *et al*. suggested that compound may also be aggregated in the solid state due to H-bonding and π-π stacking interactions which is also in agreement with the UV-vis measurements during the sol-to-gel transition. In contrast to the PXRD pattern of compound **104**, non-gelators **105 - 113** showed additional peaks after 17 °C, especially compounds **108** and **110** with extremely higher crystallinity than compound **104**.[185] The application of a heating ultrasound protocol instead of the heating-cooling cycle allows not only the formation of alcogels that could otherwise not be formed, but it also decreases both CGC and gelation times in comparison to the heating-cooling treatment.[185] Moreover, Diaz *et al*. revealed that the nature of the solvent has a remarkable effect on the morphology of the aggregates and some gels also exemplify the strong competition between gelation and macroscopic crystallisation typically observed in weak physical gels.[185] Furthermore, these alcogels were also reported to possess other interesting features such as thixotropic behaviour and phase selective gelation of non-miscible alcohol/water mixtures.[185]

Recently, Costa *et al*. synthesised amphiphilic LMWHs **114 - 116** (Figure 3.17).[186] The addition of NaOH triggers the self-assembly and hydrogelation of **114** in minutes at a pH range of 3 - 9, with or without heating.[186] Similarly, LMWH **115** also gels, but requires heating and the critical gelation concentration is higher.[186] However, after similar treatment, LMWH **116** remains as a suspension, even with excessive sonification and heating.[186] Costa *et al*. reported the different morphologies observed in LMWG **114 - 116** and the failure of hydrogel formation of **116** to be ascribed to the influence of peripheral substituents on the self-assembly of the precursor hydrogelators.[186]

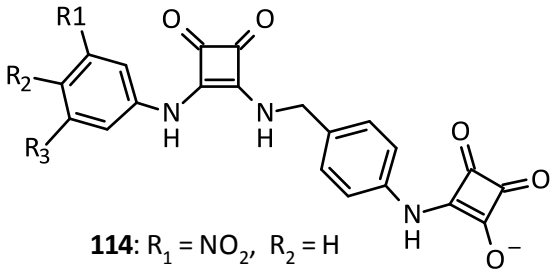

114: $R_1 = NO_2$, $R_2 = H$
115: $R_1 = H$, $R_2 = CF_3$
116: $R_1 = H$, $R_2 = H$

Figure 3.17: *Structure of amphiphilic squaramide based LMWHs **114 - 116** studied by Costa and co-workers.*[186]

To further explore the initial self-assembly events, Costa *et al*. studied the evolution of the ^1H NMR spectra of solutions **114** in different solvent mixtures $DMSO_{d6}/H_2O$.[186] Upon increasing the amount of water in the solvent mixture, all aromatic protons were reported to exhibit significant upfield shifts, which indicate the growing influence of the aromatic stacking interactions that occur in water.[186] The HRMS spectra of **115** show an intense base signal at m/z 433.0789 assigned to the monomer anion with 44% contribution of the doubly charged dimer.[186] The base signal of **115** appears at m/z 524.0681 and the contribution of the dimer increases to 60%.[186] However, the molecular signal of **116** at m/z 389.3670 contains less than 3% of the dimer, which indicates the low aggregation ability of 3.[186] Finally, Costa and co-workers reported LMWH **114** to be thermoreversible, thixotropic, injectable, and can be loaded with a substantial amount of zwitterionic biomolecules, which are rarely used as payloads.[186]

3.10 Conclusion

This chapter gave a detailed insight on the definition, formation, classification, and characterisation of a gel. It also gave a brief introduction on the topic of supramolecular gels with some examples of current research on amide, urea and squaramide based LMWGs. The design and sythesis of our novel squaramide based LMWOGs will be discussed in the next chapter.

Chapter 4 – Synthesis and Characterisation of Potential Novel Squaramide Based Low Molecular Weight Oragano-Gelators (LMWOGs)

4.1 Introduction

As discussed in Chapters one and two, urea and squaramides units not only constitute ideal anion binding sites, but also act as useful motifs for supramolecular architectures[185, 186] *via* intra- or inter- molecular H-bonding and self-assembly interactions which the gelation processes of soft materials. Ureas are attractive scaffolds for the design of LMWGs due to the urea α-tape motif which allows urea based LMWGs to undergo self-assembly.[176] This key supramolecular interaction that results from urea self–association to form a 6-membered hydrogen bonded ring based on two donors and one carbonyl acceptor has been used extensively in supramolecular self-assembly.[177]

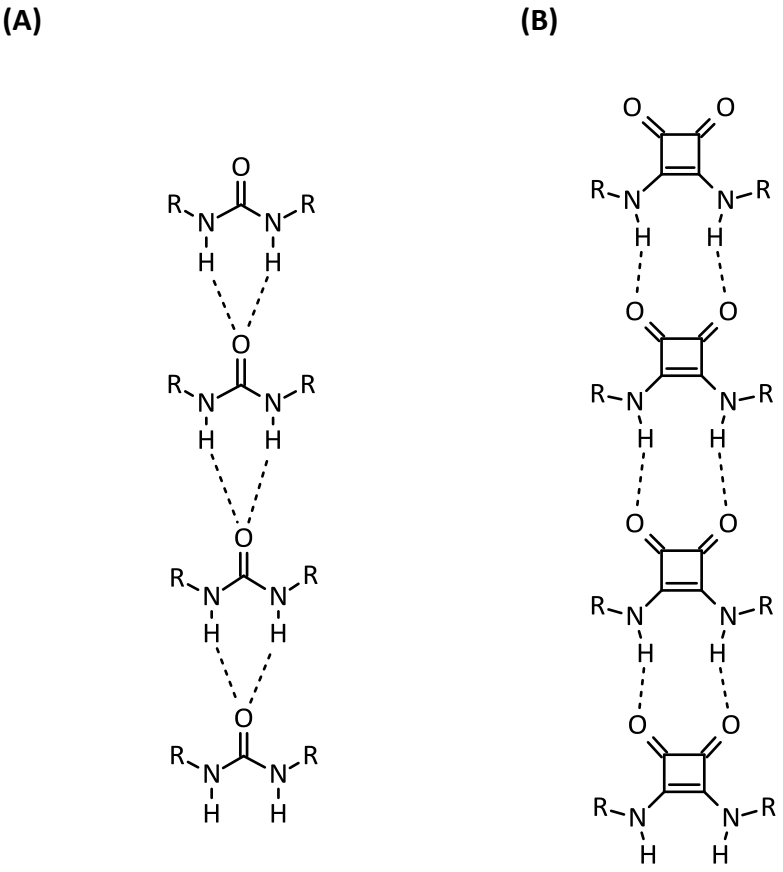

Figure 4.1: (A) *Urea hydrogen bonding via the urea α-tape motif.* ***(B)*** *Squaramide hydrogen bonding via the urea α-tape motif.*

However, squaramides are more interesting scaffolds compared to their urea counterparts for the design of LMWGs due to their enhanced hydrogen bond donor-acceptor ability (Figure 4.1). Squaramides are extremely advantageous

scaffolds for LMWGs assembly, because they can establish synergistic H-bonding/aromaticity relationships that control the outcome of the aggregation process[183] and trigger self-assembly process which results in gel formation. Therefore, research on this project has centred on the development of novel di-squaramide based low molecular weight organogelators (LMWOGs). In particular, we have focused on the development of novel LMWOGs based on three linker families.

The overall aim of the work presented in this Chapter is to synthesise three families of novel LMWOGs based on their linker and a preliminary study of their gelation ability in a range of organic solvents. Firstly, a description of the design of each of the gelator family is given. This is followed by the synthesis and a discussion of the characterisation of each of the novel LMWOGs. Finally, a preliminary gelation test of all novel compounds was carried out in different solvents to determine the formation of novel LMWOGs.

4.2 Design Requirements

The design of the novel LMWOGs will be based on three different requirements which include; the linker, the squaramide motif and the variable R groups as outlined in Figure 4.2.

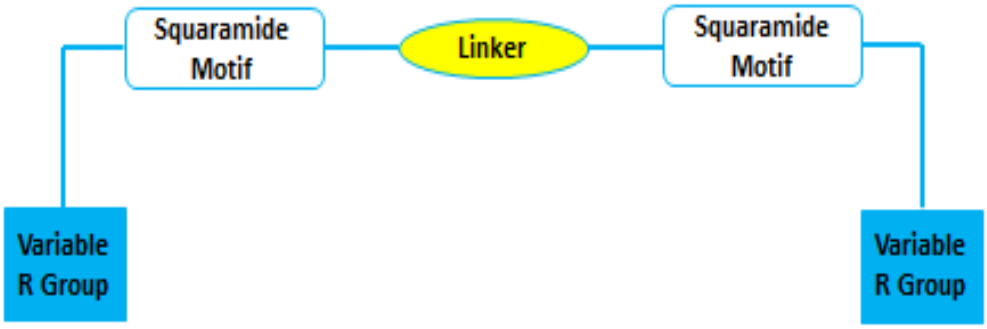

Figure 4.2: *Schematic representation of potential di-squaramide based low molecular weight organogelators (LMWOGs).*

4.2.1 The Linker

Three different linkers **117, 120** and **121** were exploited in the design of the novel LMWOGs as shown in Figure 4.3. The influence of linkers **117, 120** and **121** on the urea motif has been reported in the literature to trigger gel formation in organic solvents.[168, 187] Linker **120** was introduced into the design of the novel compounds to promote potential stacking interactions via increased structural rigidity, which is ascribed to the reduced degrees of rotation by the presence of the four methyl groups. Linker **117** was introduced into the design of the novel compounds to act as comparison for linker **121** which is less prone to aromatic stacking. Linker **117** triggers aromatic stacking which is disrupted by the ethyl groups on linker **121**, creating a balance between the stacking interaction and potential gel formation which are key characteristics to promote gelation behaviour.

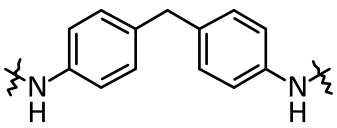

117

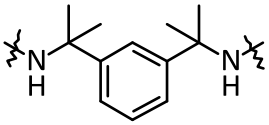

120

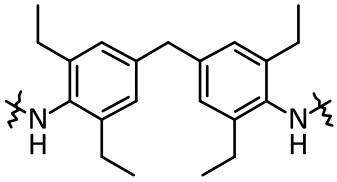

121

Figure 4.3: *Structure of linkers exploited in the design of potential novel LMWOGs.*

4.2.2 The Squaramide Motif

Squaramides have the capacity for selectively binding to different hydrogen bond acceptors *via* their acidic NH groups resulting in the formation of multiple and self-complementary H-bonds.[185] These interesting scaffolds can also pack with each other *via* $\pi - \pi$ interaction between the cyclobutenedione rings due to the planarity and aromacity.[188] In the design of our novel LMWOGs, we foresaw that the $\pi - \pi$ interaction between the cyclobutenedione rings the remarkable hydrogen bonding donor ability of the squaramide motif could be utilised (Figure 4.1).

4.2.3 The Variable R Groups

The R groups were varied to provide a diverse set of structures that will display various supramolecular interactions. The design of the novel compounds as shown in Figure 4.4. Firstly, the ability of aliphatic alkyl R groups such as n-butylamine **125** and decylamine **126** to increase solubility in organic solvents *via Van der waals* forces of interaction was incorporated into the design of the novel compounds. The introduction of aromatic ring such as in benzylamine **127** and 4-hydroxybenzylamine **128** induces aromatic stacking with additional potential H-bonding interaction through the phenol moiety in **128**. The potential of developing metallogels was also investigated by incorporating 4-(aminomethyl)pyridine **129** into the design of the novel compounds, with the potential of developing metallogel complexes *via* the nitrogen (N) atom in the pyridine ring of **129**. The position of the N atom was varied to the 3-position **130** and the 2-position **131**, to introduce a structural diversity in the design of novel compounds **146 – 148**.

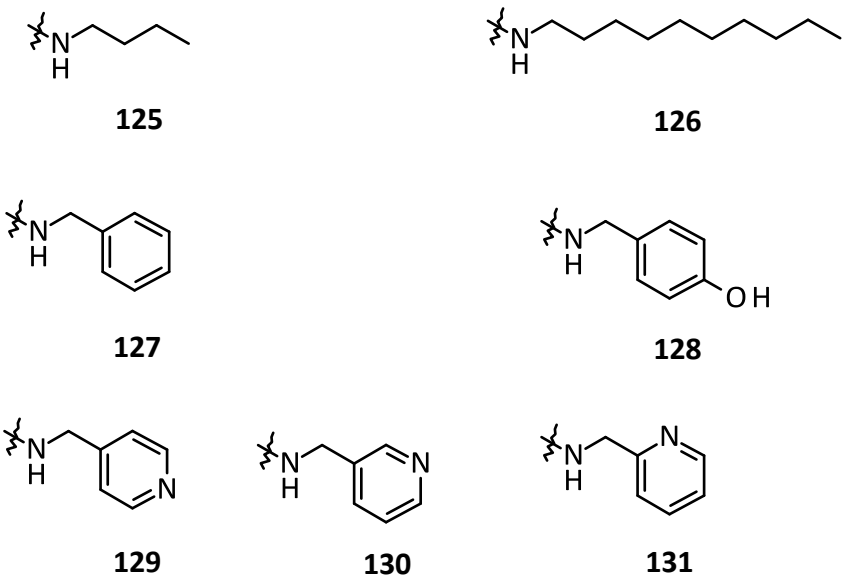

Figure 4.4: *Structure of the variable R groups exploited in the design of potential novel LMWOGs.*

With such structural diversity, we envisaged our design would give rise to a number of potential LMWG candidates. In the following chapter, the description of the synthesis and characterisation of each of the target novel compounds as outlined in

Figure 4.5 will be given. This will be followed by a summary of the gelation ability of each novel compound in polar aprotic, polar protic and non-polar solvents.

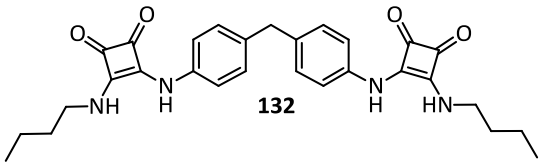

132

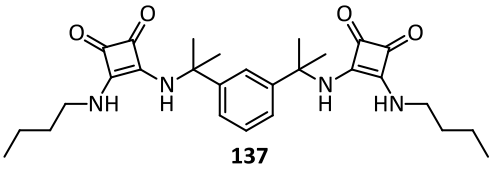

137

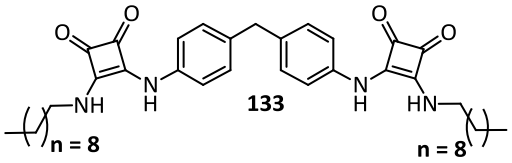

133

n = 8 **n = 8**

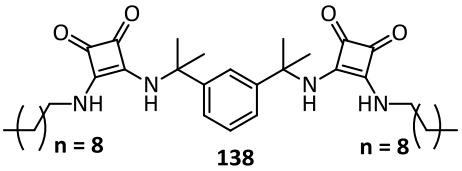

n = 8 **138** **n = 8**

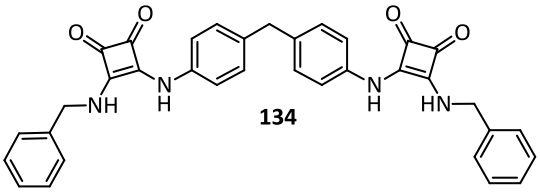

134

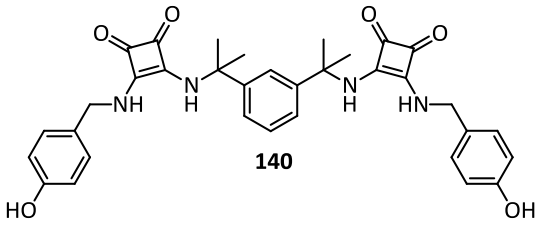

140

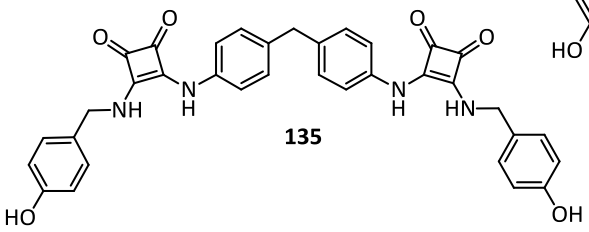

135

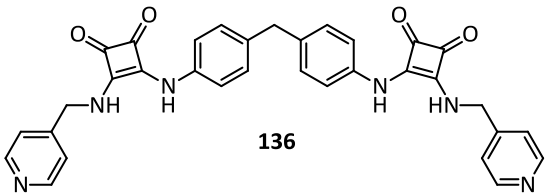

136

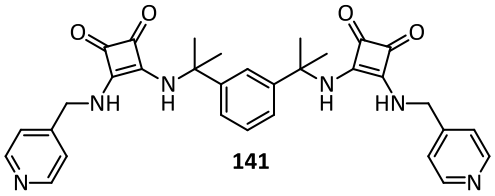

141

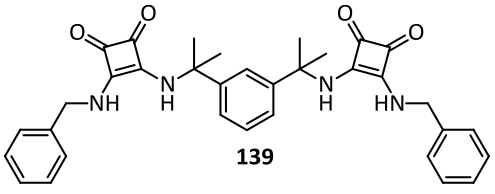

139

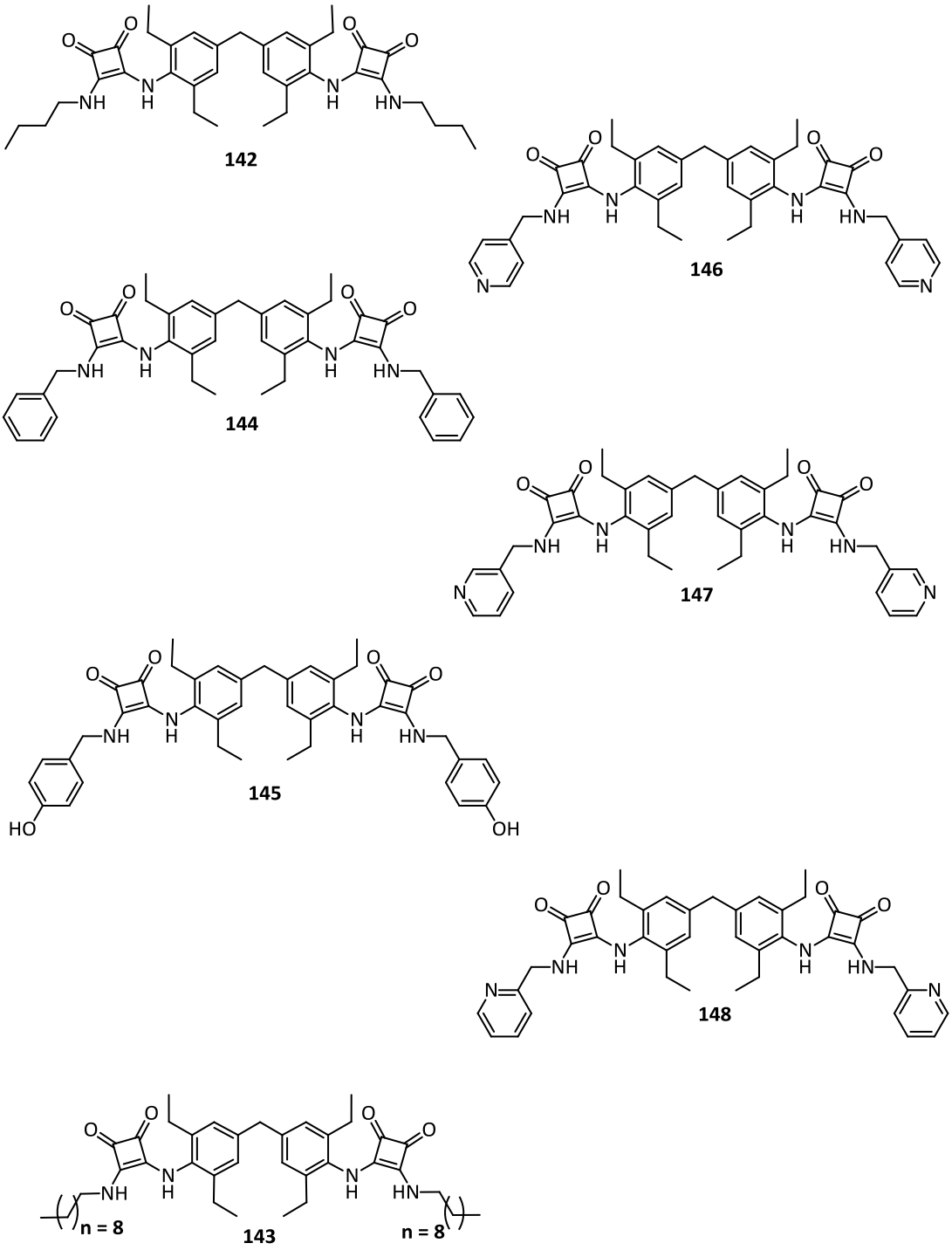

Figure 4.5: *Structure of novel target compounds.*

4.3 Synthesis

The target compounds were prepared from commercially available starting materials. All target and intermediates compounds were fully characterised using ^{1}H NMR, ^{13}C NMR, infrared spectroscopy and high resolution mass spectroscopy.

4.3.1 Synthesis of Linker 89 Target Compounds 132 – 136.

The synthesis of target compounds **132 - 136** were achieved using intermediate **122** as outlined in Scheme 4.2, using **132** as a representative example.

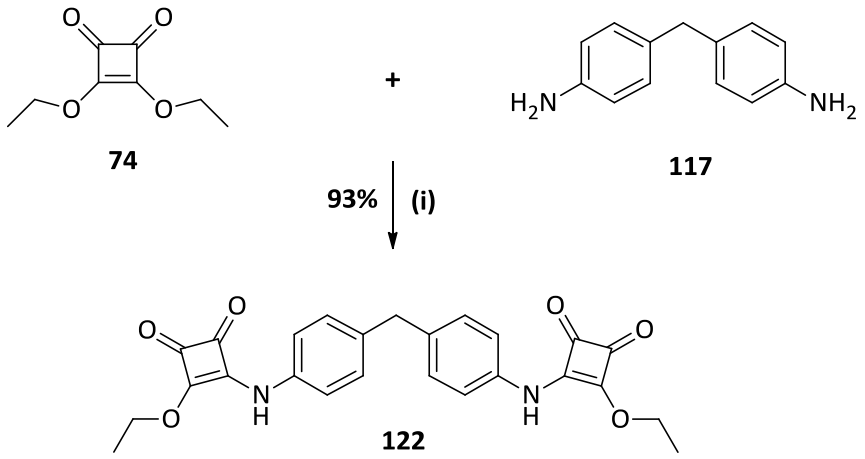

Scheme 4.1: *Synthetic pathway to intermediate* ***122 (i)*** *$Zn(OTf)_2$, EtOH.*

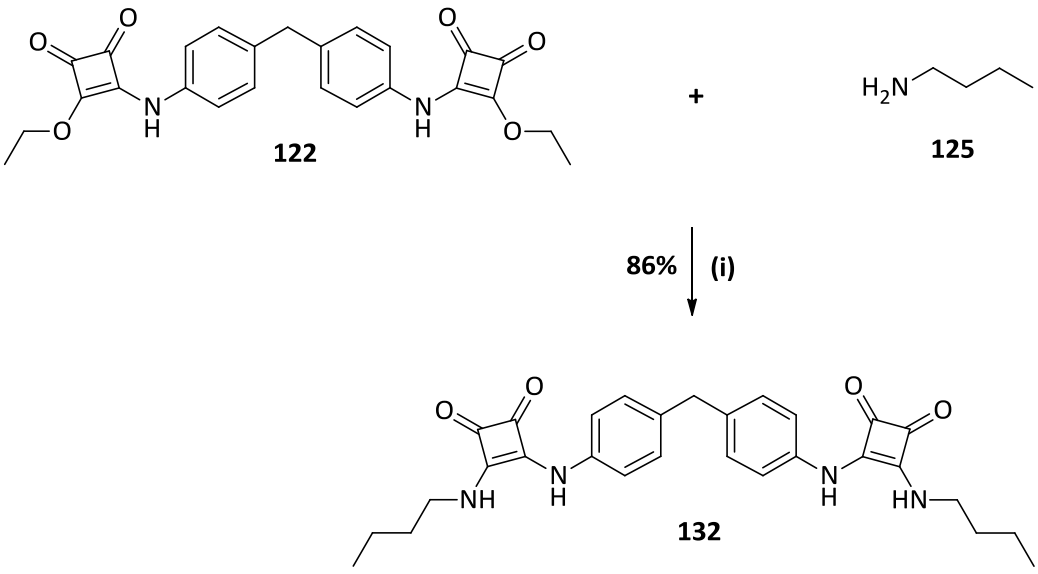

Scheme 4.2: *Synthetic pathway to* ***132 (i)*** Et_3N*, DMF.*

Firstly, intermediate **122** was synthesised as outlined in Scheme 4.1, by stirring a solution of linker **117** in EtOH with a solution of diethyl squarate **74** and zinc triflate to ensure that **74** was electrophilic enough prior to nucleophilic attack by linker **117** in EtOH. Isolation of the product yielded the desired product **122** as a tan amorphous solid in 93% yield.

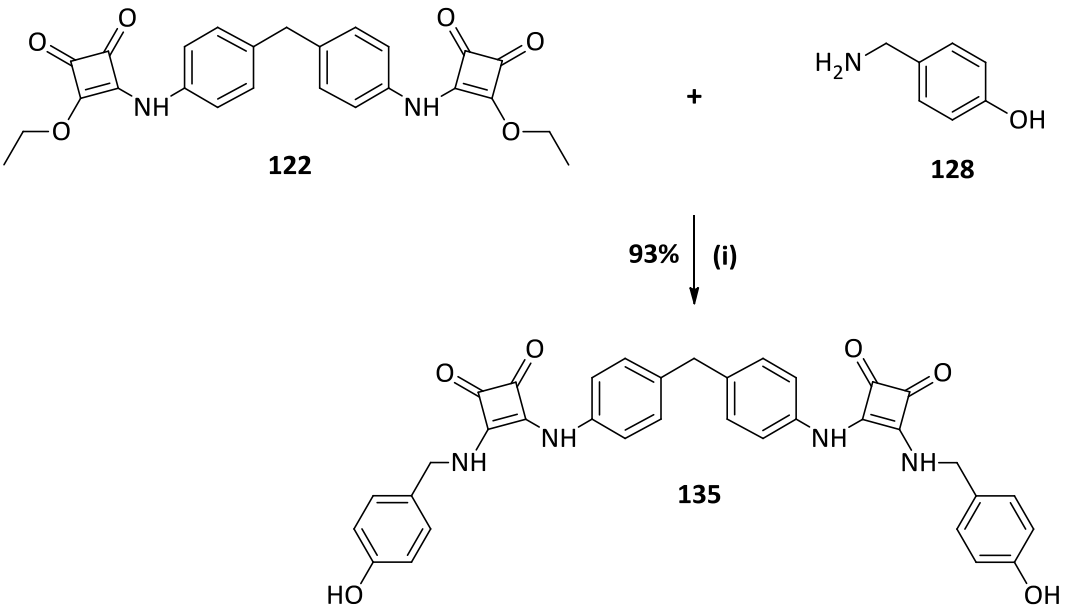

Scheme 4.3: *Synthetic pathway to* ***135 (i)*** Et_3N*, DMF.*

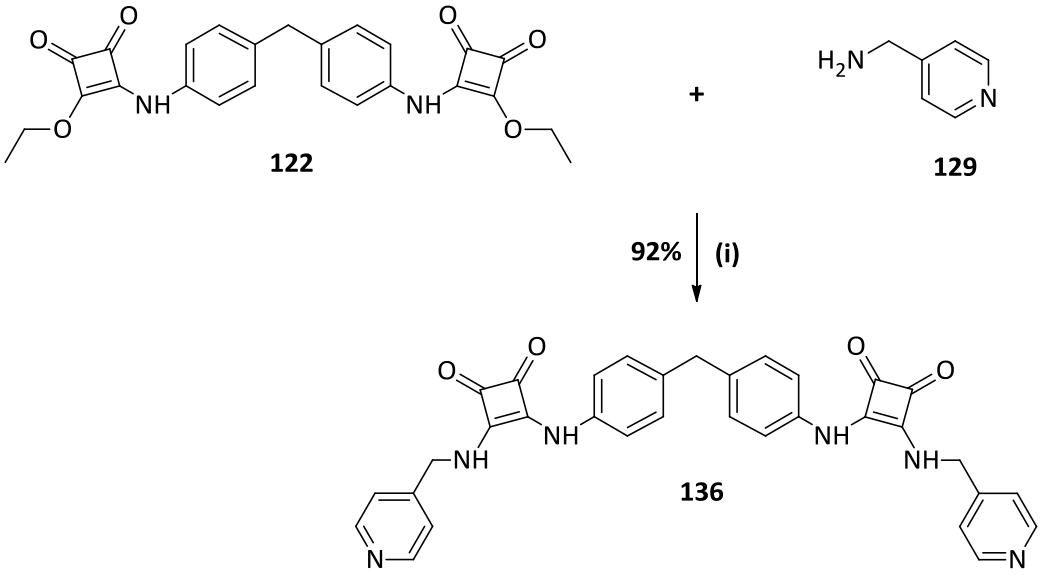

Scheme 4.4: *Synthetic pathway to* ***136 (i)*** Et_3N*, DMF.*

Compound **132** was synthesised as outlined in Scheme 4.2, *via* the nucleophilic addition of intermediate **122** to **125** in Et_3N and DMF to yield compound **132** as an off-white amorphous solid in 86% yield. The same procedure was applied to the synthesis of compounds **135** and **136** using reagent **128** and **129** respectively as outlined in Scheme 4.3 and Scheme 4.4 respectively. Compound **135** was obtained as a grey amorphous solid in 93% yield while compound **136** was obtained as beige amorphous solid in 92% yield. The synthesis of compounds **133** and **134** was attempted under the same reaction conditions as compound **132, 135** and **136** as outlined in Schemes 4.2, 4.3 and 4.4 respectively. Unfortunately, ^{1}H NMR and ^{13}C NMR analysis of compounds **133** and **134** could not be obtained due to the insoluble nature of the compounds in DMSO-*d6*. Novel compounds **132, 135** and **136** were fully characterised by ^{1}H NMR, ^{13}C NMR, HRMS and IR spectroscopy. However, the ^{13}C NMR analysis of compound **132** and **136** could not be obtained due to the insoluble nature of the compound. As a representative example the ^{1}H NMR spectrum of compound **132** is shown in Figure 4.6.

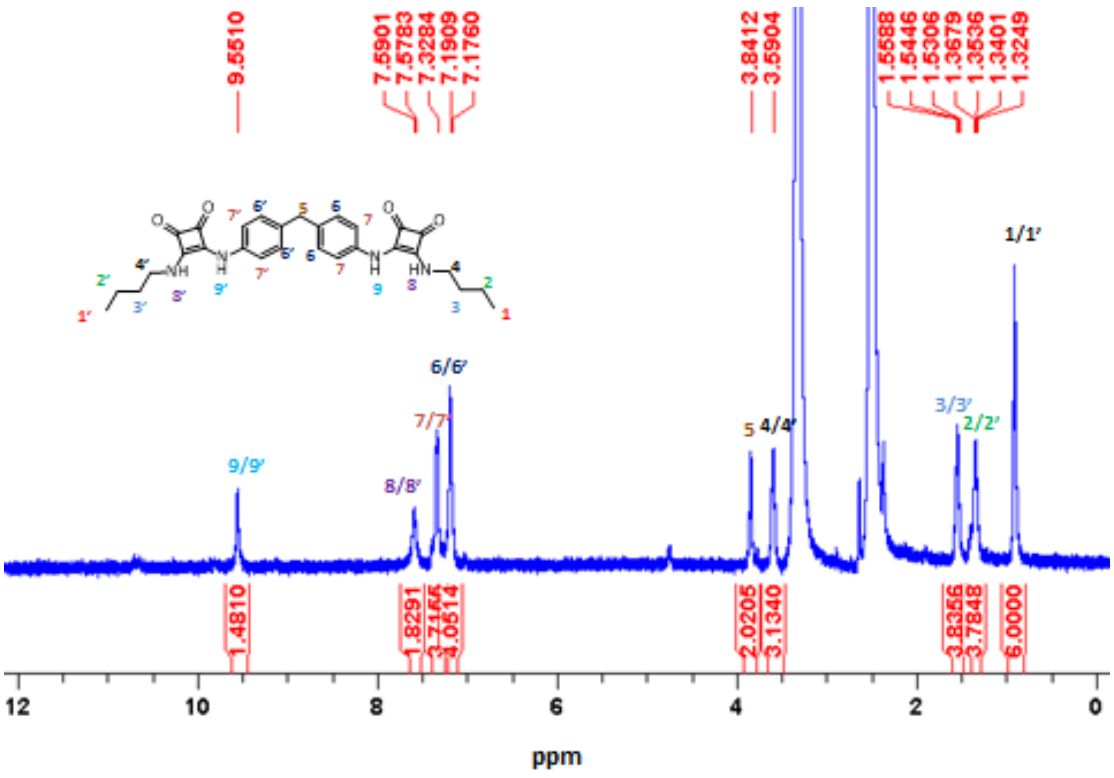

Figure 4.6: *The ^{1}H NMR spectrum of compound **132** (500.13 MHz, DMSO-$_{d6}$).*

According to Figure 4.6, nine signals can be seen in the ^{1}H NMR spectrum of compound **132**. A triplet can be seen up-field at 0.90 ppm for the six methyl protons (H1/1') which is due to the shielding effect by the four methylene protons (H2/2'). A quartet can be seen at 1.34 ppm for the four methylene protons (H2/2') while a triplet at 1.54 ppm was observed for the four methylene protons (H3/3'). A singlet was observed down field at 3.59 ppm for the four methylene protons (H4/4') due to the de-shielding effect of the electron withdrawing nitrogen atom on the two NH protons (H8/8'). A singlet at 3.84 ppm was observed for the two methylene protons (H5) due to the de-shielding effect of the two phenyl rings. A doublet was observed at 7.18 ppm for the four aromatic protons (H6/6') due to the shielding effect by the two methylene protons (H5). A broad signal was observed at 7.32 ppm for the four aromatic protons (H7/7') due to the de-shielding effect of the electron withdrawing nitrogen atom on the two NH protons (H9/9'). A broad signal at 7.58 ppm was observed for the two NH protons (H8/8') due to the shielding effect of the four methylene protons (H4/4') and the de-shielding effect of the cyclobutenedione rings. Finally, a broad signal was observed further downfield at 9.55 ppm for the two NH protons (H9/9') due to the de-shielding effect of both the phenyl and cyclobutenedione rings. Successful formation of compound **132** was also evident from accurate mass spectrometry, where **132** displayed a peak at 501.2515 corresponding to the [M + H] ion (3.68 ppm). The ^{1}H and ^{13}C NMR spectra of compounds **135** and **136** are shown in the appendix section. All other compounds were similarly characterised as outlined above.

4.3.2 Synthesis of Linker 103 Target Compounds 137 – 141

The synthesis of target compounds **137 – 141** were achieved using intermediate **123** as outlined in Scheme 4.6, using **105** as a representative example. Firstly, **119** was synthesised as outlined in Scheme 4.5, by stirring a solution of **118** in MeOH. Removal of solvent under reduced pressure yielded compound **119** as a white amorphous solid in 95% yield. Linker **120** was synthesised by refluxing a solution of compound **119** containing KOH in n-BuOH as outlined in Scheme 4.5. Removal of solvent and extraction of crude product in THF, followed by drying over Na_2SO_4 yielded linker **120** as a yellow oil in 96% yield. Intermediate **123** was synthesised

according to Scheme 4.5, by stirring a solution of linker **120** in Et_3N and EtOH with a solution of diethyl squarate **74** in EtOH. Purification of crude product *via* column chromatography yielded compound intermediate **123** as a sticky yellow residue in 74% yield.

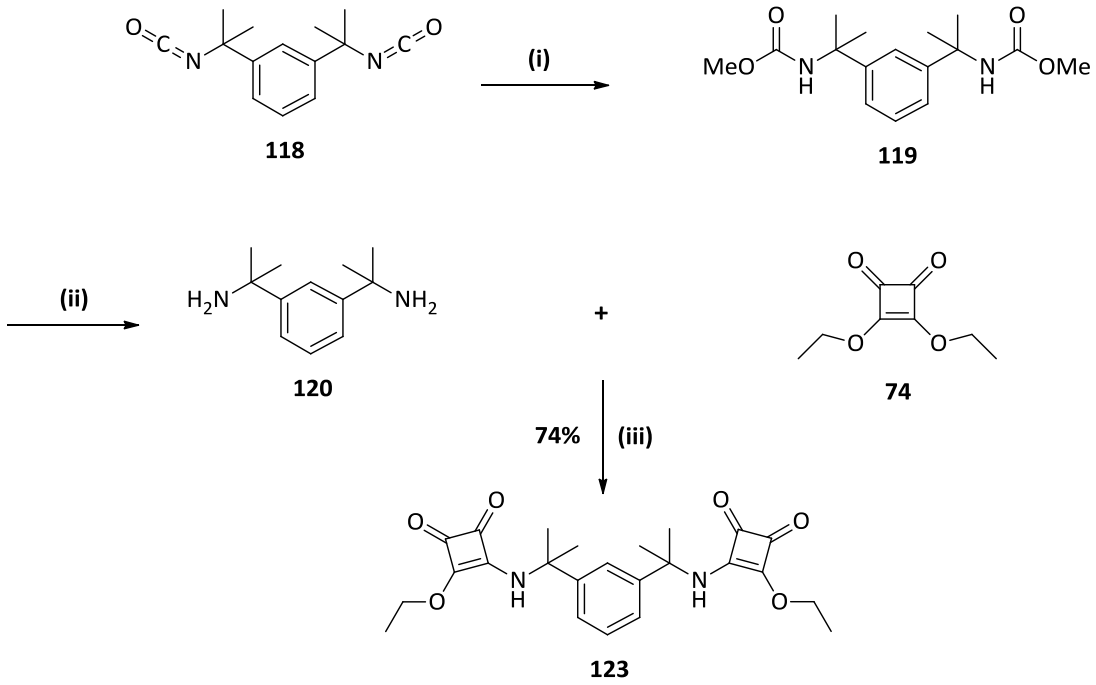

Scheme 4.5: *Synthetic pathway to intermediate* ***123*** ***(i)*** *MeOH;* ***(ii)*** *KOH, n-BuOH, reflux;* ***(iii)*** Et_3N*, EtOH.*

Finally, compound **137** was synthesised as outlined in Scheme 4.6, *via* the nucleophilic addition of intermediate **123** to **125** in Et_3N and EtOH to yield compound **137** as an off-white amorphous solid in 93% yield. The same procedure was applied to the synthesis of compound **138 -141** using reagent **126** - **129** respectively as outlined in Scheme 2.6. Isolation by suction filtration afforded the products **126, 127, 128** and **129** as off-white, white, beige and light yellow solids respectively in 79%, 76%, 84% and 96% yield. Novel compounds **137 - 141** were fully characterised by ^{1}H NMR, ^{13}C NMR, HRMS and IR spectroscopy. As a representative example the ^{1}H NMR spectrum of compound **137** is shown in Figure 4.7.

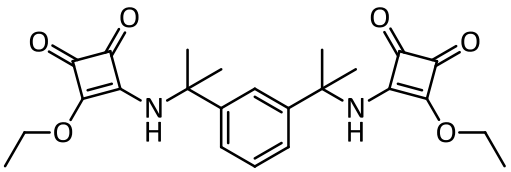

123

\+ **125 - 129**

(i)

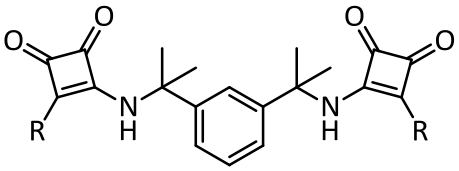

137: R = n-Bu
138: R = n-dec
139: R = Bn
140: R = CH_2-(4-HOC_6H_4)
141: R = CH_2-(4-C_5H_4N)

RNH_2 =

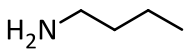

125

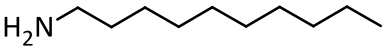

126

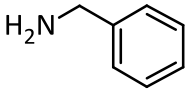

127

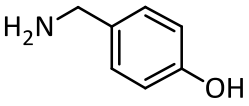

128

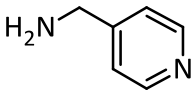

129

Scheme 4.6: *Synthetic pathway to target compounds* ***137 – 141*** *incorporating linker* ***120 (i)*** Et_3N*, EtOH.*

According to Figure 4.7, eight signals can be seen in the ^{1}H NMR spectrum of compound **137**. A triplet can be seen up-field at 0.88 ppm for the six methyl protons (H1/1') which is due to the shielding effect by the four methylene protons (H2/2'). A multiplet can be seen at 1.31 ppm for the four methylene protons (H2/2') while a multiplet at 1.48 ppm was observed for the four methylene protons (H3/3'). A singlet was observed slightly down field at 1.73 ppm for the twelve methyl protons (H4/4') due to the de-shielding effect of the aromatic phenyl ring. A quartet at 3.53 ppm was observed down-field for the four methylene protons (H5/5') due to the de-shielding effect of the electron withdrawing nitrogen atom on the two NH protons (H7/7').

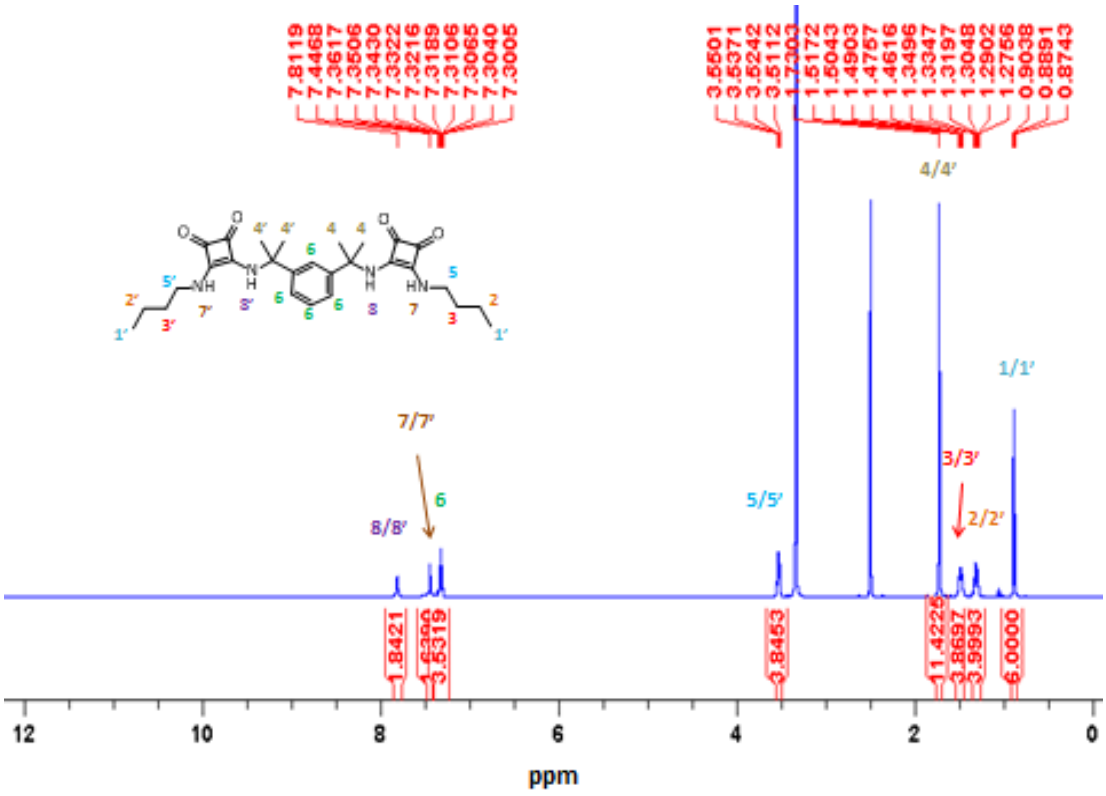

Figure 4.7: *The ^{1}H NMR spectrum of compound **137** (500.13 MHz, DMSO-$_{d6}$).*

A multiplet was observed down-field at 7.32 ppm for the four aromatic protons (H6). A singlet was observed at 7.44 ppm for the two NH protons (H7/7') due to the shielding effect by the four methylene protons (H5/5'). Finally, a singlet was observed further downfield at 7.81 ppm for the two NH protons (H8/8') due to the de-shielding effect of both the phenyl and cyclobutenedione rings. Successful

formation of compound **137** was also evident from accurate mass spectrometry, where **137** displayed a peak at 495.2985 corresponding to the [M + H] ion (3.92 ppm). The ^{1}H and ^{13}C NMR spectra of compounds **138 - 141** are shown in the appendix section. All other compounds were similarly characterised as outlined above.

4.3.3 Synthesis of Linker 110 Target Compounds 142 - 148

The synthesis of target compounds **142 - 148** were achieved using intermediate **124** as outlined in Scheme 4.8, using **142** as a representative example. Firstly, intermediate **124** was synthesised according to Scheme 2.7, by refluxing a solution of linker **121** in Et_3N and EtOH with a solution of diethyl squarate **74** in zinc triflate and EtOH. Purification of crude product *via* column chromatography yielded compound intermediate **124** as a yellow oil in 59% yield.

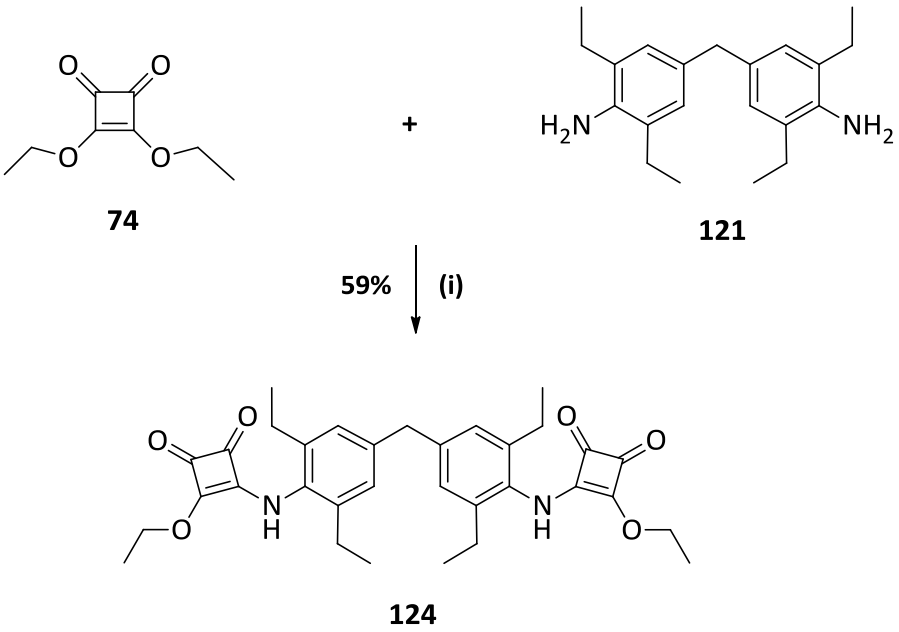

Scheme 4.7: *Synthetic pathway to intermediate* ***124*** ***(i)*** Et_3N*, Zn(OTf)$_2$, EtOH, reflux.*

Finally, compound **142** was synthesised as outlined in Scheme 2.8, *via* the nucleophilic addition of intermediates **124** to **125** in Et_3N and EtOH to yield compound **142** as an off-white amorphous solid in 55% yield. The same procedure was applied to the synthesis of compound **143 – 148** using reagent **126 - 131** respectively as outlined in Scheme 4.8. Isolation by suction filtration afforded the

products **143, 144, 145, 146, 147** and **148** as white, off-white, brown and beige solids in 33%, 59%, 27%, 68%, 66% and 61% yield respectively.

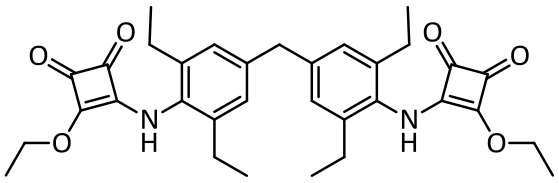

124

+ **125 -131**

(i)

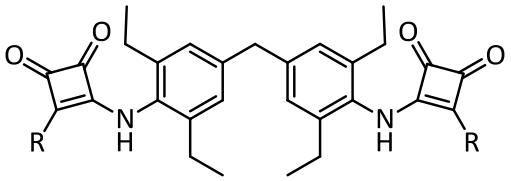

142: R = n-Bu
143: R = n-dec
144: R = Bn
145: R = CH_2-(4-HOC_6H_4)
146: R = CH_2-(4-C_5H_4N)
147: R = CH_2-(3-C_5H_4N)
148: R = CH_2-(2-C_5H_4N)

RNH_2 =

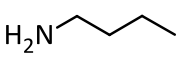

125

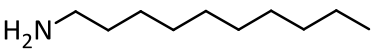

126

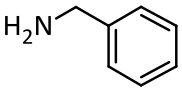

127

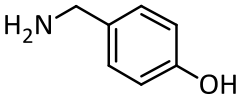

128

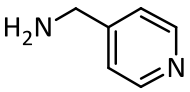

129

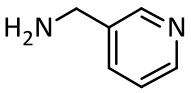

130

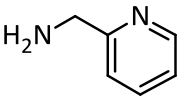

131

Scheme 4.8: *Synthetic pathway to target compounds* ***142 – 148*** *incorporating linker* ***121 (i)*** Et_3N*, EtOH.*

These novel compounds were fully characterised by ^{1}H NMR, ^{13}C NMR, HRMS and IR spectroscopy. The ^{1}H NMR spectrum of compound **142** is shown in Figure 4.8. According to Figure 4.8, seven signals can be seen in the ^{1}H NMR spectrum of compound **142**. A multiplet was observed up-field at 1.16 ppm for the eighteen methyl protons (H1/1', H5/H5') and the twelve methylene protons (H2/2', H3/3', H4/H4'). A multiplet was observed slightly down-field at 3.30 ppm for the eight methylene protons (H6/H6') due to the presence of the aromatic phenyl rings. A singlet at 3.90 ppm was also observed for the two methylene protons (H7) due to the de-shielding effect of the two aromatic phenyl rings.

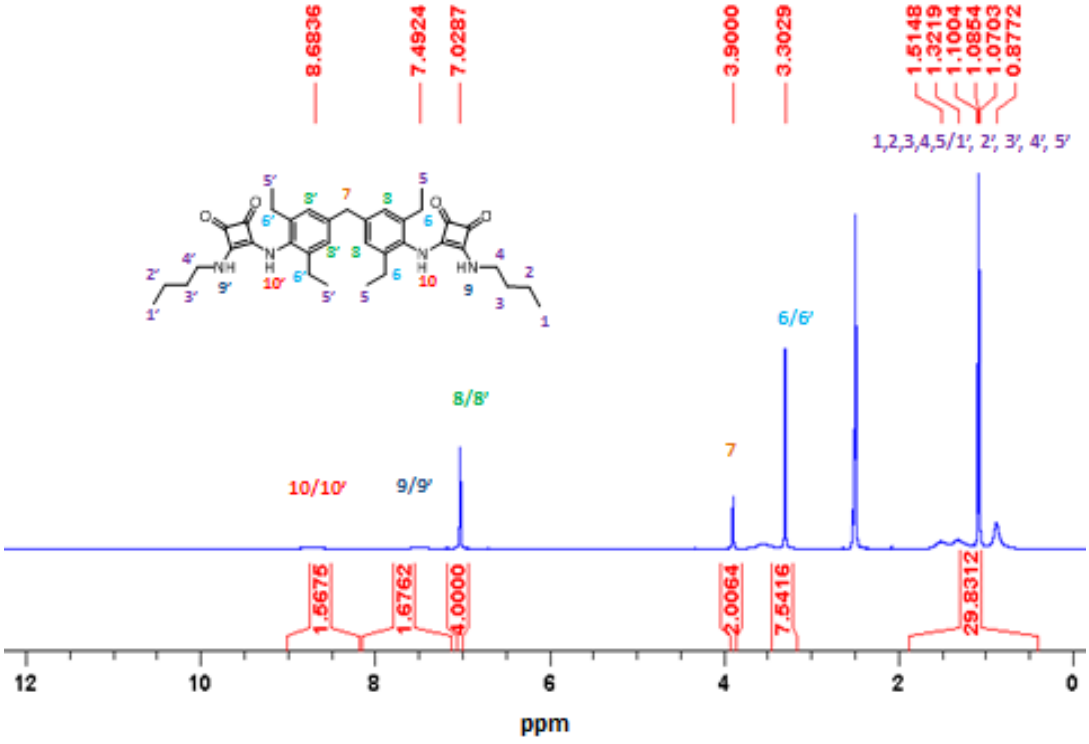

4.8: *The ^{1}H NMR spectrum of compound **142** (500.13 MHz, DMSO-$_{d6}$).*

A singlet at 3.90 ppm was also observed for the two methylene protons (H7) due to the de-shielding effect of the two aromatic phenyl rings. A singlet can be seen at 7.02 ppm for the four aromatic protons (H8/8'). A broad signal at 7.49 ppm was observed for the two NH protons (H9/9') due to the shielding effect of the four methylene protons (H4/4') and the de-shielding effect of the cyclobutenedione rings. Finally, a broad signal was observed further downfield at 8.68 ppm for the two NH protons (H10/10') due to the de-shielding effect of both the phenyl and

cyclobutenedione rings. Successful formation of compound **142** was also evident from accurate mass spectrometry, where **142** displayed a peak at 613.3767 corresponding to the [M + H] ion (3.07 ppm). The ^{1}H and ^{13}C NMR spectra of compounds **143 - 148** are shown in the appendix section. All other compounds were similarly characterised as outlined above.

4.3.4 Summary of Synthesis of Target Compounds

Three different linkers **117, 120** and **121** which have been reported in the literature to trigger gel formation in organic solvents were exploited in the design and synthesis of the target novel compounds. Linker **117** was introduced into the design of the novel compounds to act as comparison for linker **121** which is less prone to aromatic stacking. Meanwhile, the aromatic stacking interaction is disrupted by the ethyl groups on linker **121**, creating a balance between the stacking interaction and potential gel formation which are key characteristics to promote gelation behaviour. Furthermore, the potential stacking interactions triggered by structural rigidity *via* the reduced degrees of rotation by the presence of the four methyl groups was exploited in the design and synthesis of the target novel compounds.

The $\pi - \pi$ interaction and hydrogen bond donor capacity of the squaramide motif *via* their acidic NH groups was exploited in potential formation of multiple and self-complementary H-bonds which could be advantageous to the self-assembly and self-aggregation process of a gel.

Finally, a diverse set of structures that will take advantage of various supramolecular interactions were developed by varying the R groups in the design and synthesis of the target squaramide compounds. The ability of aliphatic alkyl R groups to increase solubility in organic solvents *via Van der waals* forces of interaction was exploited into the design and synthesis of the target novel compounds. The aromatic stacking interaction of the phenyl ring and the potential H-bonding interaction of the phenol moiety were also explored in the design and synthesis of the target novel compounds. The potential of developing metallogels *via* the nitrogen (N) atom of the pyridine ring was also investigated.

In summary, we have successfully developed potential LMWOGs based on three different linker families **117, 120** and **121**. However, the synthesis of compounds **133** and **134** was unsuccessful due to the insoluble nature of the compounds in majority of organic solvents. The preliminary gelation test conducted for all novel compounds in different solvents will be discussed next.

4.4 Preliminary Gelation Test of all Novel Compounds

Organogels are classified according to the solvent they are surrounded by, in which they can be formed in organic solvents such as polar, protic, polar aprotic and non-polar solvents. The non-covalent interactions required to promote gelation in organogels is dependent on the solvent, which is mostly achieved by dipolar interactions such as H-bonding. It has been observed that squaramides exhibit significantly higher H-bonding abilities[110, 183] compared to their urea analogues[156, 176, 177, 181] and that this results in superior self-assembly interactions. With this in mind, preliminary gelation test of all novel compounds was carried out in different solvents which include non-polar, polar aprotic and polar protic solvents, to determine the formation of novel LMWOGs.

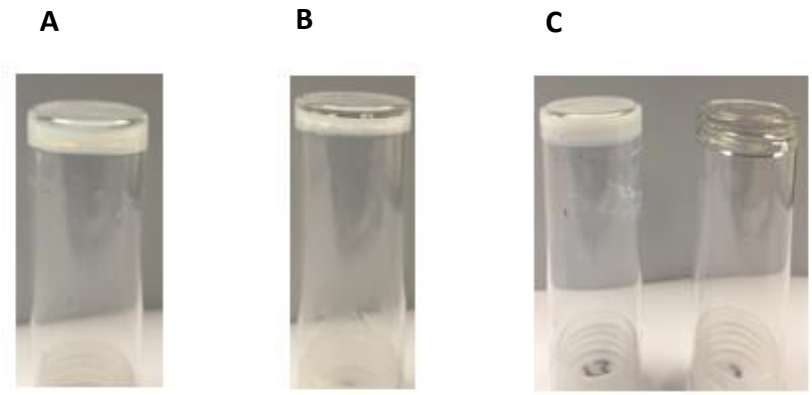

Figure 4.9: *Representative photographs of up-side down vials containing LMWOGs prepared via heating-ultrasound (H-C) and heating-cooling (H-U).* ***(A)*** *Gelator* ***137*** *in DMSO.* ***(B)*** *Gelator* ***138*** *in DMF.* ***(C)*** *Gelator* ***143*** *in EtOH (left) and in toluene (right).*

The preliminary gelation tests were performed by dissolving 10 mg of each novel compound in 0.5 ml of eight different solvents. This was achieved by sonification of each sample followed by heating via a heat gun and cooling at room temperature

for 24 hours. A summary of the results obtained from the preliminary gelation test of all novel compounds in different solvents are detailed in Table 4.1.

Table 4.1: Summary of the results obtained from the preliminary gelation test of all novel compounds in different solvents.

Novel Compounds	Organic Solvents							
	Polar Protic	Polar Aprotic			Non-Polar			
	EtOH	DMSO	MeCN	DMF	$CHCl_3$	Toluene	DCM	Pet.Ether
132	I	PS	I	I	I	I	I	I
135	I	S	I	I	I	I	I	I
136	I	PS	I	I	I	I	I	I
137	I	S	I	OG	I	I	I	I
138	I	PG	I	OG	I	I	I	I
139	I	S	I	I	I	I	I	I
140	I	S	I	I	I	I	I	I
141	I	S	I	S	I	I	I	I
142	I	S	I	S	I	I	I	I
143	OG	PG	I	S	PG	TG	PG	I
144	I	S	I	S	I	I	I	I
145	I	S	I	S	I	I	I	I
146	I	S	I	S	I	I	I	I
147	I	S	I	S	I	I	I	I
148	I	S	I	S	I	I	I	I

KEY

I = Compounds that are insoluble in solvent, OG = Compounds that form opaque gels in solvent, TG = Compounds that form transparent gels in solvent, S = Compounds that are soluble in solvent, PG = Compounds that partially form gels in solvent, PS = Compounds that are partially soluble in solvent.

4.4.1 Summary of Preliminary Gelation Test Results of all Novel Compounds

A summary of the preliminary gelation test results of all novel compounds will be discussed in this section.

4.4.1.1 Compounds Containing Linker 117

Linker **117** target novel compounds **132, 135** and **136** formed no gels in polar aprotic, polar protic, and non-polar solvents due to their insolubility in all the tested solvents. However, compound **135** which is fully soluble in DMSO and **132** and **136** which are partially soluble in DMSO, none of the linker **117** target compound formed a gel, despite their solubilty in DMSO.

4.4.1.2 Compounds Containing Linker 120

Linker **120** target compounds **137 – 141** are insoluble EtOH, MeCN and non-polar solvents. Compounds **139** and **140** also insoluble in DMF unlike **137** and **141** were both soluble in DMF. Whereas compound **137** formed an opaque gel in DMSO while compound **138** formed an opaque gel in DMF as shown in Figure 4.9 (A) and (B) respectively. However, compounds **138 – 141** are soluble in DMSO, with **138** forming a partial gel in DMSO.

4.4.1.3 Compounds Containing Linker 121

Furthermore, linker **121** target compounds **142, 144, 145, 146, 147** and **148** are insoluble in EtOH, MeCN and non-polar solvents with solubility in DMSO and DMF. Whereas compound **143** was insoluble in MeCN and petroleum ether with solublity in DMF. Compound **143** formed a partial gel in $CHCl_3$, DMSO and DCM. Compound **143** also formed an opaque gel in EtOH and a transparent gel in toluene as shown in Figure 4.9 (C)

4.5 Conclusion and Future work

In this Chapter, we have successfully developed an array of potential novel LMWOGs. In particular, novel LMWOGs **137** which forms opaque gels in DMSO, while **138** forms opaque gels in DMF. Whereas, **143** forms opaque gels in EtOH and transparent gels in toluene. In summary, compound derived from linker **117** are insoluble in most of all the tested organic solvent except in DMSO. This was ascribed to the formation of aromatic stacking between their molecules. Nevertheless, improved solubility in polar aprotic solvents such as DMSO and DMF was observed for compounds derived from linker **120**. However, compound **137** gels in DMSO and whereas the formation of a gel of gelator **138** was evident in DMF. This behaviour was ascribed to the presence of the butyl and decylamine R group in compound **137** and **138** respectively, to enhance the solubility in organic solvents and the presence of linker **120** to improve structural rigidity and potential stacking interactions. Furthermore, enhanced solubility in polar aprotic solvents such as DMSO and DMF was also observed for compounds derived from linker **121**. Partial gelation of compound **143** was observed in DMSO, DCM and $CHCl_3$ whereas the formation of an opaque gel was observed in EtOH while formation of a transparent gel was evident in toluene. This behaviour was also ascribed to the presence of the decylamine R group to increase the solubility in organic solvents and the presence of linker **121** to disrupt stacking interaction *via* the ethyl group and induces a balance between the stacking interaction and potential gel formation.

Future perspectives of this work will look to further investigate the gelation studies of novel LMWOGs **137, 138** and **143,** in order to further understand their gelation properties. The metallo-gellation capabilities of compounds **146 – 147** will also be investigated. This will be carried out by our collaborators, the Steed Research Group at Durham University. From our understanding of this chapter, we will investigate the design, synthesis and gelation properties of the target compounds **149 – 153** based on using linker **124**. Futhermore, we will also investigate the impact of increasing the ethyl chain on linker **124** to a propyl chain and the effect of

incorporating a thio-squaramide motif versus having a squaramide motif (Figure 4.10).

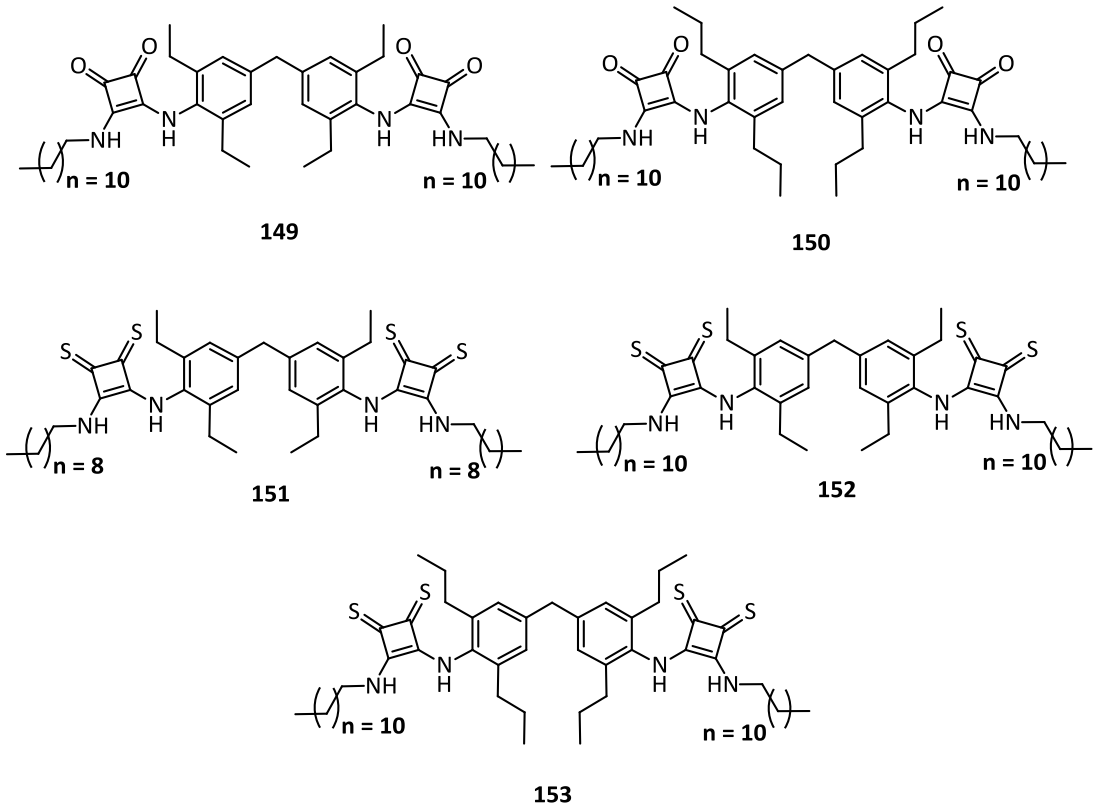

Figure 4.10: *Future target compounds.*

Chapter 5 – Conclusion

5.1 Conclusion

The work carried out in this thesis was undertaken with a goal of the preparation and study of novel squaramide based materials for sensors and soft materials. The design, synthesis and photophysical as well as anion binding properties of a set of novel squaramide based anion receptors **85 – 88** were described in Chapter 2. Whereas, the design, synthesis and preliminary gelation test of potential gelators were discussed in Chapter 4.

In Chapter 2, the novel receptors **85 – 88** were shown by ^{1}H NMR analysis and SEM analysis to self-associate at room temperature and self-dissociate at higher temperatures (343 K). According to the photophysical properties of receptors **85 – 88** in DMSO, receptor **85** and **87** have proved to be more emissive in DMSO solution compared to receptors **86** and **88** which are less emissive in DMSO solution. Furthermore, the addition of anions (AcO^-, F^-, PO_4^{3-} and SO_4^{2-}) as their TBA salts led to deprotonation events within receptors **85 – 88**, this event was evident by UV/Vis titration, fluorescence titration and ^{1}H NMR spectroscopic analysis. However, the receptors were shown to be selective towards Cl^- *via* classical H-bonding interaction between the binding site and Cl^-, resulting in a subtle colour change. The position of the binding site (top or bottom) on the signalling unit was observed to play a major role in the affinity towards Cl^- binding, this was ascribed to the number of H-bonding available in the binding pocket. This was further supported by a 1:1 binding isotherm observed for **85, 86, 87** and **88** in DMSO with a K_a value of 488.62, 273.65, 221.26 and 114.80 M^{-1} respectively. In conclusion, **85** is the most selective receptor towards Cl^- binding with **88** being the least selective. Future perspectives of this work will look to further evaluate the SEM images of novel anion receptors **85 – 88**, in order to further understand the unique morphologies of our novel receptors.

In Chapter 4, we successfully developed an array of potential novel LMWOGs and studied their gelation ability in a range of solvents. In particular, novel LMWOGs **137** which forms opaque gels in DMSO and **138** which forms opaque gels in DMF. This behaviour was ascribed to the presence of the butyl and decylamine R group in compounds **137** and **138** respectively, enhancing their

solubility in organic solvents and the presence of linker **120** to improve structural rigidity and potential stacking interactions. Furthermore, gelator **143** forms opaque gels in EtOH and transparent gels in toluene. This behaviour was also ascribed to the ability of the decylamine R group to increase the solubility in organic solvents and the presence of linker **121** to disrupt stacking interaction *via* the ethyl group and induces a balance between the stacking interaction and potential gel formation. Future perspectives of this work will look to further investigate the gelation studies of novel LMWOGs **137, 138** and **143,** in order to further understand their gelation properties. The metallo-gellation capabilities of compounds **146 – 148** will also be investigated. This will be carried out by our collaborators, the Steed Research Group at Durham University. From our understanding of this chapter, we will investigate the design, synthesis and gelation properties of the target compounds **149 – 153** based on using linker **124.** Futhermore, we will also investigate the impact of increasing the ethyl chain on linker **124** to a propyl chain and the effect of incorporating a thio-squaramide motif versus having a squaramide motif (Figure 4.10).

Chapter 6 – Experimental

6.1 Instrumentation and Reagents

Commercial materials were supplied by TCI Europe or Sigma Aldrich and were used without further purification. HPLC grade solvents were used as received. ^{1}H NMR spectra were recorded using a Bruker Avance III 500 at a frequency of 500.13 MHz, and are reported as parts per million (ppm) with $CDCl_3$ (δH 7.26 ppm) or DMSO-d_6 (δH 2.50 ppm) as an internal reference. The data are reported as chemical shift (δ), multiplicity (br = broad, s = singlet, d = doublet, t = triplet, m = multiplet), coupling constant (*J*, Hz) and relative integral. ^{13}C NMR spectra were recorded using a Bruker Avance III 500 at a frequency of 125.76 MHz and are reported as parts per million (ppm) with $CDCl_3$ (δH 77.1 ppm) or DMSO-d_6 (δH 39.5 ppm) as an internal reference. High resolution ESI spectra were recorded on an Agilent 6310 LCMS TOF. Analytical TLC was performed using pre-coated silica gel plates (Merck Kieselgel 60 F254). Flash chromatography was performed using silica gel 40-63 µM, 60 Å. Infrared absorption spectra were recorded on a Perkin Elmer Spectrum 100 FT-IR spectrometer using KBr disks. FT-IR are reported in wavenumbers (cm^{-1}). Commercial materials were supplied by TCI Europe or Sigma Aldrich and were used without further purification, unless otherwise noted. Diethyl squarate were synthesised as previously described.[189]

6.2 Spectroscopic Binding Studies

Spectroscopic titrations were performed by additions of aliquots of the putative anionic guest (AcO^-, Cl^-, F^-, PO_4^{3-}, SO_4^{2-}) as the tetrabutylammonium (TBA) salt solutions (20 mM made up in 1.199×10^{-5} M solutions of the receptors in DMSO) to a 1.199×10^{-5} M solution of the receptor in DMSO. Typically, up to 70 equivalents of the salts were added. After each addition, the resulting solution was stirred for at least 30 seconds and the absorbance was recorded. Both salt and receptor were dried under high vacuum prior to use. UV-Vis data was recorded using a Varian Cary 50 UV-Vis Spectrophotometer. The absorbance was recorded from 250 nm to 850 nm. To determine association constants for the receptor-anion complexes, global analysis of the absorbance data was carried out using the open access BindFit software program. Fluorescence titrations were carried out in parallel with the

UV/Vis absorption measurements using a Jasco FP-6300 spectrofluorometer. An example of a typical UV titration experimental layout is outlined in Table 6.1.

Table 6.1: An example of a typical UV titration experimental layout

Sample Number	Total Volume of anion added (µL)	Sample anion concentration (M)	Molar ratio Receptor:Anion
1	0.0	0.00E+00	1 : 0
2	1.8	1.20E-05	1 : 1
3	3.6	2.40E-05	1 : 2
4	5.4	3.59E-05	1 : 3
5	7.2	4.78E-05	1 : 4
6	9.0	5.98E-05	1 : 5
7	10.8	7.17E-05	1 : 6
8	12.6	8.36E-05	1 : 7
9	14.4	9.55E-05	1 : 8
10	16.2	1.07E-04	1 : 9
11	18.0	1.19E-04	1 : 10
12	27.0	1.78E-04	1 : 15
13	36.0	2.37E-04	1 : 20
14	54.0	3.53E-04	1 : 30
15	71.9	4.68E-04	1 : 40
16	89.9	5.82E-04	1 : 49
17	107.9	6.94E-04	1 : 58

Note: 3000 µL of the stock receptor solution always present, and the anion aliquots are drawn from a 20 mM sample.

6.3 NMR Binding Studies

NMR titrations were performed by additions of aliquots of the putative anionic guest (AcO^-, Cl^-, F^-, PO_4^{3-}, SO_4^{2-}) as the TBA salt solutions (200 mM made up in 2.5 × 10^{-3} M solutions of the receptors in DMSO-$_{d6}$) to a 2.5 × 10^{-3} M solution of the receptor in DMSO-$_{d6}$. Typically, up to 20 equivalents of the salts were added. Both salt and receptor were dried under high vacuum prior to use. ^{1}H NMR spectra were recorded on a Bruker Avance III 500 spectrometer at a frequency of 500.13 MHz and calibrated to the residual protio solvent peak in DMSO-d_6 (δ = 2.50 ppm). Stack plots were made using TopSpin 3.2. An example of a typical experimental layout is outlined in Table 6.2.

6.4 ^{1}H NMR Binding Studies of Novel Receptors

Procedure: A 2.5 mM stock solution of receptor was accurately prepared in the stated deuterated solvents (v/v) using a pipette (Eppendorf). Solutions of anions to be titrated were prepared in separate 3 ml Eppendorf vials and 200µL deuterated solvents (v/v) were added using pipettes. In each case, the host solution in an NMR tube was titrated with aliquots of anion stock solution and after each addition, and the ^{1}H NMR spectrum was recorded after thorough mixing at 300 K. Titrations were performed in triplicate to give accurate values. Typically a total of at least 20 equivalents of anion were added. Non-linear curve fitting of the experimentally obtained titration isotherms (equivalents of anion versus chemical shift of NH, aromatic CH and methylene CH protons) using the program TopSpin 3.2 and Microsoft excel 2010, enabled the calculation of association constants (Ka/M^{-1}) using the open access BindFit software program.[120]

Table 6.2: An example of a typical NMR titration experimental layout

Sample Number	Total Volume of Anion added (µL)	Sample Anion Concentration (M)	Molar Ratio Receptor:Anion
1	0.0	0.00E+00	5 : 0
2	1.3	4.99E-04	5 : 1
3	2.6	9.95E-04	5 : 2
4	3.9	1.49E-03	5 : 3
5	5.2	1.98E-03	5 : 4
6	6.5	2.47E-03	1 : 1
7	7.8	2.96E-03	5 : 6
8	9.1	3.44E-03	5 : 7
9	10.4	3.92E-03	5 : 8
10	11.7	4.40E-03	5 : 9
11	13.0	4.88E-03	1 : 2
12	20.0	7.51E-03	1 : 3
13	27.0	1.01E-02	1 : 4
14	41.5	1.52E-02	1 : 6
15	56.0	2.00E-02	1 : 8
16	70.5	2.46E-02	1 : 10
17	85.0	2.89E-02	1 : 12
18	100.0	3.86E-02	1 : 16
19	138.0	4.97E-02	1 : 20

Note: 500 µL of the stock receptor solution always present, and the anion aliquots are drawn from a 200 mM sample.

6.5 Synthesis and Characterisation of Compounds Described in Chapter 2

3,4-Diethoxycyclobut-3-ene-1,2-dione (74)[189]

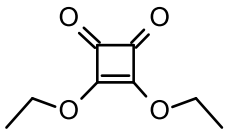

In a 250 mL round bottomed flask, squaric acid (5.00 g, 43.84 mmol, 1 eq) was dissolved in EtOH (50 mL), triethyl orthoformate (19.97 mL, 120.12 mmol, 2.74 eq) was added to the reaction mixture drop wise and the reaction mixture was heated under reflux for 24 hours. The reaction was monitored by TLC and was and concentrated on a rotary evaporator. The residue was purified by column chromatography (silica gel, DCM) to yield a clear yellow liquid (yield: 6.363 g, 85%). **^{1}H NMR,** ($CDCl_3$, 500.13 MHz) δ (ppm), *J* (Hz): 1.06 (t, *J* = 7.1, 3H, CH_3), 4.67 (q, *J* = 7.1, 2H, CH_2); **^{13}C NMR** ($CDCl_3$, 125.76 MHz): δ (ppm): 15.54, 70.51, 184.81, 189.23; **HRMS** (ESI) calcd. for $C_8H_{11}O_4$ $[M + H]^+$ 171.0652, found 171.0646; difference -3.50 ppm.

3-((3,5-Bis(trifluoromethyl)phenyl)amino)-4-ethoxycyclobut-3-ene-1,2-dione (75)

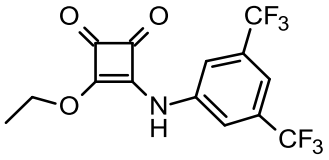

A solution of 3,5-bis(trifluoromethyl)aniline (1.835 mL, 11.75 mmol, 1eq) in EtOH (5 mL) was slowly added to a mixture of **74** (1.74 mL, 11.75 mmol, 1 eq) and zinc triflate (0.85 g, 2.35 mmol, 0.2 eq) in 5 mL EtOH. The reaction was stirred at room temperature overnight. The precipitate was collected by suction filtration and washed with EtOH and Et_2O to yield the product as an off-white amorphous solid. (3.28 g, 79%). **^{1}H NMR,** (DMSO-d_6, 500.13 MHz) δ (ppm), J (Hz): 1.41 (t, *J* = 7.1, 3H, CH_3), 4.79 (q, *J* = 7.1, 2H, CH_2), 7.78 (s, 1H, ArH), 8.03 (s, 2H, ArH), 11.19 (br, 1H, NH); **^{13}C NMR** (DMSO-d_6, 125.76 MHz): δ (ppm): 184.9, 179.7, 140.6, 131.7, 131.4, 131.2, 126.8, 124.6, 122.4, 119.9, 116.8, 70.5, 15.8; **HRMS** (ESI) calcd. for

$C_{14}H_{10}F_6NO_3$ $[M + H]^+$ 354.0559, found 354.0554; difference -1.64 ppm; **ν_{max} (KBr)/cm^{-1}:** 3254 (N-H), 3004 (ArH), 1717 (C=O), 1603 (ArH), 1278 (C-F), 1101 (C-O).

3-Ethoxy-4-((4-nitrophenyl)amino)cyclobut-3-ene-1,2-dione (76)

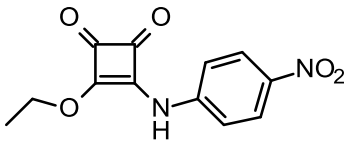

A solution of 4-nitroaniline (1.63 g, 11.75 mmol, 1 eq) in EtOH (5mL) was slowly added to a mixture of diethyl squarate (1.74 mL, 11.75 mmol, 1 eq) and zinc triflate (0.85 g, 2.35 mmol, 0.2 eq) in EtOH (5 mL). The reaction was stirred at room temperature overnight. The precipitate was collected by suction filtration and washed with EtOH and Et_2O to yield the product as an orange amorphous solid (2.901 g, 94%). **^{1}H NMR,** (DMSO-*d_6*, 500.13 MHz) δ (ppm), *J* (Hz): 1.44 (t, *J* = 7.1, 3H, CH_3), 4.80 (q, *J* = 7.1, 2H, CH_2), 7.59 (d, *J* = 9.0, 2H, ArH), 8.24 (d, *J* = 9.0, 2H, ArH), 11.22 (s, 1H, NH); **^{13}C NMR** (DMSO-*d_6*, 125.76 MHz): δ (ppm): 16.06, 70.66, 119.51, 125.75, 126.87, 142.97, 169.90, 185.25; **HRMS** (ESI) calcd. for $C_{12}H_{10}N_2NaO_5$ $[M + Na]^+$ 285.0482, found 285.0496; difference 4.84 ppm; **ν_{max} (KBr)/cm^{-1}:** 3304 (N-H), 3083 (ArH), 1715 (C=O), 1623 (ArH), 1531 (N-O), 1114 (C-O).

6-Bromo-2-ethyl-1H-benzo[de]isoquinoline-1,3(2H)-dione (78)

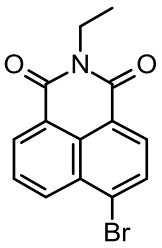

77, (2.0 g, 7.33 mmol, 1 eq) was mixed with ethylamine (0.57 mL, 8.66 mmol, 1.2 eq) in EtOH (10 mL). The reaction mixture was heated under reflux for 24 hours. The precipitate was collected by suction filtration and washed with EtOH and Et_2O to yield the product as a light tan amorphous solid. (1.74 g, 79%). **^{1}H NMR,** (DMSO-*d_6*, 500.13 MHz) δ (ppm), *J* (Hz): 1.21 (t, *J* = 7.0, 3H, CH_3), 4.06 (q, *J* = 7.0, 2H, CH_2), 7.99 (t, *J* = 8.0, 1H, ArH), 8.21 (d, *J* = 7.8, 1H, ArH), 8.32 (d, *J* = 7.8, 1H, ArH), 8.55 (m,

ArH); **^{13}C NMR** (DMSO-d_6, 125.76 MHz): δ (ppm): 163.1, 163.1, 133.0, 132.0, 131.8, 131.4, 130.3, 129.5, 129.3, 128.8, 123.3, 122.5, 35.4, 13.5; **HRMS** (ESI) calcd. for $C_{14}H_{11}BrNO_2$ $[M + H]^+$ 303.9968, found 303.9964; difference -1.11 ppm; **ν_{max} (KBr)/cm^{-1}:** 3086 (ArH), 1740 (C=O), 1456 (ArH), 1354 (C-H), 1325 (C-N), 562 (Br).

6-((2-Aminoethyl)amino)-2-ethyl-1H-benzo[de]isoquinoline-1,3(2H)-dione (79)

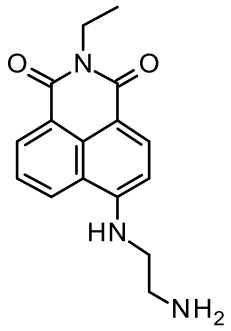

78, (1 g , 3.288 mmol, 1 eq) was stirred at room temperature overnight in neat ethylenediamine (10 mL, excess) to yield a dark orange liquid. The crude product was slowly added to deionised water (50 mL) and left to stir at room temperature for 2 hours. The precipitate was collected by suction filtration and washed with H_2O to yield the product as a yellow amorphous solid. (0.748 g, 80%). **^{1}H NMR,** (DMSO-d_6, 500.13 MHz) δ (ppm), *J* (Hz): 1.11 (t, *J* = 7.0, 3H, CH_3), 2.82 (t, *J* = 6.4, 2H, CH_2), 3.32 (t, *J* = 6.4, 2H, CH_2), 3.97 (q, *J* = 7.1, 2H, CH_2), 6.73 (d, *J* = 8.5, 1H, ArH), 7.60 (m, 1H, ArH), 8.18 (d, J = 8.5, 1H, ArH), 8.36 (dd, J = 7.3, J = 0.9, 1H, ArH), 8.63 (dd, J = 8.4, J = 0.8, 1H, ArH); **^{13}C NMR,** (DMSO-d_6, 125.76 MHz) δ (ppm): 13.7, 34.7, 46.7, 104.3, 108.1, 120.6, 122.3, 124.6, 129.0, 129.8, 131.0, 134.6, 151.3, 163.1, 164.0; **HRMS** (ESI) calcd. for $C_{16}H_{18}N_3O_2$ $[M + H]^+$ 284.1394, found 284.1389; difference -1.65 ppm; **ν_{max} (KBr)/cm^{-1}:** 3358 (N-H), 2979 (ArH), 1676 (C=O), 1461 (ArH), 1370 (C-H), 1249 (C-N).

Tert-butyl(2-aminoethyl)carbamate (81)[190]

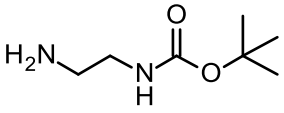

To a 500mL round bottom flask was added ethylenediamine (13.4 mL, 161.86 mmol, 10 eq) in $CHCl_3$ (100 mL). A solution of di-tert-butyl dicarbonate (4.4 g, 37.56 mmol, 1 eq) in $CHCl_3$ (50 mL) was added dropwise over 2 hours at 0°C and stirred at room for 24 hours. The reaction mixture was washed with brine, the organic layer was washed with H_2O and dried over $MgSO_4$. The filtrate was concentrated in vacuo to yield an off-white liquid. (2.012 g, 34%). **^{1}H NMR,** (DMSO-d_6, 500.13 MHz) δ (ppm), *J* (Hz): 1.36 (s, 9H, CH_3), 2.51 (d, *J* = 6.5, 2H, CH_2), 2.90 (d, *J* = 5.8, 2H, CH_2), 6.71 (s, 1H, NH); **^{13}C NMR** (DMSO-d_6, 125.76 MHz): δ (ppm): 28.7, 31.7, 42.0, 44.1, 77.8, 79.6, 156.1.

Tert-butyl(2-(6-nitro-1,3-dioxo-1H-benzo[de]isoquinolin-2(3H)-yl)ethyl)carbamate (82)

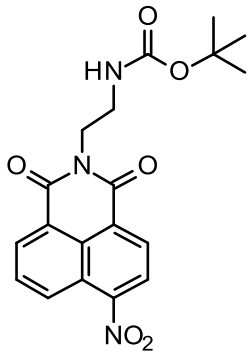

81, (0.565 mL, 3.54 mmol, 1 eq) was slowly added dropwise to a solution of **80**, (0.86 g, 3.54 mmol, 1 eq) in EtOH (20 mL). The reaction mixture was left to react in a 35 mL microwave tube for 1 hour at 110 °C, 1 mbar and 300 watts. The precipitate was collected by suction filtration and washed with EtOH and Et_2O to yield the product as a peach amorphous solid. (1.047 g, 76%). **^{1}H NMR,** (DMSO-d_6, 500.13 MHz) δ (ppm), *J* (Hz): 1.22 (s, 9H, CH_3), 3.27 (t, *J* = 6.0, 2H, CH_2), 4.14 (t, J = 6.0, 2H, CH_2), 6.88 (s, 1H, NH), 8.09 (t, *J* = 8.1, 1H, ArH), 8.55 (d, *J* = 8.0, 1H, , ArH), 8.62 (m, 2H, , ArH), 8.71 (d, *J* = 8.4, 1H, , ArH); **^{13}C NMR** (DMSO-d_6, 125.76 MHz): δ (ppm): 28.5, 38.0, 77.9, 123.1, 123.5, 124.6, 127.3, 128.9, 129.0, 129.9, 130.5, 132.0, 149.5, 156.2, 162.8, 163.6; **HRMS** (ESI) calcd. for $C_{38}H_{38}N_6NaO_{12}$ $[2M + Na]^+$ 794.2471, found 794.2493; difference 2.8 ppm; **ν_{max} (KBr)/cm^{-1}:** 3401 (N-H), 2977 (ArH), 1714 (C=O), 1593 (ArH), 1523 (N-O), 1365 (C-H), 1192 (C-N).

2-(2-Aminoethyl)-6-nitro-1H-benzo[de]isoquinoline-1,3(2H)-dione (83)

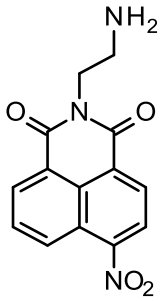

82, (1.02 g, 2.647 mmol, 1 eq) was dissolved in (TFA : DCM, 50 : 50) (6 mL) and was stirred at room temperature overnight. The solvent was removed under reduced pressure to yield a beige amorphous solid. (0.70 g, 93%). **^{1}H NMR,** (DMSO-d_6, 500.13 MHz) δ (ppm), *J* (Hz): 3.17 (m, 2H, CH_2), 4.33 (t, *J* = 5.6, 2H, CH_2), 7.81 (br, 2H, NH_2), 8.13 (m, 1H, ArH), 8.58 (d, *J* = 7.9, 1H, ArH), 8.66 (m, 2H, ArH), 8.76 (dd, J = 8.69, J = 0.8, 1H, ArH); **^{13}C NMR** (DMSO-d_6, 125.76 MHz): δ (ppm): 37.9, 38.2, 123.2, 123.4, 124.7, 127.2, 128.9, 129.4, 130.1, 130.6, 132.2, 149.7, 163.3, 164.0; **HRMS** (ESI) calcd. for $C_{14}H_{12}N_3O_4$ $[M + H]^+$ 286.0822, found 286.0800; difference -7.88 ppm; **ν_{max} (KBr)/cm^{-1}:** 3078 (ArH), 1712 (C=O), 1595 (ArH), 1525 (N-O), 1437 (C-H), 1247 (C-N).

6-Amino-2-(2-aminoethyl)-1H-benzo[de]isoquinoline-1,3(2H)-dione (84)

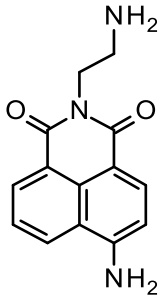

Pd/C (approx. 0.2 g) was added to a solution of **83**, (1.00 g, 3.50 mmol) dissolved in MeOH (40 mL). The reaction was placed under a H_2 atmosphere and left to stir at room temperature for 3 hours. The reaction was filtered through a pad of celite and washed with excess MeOH, the filtrate was removed under reduced pressure to yield a mustard amorphous solid. (0.673 g, 75%). **^{1}H NMR,** (DMSO-d_6, 500.13 MHz) δ (ppm), *J* (Hz): 3.12 (m, 2H, CH_2), 4.27 (t, *J* = 6.0, 2H, CH_2), 6.86 (d, *J* = 8.4, 1H, ArH),

7.48 (s, 2H, NH_2), 7.67 (m, 1H, ArH), 7.77 (br, 2H, NH_2), 8.21 (d, J = 8.4, 1H, ArH), 8.44 (dd, J = 7.3, J = 1.05, 1H, ArH), 8.63 (dd, J = 8.4, J = 1.1, 1H, ArH); **^{13}C NMR,** (DMSO-d_6, 125.76 MHz) δ (ppm): 37.6, 38.4, 108.0, 108.6, 119.8, 122.4, 124.4, 129.9, 130.4, 131.5, 134.5, 153.3, 163.9, 164.9; **HRMS** (ESI) calcd. for $C_{14}H_{13}N_3NaO_2$ $[M + Na]^+$ 279.0930, found 279.0914; difference -5.68 ppm; **ν_{max} (KBr)/cm^{-1}:** 3419 (N-H), 3362 (N-H), 3017 (ArH), 1636 (NH), 1485 (ArH), 1429 (C-H), 1247 (C-N).

6-((2-((2-((3,5-bis(trifluoromethyl)phenyl)amino)-3,4-dioxocyclobut-1-en-1-yl)amino)ethyl)amino)-2-ethyl-1H-benzo[de]isoquinoline-1,3(2H)-dione (85)

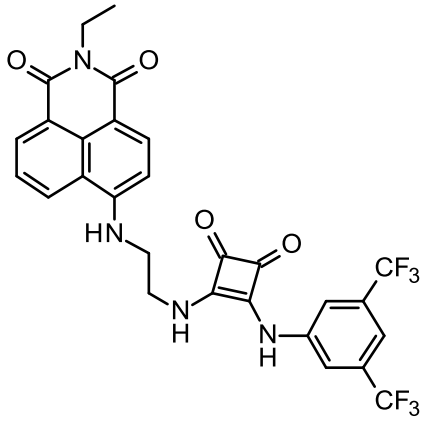

A solution of **75**, (0.436 g, 1.235 mmol, 1 eq) in EtOH (8 mL) was slowly added to a mixture of **79**, (0.35 g, 1.235 mmol, 1 eq) and Et_3N (0.689 mL, 4.94 mmol, 4 eq) in EtOH (12 mL). The reaction mixture was stirred at room temperature overnight. The precipitate was collected by suction filtration and washed with EtOH and Et_2O to yield the product as a yellow amorphous solid. (0.575 g, 78%). **^{1}H NMR at 343K,** (DMSO-d_6, 500.13 MHz) δ (ppm), *J* (Hz): 1.18 (t, *J* = 7.0, 3H, CH_3), 3.70 (q, *J* = 5.5, 2H, CH_2), 3.95 (t, *J* = 5.5, 2H, CH_2), 4.04 (q, *J* = 7.0, 2H, CH_2), 6.91 (d, *J* = 8.5, 1H, ArH), 7.47 (s, 1H, ArH), 7.63 (m, 2H, ArH), 7.80 (br, 2H, NH), 7.89 (s, 1H, ArH), 8.25 (d, *J* = 8.5, 1H, ArH), 8.39 (d, *J* = 7.0, 1H, ArH), 8.58 (d, *J* = 8.3, 1H, ArH), 9.68 (br, 1H, NH); **^{13}C NMR at 343K,** (DMSO-d_6, 125.76 MHz) δ (ppm): 13.6, 30.9, 34.6, 43.2, 44.2, 104.6, 109.1, 114.7, 118.3, 120.8, 122.5, 124.7, 128.6, 129.8, 130.9, 134.2, 141.5, 150.7, 163.1, 163.9, 171.2, 181.3; **HRMS** (ESI) calcd. for $C_{28}H_{21}F_6N_4O_4$ $[M + H]^+$ 591.1462 found 591.1439; difference -3.8 ppm; **ν_{max} (KBr)/cm^{-1}:** 3292 (N-H), 3086 (ArH), 2982 (C-H), 1796 (C=O), 1459 (C-H), 1278 (C-F), 1249 (C-N).

2-Ethyl-6-((2-((2-((4-nitrophenyl)amino)-3,4-dioxocyclobut-1-en-1-yl)amino)ethyl)amino)-1H-benzo[de]isoquinoline-1,3(2H)-dione (86)

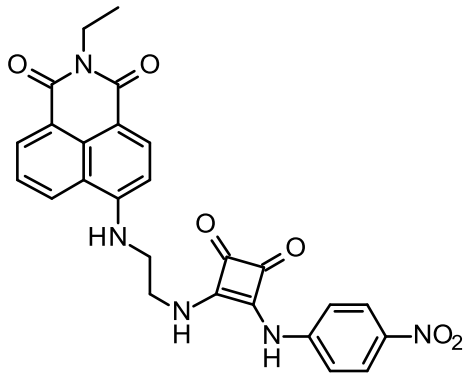

A solution of **76**, (0.324 g, 1.235 mmol, 1 eq) in EtOH (8 mL) was slowly added to a mixture of **79**, (0.35 g, 1.235 mmol, 1 eq) and Et_3N (0.689 mL, 4.94 mMol, 4 eq) in EtOH (12 mL). The reaction was stirred at room temperature. The precipitate was collected by suction filtration and washed with EtOH and Et_2O to yield the product as an orange amorphous solid. (0.453 g, 73%). **^{1}H NMR at 343K,** (DMSO-*d_6*, 500.13 MHz) δ (ppm), *J* (Hz): 1.18 (t, *J* = 7.1, 3H, CH_3), 3.70 (q, *J* = 6.0, 2H, CH_2), 3.96 (t, *J* = 6.0, 2H, CH_2), 4.03 (q, J = 7.0, 2H, CH_2), 6.91 (d, *J* = 8.5, 1H, ArH), 7.38 (br, 2H, NH), 7.64 (d, *J* = 10.7, 1H, ArH), 7.67 (d, *J* = 8.1, 2H, ArH), 8.07 (brS, 2H, ArH), 8.26 (d, *J* = 8.5, 1H, ArH), 8.42 (d, *J* = 7.2, 1H, ArH), 8.60 (d, *J* = 8.3, 1H, ArH), 9.87 (br, 1H, NH); **^{13}C NMR at 343K,** (DMSO-*d_6*, 125.76 MHz) δ (ppm): 13.6, 18.9, 34.6, 43.1, 44.2, 56.5, 104.7, 109.1, 118.1, 120.9, 122.6, 124.8, 125.6, 128.7, 129.8, 130.9, 134.2, 150.8, 163.1, 163.9, 181.3; **HRMS** (ESI) calcd. for $C_{26}H_{22}N_5O_6$ $[M + H]^+$ 500.1565, found 500.1557; difference -1.6 ppm; **ν_{max} (KBr)/cm^{-1}:** 3421 (NH), 3080 (ArH), 1797 (C=O), 1507 (N-O), 1419 (ArH), 1332 (N-O), 1246 (C-N).

6-Amino-2-(2-((2-((3,5-bis(trifluoromethyl)phenyl)amino)-3,4-dioxocyclobut-1-en-1-yl)amino)ethyl)-1H-benzo[de]isoquinoline-1,3(2H)-dione (87)

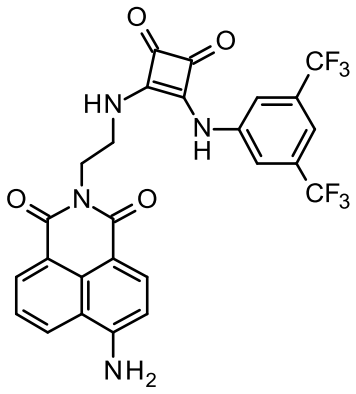

A solution of **75**, (0.14 g, 0.39 mmol, 1 eq) in EtOH (8 mL) was slowly added to a mixture of **84**, (0.1 g, 0.39 mmol, 1 eq) and Et_3N (0.217 mL, 1.56 mmol, 4 eq) in EtOH (10 mL). The reaction was stirred at room temperature overnight. The precipitate was collected by suction filtration and washed with EtOH and Et_2O to yield the product as an olive green amorphous solid. (0.123 g, 56%). **^{1}H NMR at 343K,** (DMSO-*d_6*, 500.13 MHz) δ (ppm), *J* (Hz): 3.90 (m, 2H, CH_2), 4.31 (t, *J* = 6.0, 2H, CH_2), 6.82 (d, *J* = 8.4, 1H, ArH), 7.22 (s, 2H, NH_2), 7.52 (s, 1H, ArH), 7.58 (t, *J* = 8.0, 1H, ArH), 7.89 (s, 2H, ArH), 8.15 (d, *J* = 8.4, 1H, ArH), 8.37 (d, *J* = 7.1, 1H, ArH), 8.57 (d, *J* = 8.4, 1H, ArH), 9.77 (br, 1H, NH); **^{13}C NMR at 343K,** (DMSO-*d_6*, 125.76 MHz) δ (ppm): 27.9, 42.9, 108.7, 114.8, 118.4, 119.9, 120.3, 122.2, 122.5, 124.2, 124.7, 129.0, 130.3, 131.3, 134.3, 141.7, 153.3, 163.3, 164.6, 171.4, 181.3; **HRMS** (ESI) calcd. for $C_{26}H_{17}F_6N_4O_4$ $[M + H]^+$ 565.1207, found 565.1231; difference 4.31 ppm; **ν_{max} (KBr)/cm^{-1}:** 3371 (N-H), 3254 (N-H), 1796 (C=O), 1636 (N-H), 1476 (ArH), 1378 (C-H), 1276 (C-F), 1250 (C-N).

6-Amino-2-(2-((2-((4-nitrophenyl)amino)-3,4-dioxocyclobut-1-en-1-yl)amino)ethyl)-1H-benzo[de]isoquinoline-1,3(2H)-dione (88)

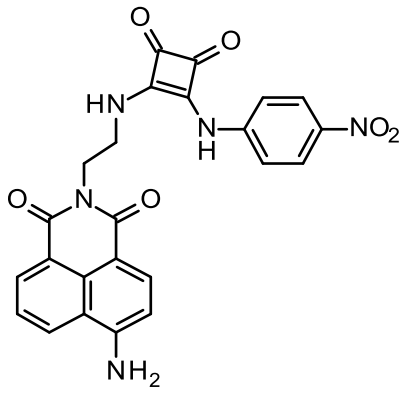

A solution of **76**, (0.1 g, 0.39 mmol, 1 eq) in EtOH (8 mL) was slowly added to a mixture of **84**, (0.1 g, 0.39 mmol, 1 eq) and Et_3N (0.217 mL, 1.56 mmol, 4 eq) in EtOH (10 mL). The reaction was stirred at room temperature overnight. The precipitate was collected by suction filtration and washed with EtOH and Et_2O to yield the product as an orange amorphous solid. (0.124 g, 67%). **^{1}H NMR at 343K,** (DMSO-d_6, 500.13 MHz) δ (ppm), *J* (Hz): 3.95 (t, *J* = 5.4, 2H, CH_2), 4.33 (t, *J* = 5.5, 2H, CH_2), 6.84 (d, *J* = 8.3, 1H, ArH), 7.23 (brS, 2H, ArH), 7.40 (br, 2H, NH_2), 7.60 (t, *J* = 7.8, 1H, ArH), 8.08 (m, 2H, ArH), 8.17 (d, *J* = 8.4, 1H, ArH), 8.40 (d, *J* = 6.8, 1H, ArH), 8.59 (d, *J* = 7.8, 1H, ArH), 9.67 (br, 1H, NH) (16 H and not the expected 17 H signals are recorded for this compound); **^{13}C NMR at 343K,** (DMSO-d_6, 125.76 MHz) δ (ppm): 16.0, 43.0, 108.2, 108.7, 118.1, 120.0, 122.3, 124.3, 125.4, 125.7, 129.0, 130.3, 131.4, 134.3, 142.0, 145.7, 153.2, 162.6, 163.6, 164.6, 171.5, 181.3 (although not symmetrical the squaramide 13C signals appeared as coincident in this spectrum); **HRMS** (ESI) calcd. for $C_{24}H_{18}N_5O_6$ $[M + H]^+$ 472.1252, found 472.1248; difference -0.79 ppm; **ν_{max} (KBr)/cm^{-1}:** 3361 (N-H), 3250 (N-H), 1796 (C=O), 1622 (N-H), 1504 (N-O), 1432 (ArH), 1368 (C-H), 1328 (N-O), 1247 (C-N).

6.6 Synthesis and Characterisation of Compounds Described in Chapter 4

4,4'-((Methylenebis(4,1-phenylene))bis(azanediyl))bis(3-ethoxycyclobut-3-ene-1,2-dione) (122)

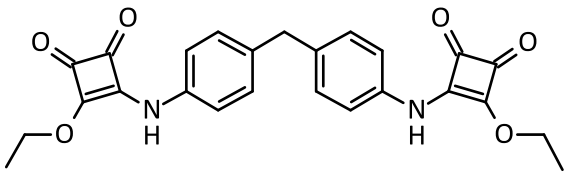

A solution of **117**, (0.037 g, 0.19 mmol, 1 eq) in EtOH (3 mL) was slowly added to a mixture of **74**, (0.1 g, 0.58 mmol, 3 eq) and zinc triflate (0.014 g, 0.038 mmol, 0.2) in EtOH (5 mL). The reaction was stirred at room temperature for 24 hours. The precipitate was collected by suction filtration and washed with EtOH and Et_2O to yield the product as a tan amorphous solid. (0.079 g, 93%). **^{1}H NMR,** (DMSO-d_6, 500.13 MHz) δ (ppm), *J* (Hz): 1.40 (t, *J* = 7.1, 6H, CH_3), 3.86 (s, 2H, CH_2), 4.74 (q, *J* = 7.1, 4H, CH_2), 7.27 (d, *J* = 8.5, 4H, ArH), 7.19 (m, 4H, ArH), 10.69 (s, 2H, NH); **^{13}C NMR,** (DMSO-d_6, 125.76 MHz) δ (ppm): 10.4, 16.1, 46.2, 69.9, 120.2, 129.6, 136.4, 137.6, 169.9, 184.0; **HRMS** (ESI) calcd. for $C_{25}H_{23}N_2O_6$ $[M + H]^+$ 447.1551, found 447.1540; difference -2.31 ppm.

4,4'-((Methylenebis(4,1-phenylene))bis(azanediyl))bis(3-(butylamino)cyclobut-3-ene-1,2-dione) (132)

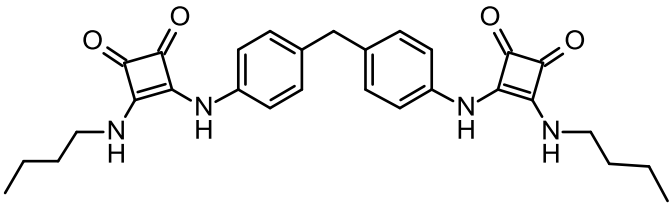

A mixture of **125**, (0.22 mL, 2.24 mmol, 2 eq) and Et_3N (0.63 mL, 4.48 mmol, 1 eq) in DMF (5 mL) was slowly added to a solution of **122**, (0.5 g, 1.12 mmol) in DMF (5 mL), the reaction mixture was stirred at room temperature for 24 hours. The precipitate was collected by suction filtration and washed with EtOH and Et_2O to yield the product as an off-white amorphous solid. (0.482 g, 86%). **^{1}H NMR,** (DMSO-d_6, 500.13 MHz) δ (ppm), *J* (Hz): 0.90 (t, *J* = 7.2, 6H, CH_3), 1.34 (q, *J* = 6.7, 4H, CH_2),

1.54 (t, *J* = 7.0, 4H, CH_2), 3.59 (s, 4H, CH_2), 3.84 (s, 2H, CH_2), 7.18 (d, *J* = 7.8, 4H, ArH), 7.32 (brS, 4H, ArH), 7.58 (br, 2H, NH), 9.55 (br, 2H, NH); **HRMS** (ESI) calcd. for $C_{29}H_{33}N_4O_4$ $[M + H]^+$ 501.2496, found 501.2515; difference 3.68 ppm; **ν_{max} (KBr)/cm^{-1}:** 3251 (N-H), 3045 (ArH), 1793 (C=O), 1615 (ArH), 1470 (C-H).

4,4'-((Methylenebis(4,1-phenylene))bis(azanediyl))bis(3-((4-hydroxybenzyl)amino)cyclobut-3-ene-1,2-dione) (135)

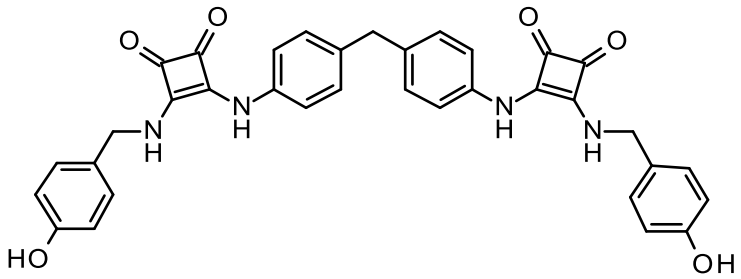

A mixture of **128**, (0.276 g, 2.24 mmol, 2 eq) and Et_3N (0.63 mL, 4.48 mmol, 4 eq) in DMF (5 mL) was slowly added to a solution of **122**, (0.5 g, 1.12 mmol, 1 eq) in DMF (5 mL), the reaction mixture was stirred at room temperature for 24 hours. The precipitate was collected by suction filtration and washed with EtOH and Et_2O to yield the product as a grey amorphous solid. (0.622 g, 93%). **^{1}H NMR,** (DMSO-*d_6*, 500.13 MHz) δ (ppm), *J* (Hz): 3.83 (d, *J* = 8.3, 2H, CH_2), 4.66 (s, 4H, CH_2), 6.75 (d, *J* = 8.3, 4H, ArH), 7.16 (m, 8H, ArH), 7.31 (d, *J* = 8.0, 4H, ArH), 7.91 (br, 2H, OH), 9.5 (s, 4H, NH); **^{13}C NMR** (DMSO-*d_6*, 125.76 MHz): δ (ppm): 16.1, 31.2 47.3, 69.9, 115.8, 118.6, 129.0, 129.6, 129.9, 136.1, 136.3, 137.4, 137.4, 157.4, 162.8, 164.1, 169.0, 180.0, 184.3; **HRMS** (ESI) calcd. for $C_{35}H_{29}N_4O_6$ $[M + H]^+$ 601.2082, found 601.2096; difference 2.32 ppm; **ν_{max} (KBr)/cm^{-1}:** 3249 (N-H), 3194 (O-H), 3042 (ArH), 1795 (C=O), 1613 (ArH), 1467 (C-H), 1251 (C-O).

4,4'-((Methylenebis(4,1-phenylene))bis(azanediyl))bis(3-((pyridin-4-ylmethyl)amino)cyclobut-3-ene-1,2-dione) (136)

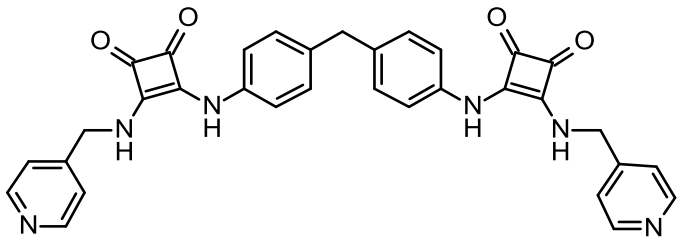

A mixture of **129**, (0.277 mL, 2.24 mmol, 2 eq) and Et_3N (0.63 mL, 4.48 mmol, 4 eq) in DMF (5 mL) was slowly added to a solution of **122**, (0.5 g, 1.12 mmol, 1 eq) in DMF (5 mL). The reaction mixture was stirred at room temperature for 24 hours. The precipitate was collected by suction filtration and washed with EtOH and Et_2O to yield the product as a beige amorphous solid. (0.587 g, 92%). **^{1}H NMR,** (DMSO-d_6, 500.13 MHz) δ (ppm), *J* (Hz): 3.84 (s, 2H, CH_2), 4.83 (d, *J* = 5.6, 4H, CH_2), 7.18 (d, *J* = 7.4, 4H, ArH), 7.32 (d, *J* = 7.7, 4H, ArH), 7.35 (d, *J* = 4.6, 4H, ArH), 8.02 (s, 2H, NH), 8.55 (m, 4H, ArH), 9.72 (s, 2H, NH); **HRMS** (ESI) calcd. for $C_{33}H_{27}N_6O_4$ $[M + H]^+$ 571.2088, found 571.2095; difference 1.22 ppm; **ν_{max} (KBr)/cm^{-1}:** 3245 (N-H), 3038 (ArH), 1793 (C=O), 1656 (C=N), 1614 (ArH), 1467 (C-H), 1210 (C-N).

Dimethyl (1,3-phenylenebis(propane-2,2-diyl))dicarbamate (119)

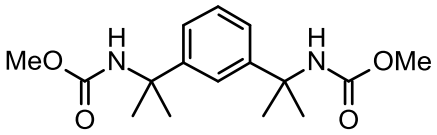

A solution of **118**, (10 mL, 43 mmol) in MeOH (30 mL) was stirred for 3 days at ambient conditions. The solvent was removed under reduced pressure to yield the crude product as a colourless gel-like residue. The residue was left to dry at room temperature to yield the product at a white amorphous solid. (12.68 g, 95%). **^{1}H NMR**, (DMSO-d_6, 500.13 MHz) δ (ppm), *J* (Hz): 1.49 (s, 12H, CH_3), 3.44 (s, 6H, CH_3), 7.12 (m, 2H, ArH), 7.18 (m, 1H, ArH), 7.30 (s, 1H, ArH), 7.46 (s, 2H, NH); **^{13}C NMR,** (DMSO-d_6, 125.76 MHz) δ (ppm): 30.1, 33.4, 51.1, 52.5, 54.9, 121.6, 121.7, 122.5, 122.8, 127.8, 148.0; **HRMS** (ESI) calcd. for $C_{16}H_{24}N_2NaO_4$ $[M + Na]^+$ 331.1628, found

331.1649; difference 6.34 ppm; **ν_{max} (KBr)/cm^{-1}:** 3318 (N-H), 3051 (ArH), 1605 (C=O), 1537 (ArH), 1443 (C-H), 1264 (C-O).

2,2'-(1,3-Phenylene)bis(propan-2-amine) (120)

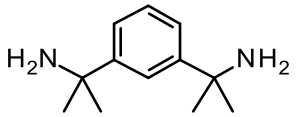

A solution of **119**, (5.40 g, 17.5 mmol, 1 eq) in n-BuOH (50 mL) containing potassium hydroxide (6.00 g, 106.94 mmol, 6.1 eq) was heated under reflux for 24 hours. Vacuum evaporation of the solvent left an oily residue which was dissolved in H_20 (25 mL) and extracted in THF (3 x 25 mL), followed by drying over Na_2SO_4 and removal of all volatile material to yield the product as a yellow oil. (3.23 g, 96%). **^{1}H NMR,** ($CDCl_3$, 500.13 MHz) δ (ppm), *J* (Hz): 1.50 (s, 12H, CH_3), 1.65 (br, 4H, NH_2), 7.29 (m, 1H, ArH), 7.35 (m, 2H, ArH), 7.69 (m, 1H, ArH); **^{13}C NMR,** ($CDCl_3$, 125.76 MHz) δ (ppm): 32.98, 52.57, 120.88, 122.61, 127.96, 150.20; **HRMS** (ESI) calcd. for $C_{24}H_{41}N_4$ $[2M + H]^+$ 386.3356, found 386.3345; difference -2.85 ppm.

4,4'-((1,3-Phenylenebis(propane-2,2-diyl))bis(azanediyl))bis(3-ethoxycyclobut-3-ene-1,2-dione) (123)

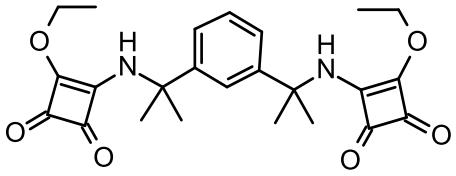

A mixture of **120**, (0.113 g, 0.58 mmol, 1 eq) and Et_3N (0.32 mL, 2.32 mmol, 4 eq) in EtOH (5 mL) was slowly added to a solution of **74**, (0.26 mL, 1.76 mmol, 3 eq) in EtOH (5 mL), the reaction mixture was stirred at room temperature for 24 hours. The reaction was monitored by TLC and was concentrated on a rotary evaporator to yield a yellow residue. The crude product was purified by column chromatography (silica gel, 3% MeOH in DCM). The solvent was removed under reduced pressure to yield a sticky yellow residue. (0.189 g, 74%). **^{1}H NMR,** ($CDCl_3$, 500.13 MHz) δ (ppm), *J* (Hz): 1.13 (m, 6H, CH_3), 1.68 (s, 12H, CH_3), 4.44 (m, 4H, CH_2), 7.19 (brS, 2H, ArH), 7.43 (brS, 1H, ArH), 7.93 (brS, 1H, ArH); **^{13}C NMR,** ($CDCl_3$, 125.76 MHz) δ (ppm):

15.3, 30.8, 53.5, 58.4, 68.6, 121.8, 123.3, 128.5, 146.8, 172.0, 176.3, 184.1, 190.1; **HRMS** (ESI) calcd. for $C_{24}H_{29}N_2O_6$ $[M + H]^+$ 441.2020, found 441.2011; difference -2.05 ppm.

4,4'-((1,3-phenylenebis(propane-2,2-diyl))bis(azanediyl))bis(3-(butylamino)cyclobut-3-ene-1,2-dione) (137)

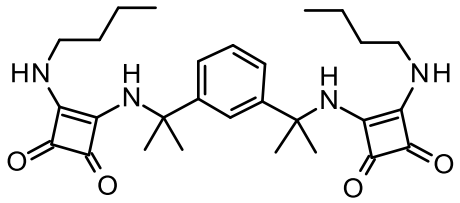

A mixture of **125**, (0.27 mL, 2.72 mmol, 4 eq) and Et_3N (0.38 mL, 2.72 mmol, 4 eq) in EtOH (5 mL) was slowly added to a solution of **123**, (0.30 g, 0.68 mmol, 1 eq) in EtOH (5 mL). The reaction mixture was stirred at room temperature for 24 hours. The precipitate was collected by suction filtration and washed with EtOH and Et_2O to yield the product as an off-white amorphous solid. (0.315 g, 93%). **^{1}H NMR,** (DMSO-d_6, 500.13 MHz) δ (ppm), *J* (Hz): 0.88 (t, *J* = 7.4, 6H, CH_3), 1.31 (m, 4H, CH_2), 1.48 (m, 4H, CH_2), 1.73 (s, 12H, CH_3), 3.53 (q, *J* = 6.5, 4H, CH_2), 7.32 (m, 4H, ArH), 7.44 (s, 2H, NH), 7.81 (s, 2H, NH); **^{13}C NMR,** (DMSO-d_6, 125.76 MHz) δ (ppm): 13.9, 19.4, 30.9, 33.1, 43.5, 57.8, 79.6, 122.3, 124.1, 128.8, 147.5, 168.3, 169.1, 180.9, 183.3; **HRMS** (ESI) calcd. for $C_{28}H_{39}N_4O_4$ $[M + H]^+$ 495.2966, found 495.2985; difference 3.92 ppm; **ν_{max} (KBr)/cm^{-1}:** 3233 (N-H), 2959 (ArH), 1792 (C=O), 1578 (ArH), 1457 (C-H).

4,4'-((1,3-Phenylenebis(propane-2,2-diyl))bis(azanediyl))bis(3-(decylamino)cyclobut-3-ene-1,2-dione) (138)

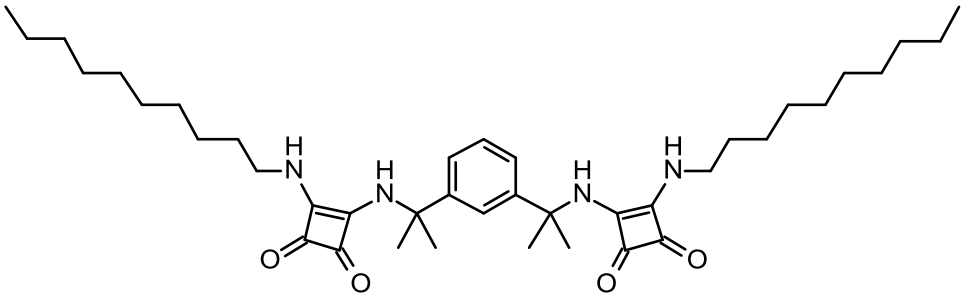

A mixture of **126**, (0.55 mL, 2.72 mmol, 4 eq) and Et_3N (0.38 mL, 2.72 mmol, 4 eq) in EtOH (5 mL) was slowly added to a solution of **123**, (0.30 g, 0.68 mmol, 1 eq) in EtOH (5 mL). The reaction mixture was stirred at room temperature for 24 hours. The precipitate was collected by suction filtration and washed with EtOH and Et_2O to yield the product as an off-white amorphous solid. (0.358 g, 79%). **^{1}H NMR,** (DMSO-d_6, 500.13 MHz) δ (ppm), *J* (Hz): 0.85 (t, *J* = 6.8, 6H, CH_3), 1.25 (m, 28H, CH_2), 1.49 (t, J = 6.7, 4H, CH_2), 1.72 (s, 12H, CH_3), 7.32 (m, 3H, ArH), 7.44 (s, 1H, ArH), 7.80 (br, 2H, NH); **^{13}C NMR,** (DMSO-d_6, 125.76 MHz) δ (ppm): 14.4, 22.5, 26.3, 29.0, 29.1, 29.4, 29.5, 30.9, 31.1, 31.7, 43.8, 57.8, 122.3 124.1, 128.7, 147.5, 168.3, 169.1, 183.2; **HRMS** (ESI) calcd. for $C_{80}H_{125}N_8O_8$ $[2M + H]^+$ 1325.9615, found 1325.9669; difference 4.08 ppm; **ν_{max} (KBr)/cm^{-1}:** 3224 (N-H), 2923 (ArH), 1792 (C=O), 1571 (ArH), 1458 (C-H).

4,4'-((1,3-Phenylenebis(propane-2,2-diyl))bis(azanediyl))bis(3-(benzylamino)cyclobut-3-ene-1,2-dione) (139)

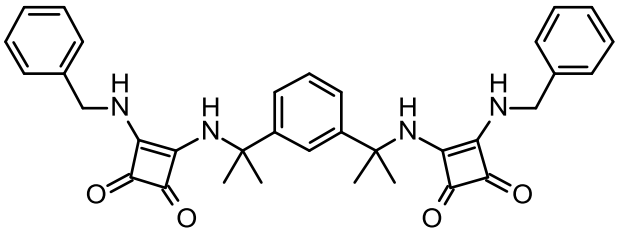

A mixture of **127**, (0.297 mL, 2.72 mmol, 4 eq) and Et_3N (0.38 mL, 2.72 mmol, 4 eq) in EtOH (5 mL) was slowly added to a solution of **123**, (0.30 g, 0.68 mmol, 1 eq) in EtOH (5 mL). The reaction mixture was stirred at room temperature for 24 hours.

The precipitate was collected by suction filtration and washed with EtOH and Et_2O to yield the product as a white amorphous solid. (0.29 g, 76%). **^{1}H NMR,** (DMSO-d_6, 500.13 MHz) δ (ppm), *J* (Hz): 1.71 (s, 12H, CH_3), 4.73 (d, *J* = 6.1, 4H, CH_2), 7.34 (m, 14H, ArH), 7.85 (br, 4H, NH); **^{13}C NMR,** (DMSO-d_6, 125.76 MHz) δ (ppm): 30.8, 47.4, 56.5, 57.9, 122.3, 124.1, 128.0, 128.1, 128.8, 129.1, 139.1, 147.4, 168.5, 168.7, 183.3; **HRMS** (ESI) calcd. for $C_{34}H_{35}N_4O_4$ $[M + H]^+$ 563.2653, found 563.2673; difference 3.55 ppm; **ν_{max} (KBr)/cm^{-1}:** 3229 (N-H), 2966 (ArH), 1793 (C=O), 1442 (C-H).

4,4'-((1,3-Phenylenebis(propane-2,2-diyl))bis(azanediyl))bis(3-((4-hydroxybenzyl)amino)cyclobut-3-ene-1,2-dione) (140)

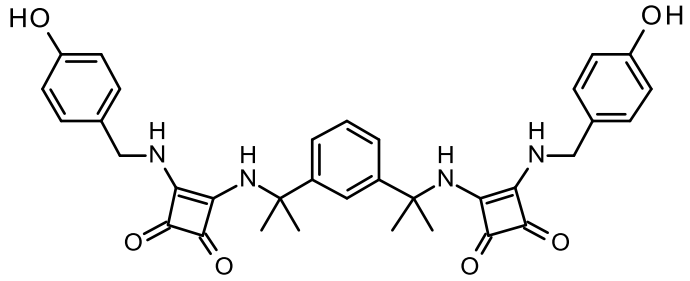

A mixture of **128**, (0.34 g, 2.72 mmol, 4 eq) and Et_3N (0.38 mL, 2.72 mmol, 4 eq) in EtOH (5 mL) was slowly added to a solution of **123**, (0.30 g, 0.68 mmol, 1 eq) in EtOH (5 mL). The reaction mixture was stirred at room temperature for 24 hours. The precipitate was collected by suction filtration and washed with EtOH and Et_2O to yield the product as a beige amorphous solid. (0.339 g, 84%). **^{1}H NMR,** (DMSO-d_6, 500.13 MHz) δ (ppm), *J* (Hz): 1.71 (s, 12H, CH_3), 4.60 (s, 4H, CH_2), 6.75 (d, *J* = 7.9, 4H, ArH), 7.14 (d, *J* = 7.6, 4H, ArH), 7.29 (brS, 3H, ArH), 7.42 (s, 1H, ArH), 7.71 (s, 2H, NH), 7.80 (s, 2H, NH), 9.41 (br, 2H, OH); **^{13}C NMR** (DMSO-d_6, 125.76 MHz): δ (ppm): 12.2, 19.0, 30.8, 46.1, 47.1, 56.5, 57.8, 115.8, 122.3, 124.1, 147.4, 157.3, 168.4, 168.5, 181.0, 183.3; **HRMS** (ESI) calcd. for $C_{34}H_{35}N_4O_6$ $[M + H]^+$ 595.2551, found 595.2568; difference 2.85 ppm; **ν_{max} (KBr)/cm^{-1}:** 3223 (N-H), 2972 (ArH), 1792 (C=O) 1570 (ArH), 1367 (C-H), 1230 (C-O).

4,4'-((1,3-Phenylenebis(propane-2,2-diyl))bis(azanediyl))bis(3-((pyridin-4-ylmethyl)amino)cyclobut-3-ene-1,2-dione) (141)

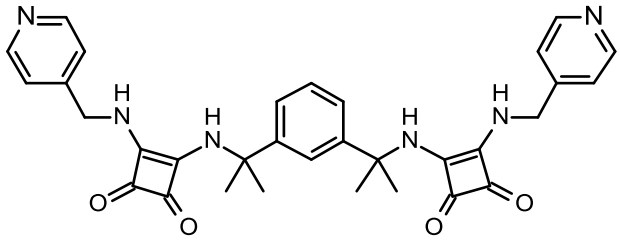

A mixture of **129**, (0.276 mL, 2.72 mmol, 4 eq) and Et_3N (0.38 mL, 2.72 mmol, 4 eq) in EtOH (5 mL) was slowly added to a solution of **123**, (0.30 g, 0.68 mmol, 1 eq) in EtOH (5 mL). The precipitate was collected by suction filtration and washed with EtOH and Et_2O to yield the product as a light yellow amorphous solid. (0.372 g, 96%). **^{1}H NMR,** (DMSO-*d_6*, 500.13 MHz) δ (ppm), *J* (Hz): 1.73 (s, 12H, CH_3), 4.77 (d, *J* = 6.4, 4H, CH_2), 7.35 (m, 8H, ArH), 7.97 (br, 4H, NH), 8.54 (m, 4H, ArH); **^{13}C NMR** (DMSO-*d_6*, 125.76 MHz): δ (ppm): 30.9, 44.1, 46.2, 58.0, 121.8, 122.3, 122.6, 122.9, 123.5, 124.2, 128.8, 147.5, 148.1, 149.8, 150.3, 168.8, 168.8, 181.5, 183.2; **HRMS** (ESI) calcd. for $C_{32}H_{33}N_6O_4$ $[M + H]^+$ 565.2558, found 565.2572; difference 2.47 ppm; **ν_{max} (KBr)/cm^{-1}:** 3236 (N-H), 2967 (ArH), 1794 (C=O) 1667 (C=N), 1535 (ArH), 1413 (C-H), 1209 (C-N).

4,4'-((Methylenebis(2,6-diethyl-4,1-phenylene))bis(azanediyl))bis(3-ethoxycyclobut-3-ene-1,2-dione) (124)

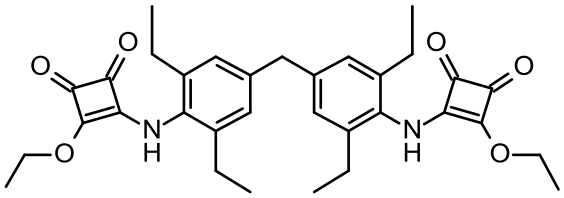

A mixture of **121**, (0.2 g, 0.644 mmol, 1 eq) and Et_3N (0.55 mL, 3.86 mmol, 6.0 eq) in EtOH (5 mL) was slowly added to a mixture of **74**, (0.286 mL, 1.932 mmol, 3 eq) and zinc triflate (0.047 g, 0.13 mmol, 0.2 eq) in EtOH (5 mL), the reaction mixture was heated under reflux for 7 days. The reaction was monitored by TLC and was concentrated on a rotary evaporator to yield a dark yellow residue. The crude

product was purified by column chromatography (silica gel, 3% MeOH in DCM). The solvent was removed under reduced pressure to yield the product as a yellow liquid. (0.23 g, 59%). **^{1}H NMR,** ($CDCl_3$, 500.13 MHz) δ (ppm), *J* (Hz): 1.16 (m, 18H, CH_3), 2.57 (m, 8H, CH_2), 3.95 (s, 2H, CH_2), 4.57 (brS, 4H, CH_2), 6.92 (s, 4H, ArH), 8.11 (br, 2H, NH); **^{13}C NMR,** ($CDCl_3$, 125.76 MHz) δ (ppm): 13.57, 14.60, 23.68, 40.32, 68.55, 126.07, 129.84, 140.08, 140.37, 171.14, 177.99, 182.74, 188.66; **HRMS** (ESI) calcd. for $C_{33}H_{39}N_2O_6$ $[M + H]^+$ 559.2803, found 559.2789; difference -2.39 ppm.

4,4'-((Methylenebis(2,6-diethyl-4,1-phenylene))bis(azanediyl))bis(3-(butylamino)cyclobut-3-ene-1,2-dione) (142)

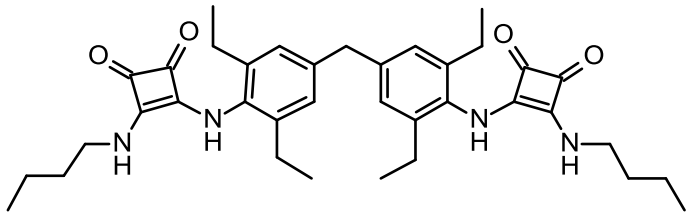

A mixture of **125**, (0.21 mL, 2.15 mmol, 4 eq) and Et_3N (0.30 mL, 2.15 mmol, 4 eq) in EtOH (5 mL) was slowly added to a solution of **124**, (0.30 g, 0.54 mmol, 1 eq) in EtOH (5 mL). The reaction mixture was stirred at room temperature for 24 hours. The precipitate was collected by suction filtration and washed with EtOH and Et_2O to yield the product as an off-white amorphous solid (0.182 g, 55%). **^{1}H NMR,** (DMSO-d_6, 500.13 MHz) δ (ppm), *J* (Hz): 1.16 (m, 30H, CH_2 and CH_3), 3.30 (m, 8H, CH_2), 3.90 (s, 2H, CH_2), 7.02 (s, 4H, ArH), 7.49 (br, 2H, NH), 8.68 (br, 2H, NH); **^{13}C NMR,** (DMSO-d_6, 125.76 MHz) δ (ppm): 14.0, 14.8, 19.4, 24.7, 33.2, 43.7, 79.6, 127.0, 132.5, 140.6, 141.2, 167.6, 168.7, 181.7, 184.3; **HRMS** (ESI) calcd. for $C_{37}H_{49}N_4O_4$ $[M + H]^+$ 613.3748, found 613.3767; difference 3.07 ppm; **ν_{max} (KBr)/cm^{-1}:** 3238 (N-H), 2963 (ArH), 1796 (C=O), 1527 (ArH), 1445 (C-H).

4,4'-((Methylenebis(2,6-diethyl-4,1-phenylene))bis(azanediyl))bis(3-(decylamino)cyclobut-3-ene-1,2-dione) (143)

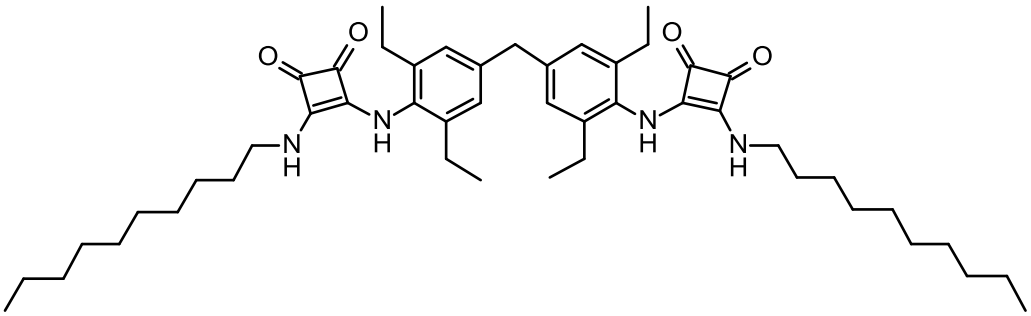

A mixture of **126,** (0.43 mL, 2.15 mmol, 4 eq) and Et_3N (0.30 mL, 2.15 mmol, 4 eq) in EtOH (5 mL) was slowly added to a solution of **124**, (0.30 g, 0.54 mmol, 1 eq) in EtOH (5 mL). The reaction mixture was stirred at room temperature for 24 hours. The precipitate was collected by suction filtration and washed with EtOH and Et_2O to yield the product as a white amorphous solid. (0.139 g, 33%). **^{1}H NMR,** (DMSO-d_6, 500.13 MHz) δ (ppm), *J* (Hz): 0.85 (t, *J* = 6.8, 6H, CH_3), 1.08 (t, *J* = 7.5, 12H, CH_3), 1.51 (m, 32H, CH_2), 2.52 (m, 8H, CH_2), 3.54 (brS, 4H, CH_2), 3.90 (s, 2H, CH_2), 7.02 (s, 4H, ArH), 7.48 (br, 2H, NH), 8.66 (br, 2H, NH); **^{13}C NMR,** (DMSO-d_6, 125.76 MHz) δ (ppm): 184.3, 168.7, 168.6, 167.5, 141.5, 141.1, 140.6, 127.0, 79.6, 79.4, 79.1, 31.7, 31.1, 29.4, 29.3, 29.1, 29.0, 26.2, 24.7, 22.5, 14.8, 14.4; **HRMS** (ESI) calcd. for $C_{49}H_{73}N_4O_4$ $[M + H]^+$ 781.5626, found 781.5672; difference 5.82 ppm; **ν_{max} (KBr)/cm^{-1}:** 3245 (N-H), 2925 (ArH), 1797 (C=O), 1528 (ArH), 1441 (C-H).

4,4'-((Methylenebis(2,6-diethyl-4,1-phenylene))bis(azanediyl))bis(3-(benzylamino)cyclobut-3-ene-1,2-dione) (144)

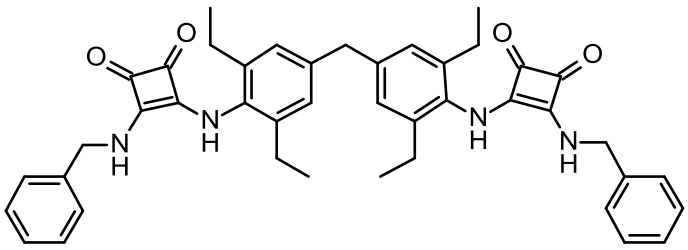

A mixture of **127**, (0.24 mL, 2.15 mmol, 4 eq) and Et_3N (0.30 mL, 2.15 mmol, 4 eq) in EtOH (5 mL) was slowly added to a solution of **124**, (0.30 g, 0.54 mmol, 1 eq) in

EtOH (5 mL). The reaction mixture was stirred at room temperature for 24 hours. The precipitate was collected by suction filtration and washed with EtOH and Et_2O to yield the product as an off-white amorphous solid. (0.219 g, 59%). **^{1}H NMR,** (DMSO-d_6, 500.13 MHz) δ (ppm), *J* (Hz): 1.04 (t, *J* = 7.1, 12H, CH_3), 3.30 (m, 8H, CH_2), 3.88 (s, 2H, CH_2), 4.77 (s, 4H, CH_2), 7.00 (s, 4H, ArH), 7.32 (m, 10H, ArH), 7.92 (br, 2H, NH), 8.69 (br, 2H, NH); **^{13}C NMR,** (DMSO-d_6, 125.76 MHz) δ (ppm): 184.4, 168.3, 167.8, 141.2, 140.6, 139.3, 132.4 129.0, 128.8, 128.6, 128.4, 127.8, 127.3, 127.2, 127.0, 126.6, 79.6, 47.3, 24.6, 14.8; **HRMS** (ESI) calcd. for $C_{43}H_{45}N_4O_4$ $[M + H]^+$ 681.3435, found 681.3447; difference 1.7 ppm; **ν_{max} (KBr)/cm^{-1}:** 3225 (N-H), 2964 (ArH), 1797 (C=O), 1527 (ArH), 1451 (C-H).

4,4'-((Methylenebis(2,6-diethyl-4,1-phenylene))bis(azanediyl))bis(3-((4-hydroxybenzyl)amino)cyclobut-3-ene-1,2-dione) (145)

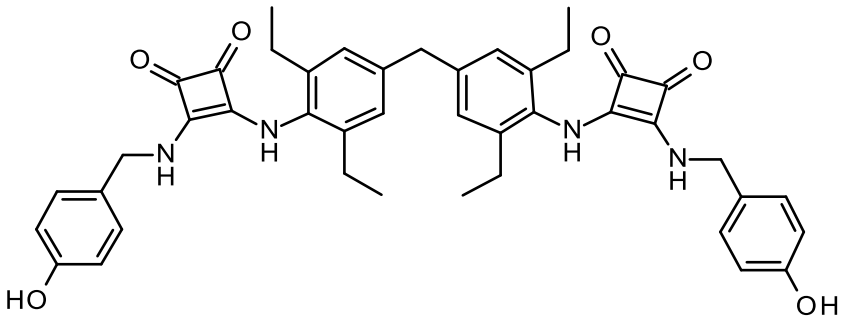

A mixture of **128**, (0.31 g, 2.52 mmol, 4 eq) and Et_3N (0.35 mL, 2.52 mmol, 4 eq) in EtOH (5 mL) was slowly added to a solution of **124**, (0.35 g, 0.63 mmol, 1 eq) in EtOH (5 mL). The reaction mixture was stirred at room temperature for 24 hours. The precipitate was collected by suction filtration and washed with EtOH and Et_2O to yield the product as a brown amorphous solid. (0.122 g, 27%). **^{1}H NMR,** (DMSO-d_6, 500.13 MHz) δ (ppm), J (Hz): 1.04 (s, 12H, CH_3), 3.87 (s, 2H, CH_2), 4.64 (s, 4H, CH_2), 6.74 (s, 4H, ArH), 7.08 (m, 8H, ArH), 7.85 (br, 2H, NH), 8.64 (br, 2H, NH), 9.39 (br, 2H, OH), 2.42 (8H, CH_2 under solvent peak according to COSY); **^{13}C NMR,** (DMSO-d_6, 125.76 MHz) δ (ppm): 12.2, 14.2, 24.6, 46.2, 47.0, 115.3, 115.8, 127.0, 129.5, 132.5, 141.1, 157.2, 167.7, 168.2, 184.4; **HRMS** (ESI) calcd. for $C_{43}H_{45}N_4O_6$ $[M + H]^+$ 713.3334, found 713.3356; difference 3.08 ppm; **ν_{max} (KBr)/cm^{-1}:** 3236 (N-H), 2966 (ArH), 1798 (C=O), 1578 (ArH), 1444 (C-H), 1257 (C-O).

4,4'-((methylenebis(2,6-diethyl-4,1-phenylene))bis(azanediyl))bis(3-((pyridin-4-ylmethyl)amino)cyclobut-3-ene-1,2-dione) (146)

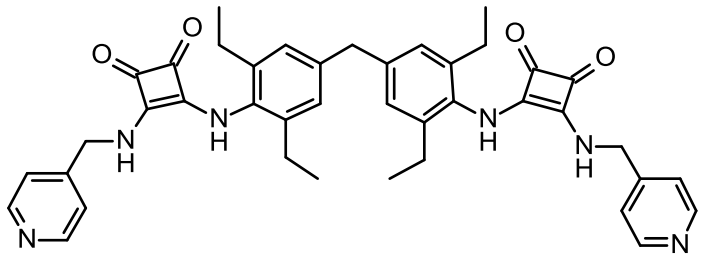

A mixture of **129**, (0.256 mL, 2.52 mmol, 4 eq) and Et_3N (0.35 mL, 2.52 mmol, 4 eq) in EtOH (5 mL) was slowly added to a solution of **124,** (0.35 g, 0.63 mmol, 1 eq) in EtOH (5 mL). The reaction mixture was stirred at room temperature for 24 hours. The precipitate was collected by suction filtration and washed with EtOH and Et_2O to yield the product as a beige amorphous solid. (0.292 g, 68%). **^{1}H NMR,** (DMSO-*d_6*, 500.13 MHz) δ (ppm), *J* (Hz): 1.05 (t, *J* = 7.0, 12H, CH_3), 2.44 (q, *J* = 7.4, 8H, CH_2), 3.89 (s, 2H, CH_2), 4.82 (s, 4H, CH_2), 7.01 (brS, 4H, ArH), 7.35 (brS, 4H, ArH), 7.96 (br, 2H, NH), 8.56 (brS, 4H, ArH), 8.80 (s, 2H, NH); **^{13}C NMR** (DMSO-*d_6*, 125.76 MHz): δ (ppm): 13.8, 14.8, 19.0, 24.6, 41.1, 46.2, 56.5, 122.4, 127.0, 127.2, 141.3, 148.4, 150.2, 168.0, 168.5, 182.2; **HRMS** (ESI) calcd. for $C_{41}H_{43}N_6O_4$ $[M + H]^+$ 683.3340, found 683.3326; difference -2.04 ppm **ν_{max} (KBr)/cm^{-1}:** 3240 (N-H), 2967 (ArH), 1797 (C=O), 1674 (C=N), 1581 (ArH), 1464 (C-H), 1211 (C-N).

4,4'-((Methylenebis(2,6-diethyl-4,1-phenylene))bis(azanediyl))bis(3-((pyridin-3-ylmethyl)amino)cyclobut-3-ene-1,2-dione) (147)

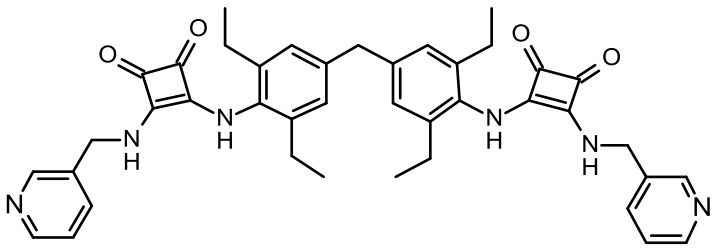

A mixture of **130,** (0.256 mL, 2.52 mmol, 4 eq) and Et_3N (0.35 mL, 2.52 mmol, 4 eq) in EtOH (5 mL) was slowly added to a solution of **124**, (0.35 g, 0.63 mmol, 1 eq) in EtOH (5 mL). The reaction mixture was stirred at room temperature for 24 hours.

The precipitate was collected by suction filtration and washed with EtOH and Et_2O to yield the product as a beige amorphous solid. (0.284 g, 66%). **^{1}H NMR,** (DMSO-*d_6*, 500.13 MHz) δ (ppm), *J* (Hz): 1.03 (t, *J* = 7.3, 12H, CH_3), 2.45 (m, 8H, CH_2), 3.88 (s, 2H, CH_2), 4.80 (m, 4H, CH_2), 7.00 (s, 4H, ArH), 7.49 (d, *J* = 5.1, 2H, ArH), 7.76 (m, 2H, ArH), 8.60 (m, 4H, ArH), 8.75 (s, 2H, NH); **^{13}C NMR** (DMSO-*d_6*, 125.76 MHz): δ (ppm): 13.8, 14.8, 24.6, 41.1, 45.0, 123.9, 124.1, 126.6, 127.1, 132.4, 134.9, 135.6, 140.6, 141.3, 149.1, 168.0, 168.3, 184.3; **HRMS** (ESI) calcd. for $C_{41}H_{43}N_6O_4$ $[M + H]^+$ 683.3340, found 683.3333; difference -1.1 ppm; **ν_{max} (KBr)/cm^{-1}:** 3225 (N-H), 2964 (ArH), 1798 (C=O), 1664 (C=N), 1425 (C-H), 1210 (C-N).

4,4'-((methylenebis(2,6-diethyl-4,1-phenylene))bis(azanediyl))bis(3-((pyridin-2-ylmethyl)amino)cyclobut-3-ene-1,2-dione) (148)

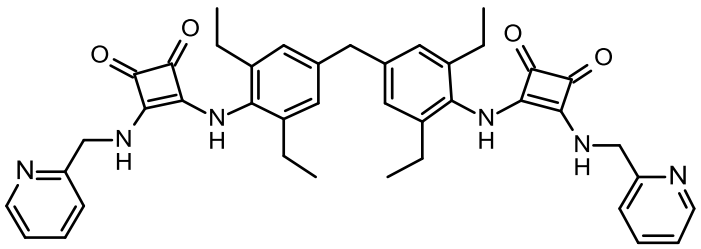

A mixture of **131**, (0.256 mL, 2.52 mmol, 4 eq) and Et_3N (0.35 mL, 2.52 mmol, 4 eq) in EtOH (5 mL) was slowly added to a solution of **124**, (0.35 g, 0.63 mmol, 1 eq) in EtOH (5 mL). The reaction mixture was stirred at room temperature for 24 hours. The precipitate was collected by suction filtration and washed with EtOH and Et_2O to yield the product as a beige amorphous solid. (0.264 g, 61%). **^{1}H NMR,** (DMSO-*d_6*, 500.13 MHz) δ (ppm), *J* (Hz): 1.06 (m, 12H, CH_3), 3.90 (s, 2H, CH_2), 4.90 (s, 4H, CH_2), 7.02 (s, 4H, ArH), 7.37 (brS, 4H, ArH), 7.82 (s, 2H, ArH), 8.11 (br, 2H, NH), 8.59 (s, 2H, ArH), 8.88 (br, 2H, NH), 2.48 (8H, CH_2 under solvent peak according to COSY); **^{13}C NMR** (DMSO-*d_6*, 125.76 MHz): δ (ppm): 14.9, 19.0, 24.6, 41.0, 48.7, 56.5, 122.0, 123.1, 127.0, 132.5, 137.6, 140.6, 141.2, 149.5, 157.7, 167.9, 168.6, 184.4; **HRMS** (ESI) calcd. for $C_{41}H_{43}N_6O_4$ $[M + H]^+$ 683.3340, found 683.3342; difference 0.24 ppm; **ν_{max} (KBr)/cm^{-1}:** 3245 (N-H), 2966 (ArH), 1797 (C=O), 1674 (C=N), 1583 (ArH), 1437 (C-H), 1212 (C-N).

Chapter 7 – References

7.1 References

1. Caltagirone, C.; Gale, P. A.; *Chem. Soc. Rev.*, **2009**, 38, 520-563.
2. C. Lin, C.; Simov V.; Drueckhammer, D. G.; *J. Org. Chem.*, **2007**, 72, 1742-1746.
3. T. Zieliński, T.; Jurczak, J.; *Tetrahedron Lett.*, **2005**, 61, 4081-4089.
4. Pfeffer, F. M.; Lim, K. F., Sedgwick, K. J.; *Org. Biomol. Chem.*, **2007**, 5, 1795-1799.
5. Bondy, C. R.; Loeb, S. J.; *Coord. Chem. Rev.*, **2003**, 240, 77-99.
6. Huggins, M. T.; Butler, T.; Barber, P.; Hunt, J.; *Chem. Commun.*, **2009**, 5254-5256.
7. Hughes, M. P.; Smith, B. D.; *J. Org. Chem.*, **1997**, 62, 4492-4499.
8. Santacroce, P. V.; Davis, J. T.; Light, M. E.; Gale, P. A.; Iglesias-Sánchez, J. C.; Prados, P.; Quesada, R.; *J. Am. Chem. Soc.*, **2007**, 129, 1886-1887.
9. Fan, E.; Vicent, C.; Hamilton, A. D.; *New J. Chem.*, **1997**, 21, 81-85.
10. Connon, S. J.; *Chem. Eur. J.*, **2006**, 12, 5418-5427.
11. Kotke, M.; Schreiner, P. R.; *Tetrahedron Lett.*, **2006**, 62, 434-439.
12. Jones, C. E. S.; Turega, S. M.; Clarke, M. L.; Philp, D.; *Tetrahedron Lett.*, **2008**, 49, 4666-4669.
13. Raheem, I. T.; Thiara, P. S.; Peterson, E. A.; Jacobsen, E. N.; *J. Am. Chem. Soc.*, **2007**, 129, 13404-13405.
14. Reisman, S. E.; Doyle, A. G.; Jacobsen, E. N.; *J. Am. Chem. Soc.*, **2008**, 130, 7198-7199.
15. Sohtome, Y.; Takemura, N.; Takagi, R.; Y. Hashimoto, Y.; Nagasawa, K.; *Tetrahedron Lett.*, **2008,** 64, 9423-9429.
16. Zhang, Z.; Schreiner, P. R.; *Chem. Soc. Rev.*, **2009**, 38, 1187-1198.
17. Zuend, S. J.; Jacobsen, E. N.; *J. Am. Chem. Soc.*, **2009**, 131, 15358-15374.
18. Sessler, J. L.; Gale, P. A.; Cho, W. S.; *Anion Receptor Chemistry*; RSC., **2006**.
19. Li, A. F.; Wang, J. H.; F. Wang, F.; Jiang, Y. B.; *Chem. Soc. Rev.*, **2010**, 39, 3729-3745.
20. Gale, P. A.; Caltagirone, C.; *Chem. Soc. Rev.*, **2015,** 44, 4212-4227.
21. Davis, A. P.; Sheppard D. N.; Smith, B. D.; *Chem. Soc. Rev.*, **2007**, 36**,** 348-357.

22. Rowe, S. M.; Miller, S.; Sorscher, E. J.; *N. Engl. J. Med.*, **2005,** 352, 1992-2001.

23. Yang, L.; Li, X.; Yang, J.; Qu, Y.; Hua, J.; *ACS Appl. Mater. Interfaces.*, **2013**, 5, 1317-1326.

24. Shao, J.; Qiao, Y. H.; Lin, H.; Lin, H. K., *J. Incl. Phenom. Macrocycl. Chem.*, **2008**, 62, 99.

25. Taylor, B. R.; Sosa, R.; Stone, W. J.; *Am. J. Med.,* **2010,** 123.

26. Xu, L.; Xu, Y.; Zhu, W.; Xu, Z.; Chen, M.; Qian, X.; *New J. Chem*, **2012,** 36, 1435-1438.

27. Gerlach, R. F.; De Souza, A. P.; Cury, J. A.; Line, S. R. P.; *Eur J. Oral. Sci.*, **2000**, 108, 48-53.

28. Zhang, J. F.; Lim, C. S.; Bhuniya, S.; Cho, B. R.; Kim, J. S.; *Org. Lett.*, **2011**, 13, 1190-1193.

29. Kumar, M.; Kumar, R.; Bhalla V.; *Org. Biomol. Chem.*, **2011**, 9, 8237-8245.

30. Swamy, K. M. K.; Lee, Y. J.; Lee, H. N.; Chun, J.; Kim, Y.; Kim, S. J.; Yoon, J.; *J. Org. Chem.,* **2006**, 71, 8626-8628.

31. Rhee, H. W.; Choi, S. J.; Yoo, S. H.; Jang, Y. O.; Park, H. H.; Pinto, R. M. A.; Cameselle, J. C.; Sandoval, F. J.; Roje, S.; Han, K.; *J. Am. Chem. Soc.*, **2009,** 131, 10107-10112.

32. Beck, G. R.; Zerler, B.; Moran, E.; *Proc. Natl. Acad. Sci.*, **2000**, 97, 8352-8357.

33. Schenk, T.; Appels, N.; Van Elswijk, D. A.; Irth, H.; Tjaden, U. R.; Van Der Greef, J.; *Anal. Biochem.,* **2003,** 316, 118-126.

34. Smith, V. H.; Schindler, D. W.; *Trends Ecol. Evol.,* **2009,** 24, 201-207.

35. Katayev, E. A.; Ustynyuk, Y. A.; Sessler, J. L.; *Coord. Chem. Rev.*, **2006,** 250, 3004-3037.

36. Moyer, B. A.; Custelcean, R.; Hay, B. P.; Sessler, J. L.; Bowman-James, K.; Day, V. W.; Kang, S. O.; *Inorg. Chem.*, **2012,** 52, 3473-3490.

37. Beer, P. D.; Gale, P. A.; *Angew. Chem. Int. Ed.,* **2001**, 40, 486-516.

38. Shriver, D. F.; Biallas, M. J.; *J. Am. Chem. Soc.*, **1967,** 89, 1078-1081.

39. Park, C. H.; Simmons, H. E.; *J. Am. Chem. Soc.*, **1968,** 90, 2431-2432.

40. Bowman-James, K.; *Acc. Chem. Res.*, **2005,** 38, 671-678.

41. Graf, E. J.; Lehn, M.; *J. Am. Chem. Soc.*, **1976,** 98, 6403-6405.

42. Kavallieratos, K.; de Gala, S. R.; Austin, D. J.; Crabtree, R. H.; *J. Am. Chem. Soc.*, **1997,** 119, 2325-2326.
43. Kubik, S.; *Chem. Soc. Rev.*, **2010,** 39, 3648-3663.
44. Ojida, A.; Takashima, I.; Kohira, T.; Nonaka, H.; Hamachi, I.; *J. Am. Chem. Soc.*, **2008,** 130, 12095-12101.
45. Kim, Y.; Gabbaï, F. O. P.; *J. Am. Chem. Soc.*, **2009,** 131, 3363-3369.
46. Fowler, C. J.; Haverlock, T. J.; Moyer, B. A.; Shriver, J. A.; Gross, D. E.; Marquez, M.; Sessler, J. L.; Hossain, M. A.; Bowman-James, K.; *J. Am. Chem. Soc.*, **2008,** 130, 14386-14387.
47. Butler, S. J.; *Chem. Commun.*, **2015,** 51, 10879-10882.
48. Steed, J. W.; *Chem. Soc. Rev.*, **2009,** 38, 506-519.
49. Mercer, D. J.; Loeb, S. J.; *Chem. Soc. Rev.*, **2010,** 39, 3612-3620.
50. Butler, S. J.; *Chem. Eur. J.*, **2014,** 20, 15768-15774.
51. Bazzicalupi, C.; Bencini, A.; Lippolis, V.; *Chem. Soc. Rev.*, **2010,** 39, 3709-3728.
52. Schottel, B. L.; Chifotides, H. T.; Dunbar, K. R.; *Chem. Soc. Rev.*, **2008,** 37, 68-83.
53. Galbraith, E.; James, T. D.; *Chem. Soc. Rev.*, **2010,** 39, 3831-3842.
54. Gale, P. A.; *Acc. Chem. Res.*, **2006**, 39, 465-475.
55. Kang, S. O.; Begum, R. A.; Bowman-James, K.; *Angew. Chem. Int. Ed.,* **2006,** 45, 7882-7894.
56. Gale, P. A.; *Chem. Soc. Rev.*, **2010,** 39, 3746-3771.
57. Bates, G. W.; Gale, P. A.; Light, M. E.; Ogden, M. I.; Warriner, C. N.; *Dalton Trans.,* **2008,** 4106-4112.
58. Dydio, P.; Lichosyt, D.; Jurczak, J.; *Chem. Soc. Rev.*, **2011,** 40, 2971-2985.
59. Caltagirone, C.; Hiscock, J. R.; Hursthouse, M. B.; Light, M. E.; Gale, P. A.; *Chem. Eur. J.*, **2008,** 14, 10236-10243.
60. Kang, S. O.; Hossain, M. A.; Bowman-James, K.; *Coord. Chem. Rev.,* **2006,** 250, 3038-3052.
61. Amendola, V.; Bergamaschi, G.; Boiocchi, M.; Fabbrizzi, L.; Milani, M.; *Chem. Eur. J.*, **2010,** 16, 4368-4380.

62. Rostami, A.; Colin, A.; Li, X. Y.; Chudzinski, M. G.; Lough, A. J.; Taylor, M. S.; *J. Org. Chem.,* **2010,** 75, 3983-3992.

63. Gómez, D. E.; Fabbrizzi, L.; Licchelli, M.; Monzani, E.; *Org. Biomol. Chem.*, **2005,** 3, 1495-1500.

64. Brooks, S. J.; Gale, P. A.; Light, M. E.; *Chem. Commun.*, **2006,** 4344-4346.

65. Dahan, A.; Ashkenazi, T.; Kuznetsov, V.; Makievski, S.; Drug, E.; Fadeev, L.; Bramson, M.; Schokoroy, S.; Rozenshine-Kemelmakher, E.; Gozin, M.; *J. Org. Chem.,* **2007,** 72, 2289-2296.

66. Boyle, E. M.; McCabe, T.; Gunnlaugsson, T.; *Supramol. Chem.,* **2010,** 22, 586-597.

67. Chmielewski, M. J.; Jurczak, J.; *Tetrahedron Lett.*, **2005,** 46, 3085-3088.

68. Kavallieratos, K.; Bertao, C. M.; Crabtree, R. H.; *J. Org. Chem.,* **1999,** 64, 1675-1683.

69. Garcia-Tellado, F.; Goswami, S.; Chang, S. K.; Geib, S. J.; Hamilton, A. D.; *J. Am. Chem. Soc.*, **1990,** 112, 7393-7394.

70. Chang, S. K.; Van Engen, D.; Fan, E.; Hamilton, A. D.; *J. Am. Chem. Soc.*, **1991,** 113, 7640-7645.

71. Pinter, T.; Jana, S.; Courtemanche, R. J. M.; Hof, F.; *J. Org. Chem.,* **2011,** 76, 3733-3741.

72. Bates, G. W.; Triyanti, Light, M. E.; Albrecht, M.; Gale, P. A.; *J. Org. Chem.,* **2007,** 72, 8921-8927.

73. Caltagirone, C.; Gale, P. A.; Hiscock, J. R.; Hursthouse, M. B.; Light, M. E.; Tizzard, G. J.; *Supramol. Chem.,* **2009,** 21, 125-130.

74. Caltagirone, C.; Bates, G. W.; Gale, P. A.; Light, M. E.; *Chem. Commun.*, **2008,** 61-63.

75. Amendola, V.; Fabbrizzi, L.; Mosca, L.; *Chem. Soc. Rev.*, **2010,** 39, 3889-3915.

76. Gale, P. A.; Busschaert, N.; Haynes, C. J. E.; Karagiannidis, L. E.; Kirby, I. L.; *Chem. Soc. Rev.*, **2014,** 43, 205-241.

77. Smith, P. J.; Reddington, M. V.; Wilcox, C. S.; *Tetrahedron Lett.*, **1992,** 33, 6085-6088.

78. Kelly, T. R.; Kim, M. H.; *J. Am. Chem. Soc.*, **1994,** 116, 7072-7080.

79. Gunnlaugsson, T.; Kruger, P. E.; Jensen, P.; Tierney, J.; Ali, H. D. P.; Hussey, G. M.; *J. Org. Chem.,* **2005,** 70, 10875-10878.

80. Brooks, S. J.; Gale, P. A.; Light, M. E.; *Chem. Commun.*, **2005,** 4696-4698.

81. Brooks, S. J.; Edwards, P. R.; Gale, P. A.; Light, M. E.; *New J. Chem.,* **2006,** 30, 65-70.

82. Tomas, S.; Prohens, R.; Vega, M.; Rotger, M. C.; Deya, P. M.; Ballester, P.; Costa, A.; *J. Org. Chem.,* **1996,** 61, 9394-9401.

83. Prohens, R.; Tomàs, S.; Morey, J.; Deyà, P. M.; Ballester, P.; Costa, A.; *Tetrahedron Lett.*, **1998,** 39, 1063-1066.

84. Quiñonero, D.; Frontera, A.; Ballester, P.; Deyà, P. M.; *Tetrahedron Lett.*, **2000,** 41, 2001-2005.

85. Quiñonero, D.; Prohens, R.; Garau, C.; Frontera, A.; Ballester, P.; Costa, A.; Deyà, P. M.; *Chem. Phys. Lett.*, **2002,** 351, 115-120.

86. Prohens, R.; Martorell, G.; Ballester, P.; Costa, A.; *Chem. Commun.*, **2001,** 1456-1457.

87. Piña, M. N.; Rotger, M. C.; Costa, A.; Ballester, P.; Deyà, P. M.; *Tetrahedron Lett.*, **2004,** 45, 3749-3752.

88. Frontera, A.; Morey, J.; Oliver, A.; Piña, M. N.; Quiñonero, D.; Costa, A.; Ballester, P.; Deyà, P. M.; Anslyn, E. V.; *J. Org. Chem.,* **2006,** 71, 7185-7195.

89. Ambrosi, G.; Fusi, M.; Giorgi, L.; Guerri, A.; Micheloni, M.; Paoli, P.; Pontellini, R.; Rossi, P.; *Chem. Eur. J.*, **2007,** 13, 702-712.

90. Ramalingam, V.; Domaradzki, M. E.; Jang, S.; Muthyala, R. S.; *Org. Lett.* **2008,** 10, 3315-3318.

91. Malerich, J. P.; Hagihara, K.; Rawal, V. H.; *J. Am. Chem. Soc.*, **2008,** 130, 14416-14417.

92. Cheon, C. H.; Yamamoto, H.; *Tetrahedron Lett.*, **2009,** 50, 3555-3558.

93. Davis, A. P.; Draper, S. M.; Dunne, G.; Ashton, P.; *Chem. Commun.*, **1999,** 2265-2266.

94. Quiñonero, D.; Frontera, A.; Suñer, G. A.; Morey, J.; Costa, A.; Ballester, P.; Deyà, P. M.; *Chem. Phys. Lett.*, **2000,** 326, 247-254.

95. Liu, Y.; Lam, A. H. W.; Fowler F. W.; Lauher, J. W.; *Mol. Cryst. Liq. Cryst.,* **2002,** 389, 39-46.

96. Owen, R. M.; Carlson, C. B.; Xu, J.; Mowery, P.; Fasella, E.; Kiessling, L. L.; *ChemBioChem.*, **2007,** 8, 68-82.

97. Gilbert, A. M.; Antane, M. M.; Argentieri, T. M.; Butera, J. A.; Francisco, G. D.; Freeden, C.; Gundersen, E. G.; Graceffa, R. F.; Herbst, D.; Hirth, B. H.; *J. Med. Chem.,* **2000,** 43, 1203-1214.

98. Valgeirsson, J.; Nielsen, E. Ø.; Peters, D.; Mathiesen, C.; Kristensen, A. S.; Madsen, U.; *J. Med. Chem.,* **2004,** 47, 6948-6957.

99. Onaran, M. B.; Comeau, A. B.; Seto, C. T.; *J. Org. Chem.,* **2005,** 70, 10792-10802.

100. Merritt, J. R.; Rokosz, L. L.; Nelson, K. H.; Kaiser, B.; Wang, W.; Stauffer, T. M.; Ozgur, L. E.; Schilling, A.; Li, G.; Baldwin, J. J.; *Bioorg. Med. Chem. Lett.,* **2006,** 16, 4107-4110.

101. McCleland, B. W.; Davis, R. S.; Palovich, M. R.; Widdowson, K. L.; Werner, M. L.; Burman, M.; Foley, J. J.; Schmidt, D. B.; Sarau, H. M.; Rogers, M.; *Bioorg. Med. Chem. Lett.,* **2007,** 17, 1713-1717.

102. Prohens, R.; Rotger, M. C.; Piña, M. N.; Deyà, P. M.; Morey, J.; Ballester, P.; Costa, A.; *Tetrahedron Lett.*, **2001,** 42, 4933-4936.

103. Al-Sayah, M. H.; Branda, N. R.; *Thermochim. Acta.*, **2010,** 503, 28-32.

104. Amendola, V.; Fabbrizzi, L.; Mosca, L.; Schmidtchen, F. P.; *Chem. Eur. J.*, **2011,** 17, 5972-5981.

105. Gaeta, C.; Talotta, C.; Della Sala, P.; Margarucci, L.; Casapullo A.; Neri, P.; *J. Org. Chem.,* **2014,** 79, 3704-3708.

106. Elmes, R. B. P.; Turner, P.; Jolliffe, K. A.; *Org. Lett.,* **2013,** 15, 5638-5641.

107. Busschaert, N.; Elmes, R. B. P.; Czech, D. D.; Wu, X.; Kirby, I. L.; Peck, E. M.; Hendzel, K. D.; Shaw, S. K.; Chan, B.; Smith, B. D.; *Chem. Sci.*, **2014,** 5, 3617-3626.

108. Elmes, R. B. P.; Busschaert, N.; Czech, D. D.; Gale, P. A.; Jolliffe, K. A.; *Chem. Commun.*, **2015,** 51, 10107-10110.

109. Owen, R. M.; Carlson, C. B.; Xu, J.; Mowery, P.; Fasella, E.; Kiessling, L. L.; *ChemBioChem.*, **2007,** 8, 68-82.

110. Storer, R. I.; Aciro, C.; Jones, L. H.; *Chem. Soc. Rev.*, **2011,** 40, 2330-2346.

111. Zhu, Y.; Malerich, J. P.; Rawal, V. H. *Angew. Chem. Int. Ed.,* **2010,** 49, 153-156.

112. Elmes, R. B. P.; Yuen, K. K.; Jolliffe, K. A.; *Chem. Eur. J.* **2014,** 20, 7373-7380.

113. Ravikumar, I.; Ghosh, P.; *Chem. Soc. Rev.*, **2012,** 41, 3077-3098.

114. Lv, M.; Xu, H.; *Curr. Med. Chem.*, **2009,** 16, 4797-4813.

115. Ingrassia, L.; Lefranc, F.; Kiss, R.; Mijatovic, T.; *Curr. Med. Chem.*, **2009,** 16, 1192-1213.

116. Braña, M. F.; Cacho, M.; García, M. A.; de Pascual-Teresa, B.; Ramos, A.; Domínguez, M. T.; Pozuelo, J. M.; Abradelo, C.; Rey-Stolle M. F.; Yuste, M.; *J. Med. Chem.,* **2004,** 47, 1391-1399.

117. Gosztola, D.; Niemczyk, M. P.; Svec, W.; Lukas, A. S.; Wasielewski, M. R.; *The J. Phys. Chem. A.,* **2000,** 104, 6545-6551.

118. Duke, R. M.; Veale, E. B.; Pfeffer, F. M.; Kruger, P. E.; Gunnlaugsson, T.; *Chem. Soc. Rev.*, **2010,** 39, 3936-3953.

119. Cao, X.; Meng, L.; Li, Z.; Mao, Y.; Lan, H.; Chen, L.; Fan, Y.; Yi, T.; *Langmuir.*, **2014,** 30, 11753-11760.

120. Thordarson, P.; *Chem. Soc. Rev.*, **2011,** 40, 1305-1323.

121. Boiocchi, M.; Del Boca, L.; Gómez, D. E.; Fabbrizzi, L.; Licchelli, M.; Monzani, E.; *J. Am. Chem. Soc.*, **2004,** 126, 16507-16514.

122. Gunnlaugsson, T.; Glynn, M.; Tocci, G. M.; Kruger, P. E.; Pfeffer, F. M.; *Coord. Chem. Rev.,* **2006,** 250, 3094-3117.

123. Shipway, A. N.; Katz, E.; Willner, I.; *ChemPhysChem.*, **2000,** 1, 18-52.

124. Sugiyasu, K.; Fujita, N.; Shinkai, S.; *Angew. Chem. Int. Ed.*, **2004,** 116, 1249-1253.

125. Bhattacharya, S.; Krishnan-Ghosh, Y.; *Chem. Commun.*, **2001,** 185-186.

126. Lee, K. Y.; Mooney, D. J.; *Chem. Rev.*, **2001,** 101, 1869-1880.

127. Yoshimura, I.; Miyahara, Y.; Kasagi, N.; Yamane, H.; Ojida, A.; Hamachi, I.; *J. Am. Chem. Soc.*, **2004,** 126, 12204-12205.

128. Pérez, J.; Riera, L.; *Chem. Soc. Rev.*, **2008,** 37, 2658-2667.

129. Kishimura, A.; Yamashita, T.; Aida, T.; *J. Am. Chem. Soc.*, **2005,** 127, 179-183.

130. Fages, F.; *Angew. Chem. Int. Ed.*, **2006,** 45, 1680-1682.

131. Mani, F.; *Coord. Chem. Rev.*, **1992,** 120, 325-359.

132. Sadimenko, A. P.; Basson, S. S.; *Coord. Chem. Rev.*, **1996,** 147, 247-297.

133. Ward, M. D.; McCleverty, J. A.; Jeffery, J. C.; *Coord. Chem. Rev.*, **2001,** 222, 251-272.

134. Pettinari, C.; Pettinari, R.; *Coord. Chem. Rev.*, **2005,** 249, 663-691.

135. Halcrow, M. A.; *Dalton Trans.*, **2009,** 2059-2073.

136. Flory, P. J.; *Faraday Discuss.*, **1974,** 57, 7-18.

137. Sangeetha, N. M.; Maitra, U.; *Chem. Soc. Rev.*, **2005,** 34, 821-836.

138. Huang, X.; Terech, P.; Raghavan, S. R.; Weiss, R. G.; *J. Am. Chem. Soc.*, **2005,** 127, 4336-4344.

139. Aggeli, A.; Nyrkova, I. A.; Bell, M.; Harding, R.; Carrick, L.; McLeish, T. C. B.; Semenov, A. N.; Boden, N.; *Proc. Natl. Acad. Sci.*, **2001,** 98, 11857-11862.

140. Simmons, B. A.; Taylor, C. E.; Landis, F. A.; John, V. T.; McPherson, G. L.; D. K. Schwartz, D. K.; Moore, R.; *J. Am. Chem. Soc.*, **2001,** 123, 2414-2421.

141. Estroff, L. A.; Hamilton, A. D.; *Chem. Rev.,* **2004,** 104, 1201-1218.

142. van Esch, J. H.; Feringa, B. L.; *Angew. Chem. Int. Ed.*, **2000,** 39, 2263-2266.

143. Mukhopadhyay, S.; Maitra, U.; *Curr. Sci.*, **2004,** 87, 1666-1683.

144. Terech, P.; Rossat, C.; Volino, F.; *J. Colloid Interface Sci.,* **2000,** 227, 363-370.

145. Suzuki, M.; Hanabusa, K.; *Chem. Soc. Rev.*, **2010,** 39, 455-463.

146. Xie, P.; Zhang, R.; *J. Mater. Chem.*, **2005,** 15, 2529-2550.

147. Smith, D. K.; *Nat. Chem.,* **2010,** 2, 162-163.

148. Hirst, A. R.; Coates, I. A.; Boucheteau, T. R.; Miravet, J. F.; Escuder, B.; Castelletto, V.; Hamley, I. W.; Smith, D. K.; *J. Am. Chem. Soc.*, **2008,** 130, 9113-9121.

149. Terech, P.; Weiss, R. G.; *Chem. Rev.,* **1997,** 97, 3133-3160.

150. Brinksma, J.; Feringa, B. L.; Kellogg, R. M.; Vreeker, R.; van Esch, J.; *Langmuir.*, **2000,** 16, 9249-9255.

151. Abdallah, D. J.; Weiss, R. G.; *Adv. Mater.,* **2000,** 12, 1237-1247.

152. Escuder, B.; Llusar, M.; Miravet, J. F.; *J. Org. Chem.*, **2006,** 71, 7747-7752.

153. Lipowitz, V. A.; *Eur. J. Org. Chem.*, **1841,** 38, 348-355.

154. Suzuki, M.; Nakajima, Y.; Yumoto, M.; Kimura, M.; Shirai H.; Hanabusa, K.; *Langmuir.*, **2003,** 19, 8622-8624.

155. Wang, C.; Zhang, D.; Zhu, D.; *J. Am. Chem. Soc.*, **2005,** 127, 16372-16373.

156. Yang, H.; Yi, T.; Zhou, Z.; Zhou, Y.; Wu, J.; Xu, Z.; Li, F.; Huang, C.; *Langmuir.*, **2007,** 23, 8224-8230.

157. Ajayaghosh, A.; Praveen, V. K.; *Acc. Chem. Res.*, **2007,** 40, 644-656.

158. Li, Y.; Liu, K.; Liu, J.; Peng, J.; Feng, X.; Fang, Y.; *Langmuir.*, **2006,** 22, 7016-7020.

159. Webb, J. E. A.; Crossley, M. J.; Turner, P.; Thordarson, P.; *J. Am. Chem. Soc.*, **2007,** 129, 7155-7162.

160. Maeda, H.; *Chem. Eur. J.*, **2008,** 14, 11274-11282.

161. Lloyd, G. O.; Steed, J. W.; *Nat. Chem.*, **2009,** 1, 437-442.

162. Kawano, S. I.; Fujita, N.; Shinkai, S.; *J. Am. Chem. Soc.*, **2004,** 126, 8592-8593.

163. Shklyarevskiy, I. O.; Jonkheijm, P.; Christianen, P. C. M.; Schenning, A. P. H. J.; Del Guerzo, A.; Desvergne, J. P.; Meijer, E. W.; Maan, J. C.; *Langmuir.*, **2005,** 21, 2108-2112.

164. Yoshio, M.; Shoji, Y.; Tochigi, Y.; Nishikawa, Y.; Kato, T.; *J. Am. Chem. Soc.*, **2009,** 131, 6763-6767.

165. Kim, J. H.; Seo, M.; Kim, Y. J.; Kim, S. Y.; *Langmuir.*, **2009,** 25, 1761-1766.

166. Wang, S.; Shen, W.; Feng, Y.; Tian, H.; *Chem. Commun.*, **2006,** 1497-1499.

167. Naota, T.; Koori, H.; *J. Am. Chem. Soc.*, **2005,** 127, 9324-9325.

168. Piepenbrock, M. O. M.; Clarke, N.; Foster, J. A.; Steed, J. W.; *Chem. Commun.*, **2011,** 47, 2095-2097.

169. Rajamalli, P.; Prasad, E.; *Org. Lett.*, **2011,** 13, 3714-3717.

170. Kim, T. H.; Kwon, N. Y.; Lee, T. S.; *Tetrahedron Lett.*, **2010,** 51, 5596-5600.

171. Tu, T.; Fang, W.; Bao, X.; Li, X.; Dötz, K. H.; *Angew. Chem. Int. Ed.*, **2011,** 123, 6731-6735.

172. Dastidar, P.; *Chem. Soc. Rev.,* **2008,** 37, 2699-2715.

173. Piepenbrock, M. O. M.; Lloyd, G. O.; Clarke, N.; Steed, J. W.; *Chem. Rev.,* **2009,** 110, 1960-2004.

174. Fages, F.; Vögtle, F.; Žinić, M.; *Low Molecular Mass Gelator*, Springer, Berlin, Heidelberg, **2005,** 777-784.

175. Džolić, Z.; Cametti, M.; Cort, D. A.; Mandolini, L.; Žinić, M.; *Chem. Commun.*, **2007,** 3535-3537.

176. Steed, J. W.; *Chem. Soc. Rev.,* **2010,** 39, 3686-3699.

177. Bernstein, J.; Davis, R. E.; Shimoni, L.; Chang, N. L.; *Angew. Chem. Int. Ed.*, **1995,** 34, 1555-1573.

178. Stanley, C. E.; Clarke, N.; Anderson, K. M.; Elder, J. A.; Lenthall, J. T.; Steed, J. W.; *Chem. Commun.*, **2006,** 3199-3201.

179. Wang, C.; Zhang, D.; Zhu, D.; *Langmuir.*, **2007,** 23, 1478-1482.

180. Yamanaka, M.; Nakamura, T.; Nakagawa, T.; Itagaki, H.; *Tetrahedron Lett.*, **2007,** 48, 8990-8993.

181. Piepenbrock, M. O. M.; Lloyd, G. O.; Clarke, N.; Steed, J. W.; *Chem. Commun.*, **2008,** 2644-2646.

182. Xing, L. B.; Yang, B.; Wang, X. J.; Wang, J. J.; Chen, B.; Wu, Q.; Peng, H. X.; Zhang, L. P.; Tung, C. H.; Wu, L. Z.; *Langmuir.*, **2013,** 29, 2843-2848.

183. Saez Talens, V.; Englebienne, P.; Trinh, T. T.; Noteborn, W. E. M.; Voets, I. K.; Kieltyka, R. E.; *Angew. Chem. Int. Ed.*, **2015,** 127, 10648-10652.

184. Ohsedo, Y.; Miyamoto, M.; Tanaka, A.; Watanabe, H.; *New J. Chem.*, **2013,** 37, 2874-2880.

185. Schiller, J.; Alegre-Requena, J. V.; Marqués-López, E.; Herrera, R. P.; Casanovas, J.; Alemán, C.; Díaz, D. D.; *Soft Matter.*, **2016,** 12, 4361-4374.

186. López, C.; Ximenis, M.; Orvay, F.; Rotger, C.; Costa, A.; *Chem. Eur. J.,* **2017,** 23, 7590-7594.

187. Applegarth, L.; Clark, N.; Richardson, A. C.; Parker, A. D.; Radosavljevic-Evans, I.; Goeta, A. E.; Howard, J. A.; Steed, J. W.; *Chem. Commun.*, **2005,** 5423-5425.

188. Wu, D.; Jiang, R.; Luo, L.; He, Z.; You, J.; *Inorg. Chem. Front.,* **2016,** 3, 1597-1603.

189. Liu, H.; Tomooka, C. S.; Moore, H. W.; *Synth. Commun.*, **1997,** 27, 2177-2180.

190. Barros, R. C.; Gelens, E.; Bulten, E.; Tuin, A.; de Jong, M. R.; Kuijer, R.; van Kooten, T. G.; *J. Biomed. Mater. Res.*, **2017.**

Appendices

Appendix 2:

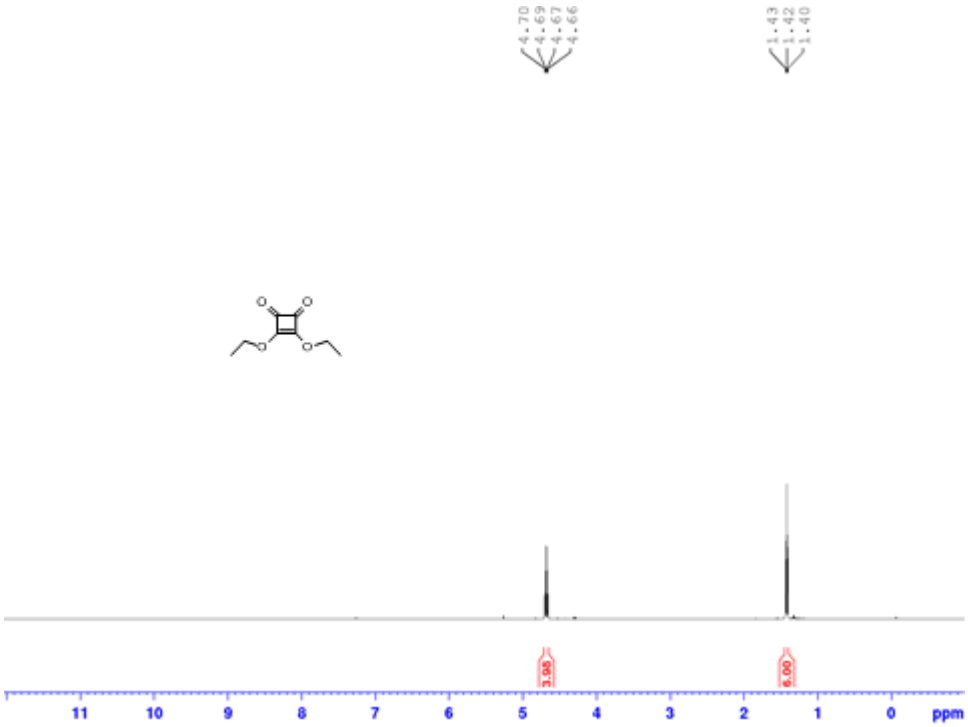

2A 1: *The ^{1}H NMR spectrum of **74** (500.13 MHz, $CDCl_3$)*

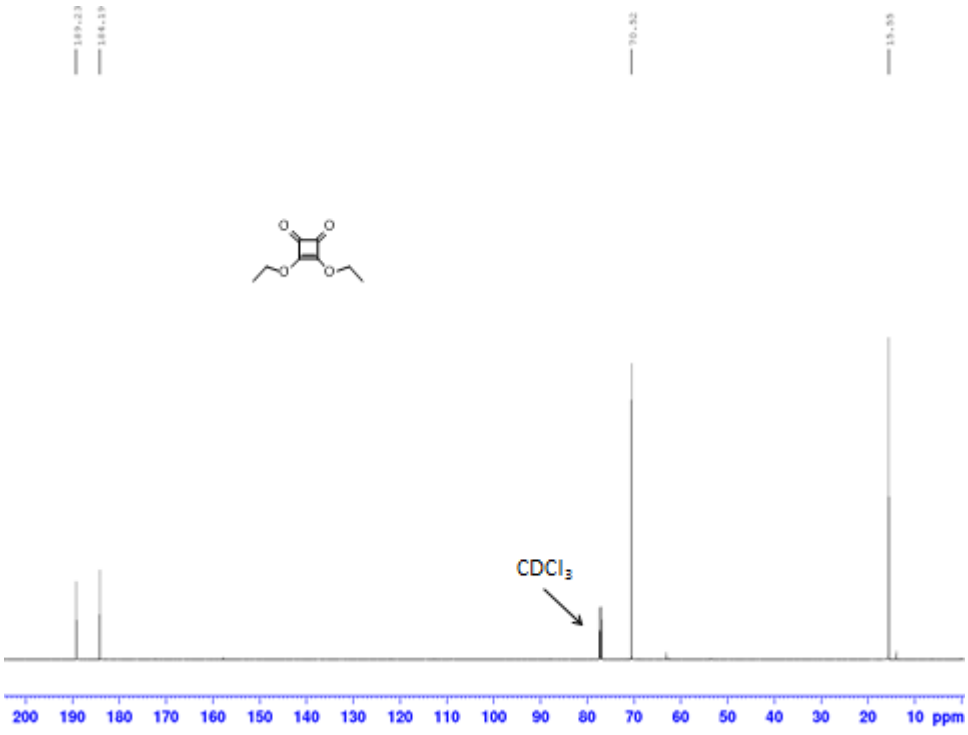

2A 2: *The ^{13}C NMR spectrum of **74** (125.76 MHz, $CDCl_3$)*

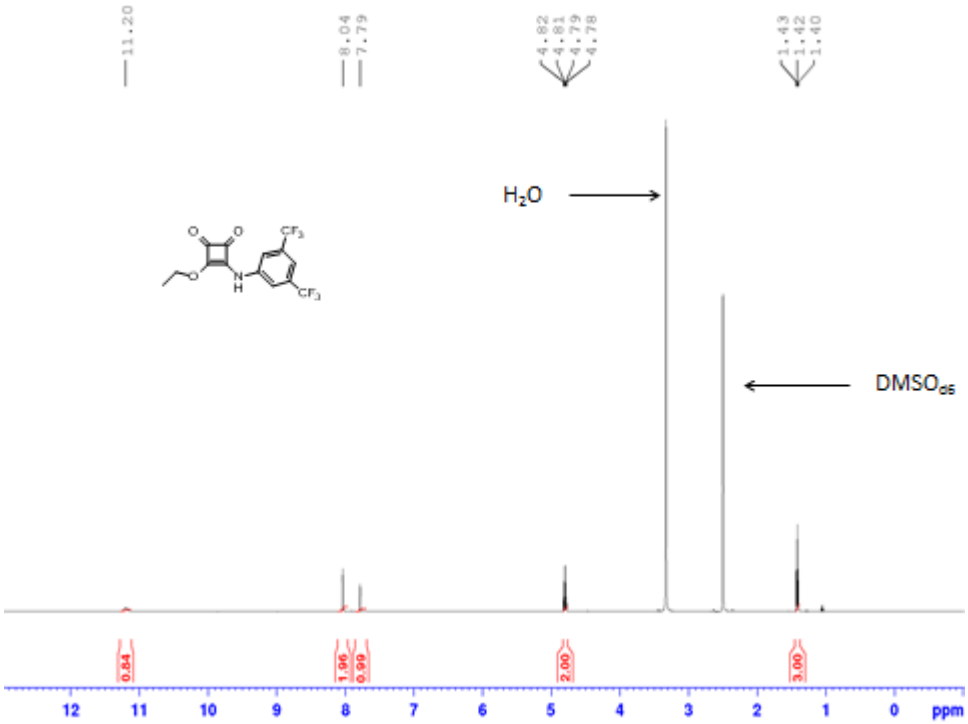

2A 3: *The ^{1}H NMR spectrum of* ***75*** *(500.13 MHz, DMSO-$_{d6}$).*

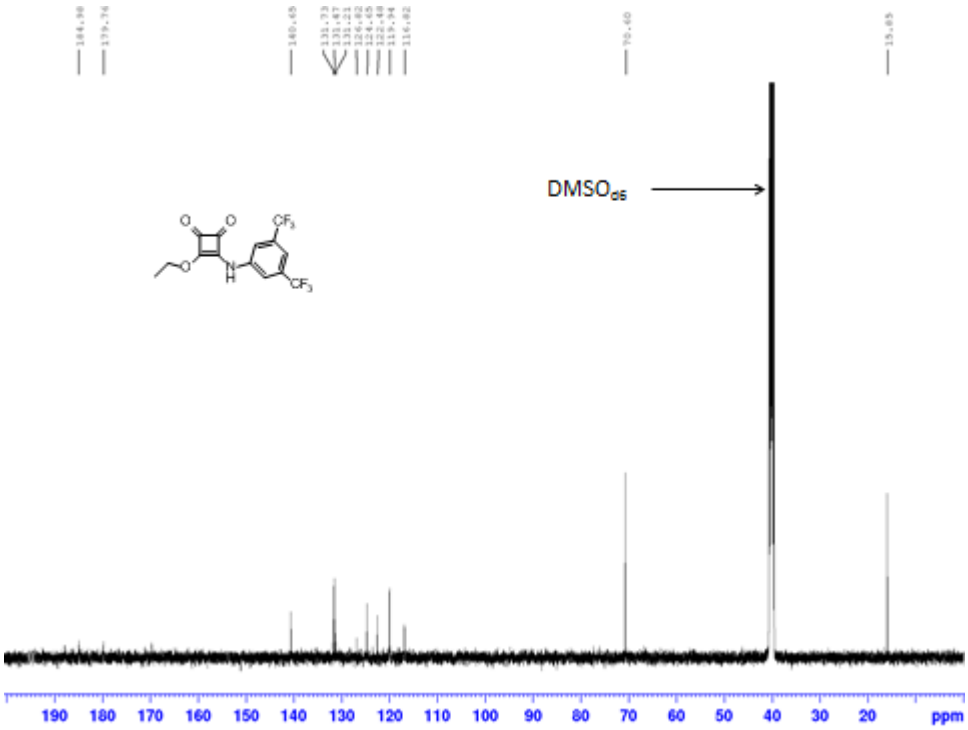

2A 4: *The ^{13}C NMR spectrum of* ***75*** *(125.76 MHz, DMSO-$_{d6}$)*

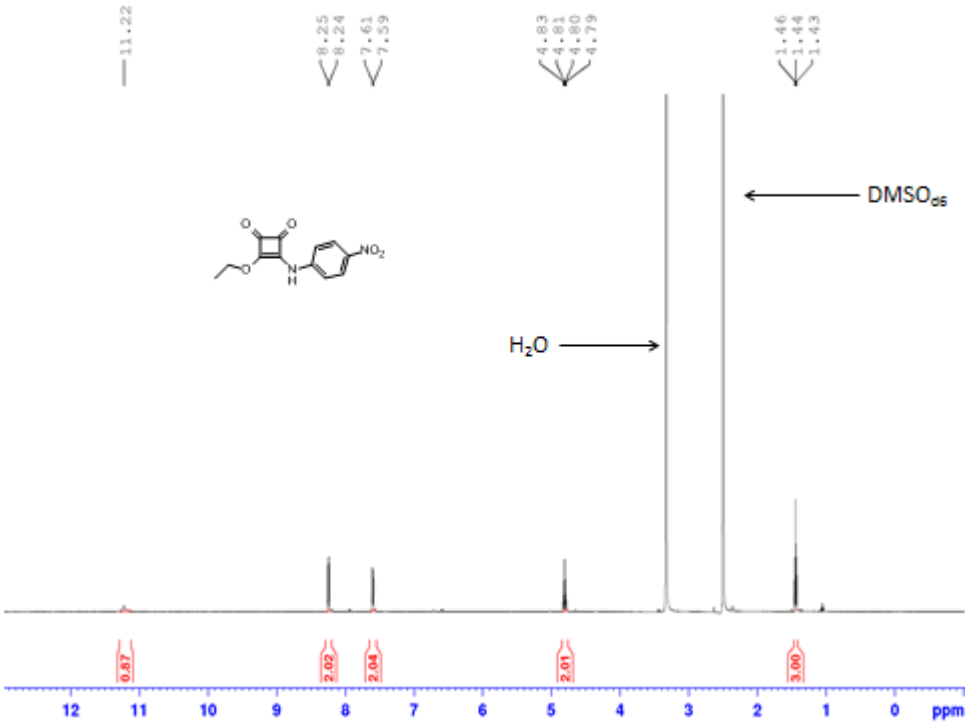

2A 5: *The ^{1}H NMR spectrum of **76** (500.13 MHz, DMSO-$_{d6}$).*

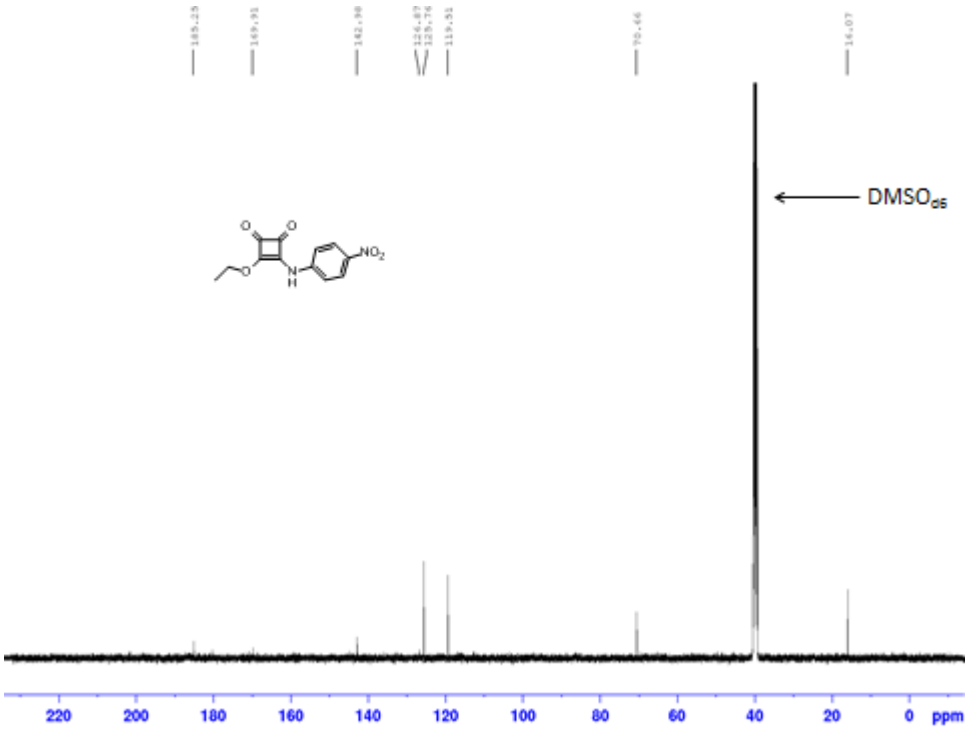

2A 6: *The ^{13}C NMR spectrum of **76** (125.76 MHz, DMSO-$_{d6}$)*

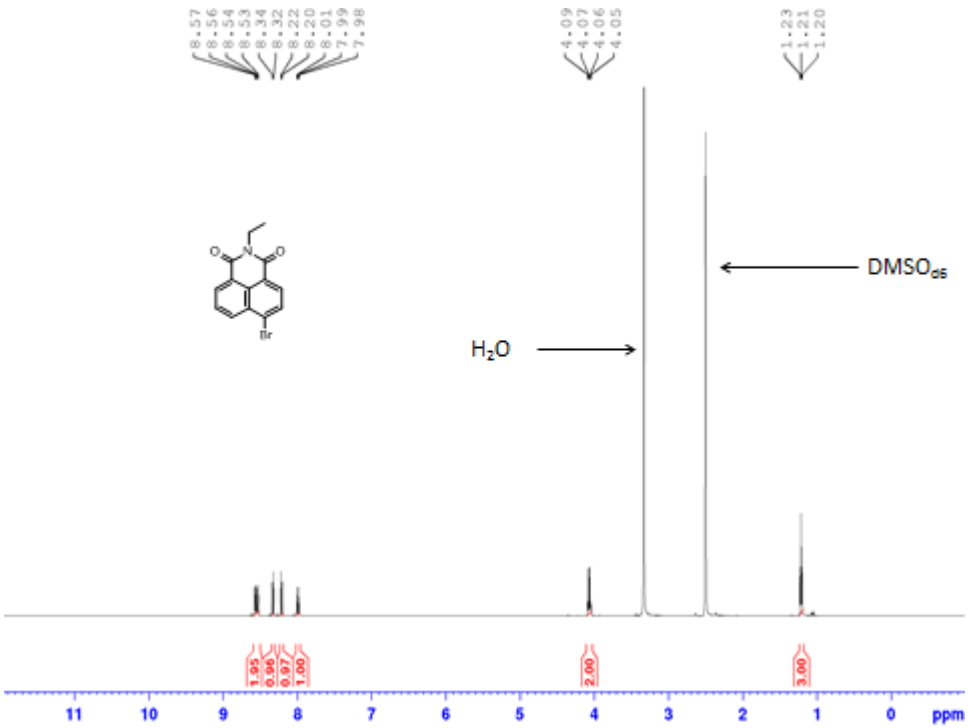

2A 7: *The ^{1}H NMR spectrum of **78** (500.13 MHz, DMSO-$_{d6}$).*

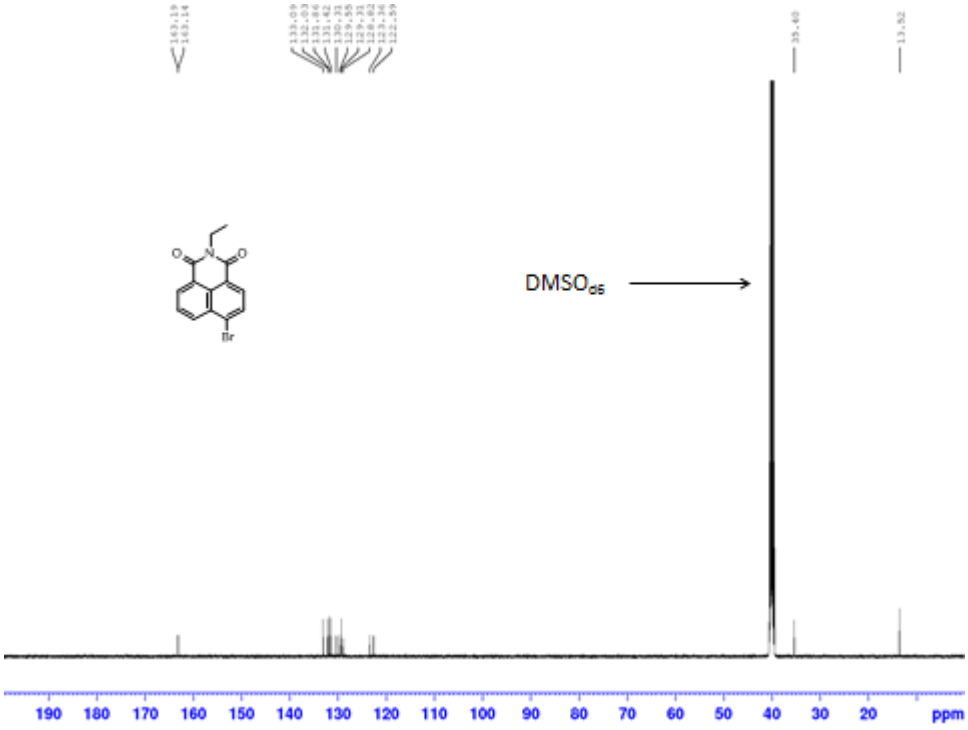

2A 8: *The ^{13}C NMR spectrum of **78** (125.76 MHz, DMSO-$_{d6}$)*

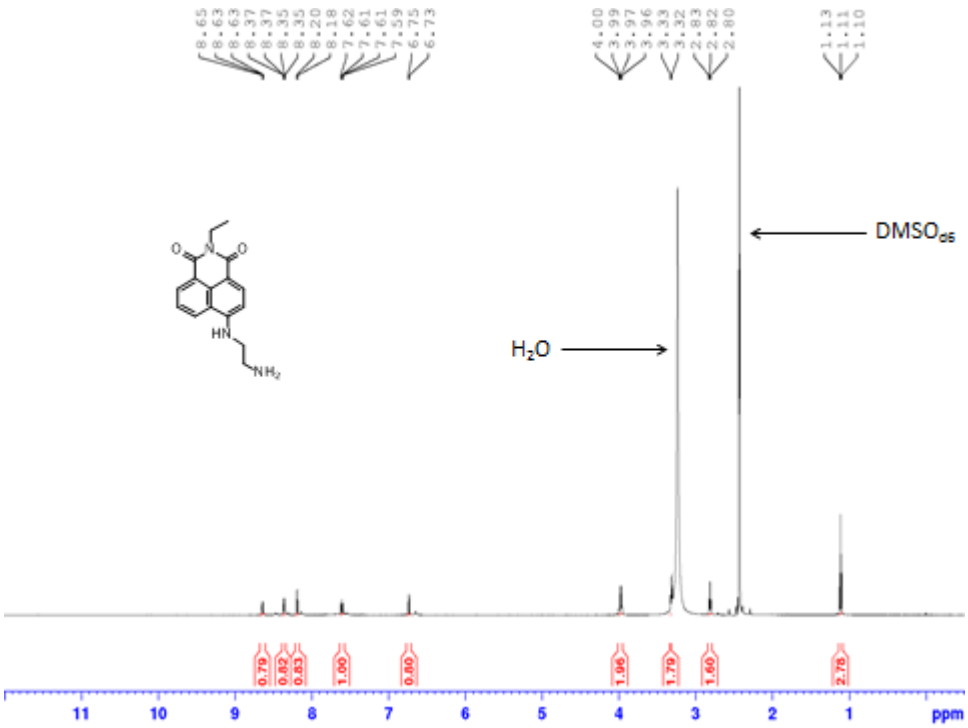

2A 9: *The ^{1}H NMR spectrum of **79** (500.13 MHz, DMSO-$_{d6}$).*

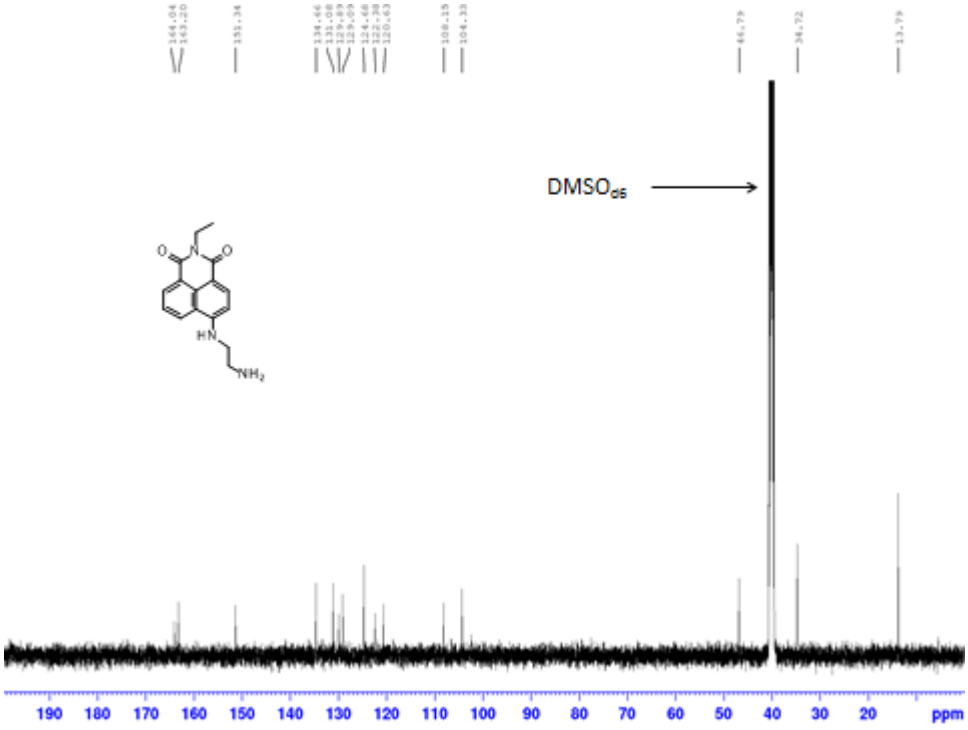

2A 10: *The ^{13}C NMR spectrum of **79** (125.76 MHz, DMSO-$_{d6}$)*

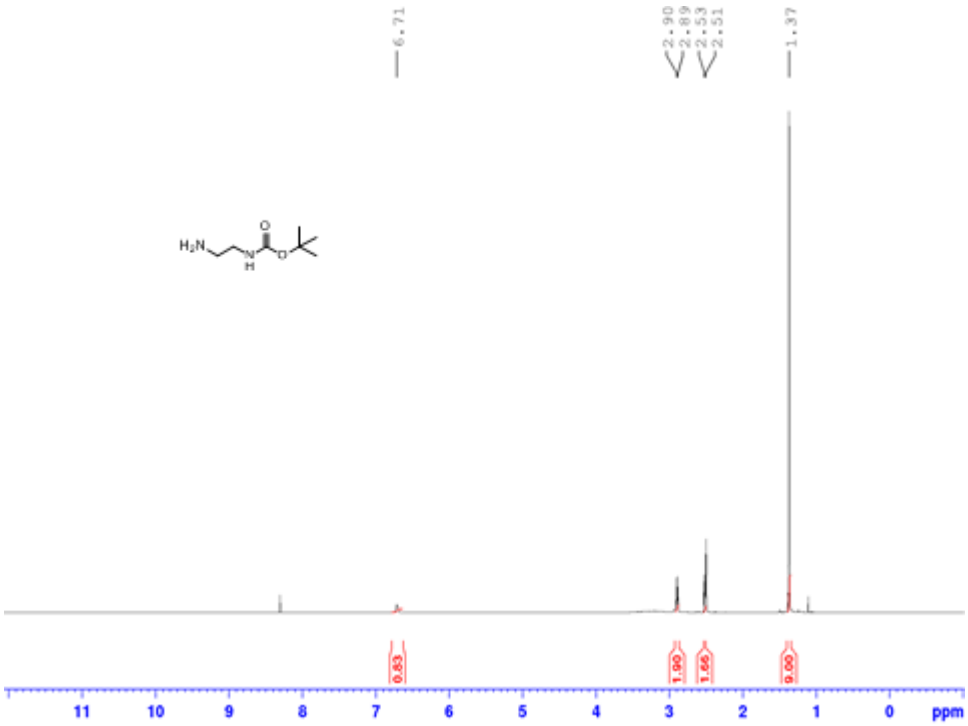

2A 11: *The ^{1}H NMR spectrum of* ***81*** *(500.13 MHz, DMSO-$_{d6}$).*

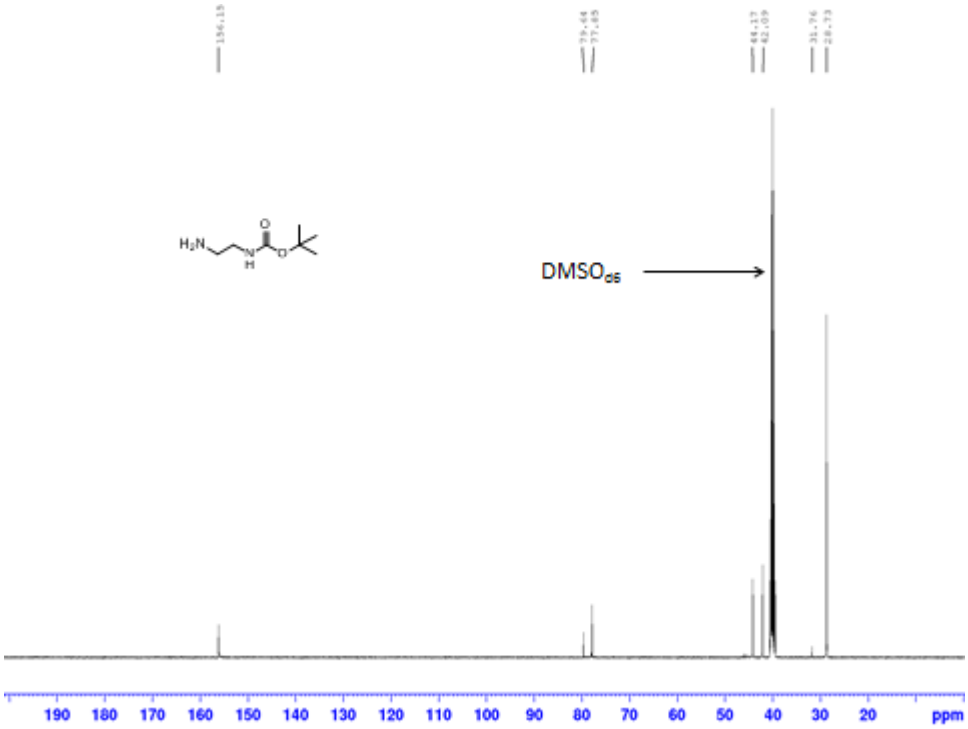

2A 12: *The ^{13}C NMR spectrum of* ***81*** *(125.76 MHz, DMSO-$_{d6}$)*

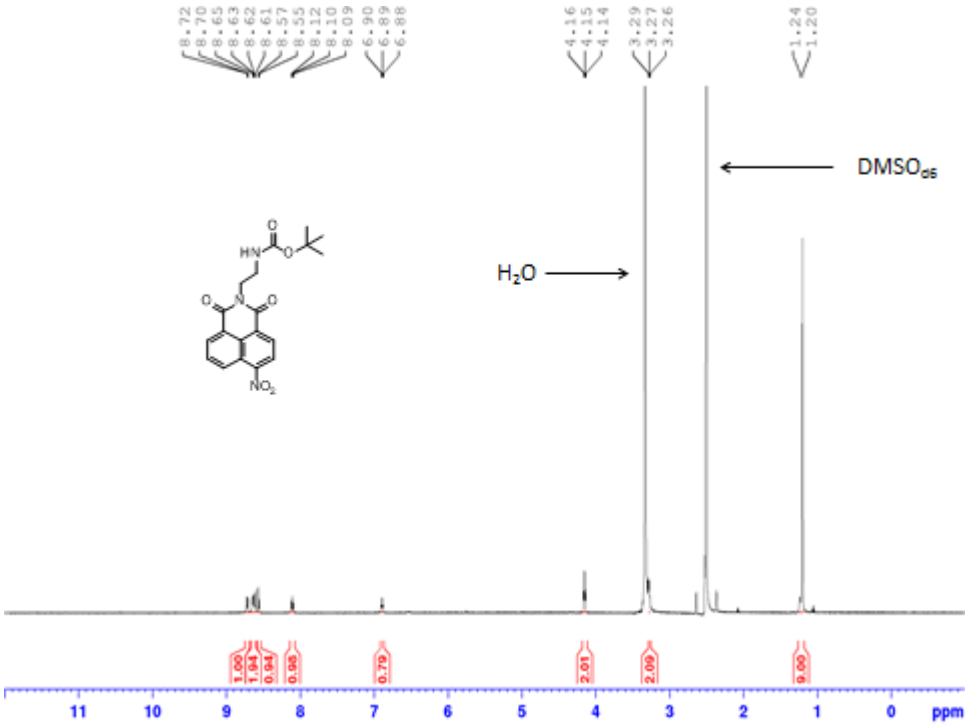

2A 13: *The ^{1}H NMR spectrum of* ***82*** *(500.13 MHz, DMSO-$_{d6}$).*

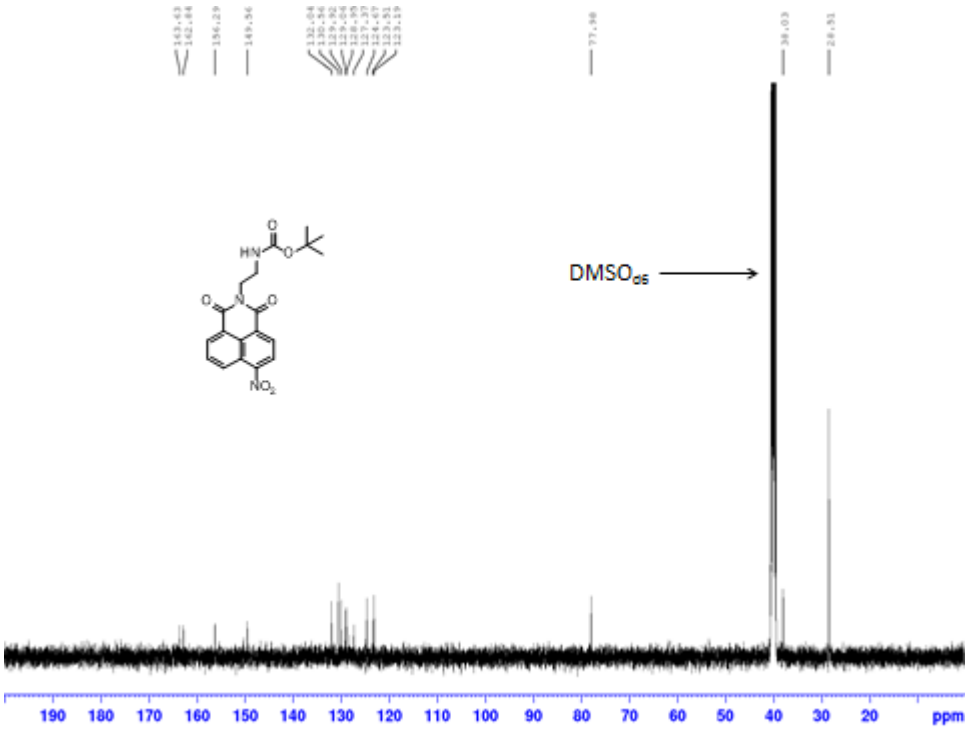

2A 14: *The ^{13}C NMR spectrum of* ***82*** *(125.76 MHz, DMSO-$_{d6}$)*

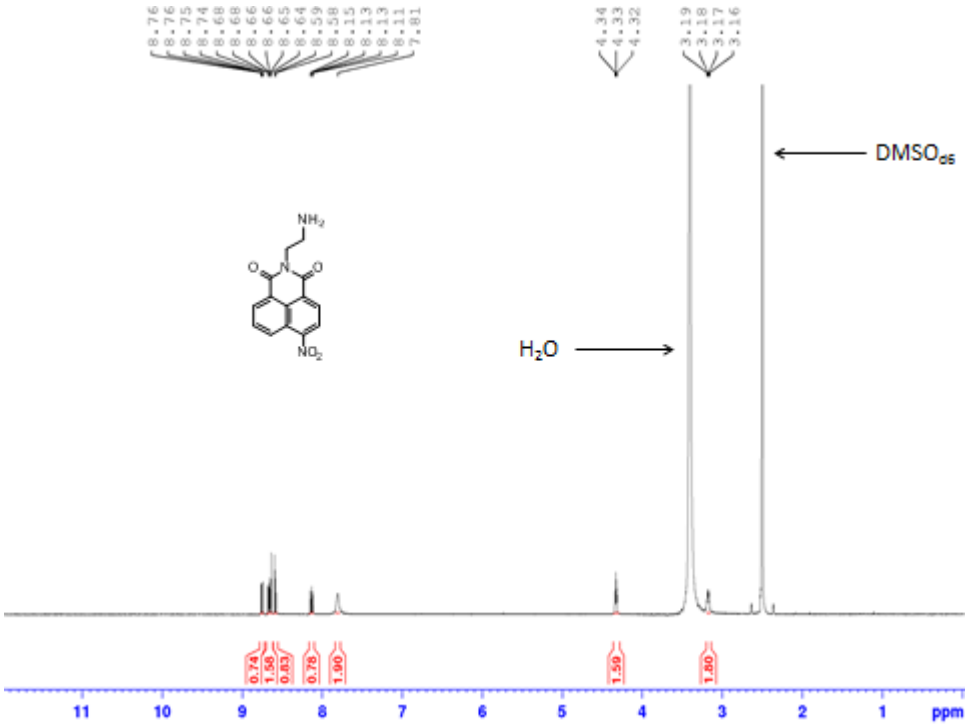

2A 15: *The ^{1}H NMR spectrum of **83** (500.13 MHz, DMSO-$_{d6}$).*

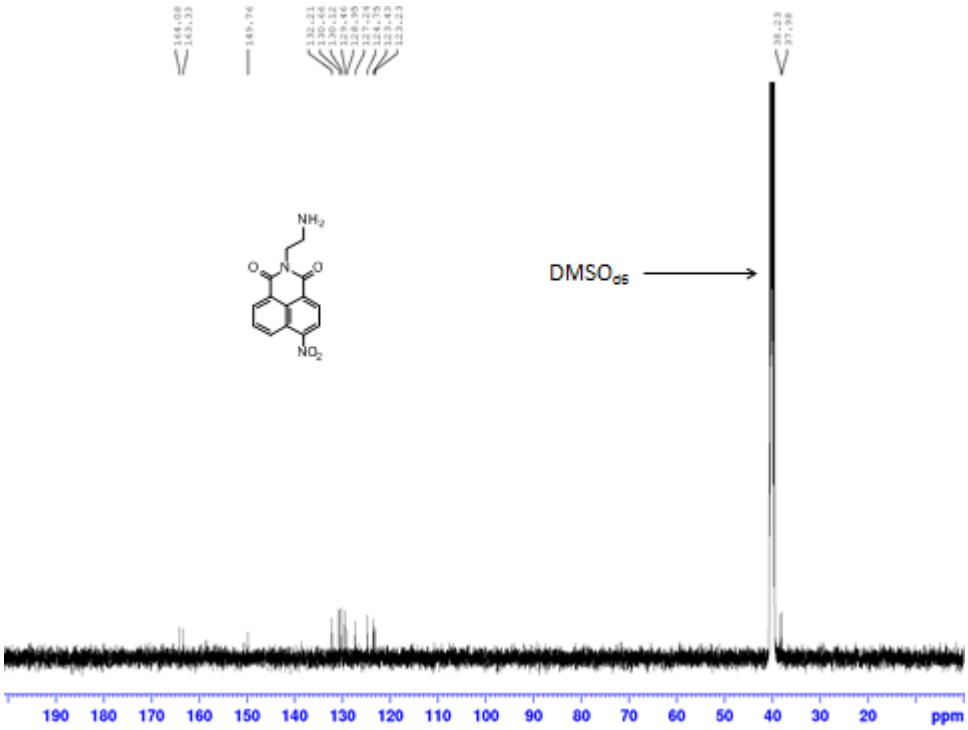

2A 16: *The ^{13}C NMR spectrum of **83** (125.76 MHz, DMSO-$_{d6}$)*

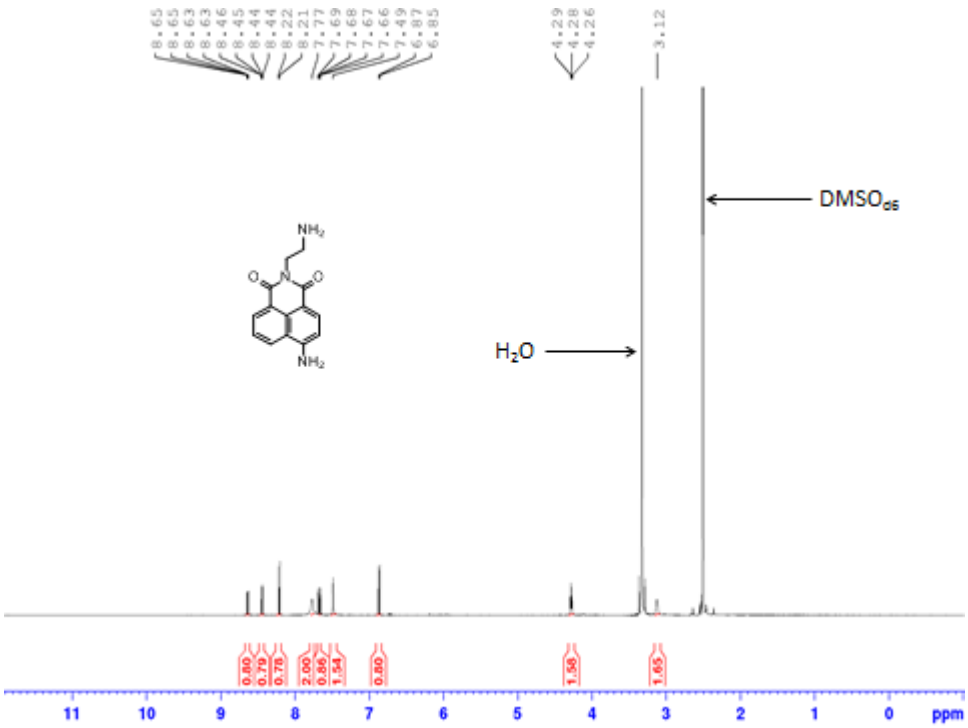

2A 17: *The ^{1}H NMR spectrum of* ***84*** *(500.13 MHz, DMSO-$_{d6}$).*

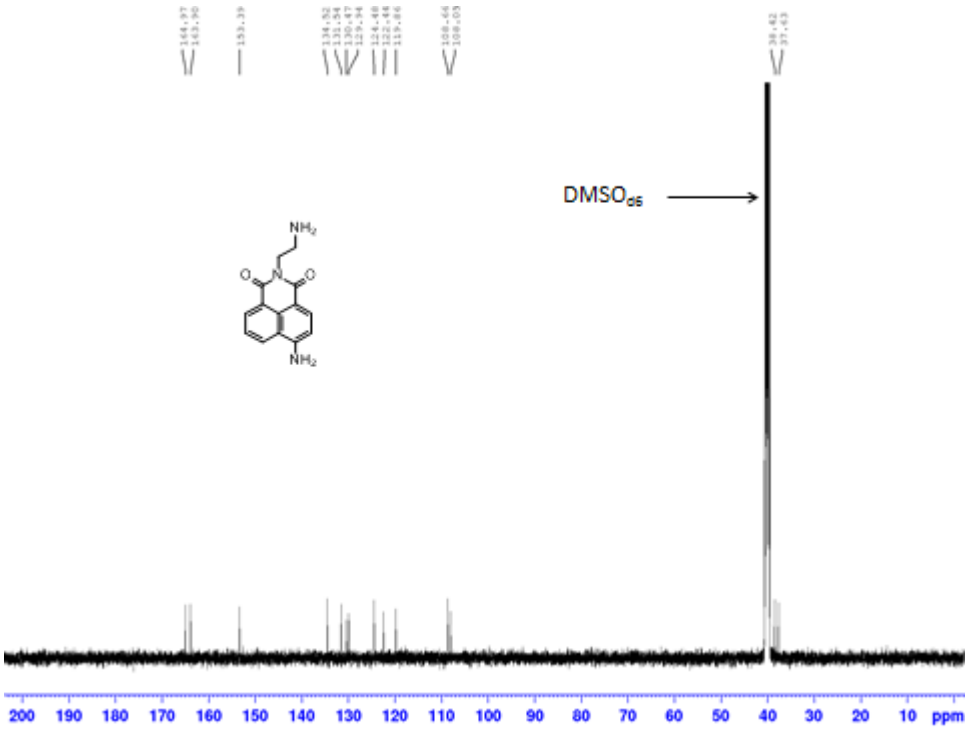

2A 18: *The ^{13}C NMR spectrum of* ***84*** *(125.76 MHz, DMSO-$_{d6}$)*

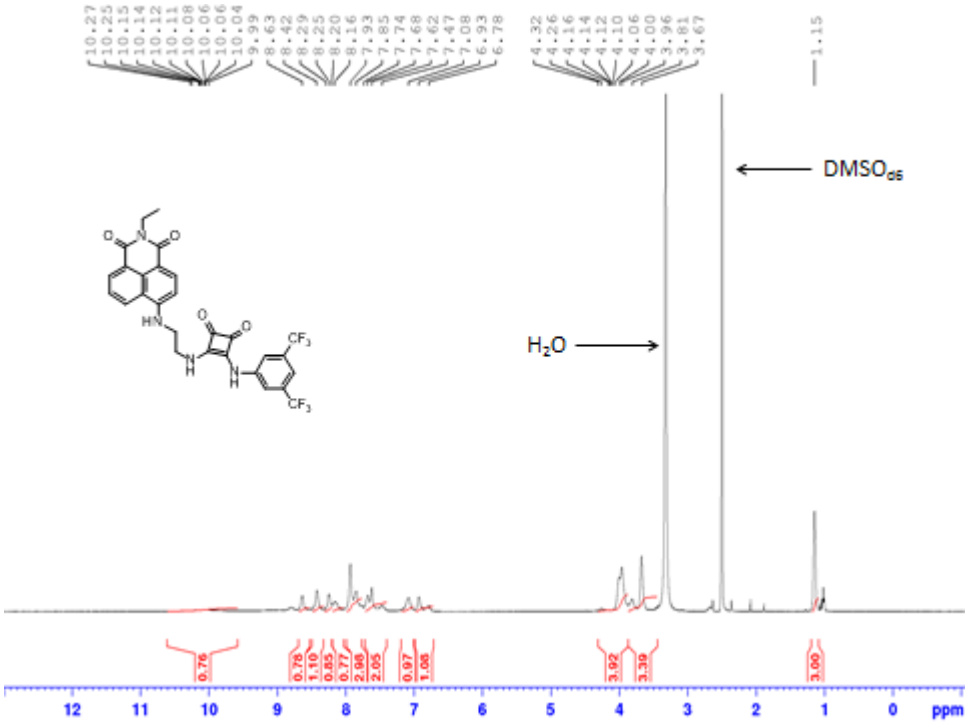

2A 19: *The ^{1}H NMR spectrum of **85** at 298 K (500.13 MHz, DMSO-$_{d6}$).*

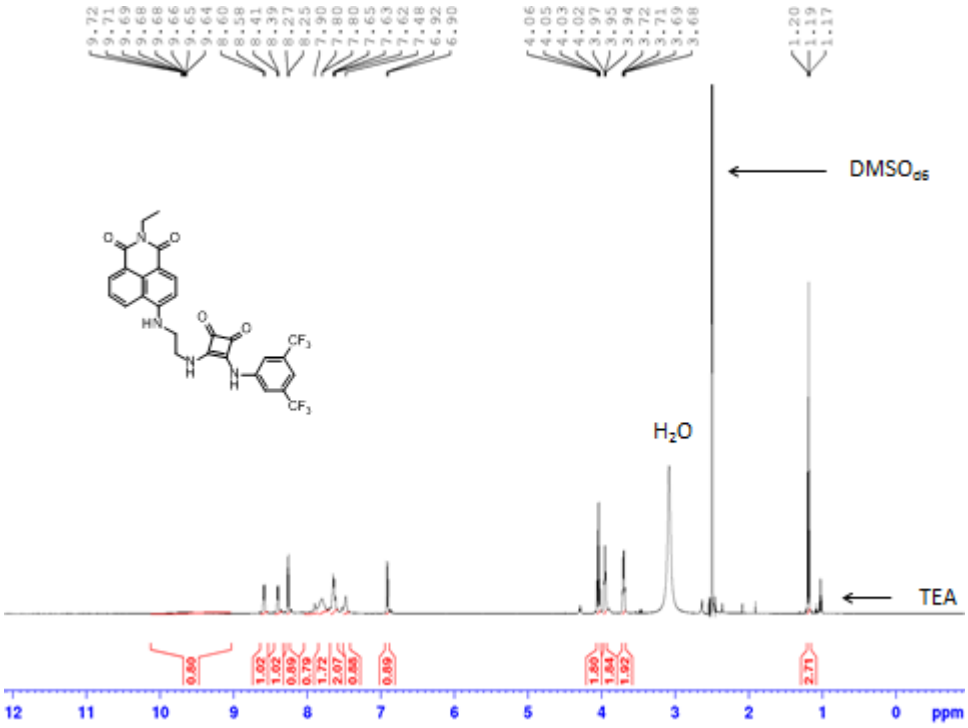

2A 20: *The ^{1}H NMR spectrum of **85** at 343 K (500.13 MHz, DMSO-$_{d6}$).*

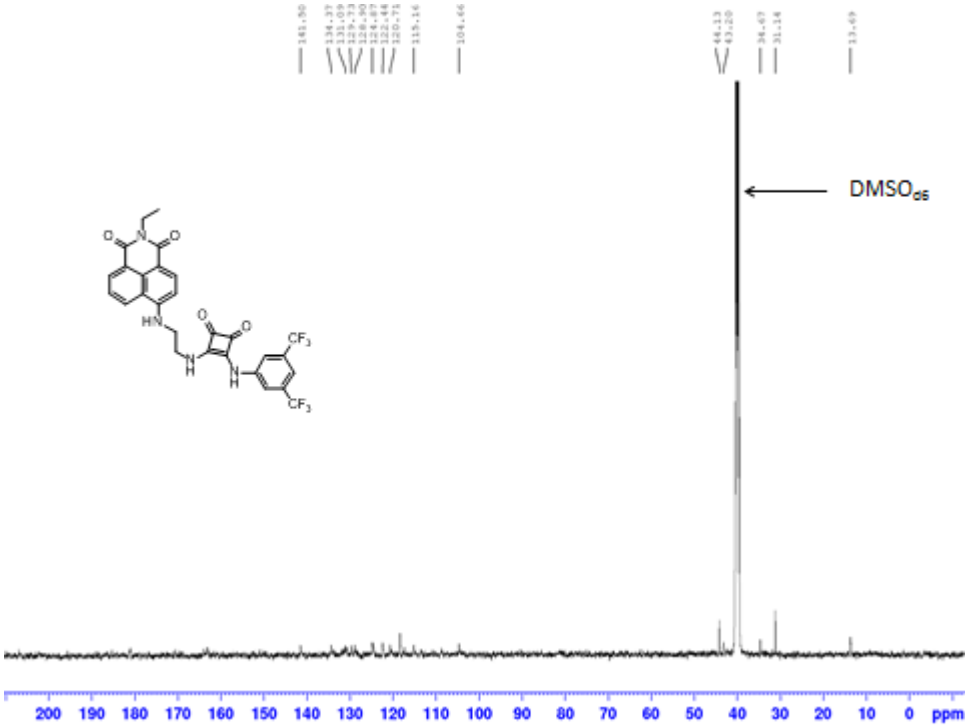

2A 21: *The ^{13}C NMR spectrum of **85** at 298 K (125.76 MHz, DMSO-$_{d6}$)*

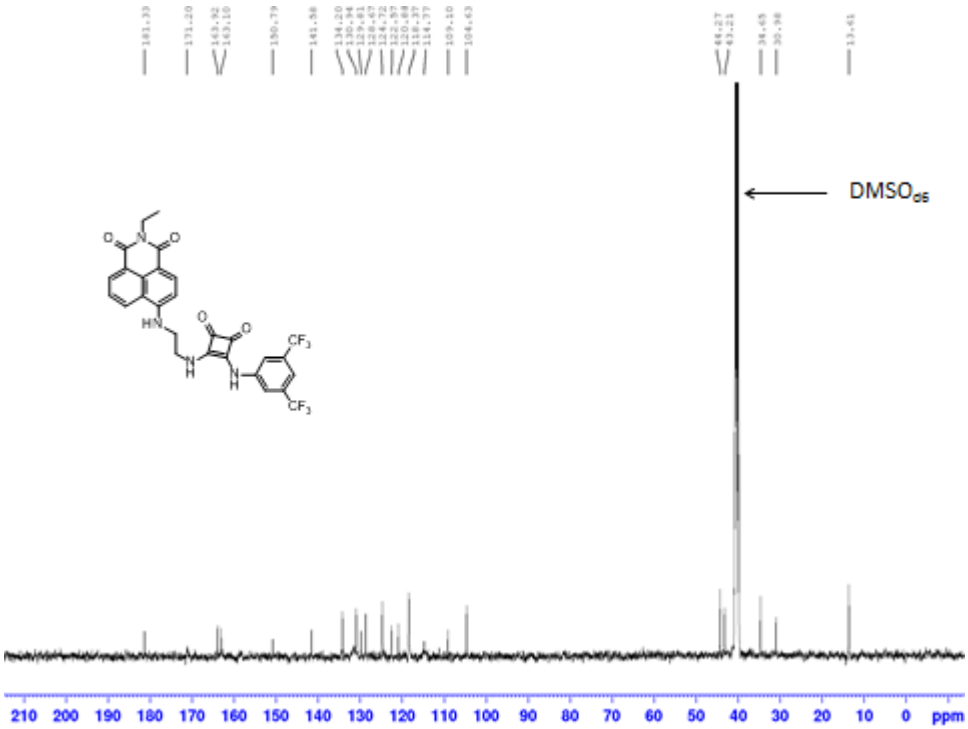

2A 22: *The ^{13}C NMR spectrum of **85** at 343 K (125.76 MHz, DMSO-$_{d6}$)*

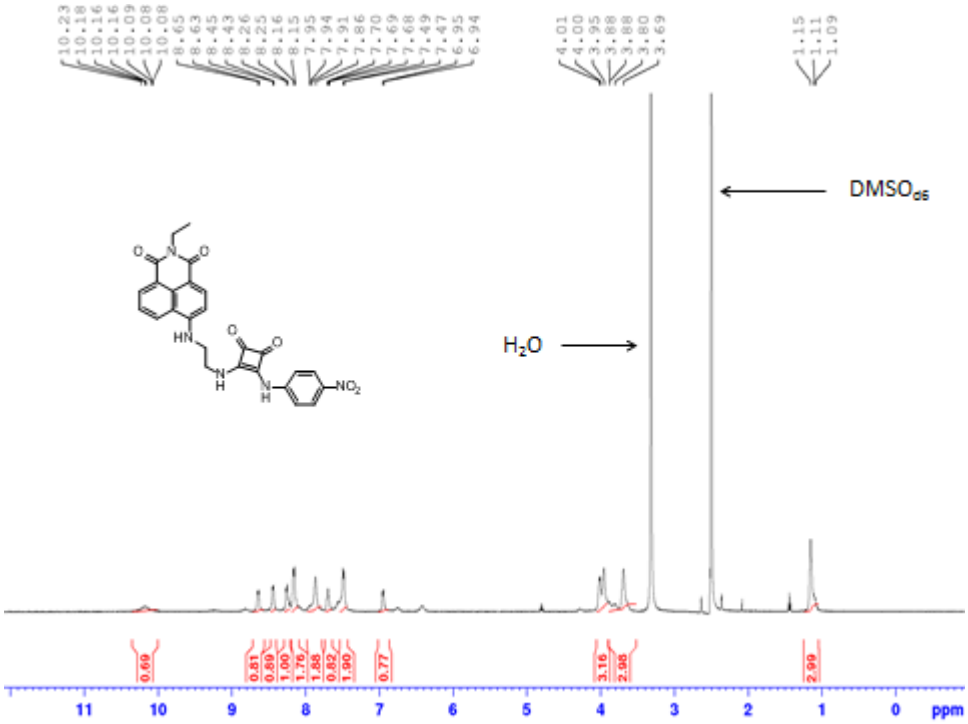

2A 23: *The ^{1}H NMR spectrum of **86** at 298 K (500.13 MHz, DMSO-$_{d6}$).*

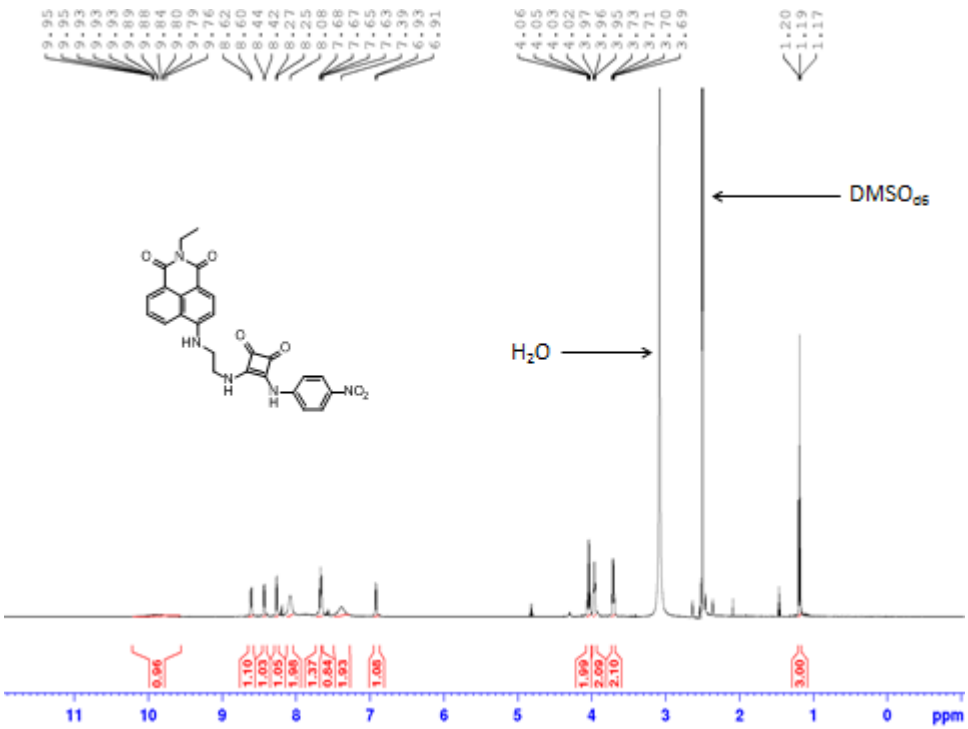

2A 24: *The ^{1}H NMR spectrum of **86** at 343 K (500.13 MHz, DMSO-$_{d6}$)*

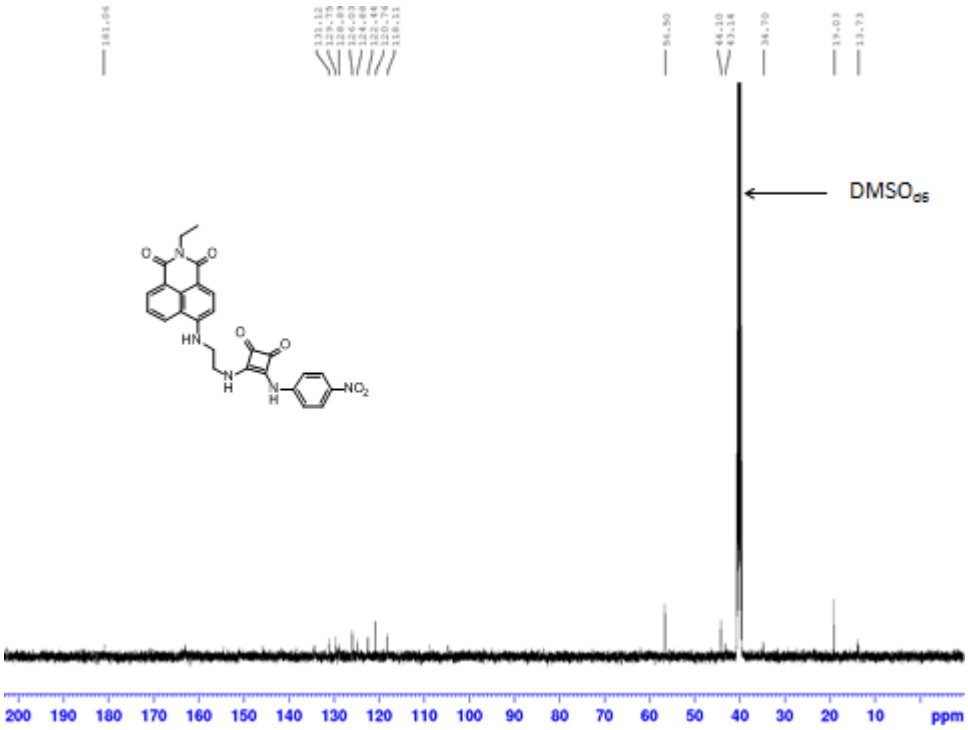

2A 25: *The ^{13}C NMR spectrum of **86** at 298 K (125.76 MHz, DMSO-$_{d6}$)*

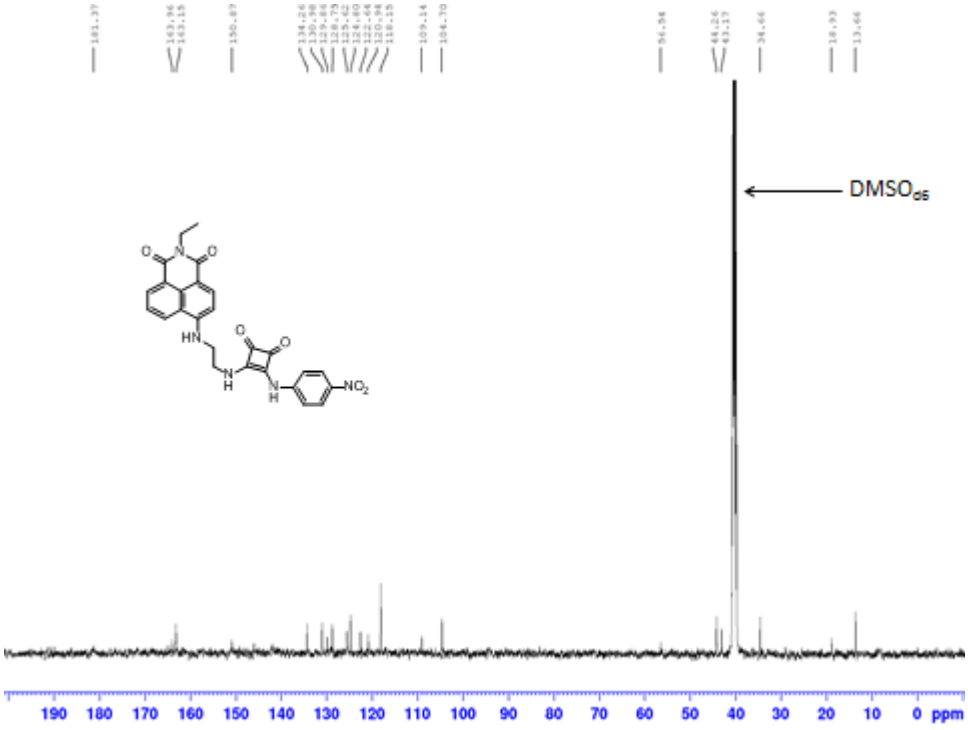

2A 26: *The ^{13}C NMR spectrum **86** at 343 K (125.76 MHz, DMSO-$_{d6}$)*

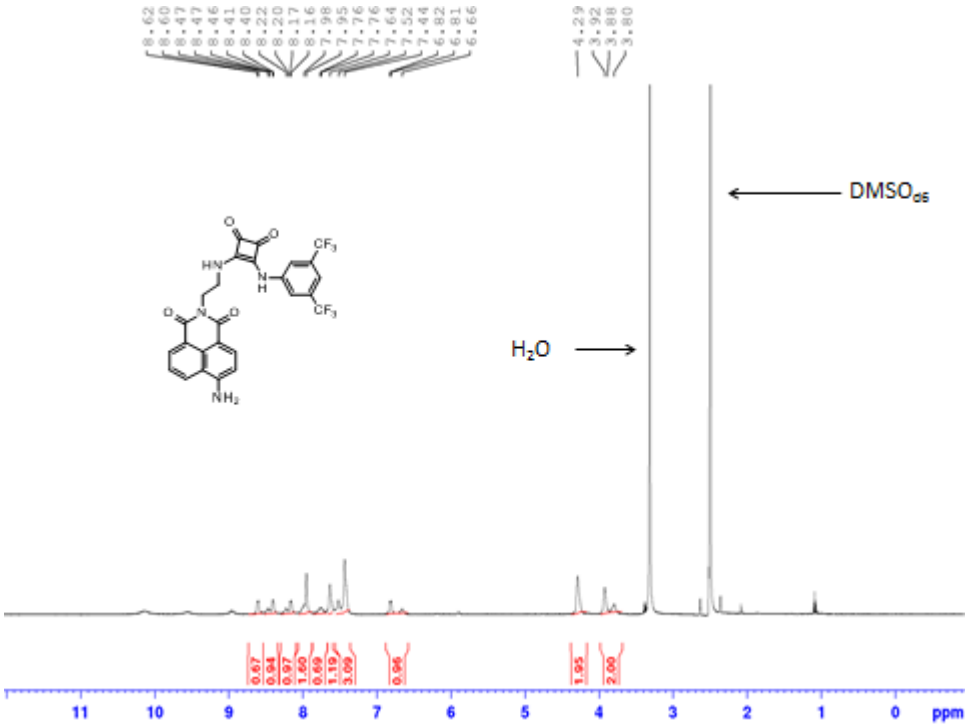

2A 27: *The ^{1}H NMR spectrum of **87** at 298 K (500.13 MHz, DMSO-$_{d6}$).*

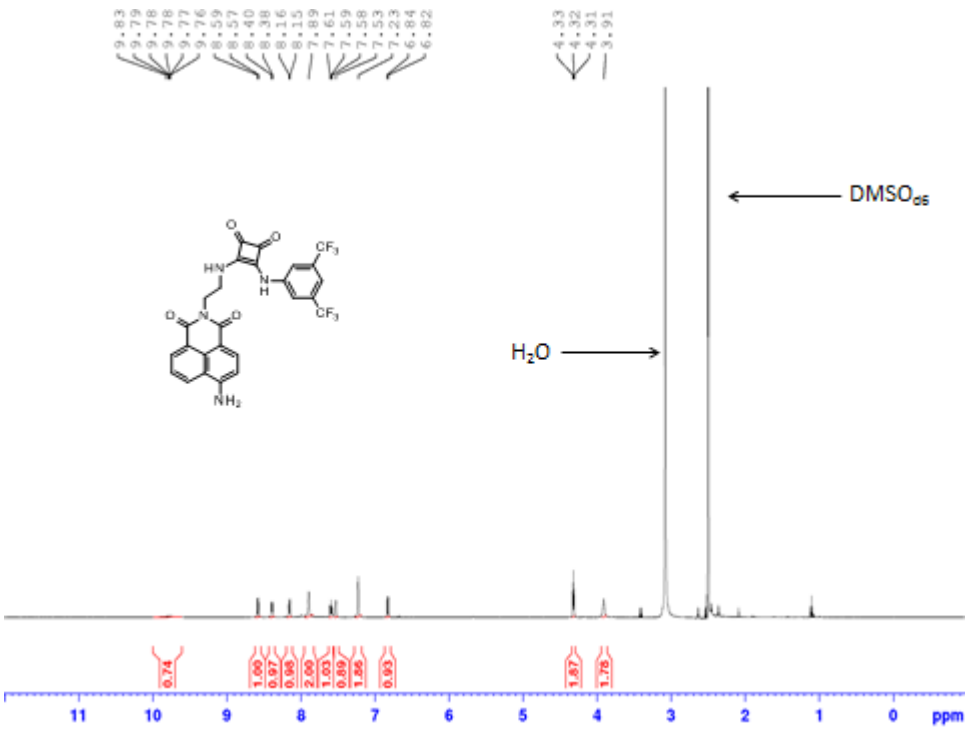

2A 28: *The ^{1}H NMR spectrum of **87** at 343 K (500.13 MHz, DMSO-$_{d6}$)*

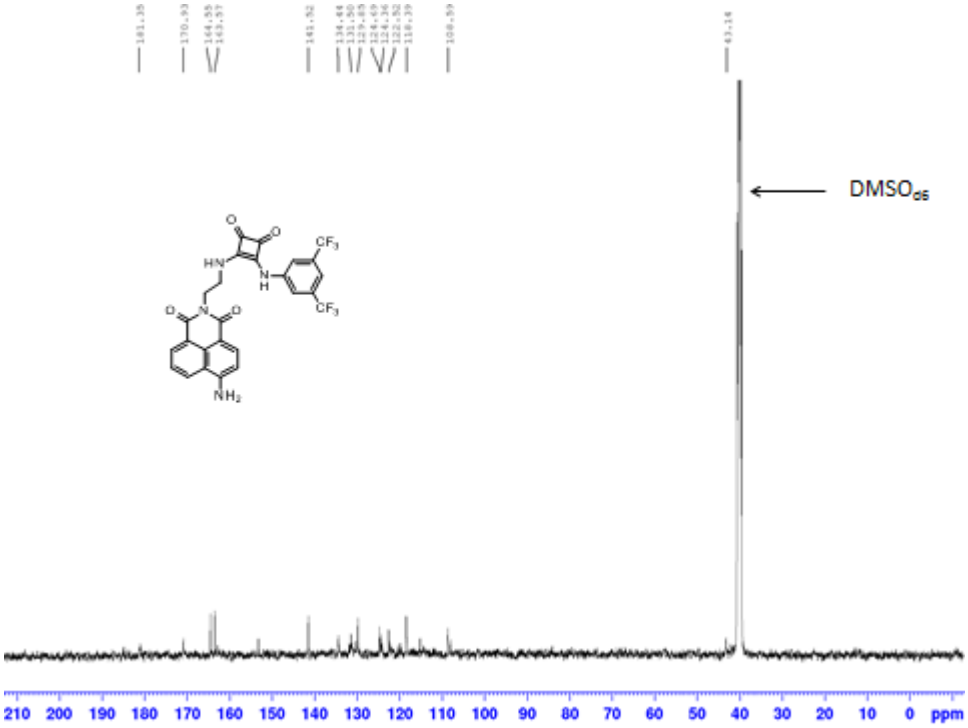

2A 29: *The ^{13}C NMR spectrum of **87** at 298 K (125.76 MHz, DMSO-$_{d6}$)*

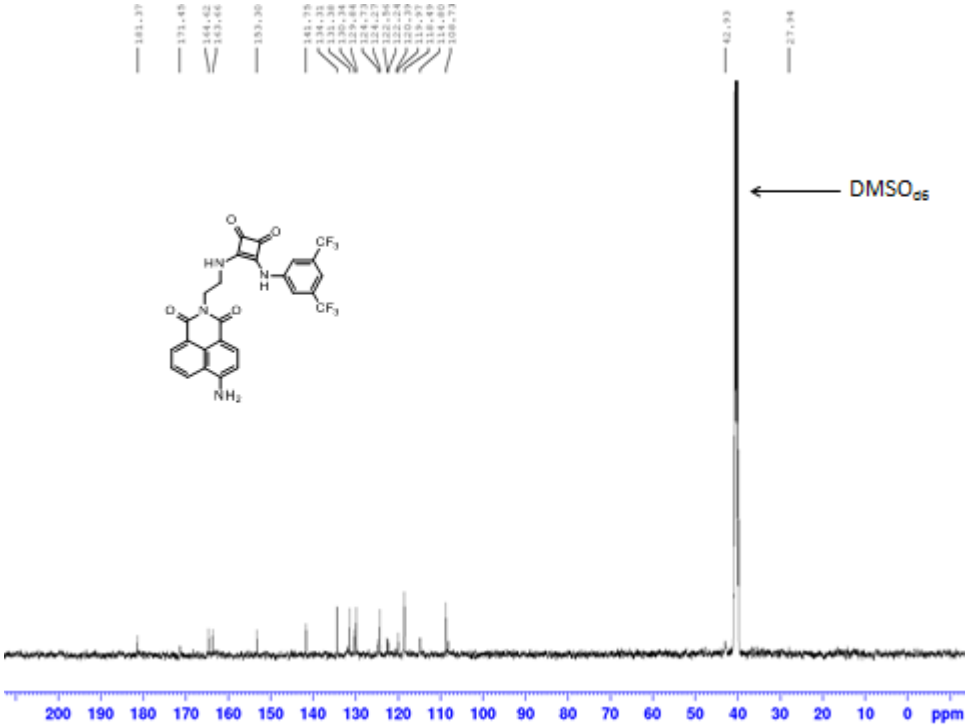

2A 30: *The ^{13}C NMR spectrum of **87** at 343 K (125.76 MHz, DMSO-$_{d6}$)*

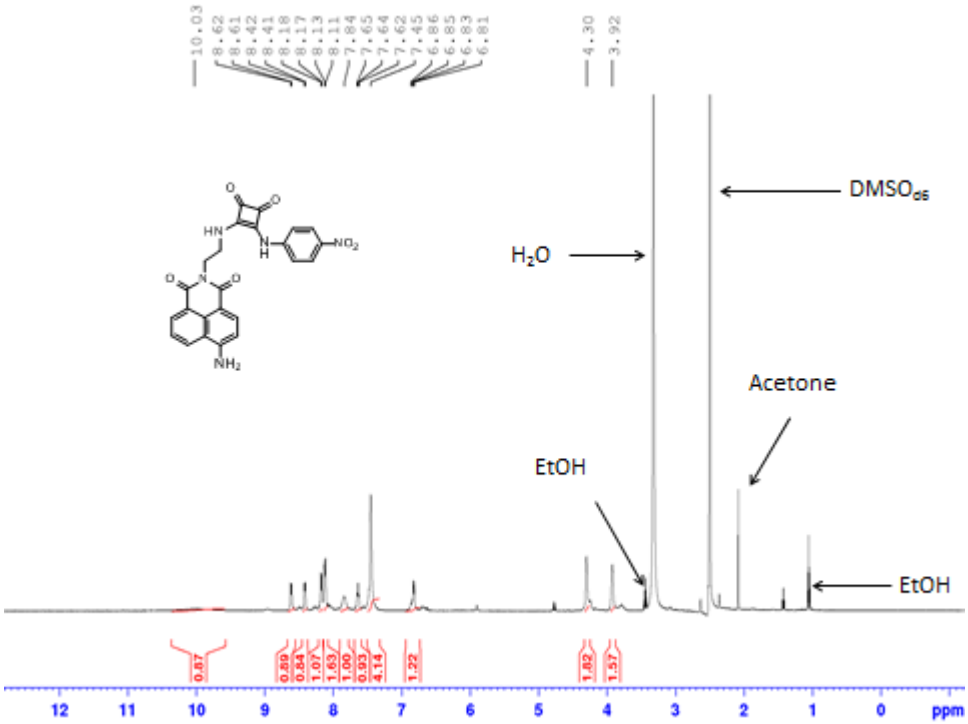

2A 31: *The ^{1}H NMR spectrum of **88** at 298 K (500.13 MHz, DMSO-$_{d6}$).*

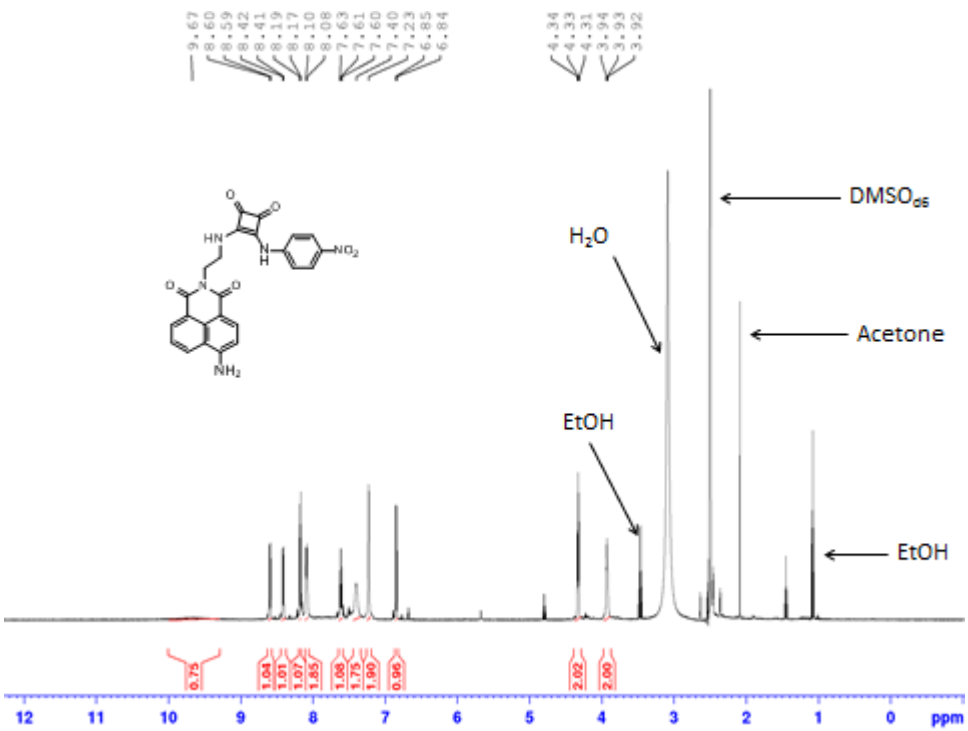

2A 32: *The ^{1}H NMR spectrum of **88** at 343 K (500.13 MHz, DMSO-$_{d6}$).*

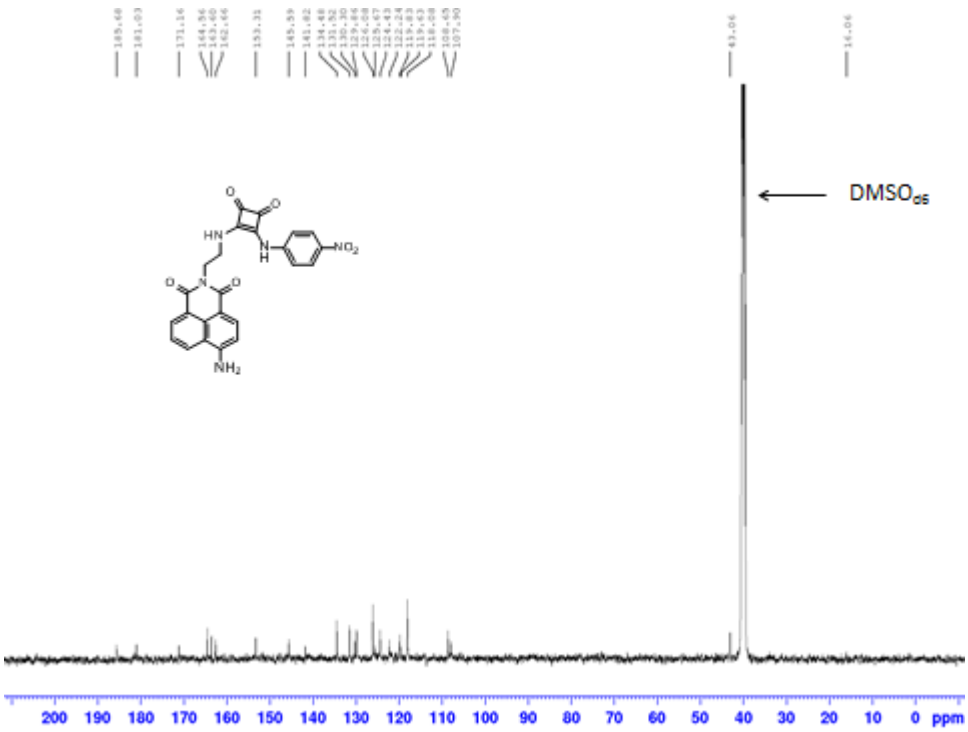

2A 33: *The ^{13}C NMR spectrum of **88** at 298 K (125.76 MHz, DMSO-$_{d6}$)*

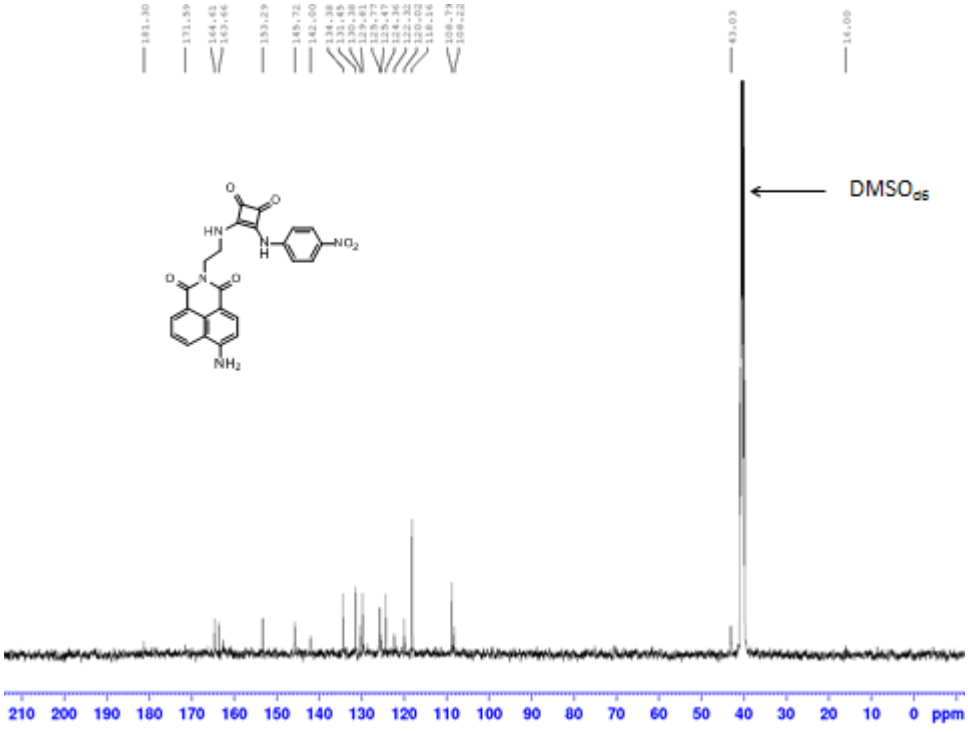

2A 34: *The ^{13}C NMR spectrum of **88** at 343 K (125.76 MHz, DMSO-$_{d6}$)*

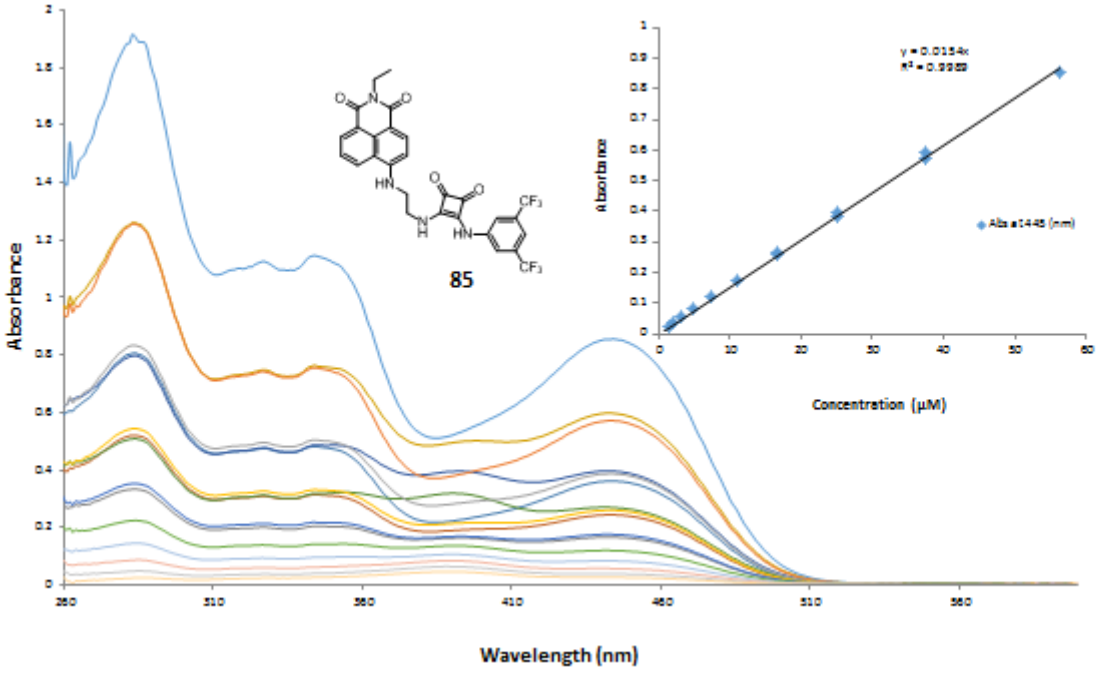

***2A 35**: Changes in UV/Visible spectra upon increasing concentration of **85** in DMSO* (0 – 57 μM). ***Inset:** Plot of absorbance at 445 nm as a function of increasing concentration of **85**.*

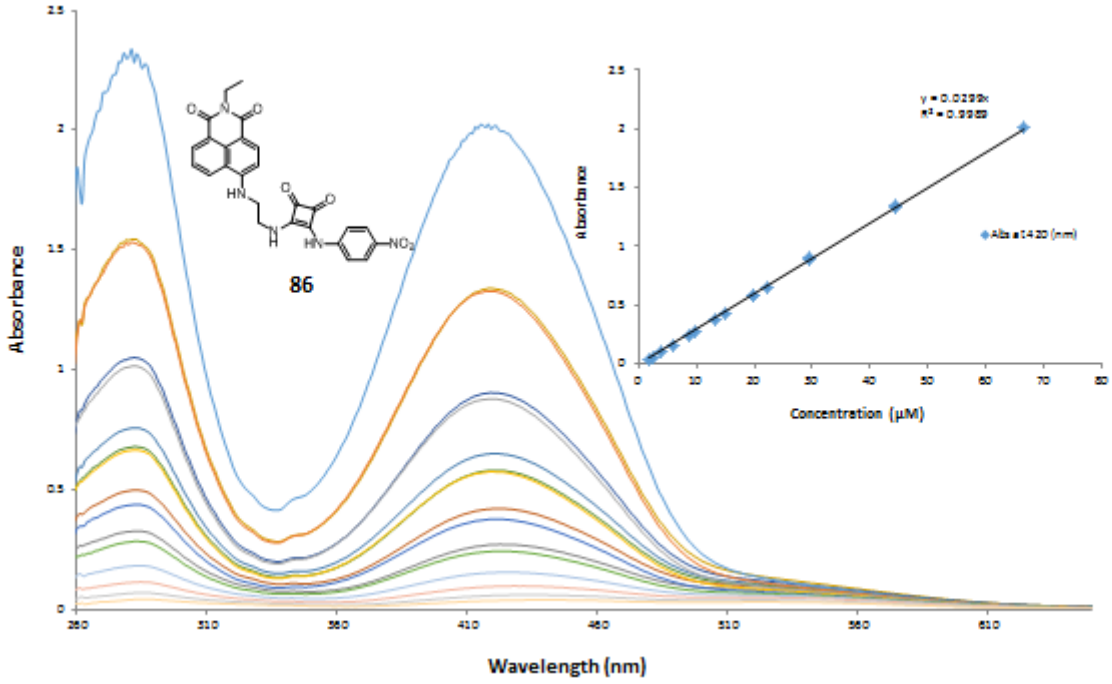

***2A 36**: Changes in UV/Visible spectra upon increasing concentration of **86** in DMSO* (0 – 67 μM). ***Inset:** Plot of absorbance at 420 nm as a function of increasing concentration of **86**.*

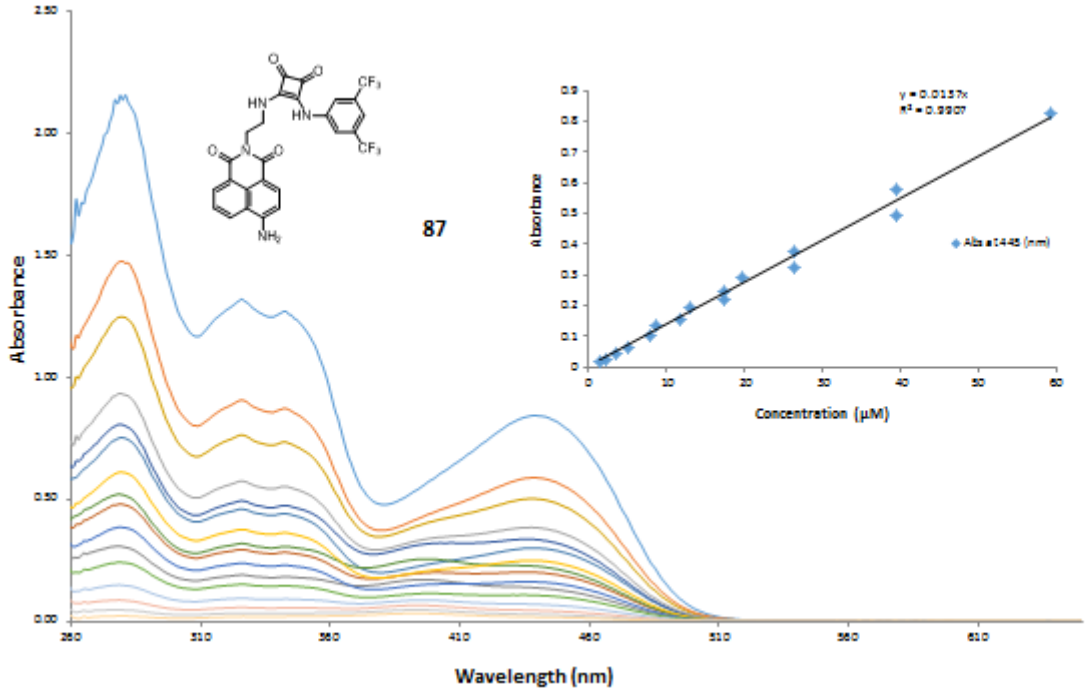

***2A 37**: Changes in UV/Visible spectra upon increasing concentration of **87** in DMSO* (0 – 60 μM). ***Inset:** Plot of absorbance at 445 nm as a function of increasing concentration of **87**.*

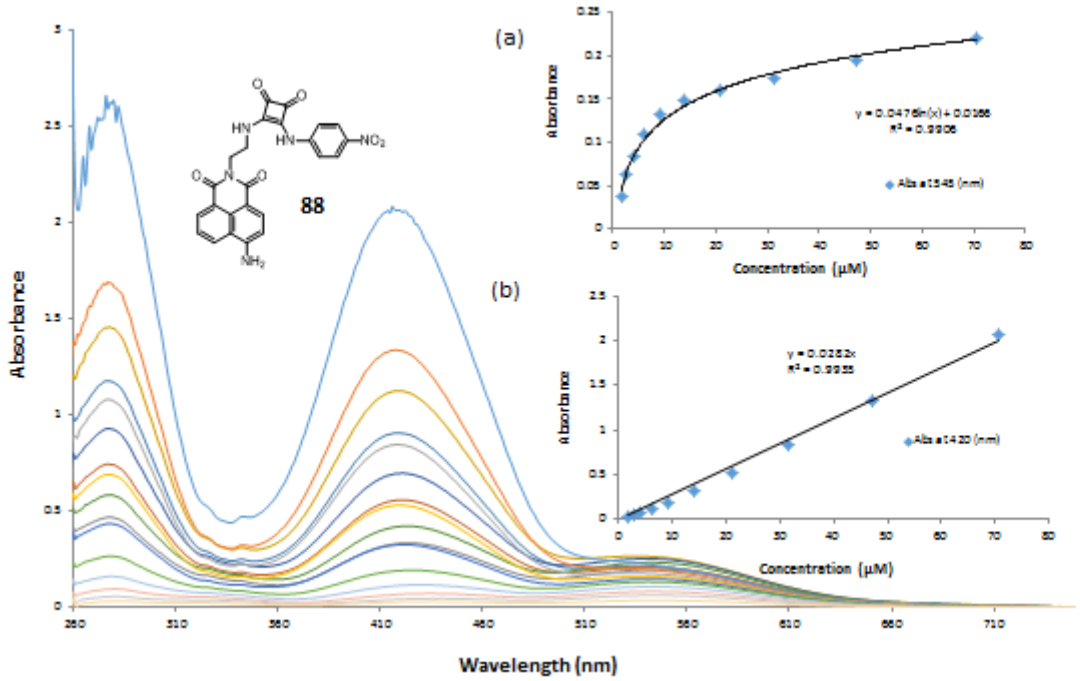

***2A 38**: Changes in UV/Visible spectra upon increasing concentration of **88** in DMSO* (0 – 70 μM). ***Inset:** Plot of absorbance at (a) 545 nm and (b) 420 nm as a function of increasing concentration of **88**.*

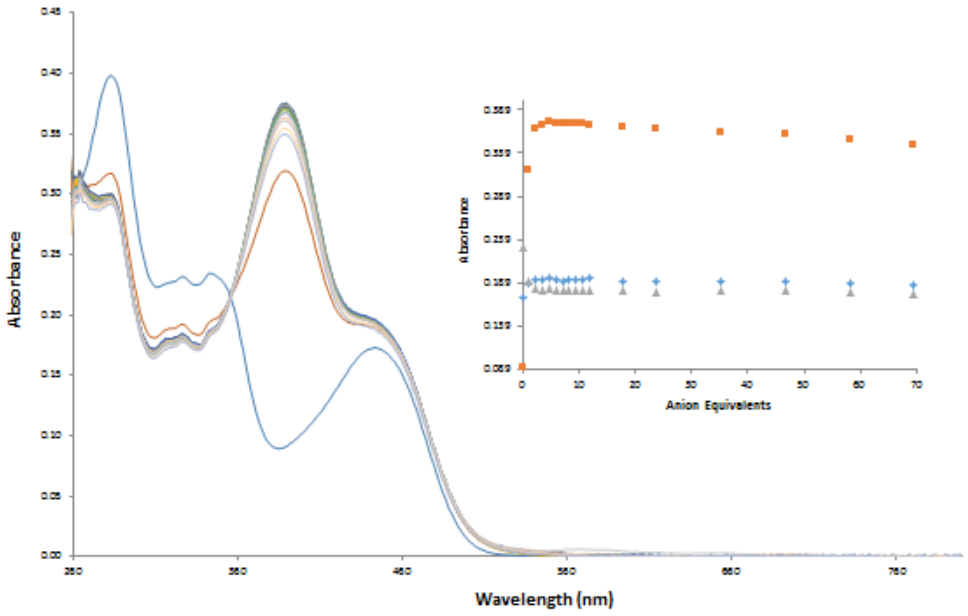

***2A 39**: Changes in the UV/Visible spectrum of **85** (11.9 µM) with increasing TBA acetate equivalents in DMSO (0 - 70 eqs). **Inset:** Plot of the change in absorbance at 325 nm (orange), 445 nm (blue) and 390 nm (grey) as a function of TBA acetate equivalents.*

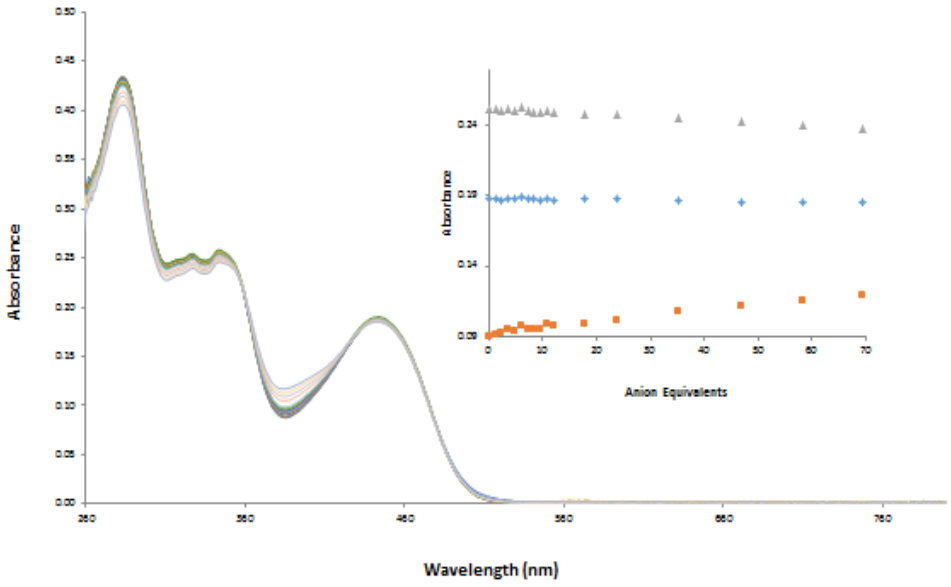

***2A 40**: Changes in the UV/Visible spectrum of **85** (11.9 µM) with increasing TBA chloride equivalents in DMSO (0 - 70 eqs). **Inset:** Plot of the change in absorbance at 390 nm (grey), 445 nm (blue) and 325 nm (orange) as a function of TBA chloride acetate equivalents.*

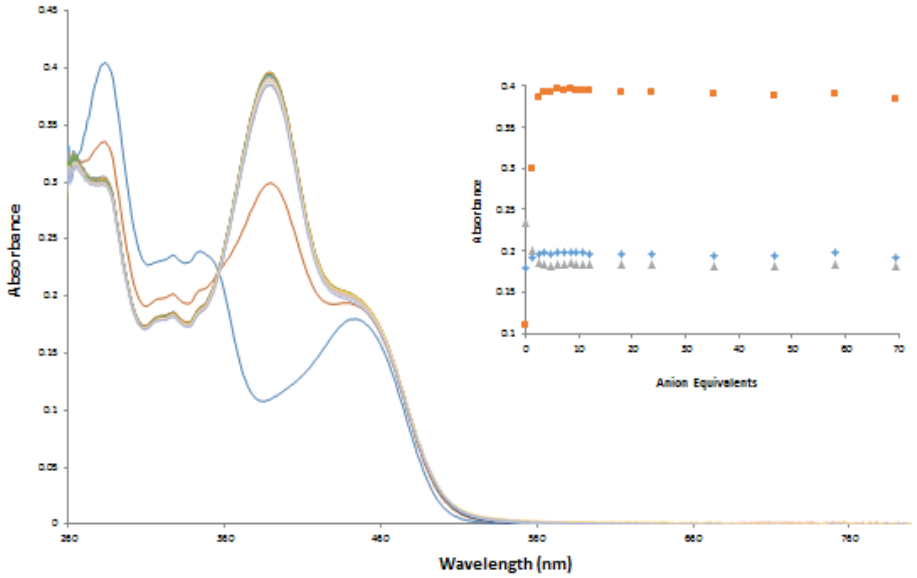

***2A 41**: Changes in the UV/Visible spectrum of **85** (11.9 µM) with increasing TBA fluoride equivalents in DMSO (0 - 70 eqs). **Inset:** Plot of the change in absorbance at 390 nm (orange), 445 nm (blue) and 325 nm (grey) as a function of TBA fluoride equivalents.*

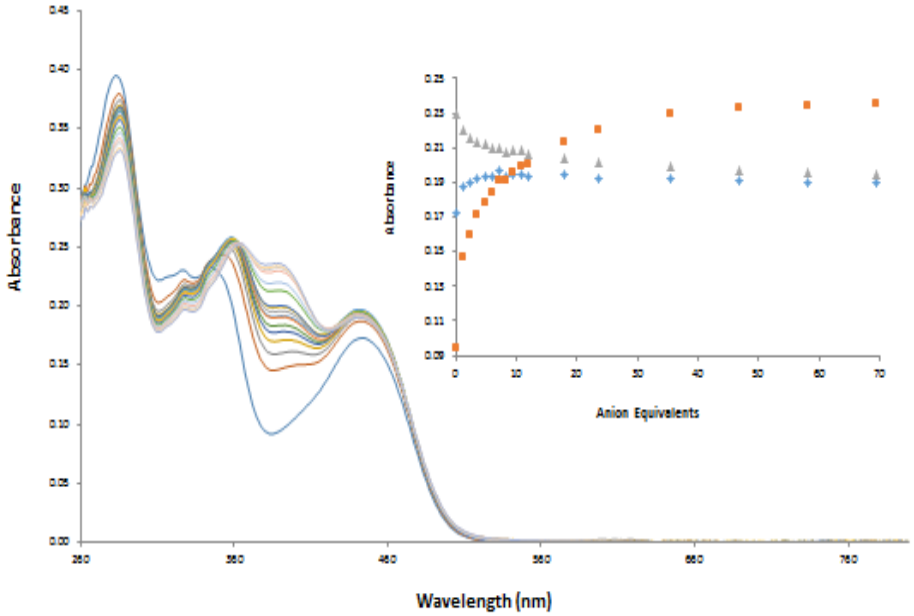

***2A 42**: Changes in the UV/Visible spectrum of **85** (11.9 µM) with increasing TBA phosphate equivalents in DMSO (0 - 70 eqs). **Inset:** Plot of the change in absorbance at 325 nm (grey), 445 nm (blue) and 390 nm (orange) as a function of TBA phosphate equivalents.*

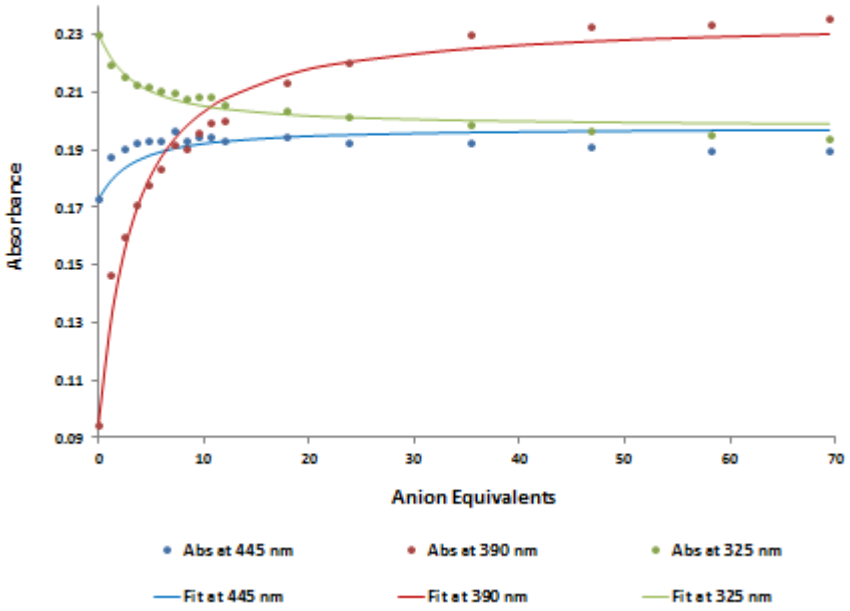

***2A 43**: Bind fit graph of UV titration of **85** (11.9 µM, DMSO) with increasing TBA phosphate equivalents in DMSO (0 - 70 eqs).*

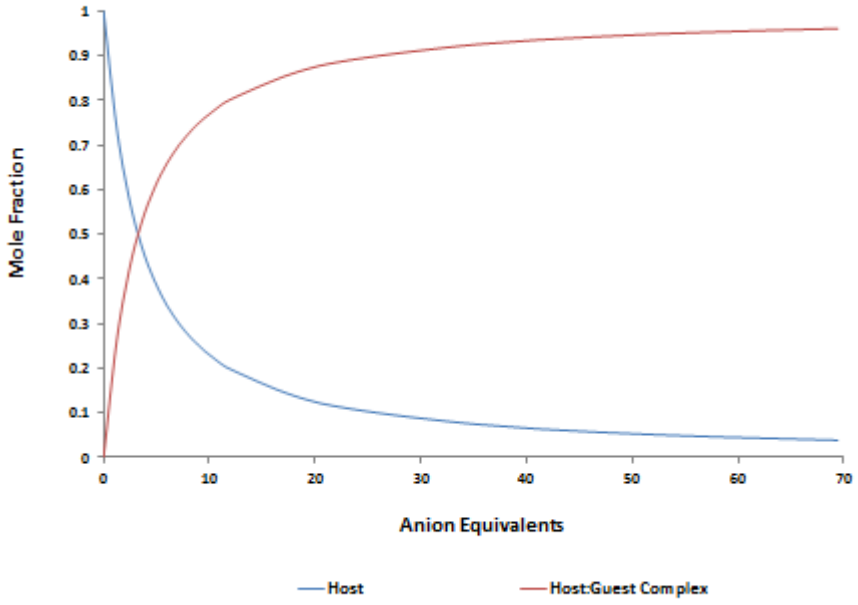

***2A 44**: Speciation graph of UV titration of **85** (11.9 µM, DMSO) with increasing TBA phosphate equivalents in DMSO (0 - 70 eqs).*

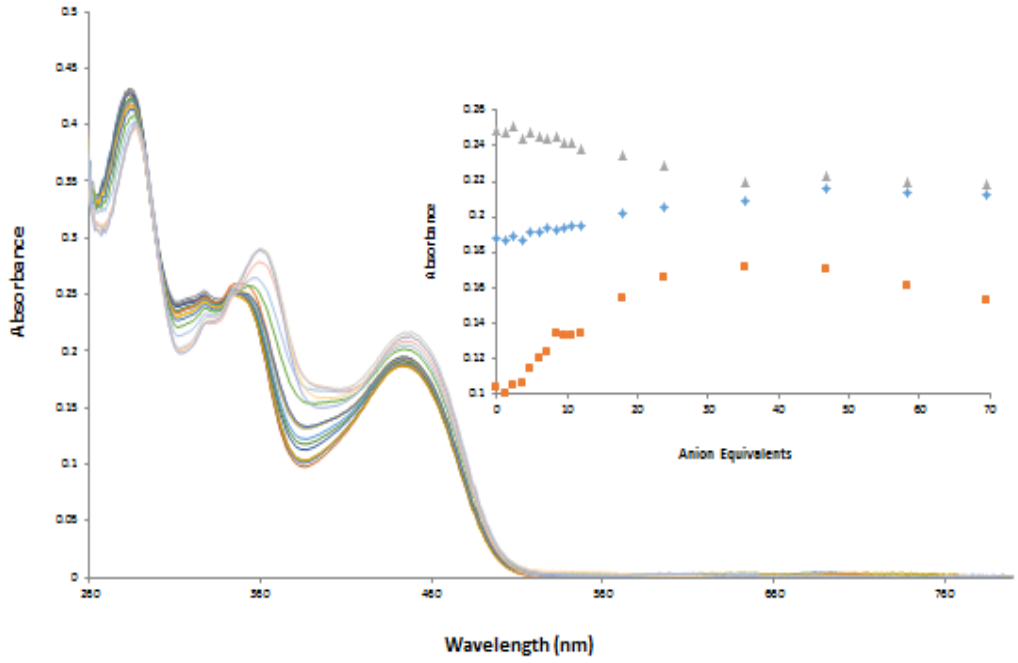

***2A 45**: Changes in the UV/Visible spectrum of **85** (11.9 µM) with increasing TBA sulphate equivalents in DMSO (0 - 70 eqs). **Inset:** Plot of the change in absorbance at 325 nm (grey), 445 nm (blue) and 390 nm (orange) as a function of TBA sulphate equivalents.*

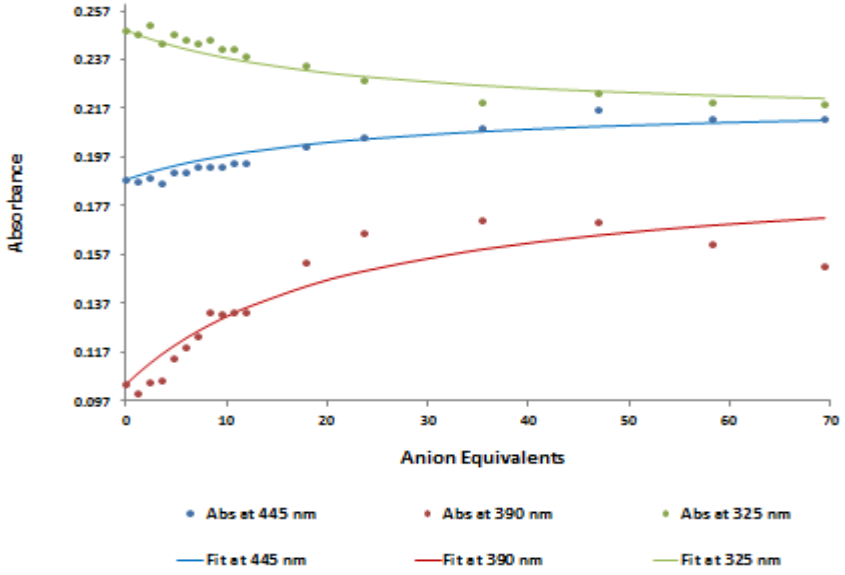

***2A 46**: Bind fit graph of UV titration of **85** (11.9 µM, DMSO) with increasing TBA sulphate equivalents in DMSO (0 - 70 eqs).*

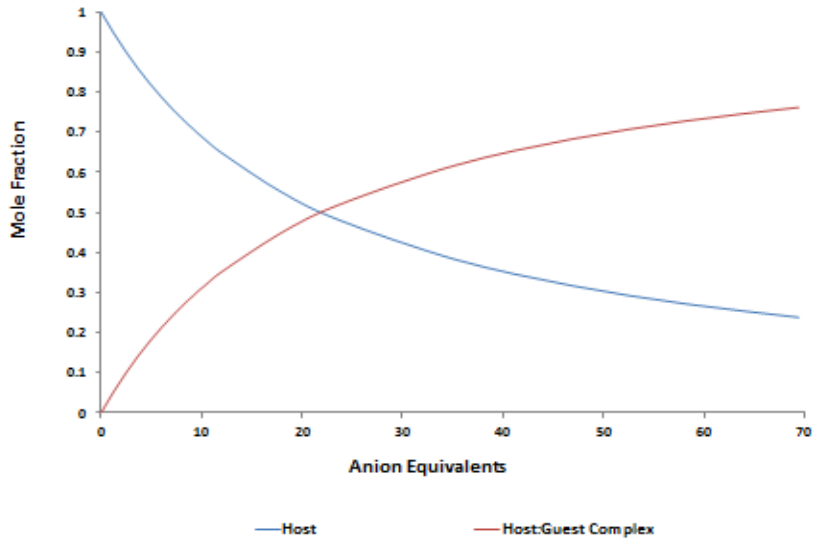

***2A 47**: Speciation graph of UV titration of **85** (11.9 µM, DMSO) with increasing TBA sulphate equivalents in DMSO (0 - 70 eqs).*

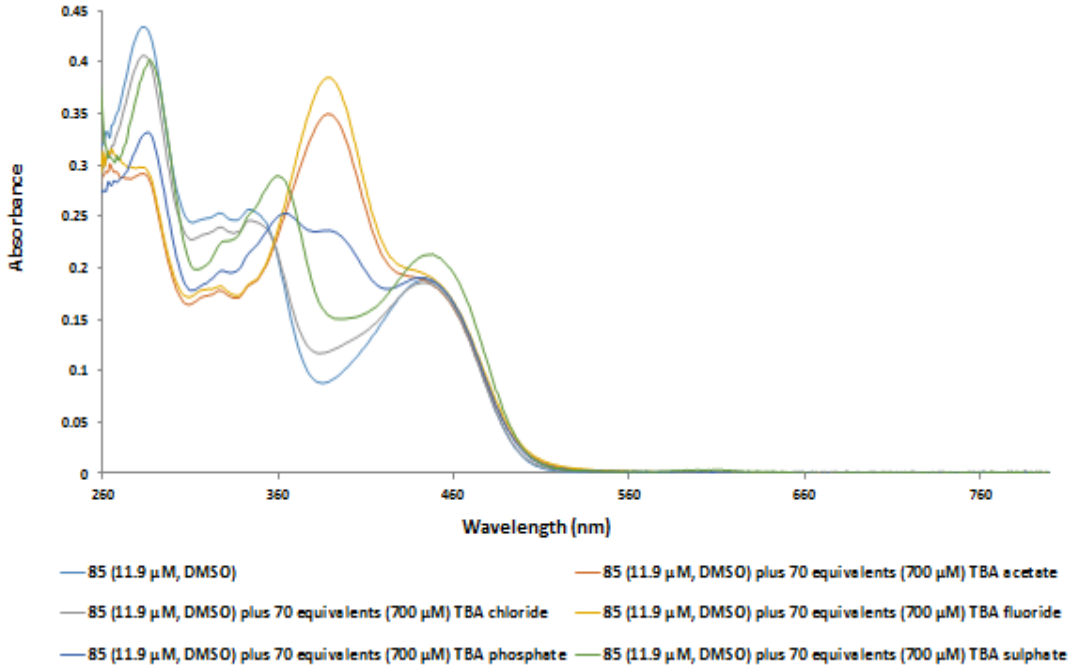

***2A 48**: Changes in the UV/Visible spectrum of **85** (11.9 µM, DMSO) with 70 equivalents (700 µM) of different solution of anions as TBA salts in DMSO (AcO^-, Cl^-, F^-, PO_4^{3-} and SO_4^{2-}).*

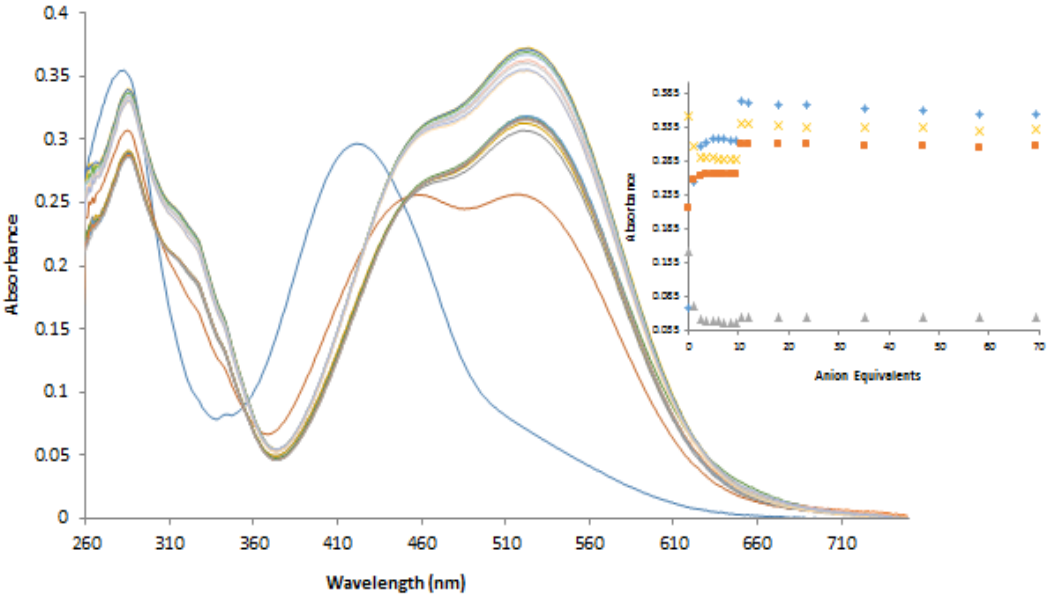

***2A 49**: Changes in the UV/Visible spectrum of **86** (11.9 μM) with increasing TBA acetate equivalents in DMSO (0 - 70 eqs). **Inset:** Plot of the change in absorbance at 285 nm (yellow), 460 nm (orange), 375 nm (grey) and 525 nm (blue) as a function of TBA acetate equivalents.*

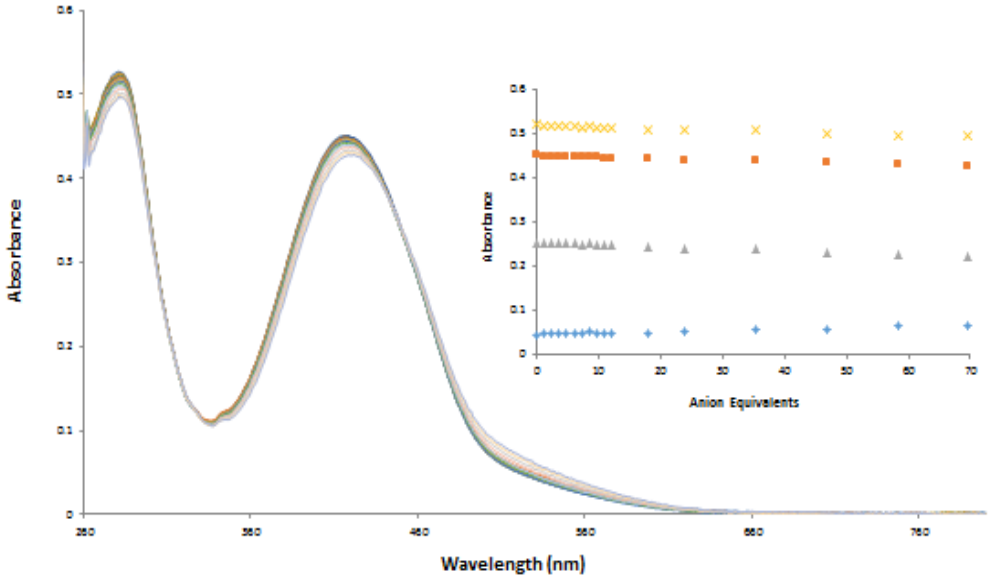

***2A 50**: Changes in the UV/Visible spectrum of **86** (11.9 μM) with increasing TBA chloride equivalents in DMSO (0 - 70 eqs). **Inset:** Plot of the change in absorbance at 285 nm (yellow), 420 nm (orange), 375 nm (grey) and 525 nm (blue) as a function of TBA chloride equivalents.*

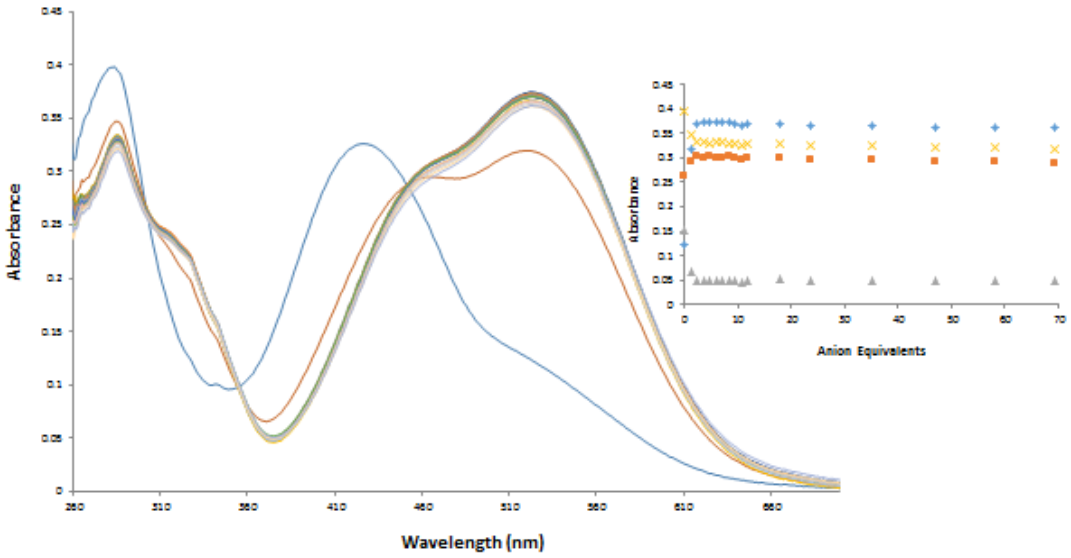

***2A 51**: Changes in the UV/Visible spectrum of **86** (11.9 µM) with increasing TBA fluoride equivalents in DMSO (0 - 70 eqs). **Inset:** Plot of the change in absorbance at 285 nm (yellow), 460 nm (orange), 375 nm (grey) and 525 nm (blue) as a function of TBA fluoride equivalents.*

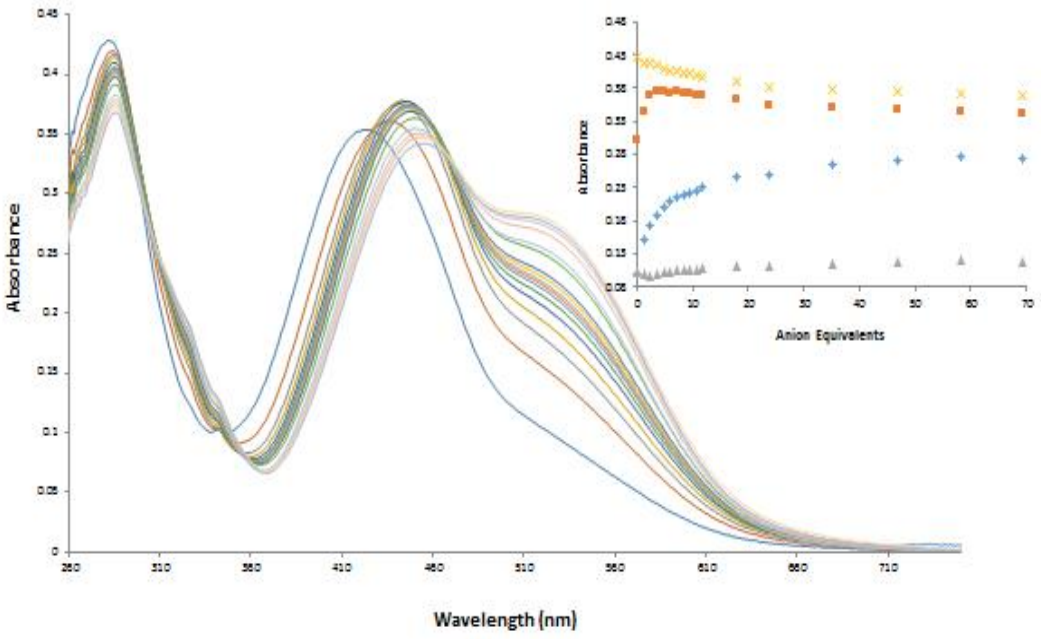

***2A 52**: Changes in the UV/Visible spectrum of **86** (11.9 µM) with increasing TBA phosphate equivalents in DMSO (0 - 70 eqs). **Inset:** Plot of the change in absorbance at 285 nm (yellow), 450 nm (orange), 345 nm (grey) and 525 nm (blue) as a function of TBA phosphate equivalents.*

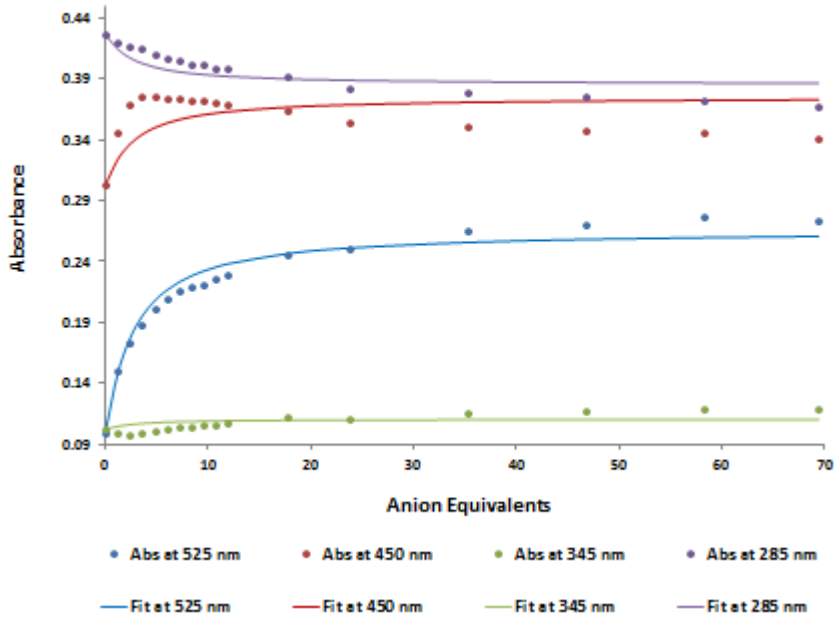

***2A 53**: Bind fit graph of UV titration of **86** (11.9 µM, DMSO) with increasing TBA phosphate equivalents in DMSO (0 - 70 eqs).*

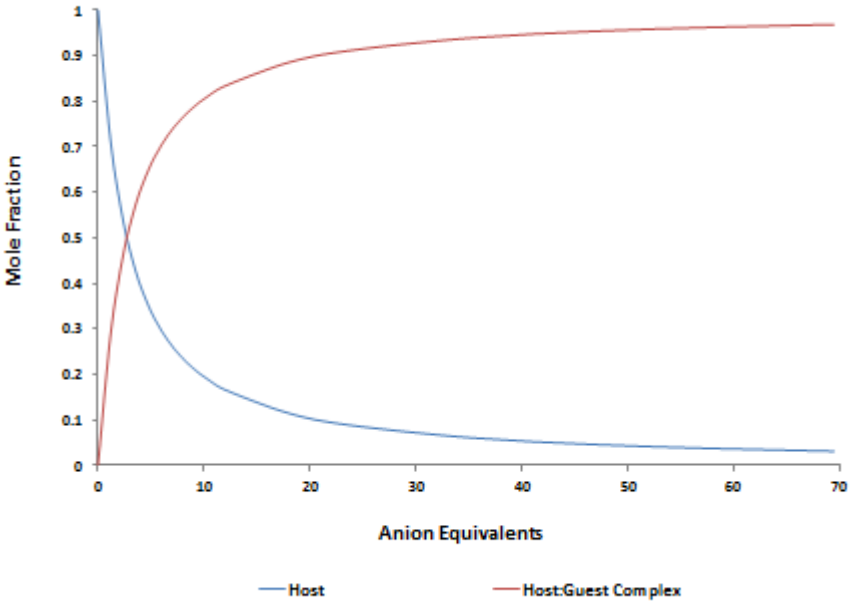

***2A 54**: Speciation graph of UV titration of **86** (11.9 µM, DMSO) with increasing TBA phosphate equivalents in DMSO (0 - 70 eqs).*

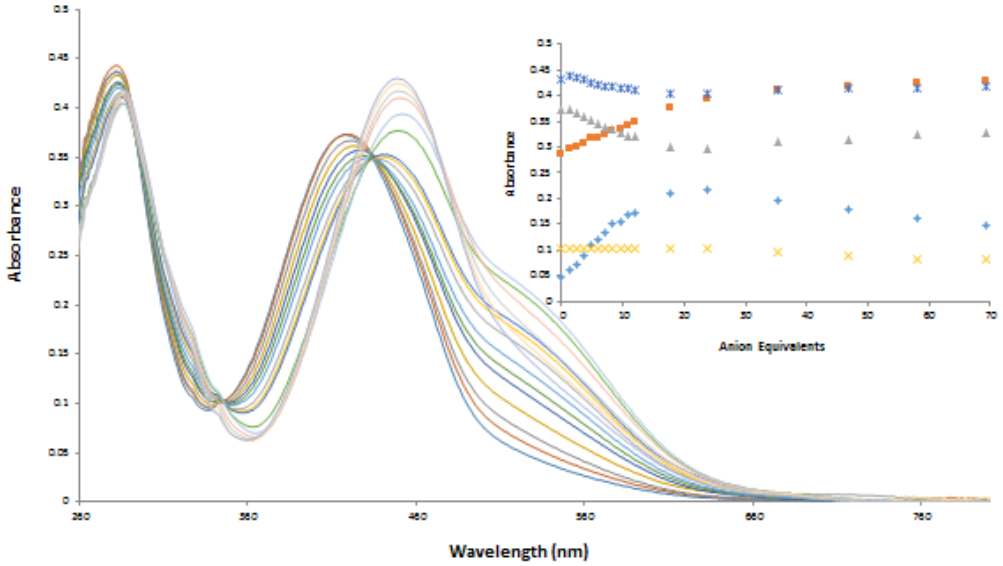

***2A 55**: Changes in the UV/Visible spectrum of **86** (11.9 µM) with increasing TBA sulphate equivalents in DMSO (0 - 70 eqs). **Inset:** Plot of the change in absorbance at 285 nm (dark blue), 420 nm (grey), 450 nm (orange), 345 nm (yellow) and 525 nm (light blue) as a function of TBA sulphate equivalents.*

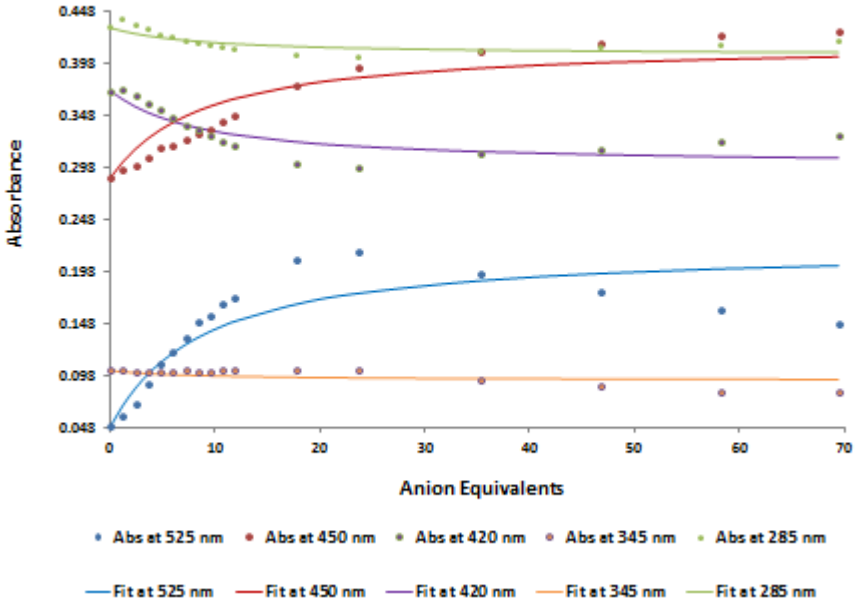

***2A 56**: Bind fit graph of UV titration of **86** (11.9 µM, DMSO) with increasing TBA sulphate equivalents in DMSO (0 - 70 eqs).*

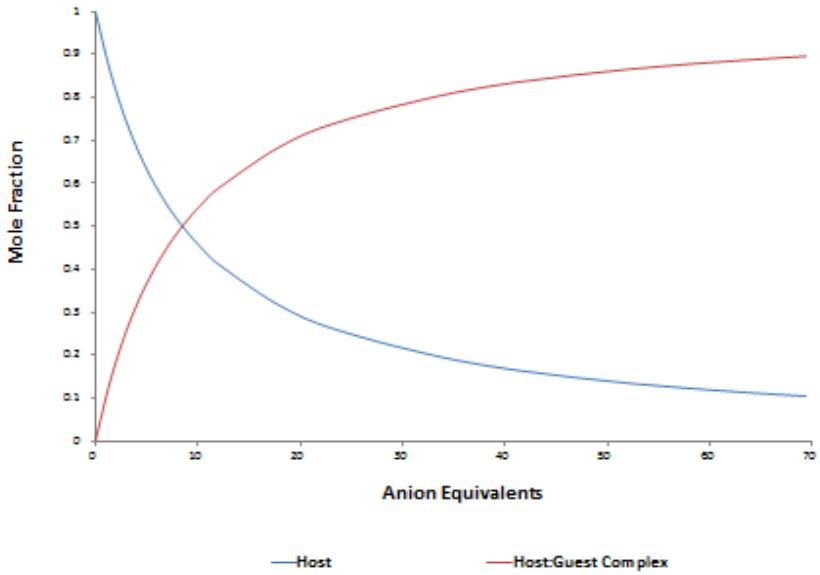

***2A 57**: Speciation graph of UV titration of **86** (11.9 µM, DMSO) with increasing TBA sulphate equivalents in DMSO (0 - 70 eqs).*

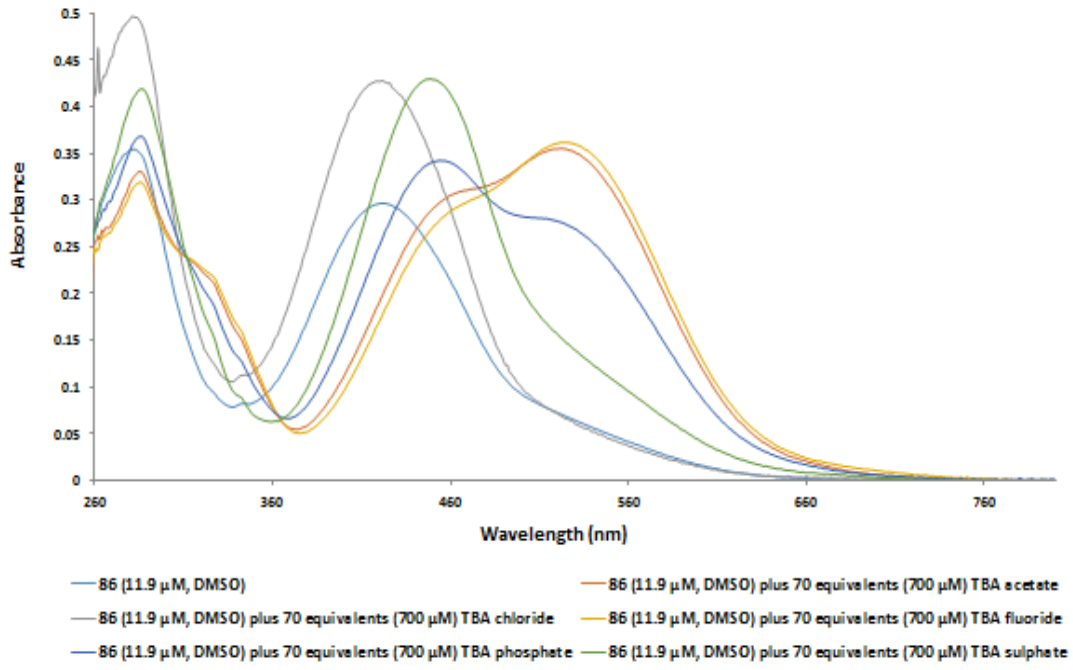

***2A 58**: Changes in the UV/Visible spectrum of **86** (11.9 µM, DMSO) with 70 equivalents (700 µM) of different solution of anions as TBA salts in DMSO (AcO^-, Cl^-, F^-, PO_4^{3-} and SO_4^{2-}).*

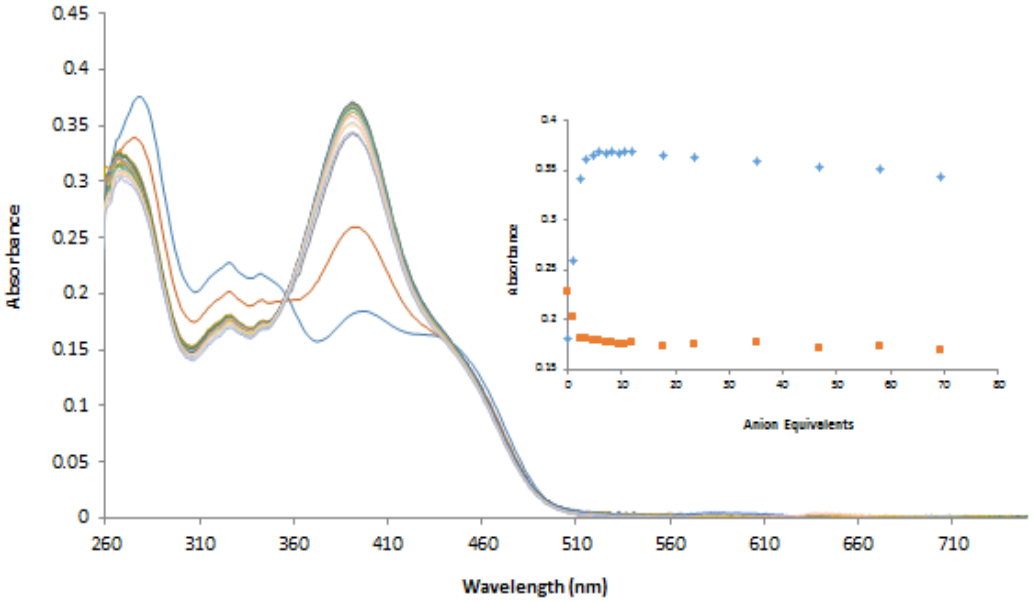

***2A 59**: Changes in the UV/Visible spectrum of **87** (11.9 µM) with increasing TBA acetate equivalents in DMSO (0 - 70 eqs). **Inset:** Plot of the change in absorbance at 325 nm (orange) and 390 nm (blue) as a function of TBA acetate equivalents.*

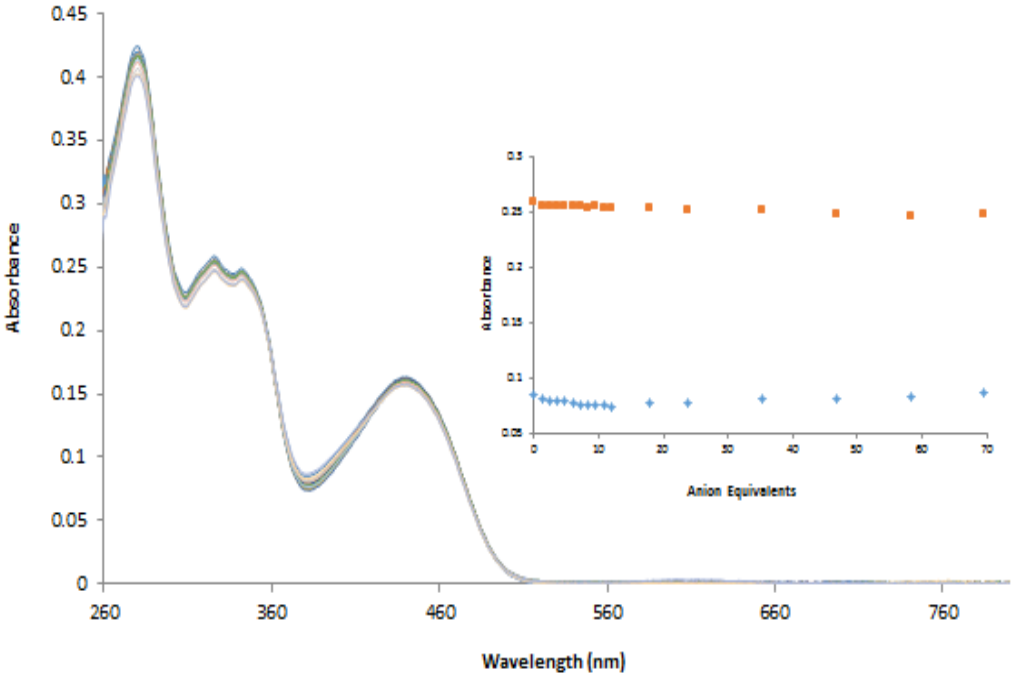

***2A 60**: Changes in the UV/Visible spectrum of **87** (11.9 µM) with increasing TBA chloride equivalents in DMSO (0 - 70 eqs). **Inset:** Plot of the change in absorbance at 325 nm (orange) and 380 nm (blue) as a function of TBA chloride equivalents.*

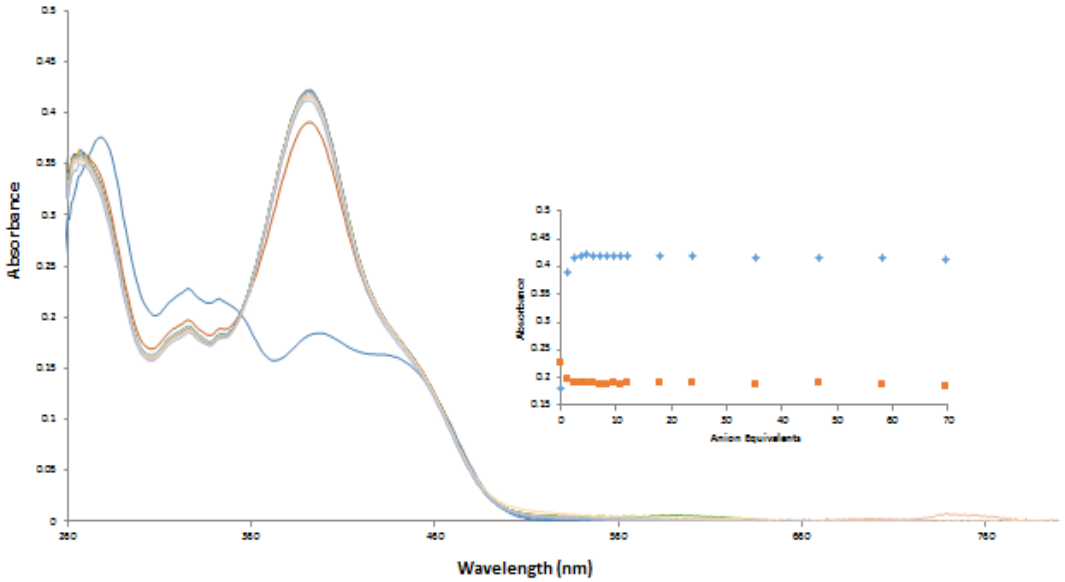

***2A 61**: Changes in the UV/Visible spectrum of **87** (11.9 µM) with increasing TBA fluoride equivalents in DMSO (0 - 70 eqs). **Inset:** Plot of the change in absorbance at 325 nm (orange) and 380 nm (blue) as a function of TBA fluoride equivalents.*

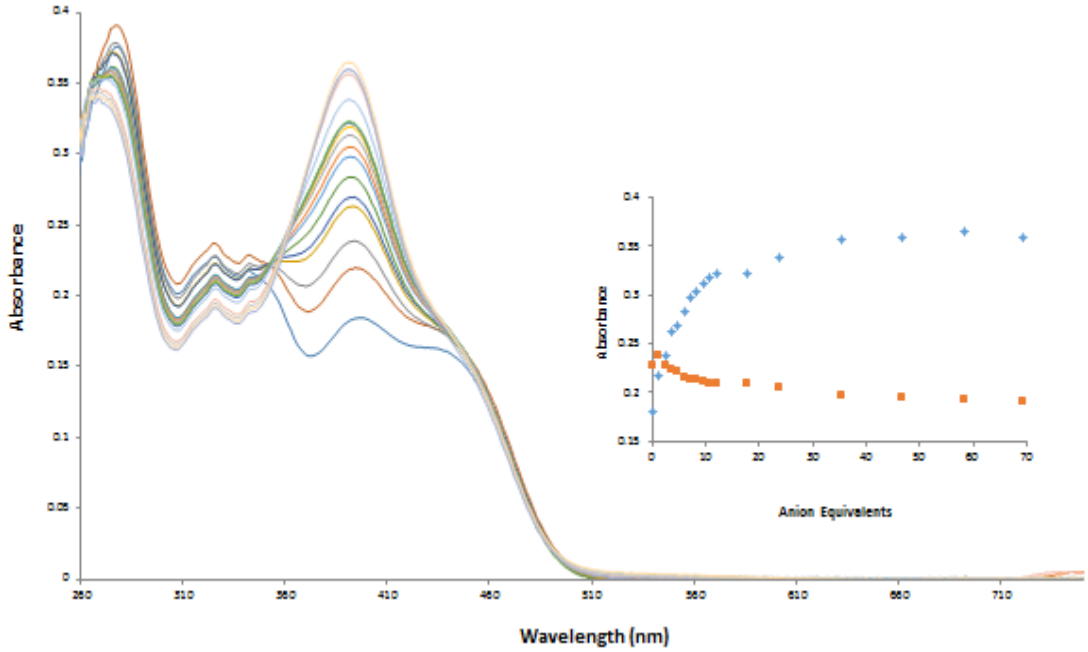

***2A 62**: Changes in the UV/Visible spectrum of **87** (11.9 µM) with increasing TBA phosphate equivalents in DMSO (0 - 70 eqs). **Inset:** Plot of the change in absorbance at 325 nm (orange) and 390 nm (blue) as a function of TBA phosphate equivalents.*

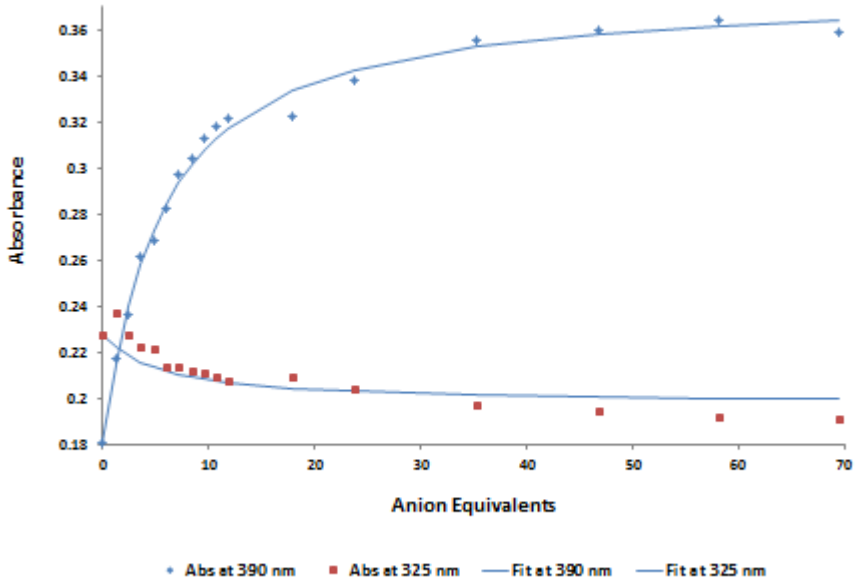

***2A 63**: Bind fit graph of UV titration of **87** (11.9 µM, DMSO) with increasing TBA phosphate equivalents in DMSO (0 - 70 eqs).*

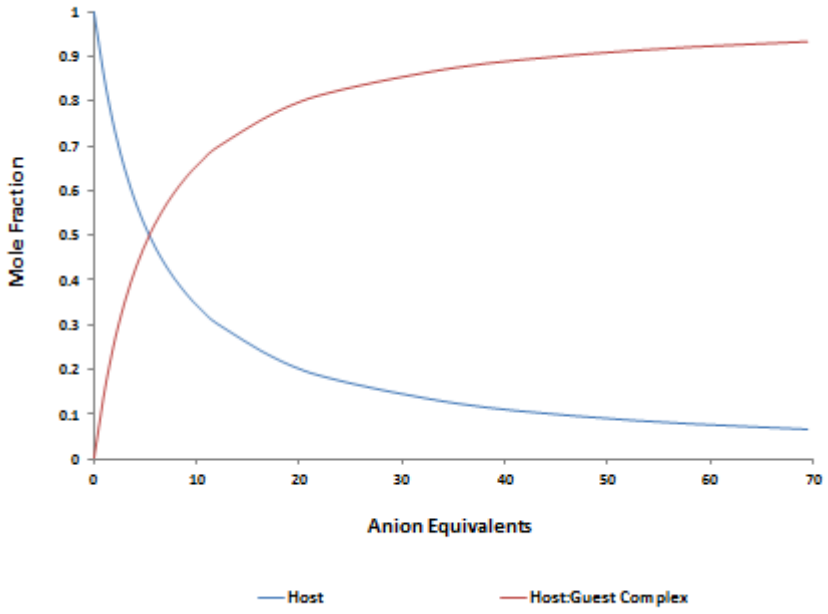

***2A 64**: Speciation graph of UV titration of **87** (11.9 µM, DMSO) with increasing TBA phosphate equivalents in DMSO (0 - 70 eqs).*

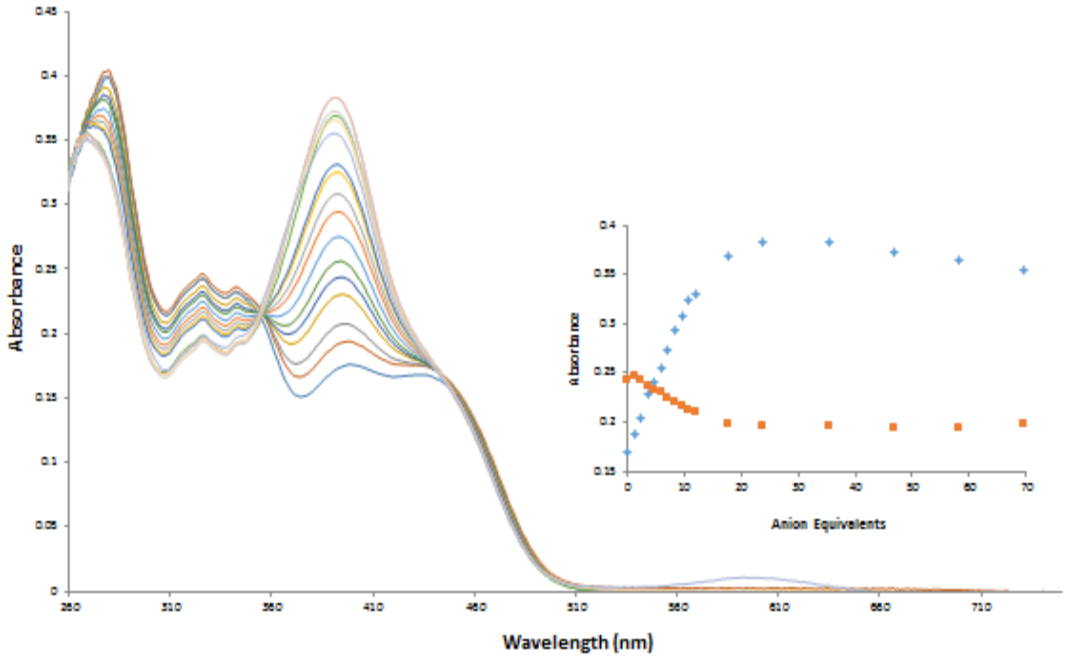

***2A 65**: Changes in the UV/Visible spectrum of **87** (11.9 µM) with increasing TBA sulphate equivalents in DMSO (0 - 70 eqs). **Inset:** Plot of the change in absorbance at 325 nm (orange) and 390 nm (blue) as a function of TBA sulphate equivalents.*

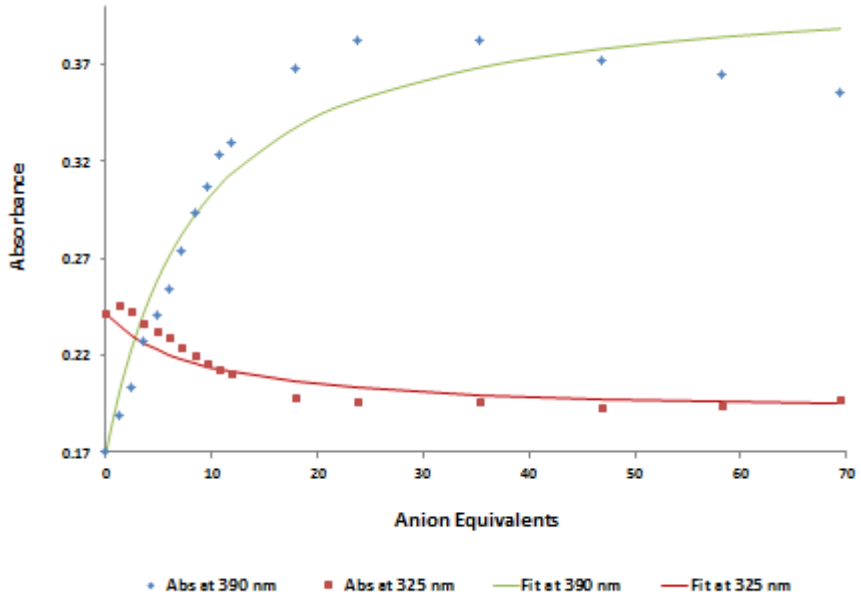

***2A 66**: Bind fit graph of UV titration of **87** (11.9 µM, DMSO) with increasing TBA sulphate equivalents in DMSO (0 - 70 eqs).*

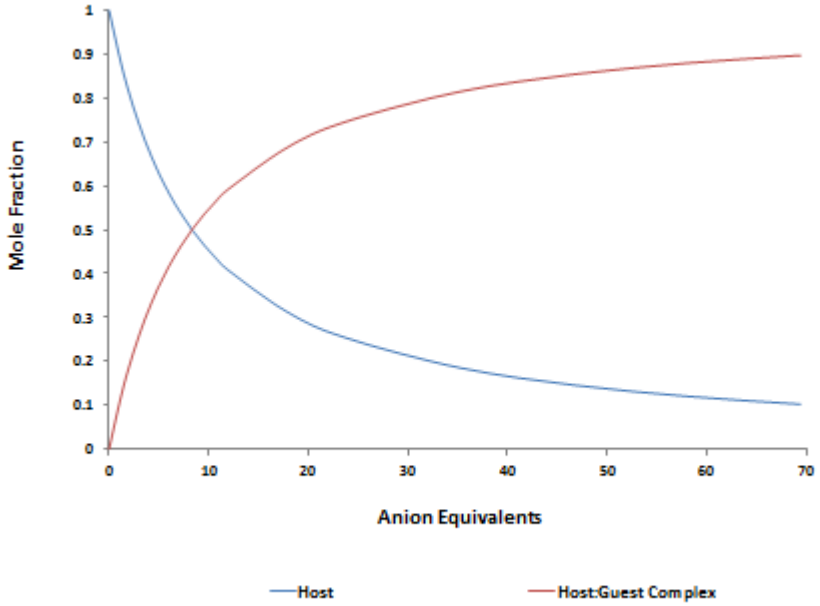

***2A 67**: Speciation graph of UV titration of **87** (11.9 µM, DMSO) with increasing TBA sulphate equivalents in DMSO (0 - 70 eqs).*

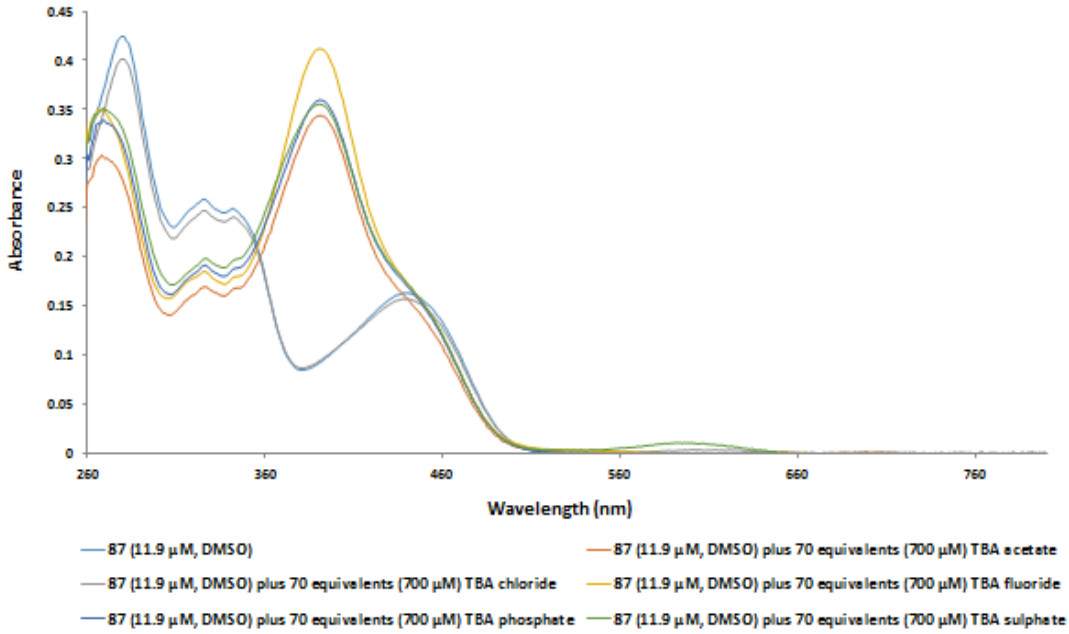

***2A 68**: Changes in the UV/Visible spectrum of **87** (11.9 µM, DMSO) with 70 equivalents (700 µM) of different solution of anions as TBA salts in DMSO (AcO^-, Cl^-, F^-, PO_4^{3-} and SO_4^{2-}).*

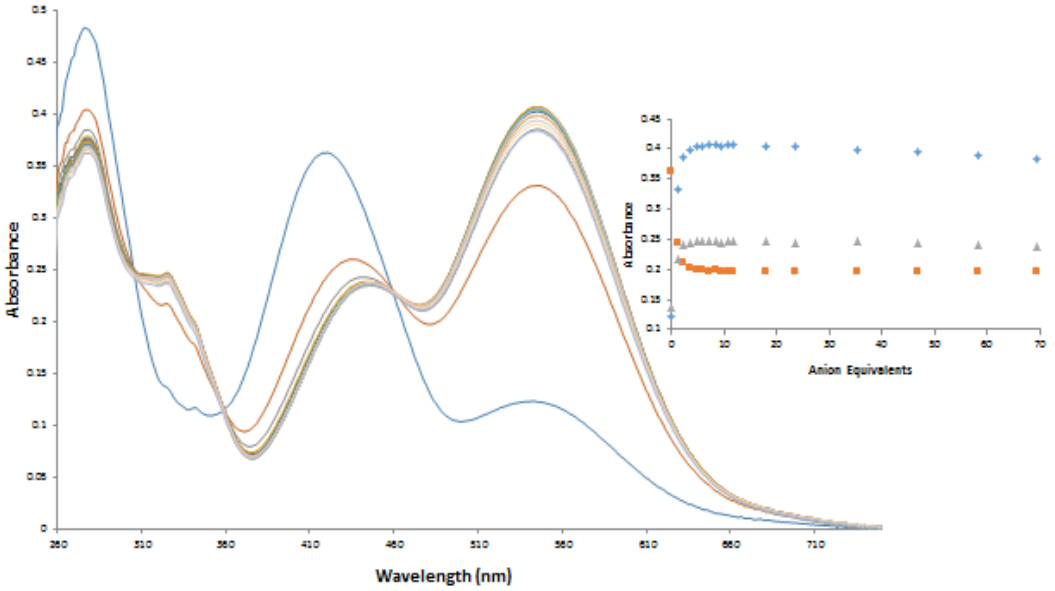

***2A 69**: Changes in the UV/Visible spectrum of **88** (11.9 µM) with increasing TBA acetate equivalents in DMSO (0 - 70 eqs). **Inset:** Plot of the change in absorbance at 420 nm (orange), 325 nm (grey) and 545 nm (blue) as a function of TBA acetate equivalents.*

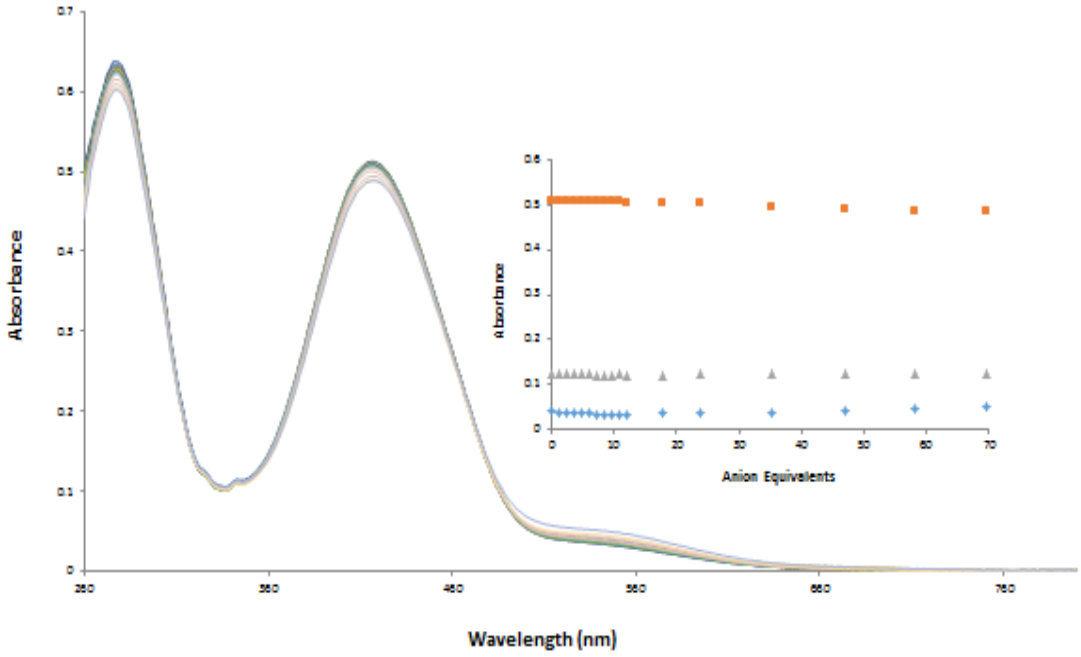

***2A 70**: Changes in the UV/Visible spectrum of **88** (11.9 µM) with increasing TBA chloride equivalents in DMSO (0 - 70 eqs). **Inset:** Plot of the change in absorbance at 420 nm (orange), 325 nm (grey) and 545 nm (blue) as a function of TBA chloride equivalents.*

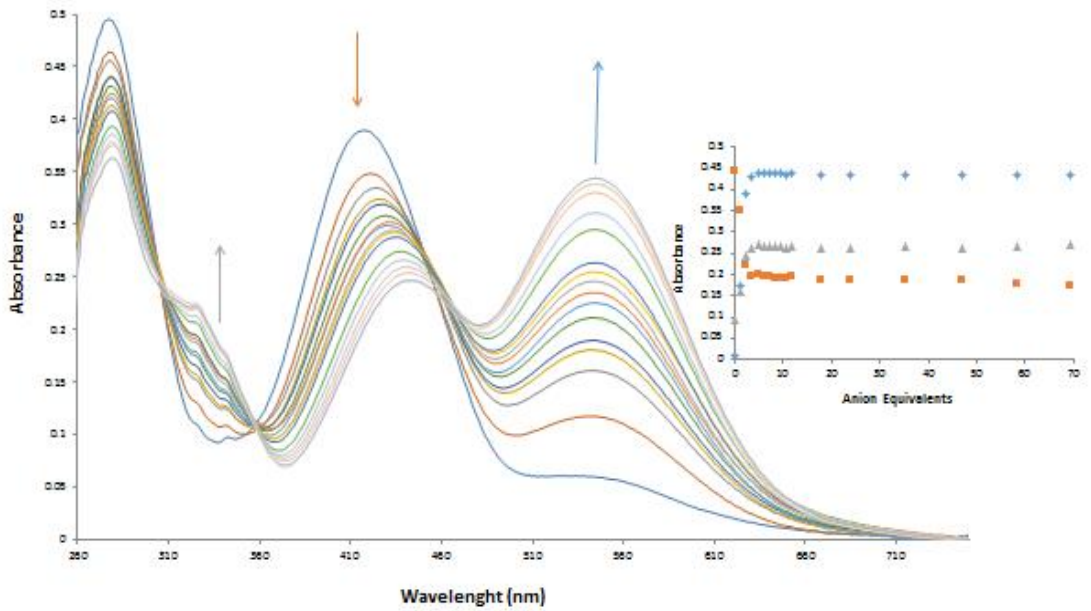

***2A 71**: Changes in the UV/Visible spectrum of **88** (11.9 µM) with increasing TBA fluoride equivalents in DMSO (0 - 70 eqs). **Inset:** Plot of the change in absorbance at 420 nm (orange), 325 nm (grey) and 545 nm (blue) as a function of TBA fluoride equivalents.*

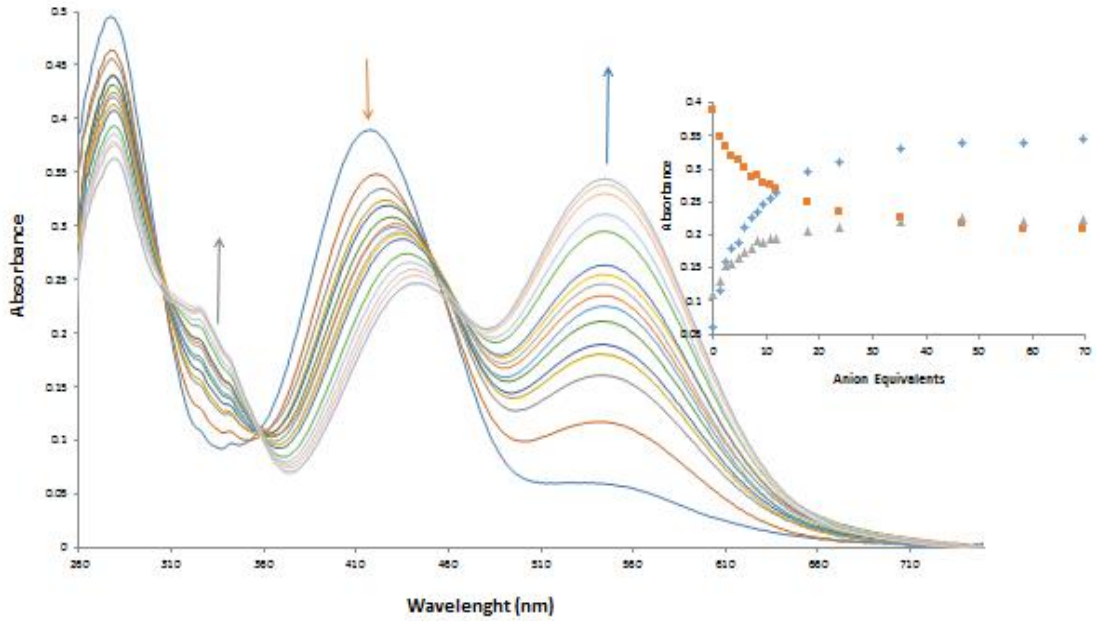

***2A 72**: Changes in the UV/Visible spectrum of **88** (11.9 µM) with increasing TBA phosphate equivalents in DMSO (0 - 70 eqs). **Inset:** Plot of the change in absorbance at 420 nm (orange), 325 nm (grey) and 545 nm (blue) as a function of TBA phosphate equivalents.*

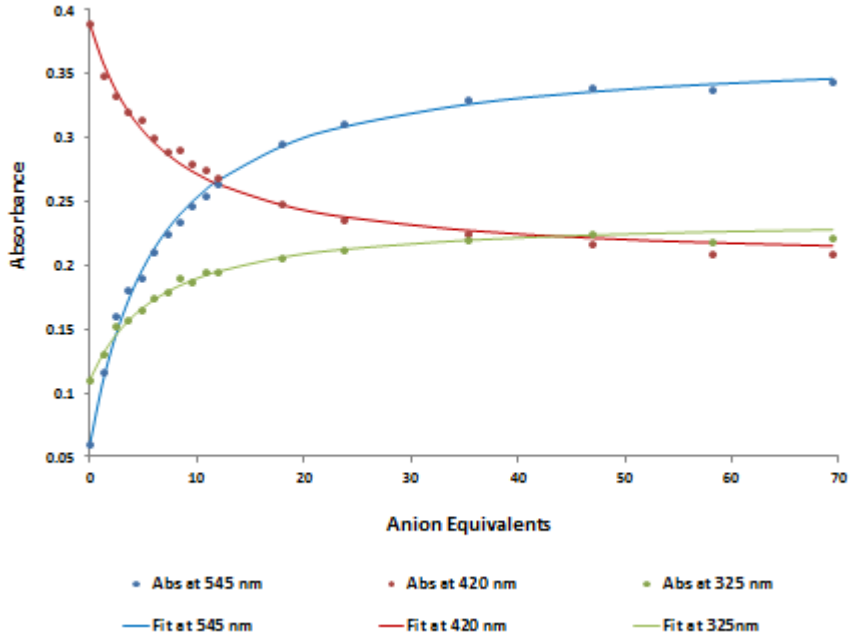

***2A 73**: Bind fit graph of UV titration of **88** (11.9 µM, DMSO) with increasing TBA phosphate equivalents in DMSO (0 - 70 eqs).*

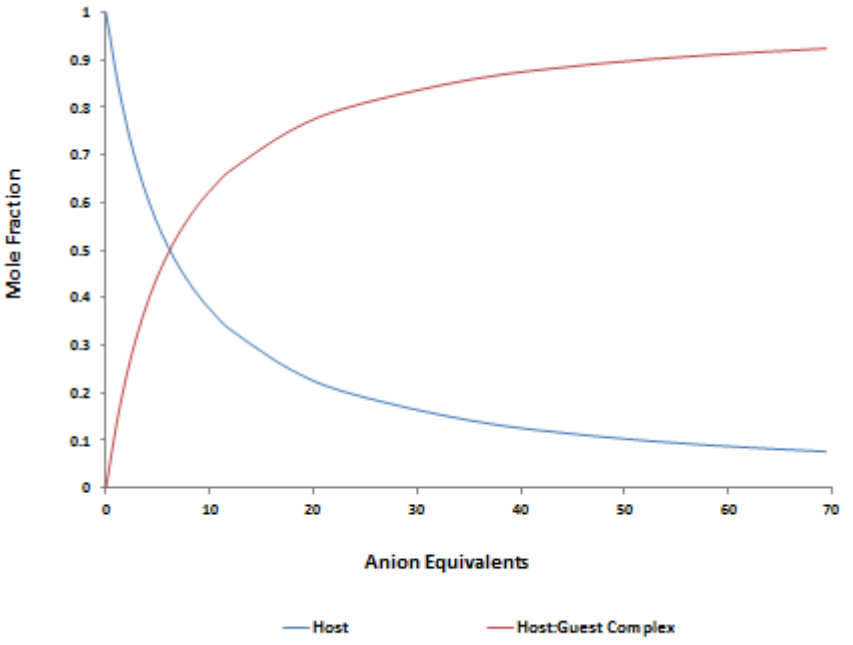

***2A 74**: Speciation graph of UV titration of **88** (11.9 µM, DMSO) with increasing TBA phosphate equivalents in DMSO (0 - 70 eqs).*

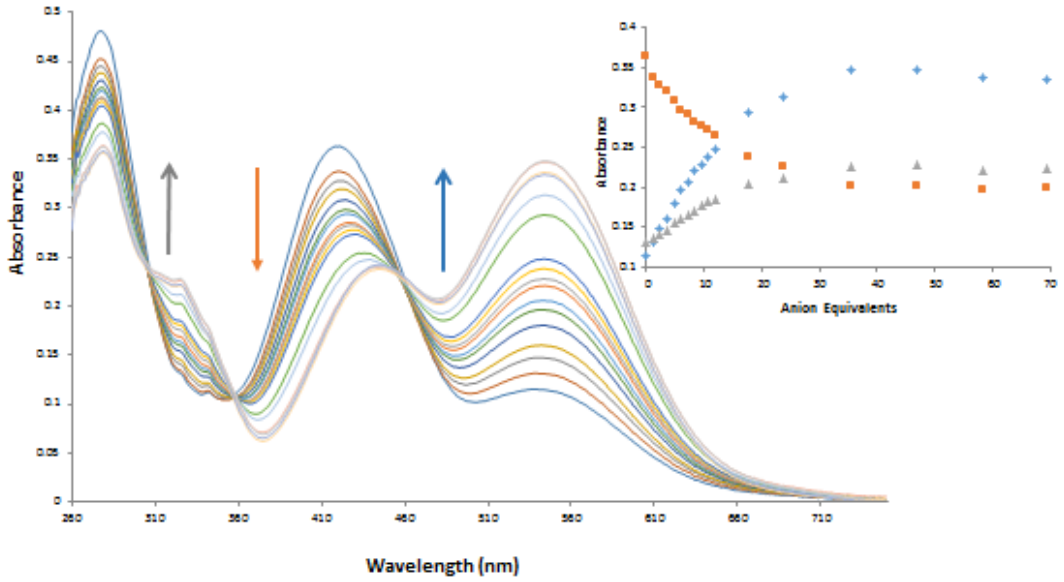

***2A 75**: Changes in the UV/Visible spectrum of **88** (11.9 µM) with increasing TBA sulphate equivalents in DMSO (0 - 70 eqs). **Inset:** Plot of the change in absorbance at 420 nm (orange), 325 nm (grey) and 545 nm (blue) as a function of TBA sulphate equivalents (0 - 70 eqs).*

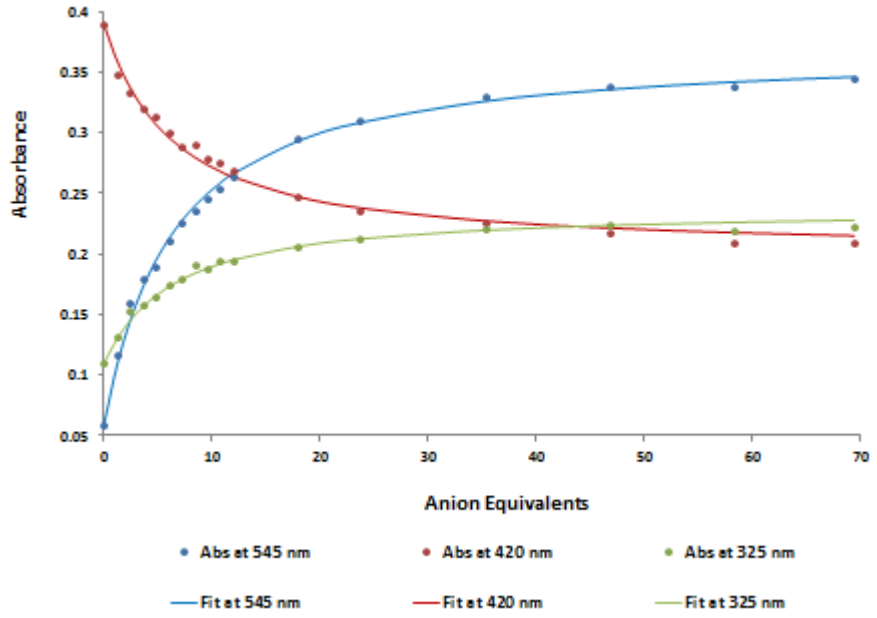

***2A 76**: Bind fit graph of UV titration of **88** (11.9 µM, DMSO) with increasing TBA sulphate equivalents in DMSO (0 - 70 eqs).*

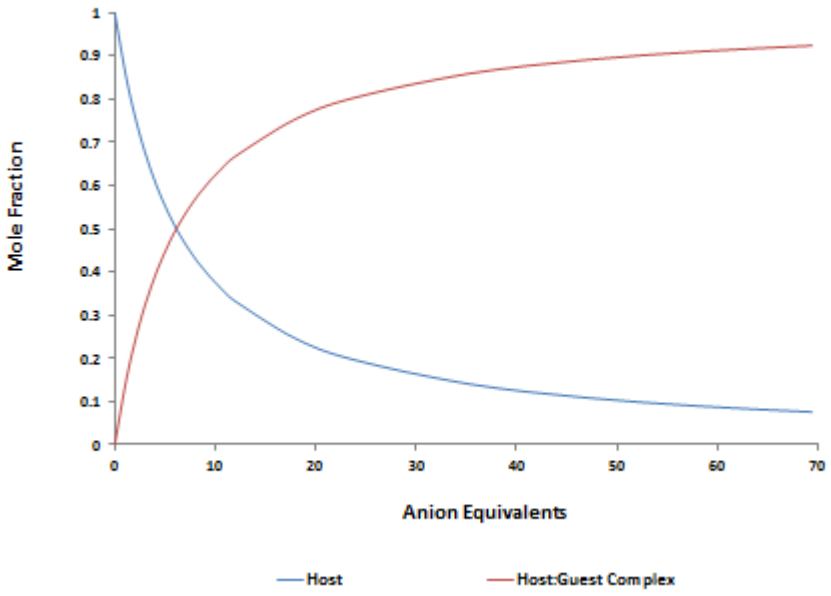

***2A 77**: Speciation graph of UV titration of **88** (11.9 µM, DMSO) with increasing TBA sulphate equivalents in DMSO (0 - 70 eqs).*

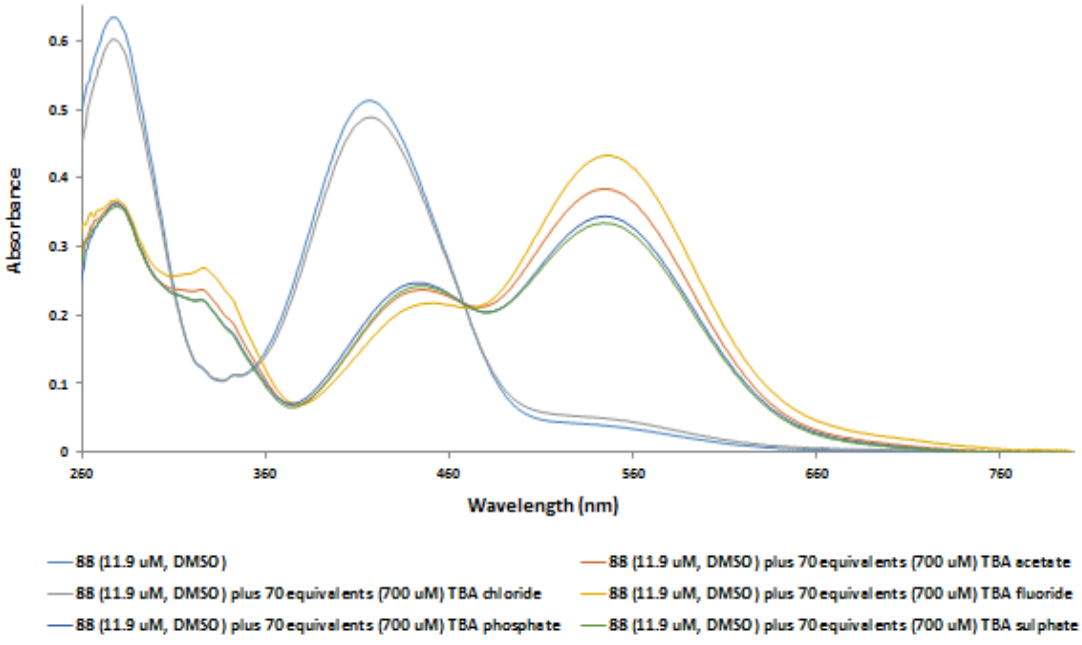

***2A 78**: Changes in the UV/Visible spectrum of **88** (11.9 µM, DMSO) with 70 equivalents (700 µM) of different solution of anions as TBA salts in DMSO (AcO^-, Cl^-, F^-, PO_4^{3-} and SO_4^{2-}).*

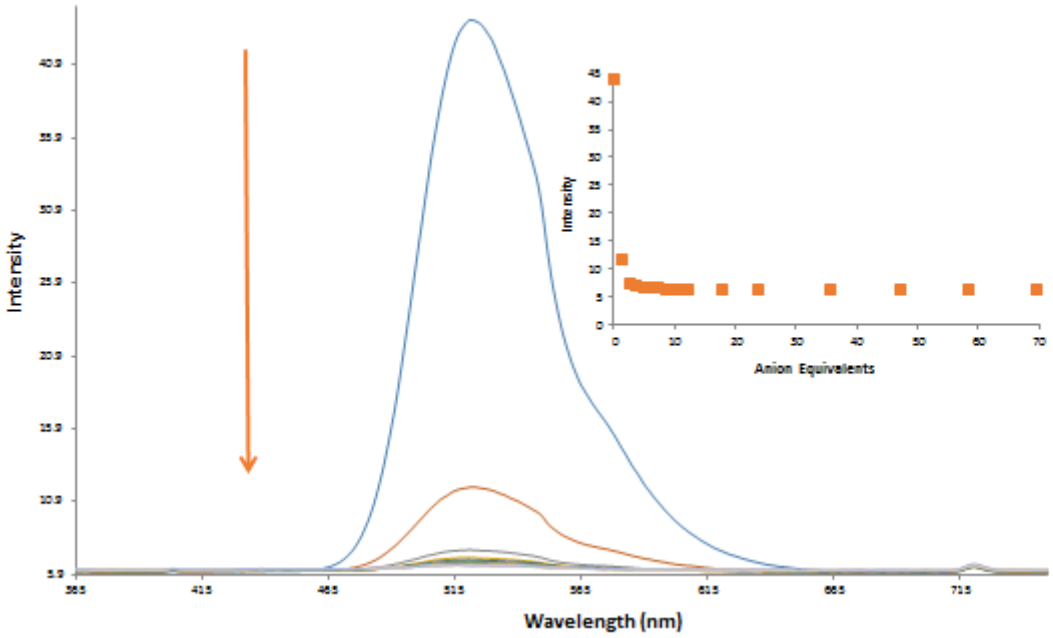

***2A 79**: Changes in the fluoresence emmission spectrum of **85** (11.9 µM) at λ_{ex} 360 nm with increasing TBA acetate equivalents in DMSO (0 – 70 eqs). **Inset:** Plot of emission intensity at 522 nm as a function of 0 – 70 equivalents of TBA acetate.*

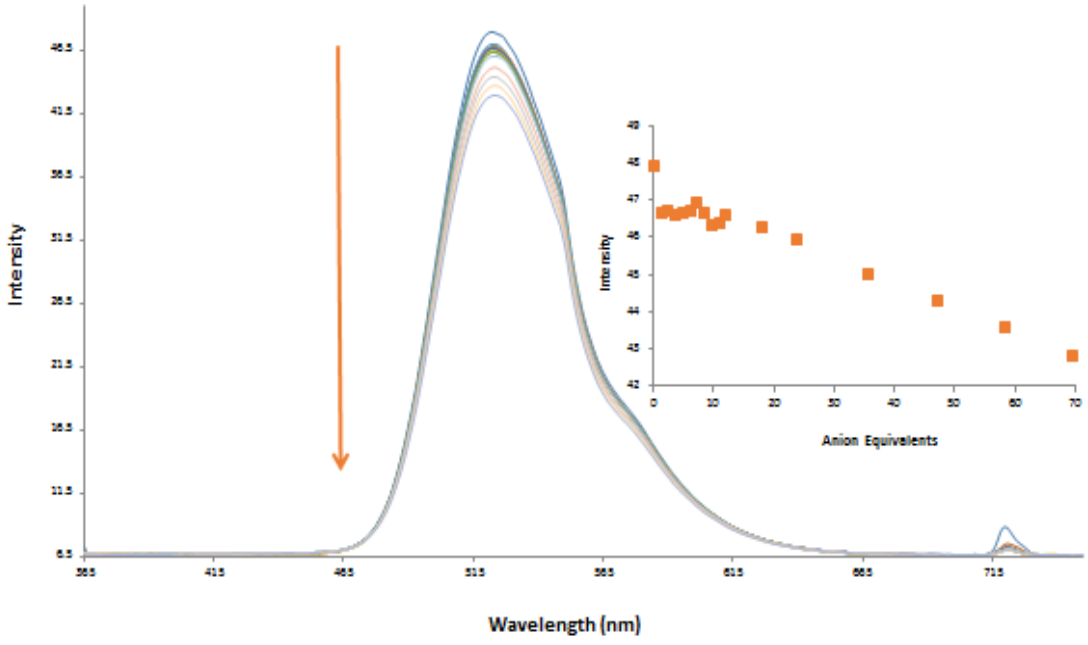

***2A 80**: Changes in the fluoresence emmission spectrum of **85** (11.9 µM) at λ_{ex} 360 nm with increasing TBA chloride equivalents in DMSO (0 – 70 eqs). **Inset:** Plot of the change in emmission intensity at 522 nm as a function of TBA chloride equivalents.*

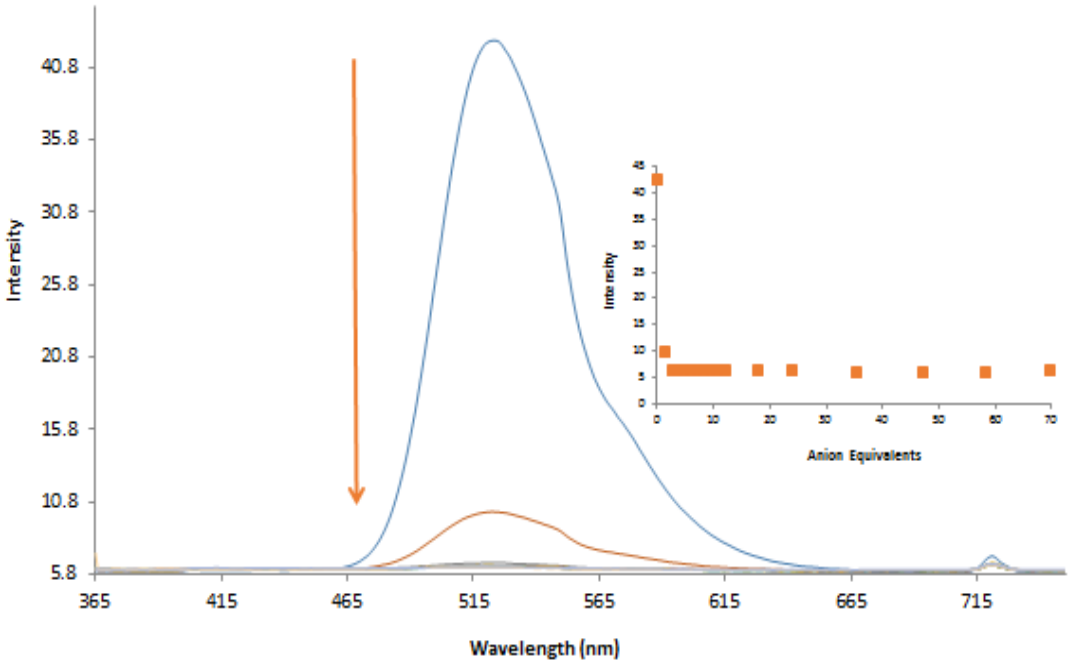

***2A 81**: Changes in the fluoresence emmission spectrum of **85** (11.9 μM) at λ_{ex} 360 nm with increasing TBA fluoride equivalents in DMSO (0 – 70 eqs). **Inset:** Plot of the change in emmission intensity at 522 nm as a function of TBA fluoride equivalents.*

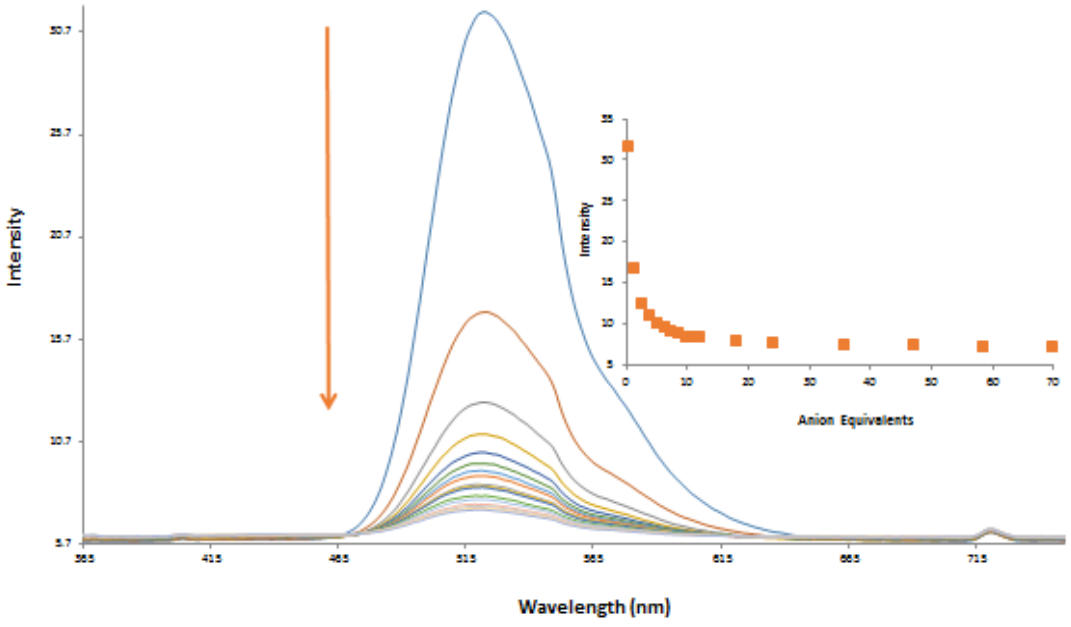

***2A 82**: Changes in the fluoresence emmission spectrum of **85** (11.9 μM) at λ_{ex} 360 nm with increasing TBA phosphate equivalents in DMSO (0 – 70 eqs). **Inset:** Plot of the change in emmission intensity at 522 nm as a function of TBA phosphate equivalents.*

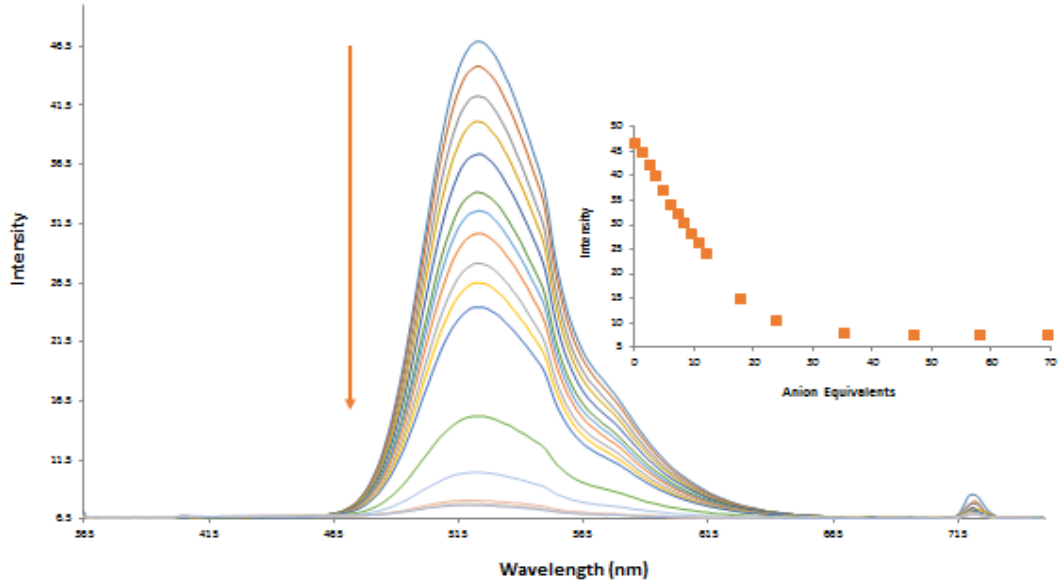

***2A 83**: Changes in the fluoresence emmission spectrum of **85** (11.9 µM) at λ_{ex} 360 nm with increasing TBA sulphate equivalents in DMSO (0 – 70 eqs). **Inset:** Plot of the change in emmission intensity at 522 nm as a function of TBA sulphate equivalents.*

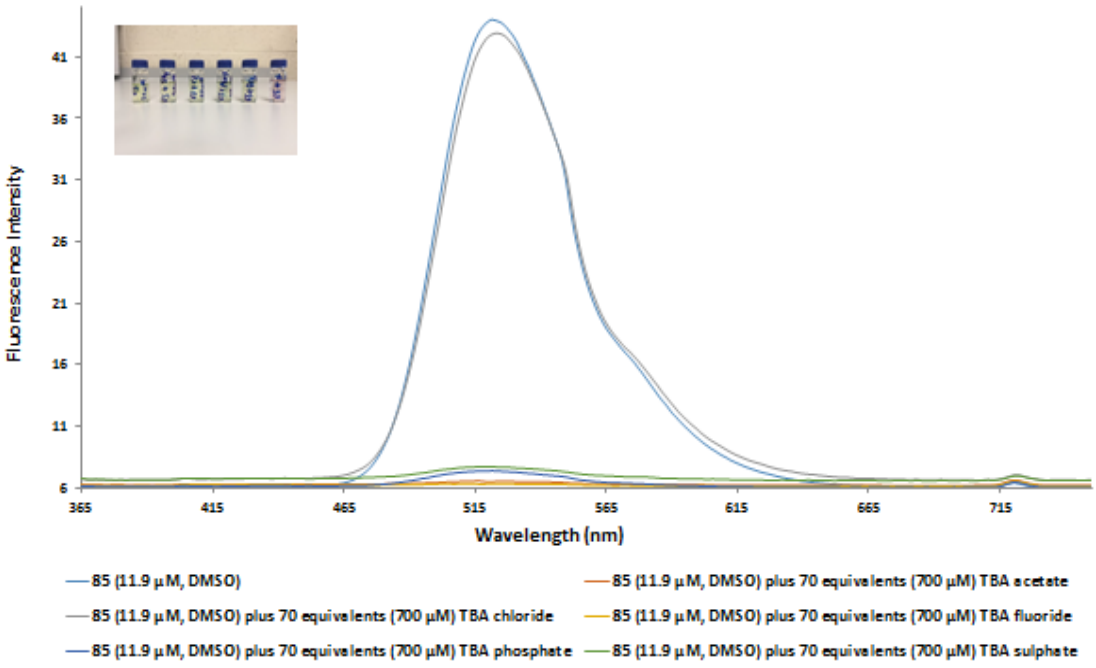

***2A 84**: Changes in the fluoresence emmission spectrum of **85** (11.9 µM, DMSO) at λ_{ex} 360 nm with 70 equivalents (700 µM) of different solution of anions as TBA salts in DMSO (AcO^-, Cl^-, F^-, PO_4^{3-} and SO_4^{2-})*

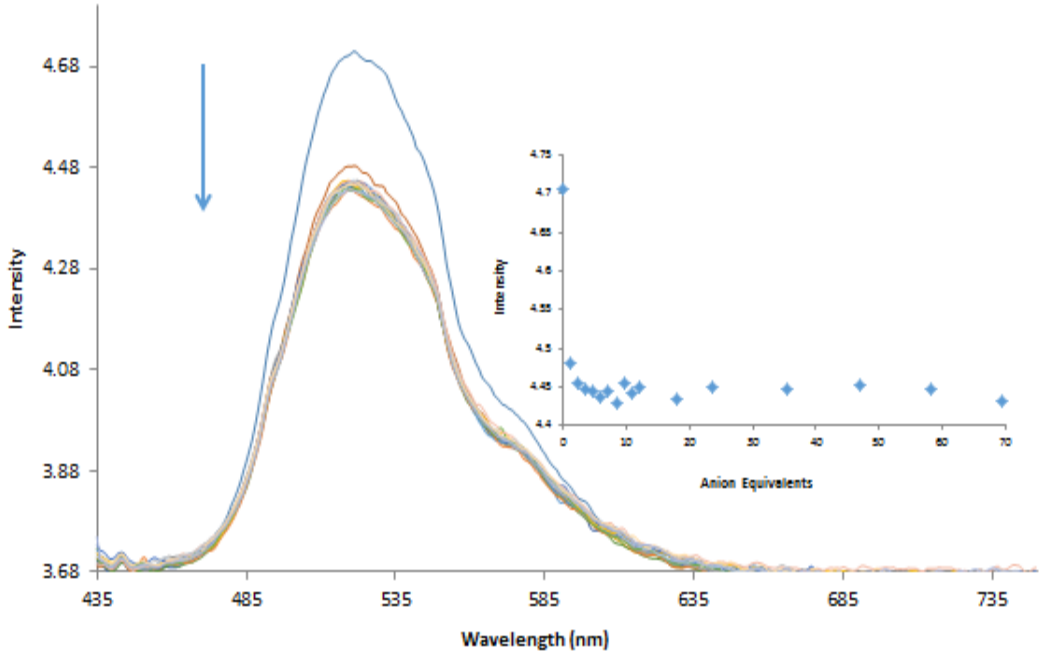

***2A 85**: Changes in the fluoresence emmission spectrum of **86** (11.9 μM) at λ_{ex} 430 nm with increasing TBA acetate equivalents in DMSO (0 – 70 eqs). **Inset:** Plot of the change in emmission intensity at 522 nm as a function of TBA acetate equivalents.*

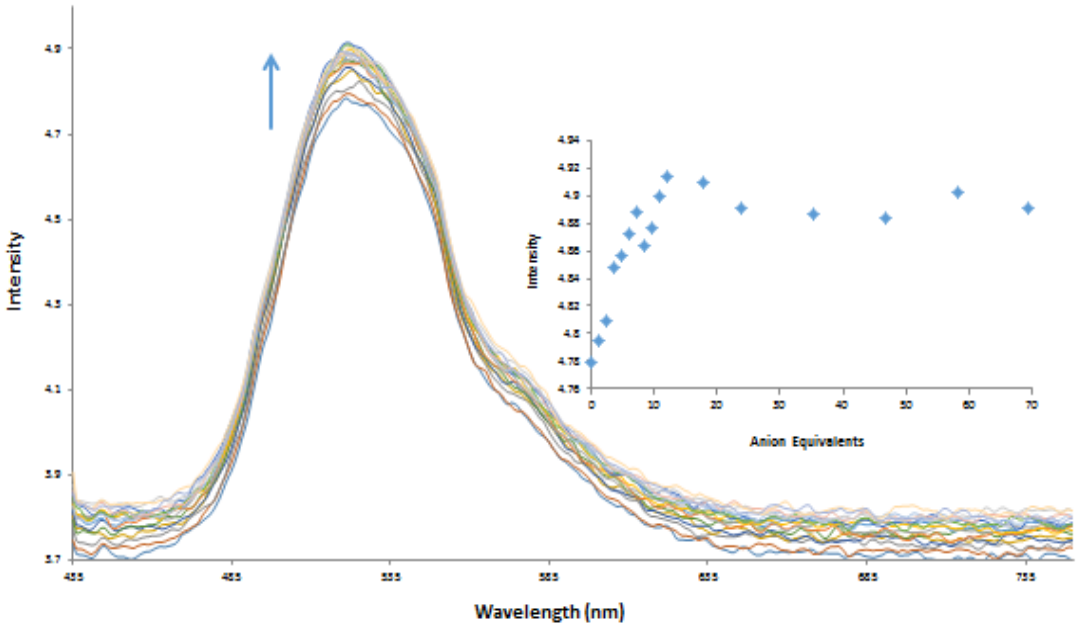

***2A 86**: Changes in the fluoresence emmission spectrum of **86** (11.9 μM) at λ_{ex} 430 nm with increasing TBA chloride equivalents in DMSO (0 – 70 eqs). **Inset:** Plot of the change in emmission intensity at 522 nm as a function of TBA chloride equivalents.*

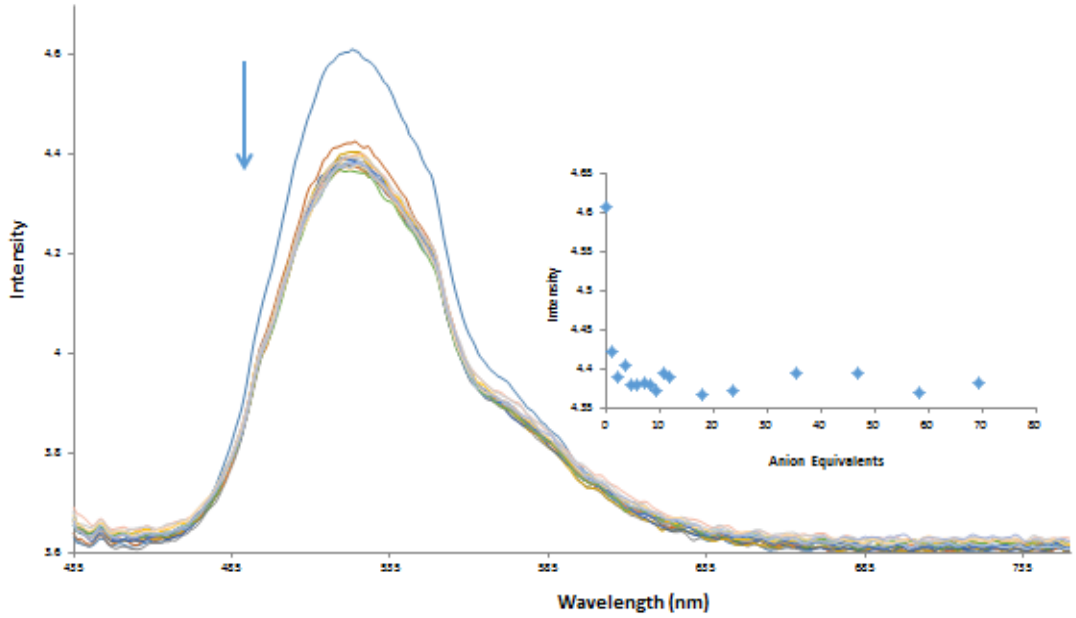

***2A 87**: Changes in the fluoresence emmission spectrum of **86** (11.9 μM) at λ_{ex} 430 nm with increasing TBA fluoride equivalents in DMSO (0 – 70 eqs). **Inset:** Plot of the change in emmission intensity at 522 nm as a function of TBA fluoride equivalents.*

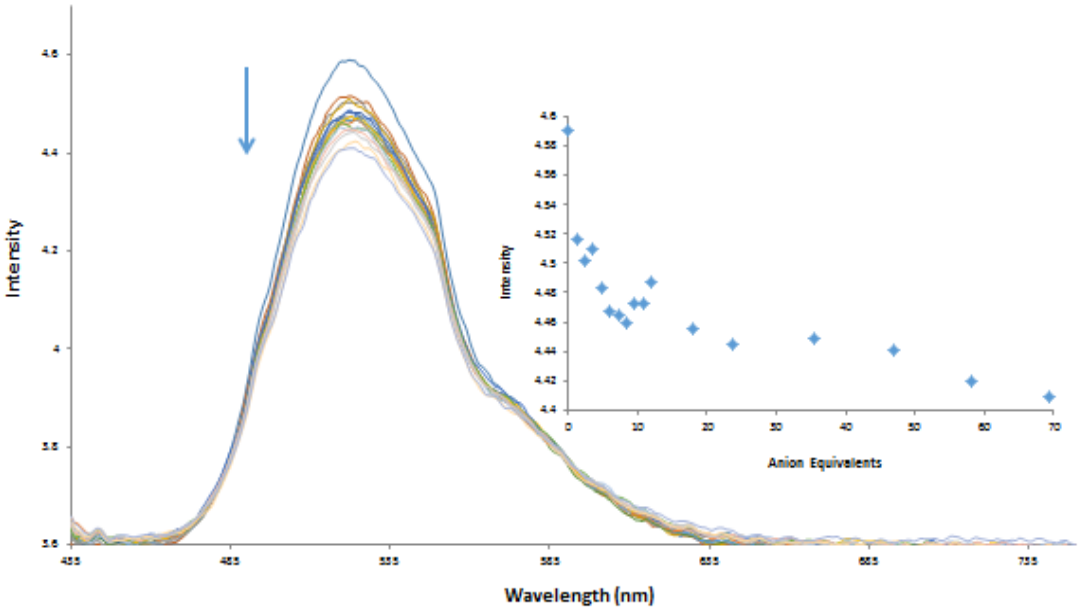

***2A 88**: Changes in the fluoresence emmission spectrum of **86** (11.9 μM) at λ_{ex} 430 nm with increasing TBA phosphate equivalents in DMSO (0 – 70 eqs). **Inset:** Plot of the change in emmission intensity at 522 nm as a function of TBA phosphate equivalents.*

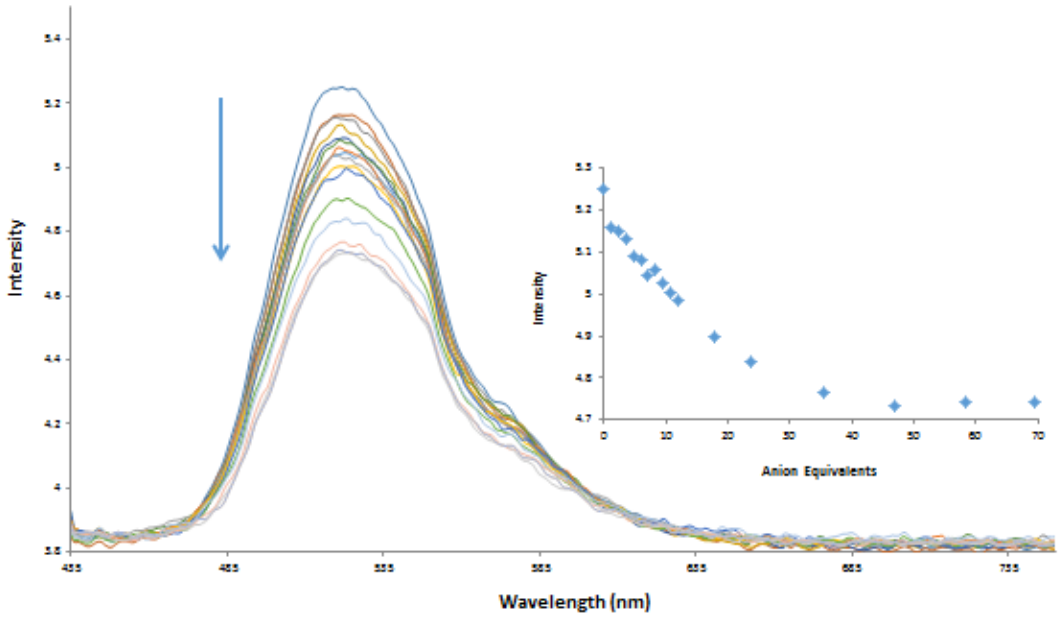

***2A 89**: Changes in the fluoresence emmission spectrum of **86** (11.9 µM) at λ_{ex} 430 nm with increasing TBA sulphate equivalents in DMSO (0 – 70 eqs). **Inset:** Plot of the change in emmission intensity at 522 nm as a function of TBA sulphate equivalents.*

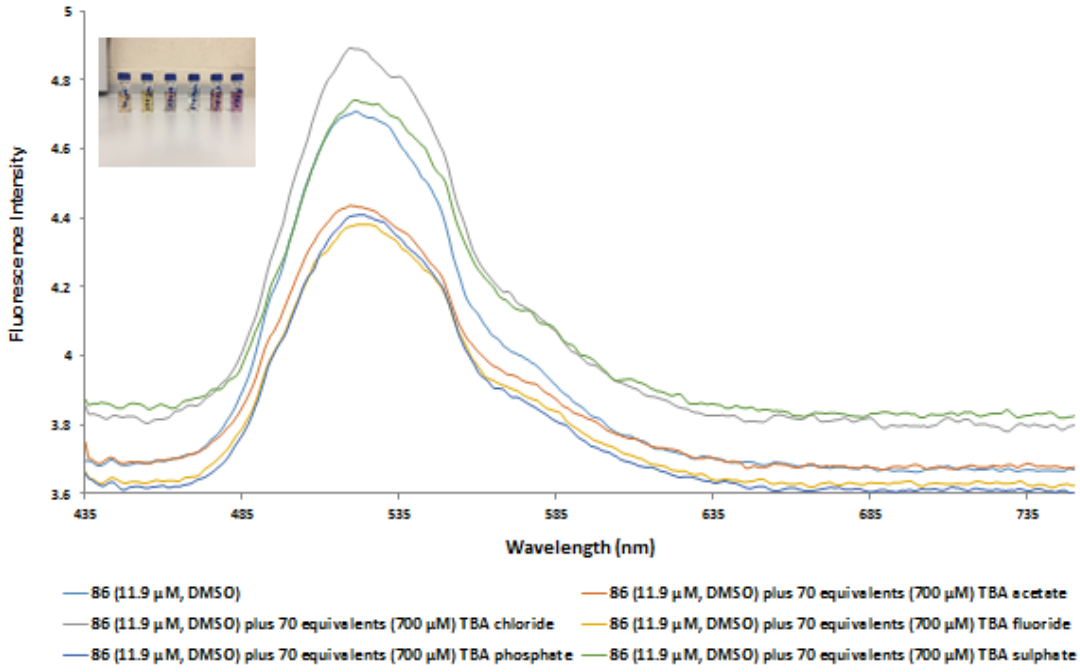

***2A 90**: Changes in the fluoresence emmission spectrum of **86** (11.9 µM, DMSO) at λ_{ex} 430 nm with 70 equivalents (700 µM) of different solution of anions as TBA salts in DMSO (AcO^-, Cl^-, F^-, PO_4^{3-} and SO_4^{2-}).*

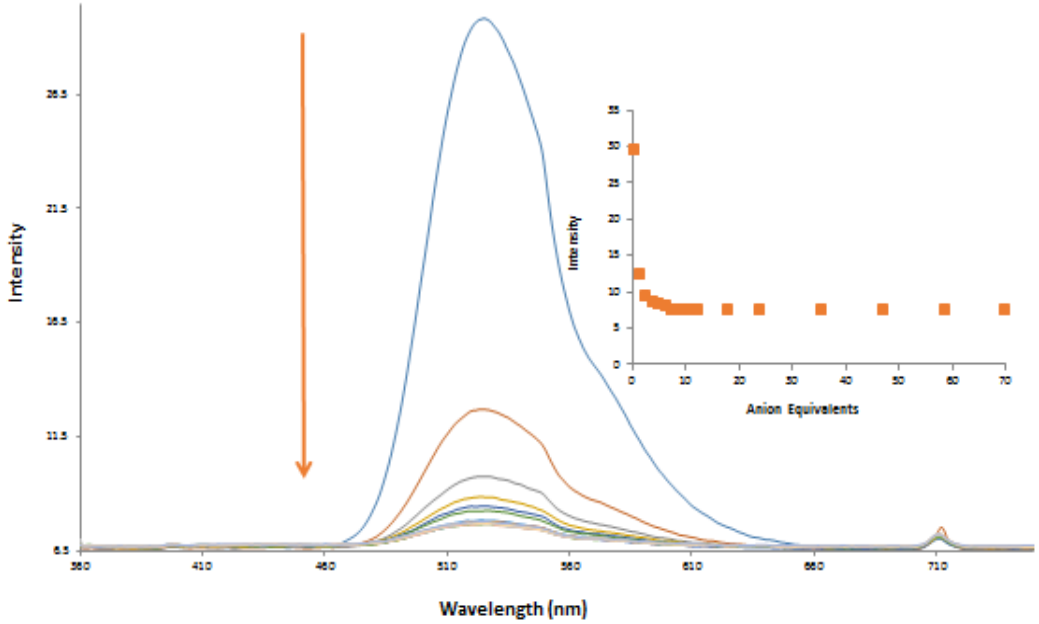

***2A 91**: Changes in the fluoresence emmission spectrum of **87** (11.9 µM) at λ_{ex} 355 nm with increasing TBA acetate equivalents in DMSO (0 – 70 eqs). **Inset:** Plot of the change in emmission intensity at 522 nm as a function of TBA acetate equivalents.*

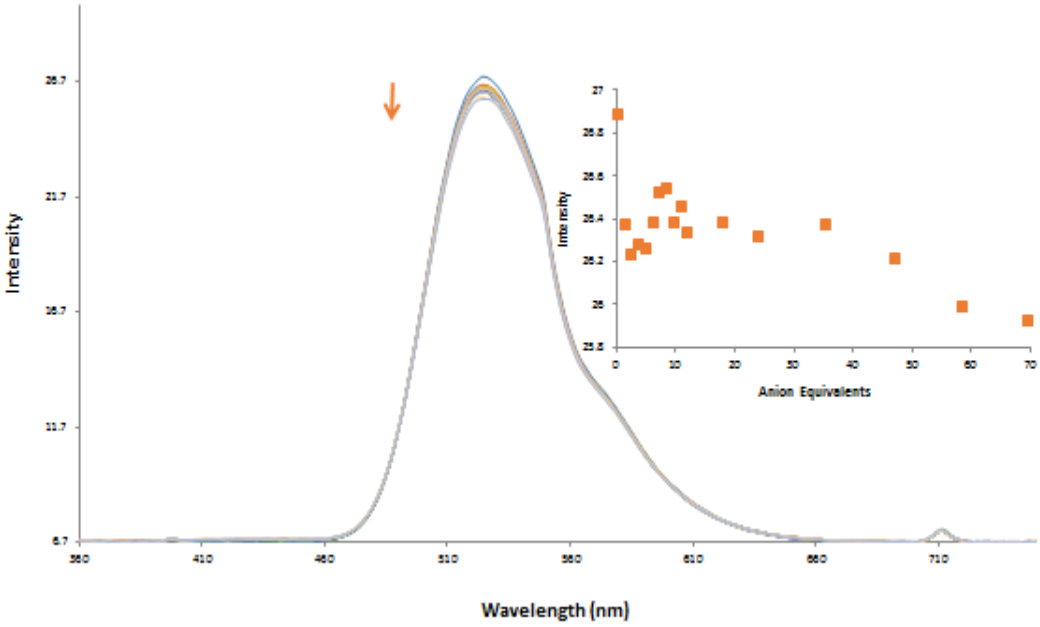

***2A 92**: Changes in the fluoresence emmission spectrum of **87** (11.9 µM) at λ_{ex} 355 nm with increasing TBA chloride equivalents in DMSO (0 – 70 eqs). **Inset:** Plot of the change in emmission intensity at 522 nm as a function of TBA chloride equivalents.*

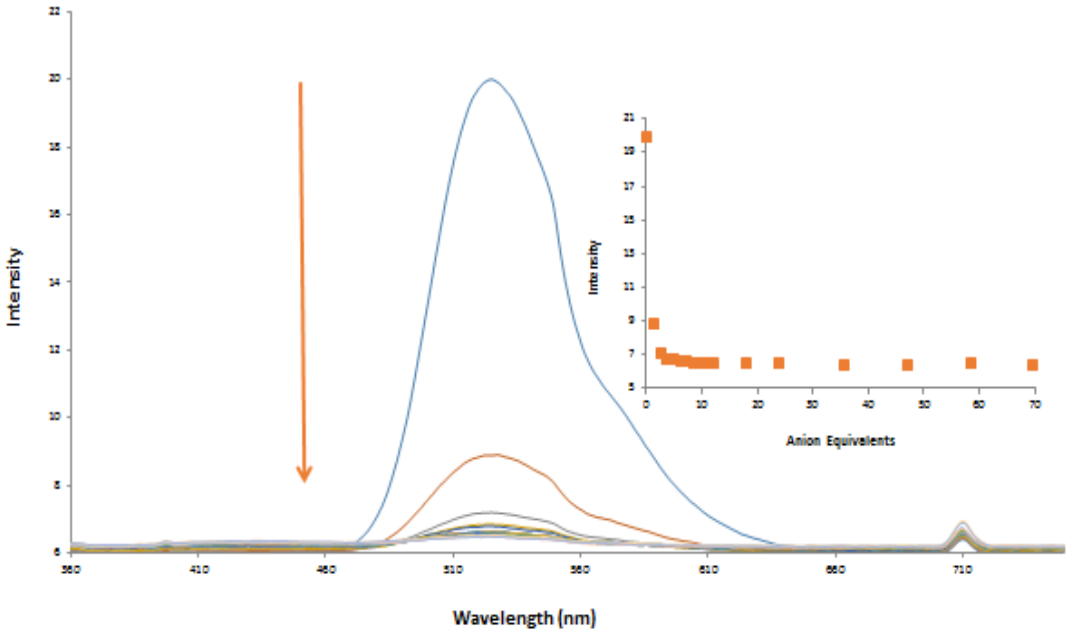

***2A 93**: Changes in the fluoresence emmission spectrum of **87** (11.9 μM) at λ_{ex} 355 nm with increasing TBA fluoride equivalents in DMSO (0 – 70 eqs). **Inset:** Plot of the change in emmission intensity at 522 nm as a function of TBA fluoride equivalents.*

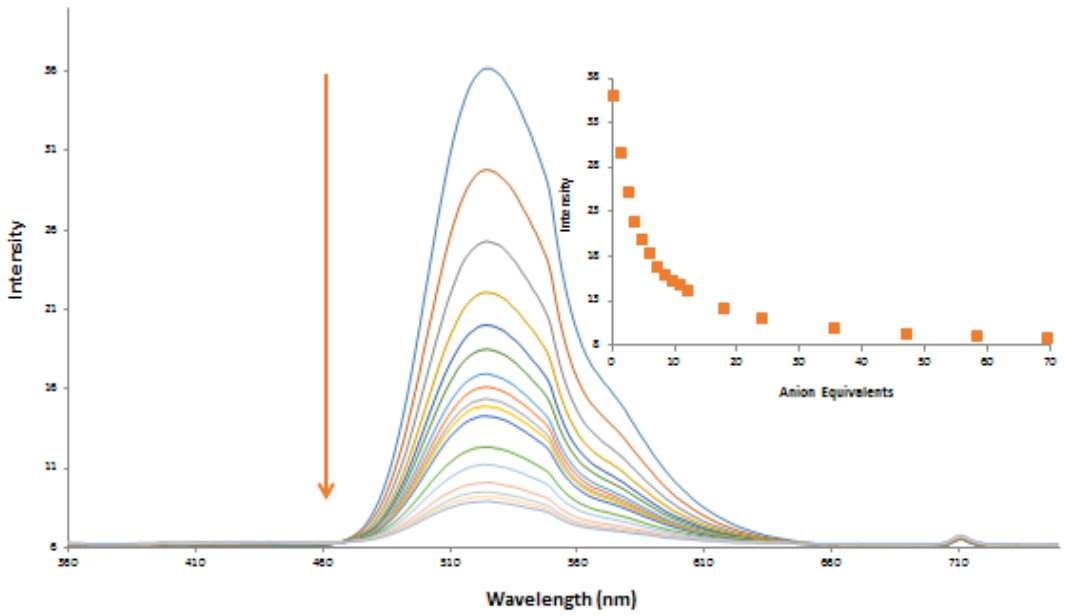

***2A 94**: Changes in the fluoresence emmission spectrum of **87** (11.9 μM) at λ_{ex} 355 nm with increasing TBA phosphate equivalents in DMSO (0 – 70 eqs). **Inset:** Plot of the change in emmission intensity at 522 nm as a function of TBA phosphate equivalents.*

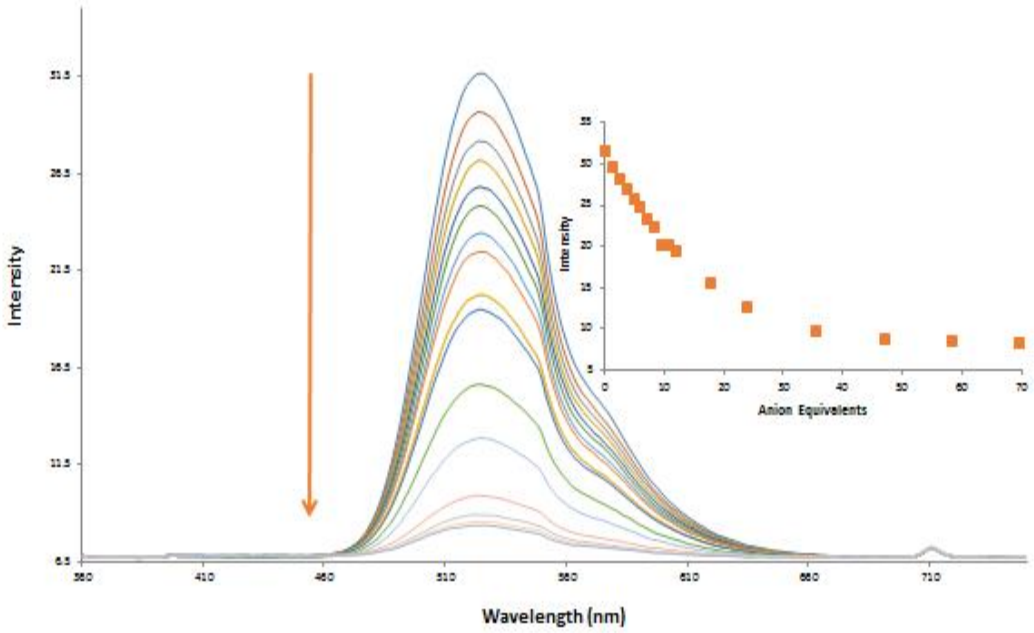

***2A 95**: Changes in the fluoresence emmission spectrum of **87** (11.9 µM) at λ_{ex} 355 nm with increasing TBA sulphate equivalents in DMSO (0 – 70 eqs). **Inset:** Plot of the change in emmission intensity at 522 nm as a function of TBA sulphate equivalents.*

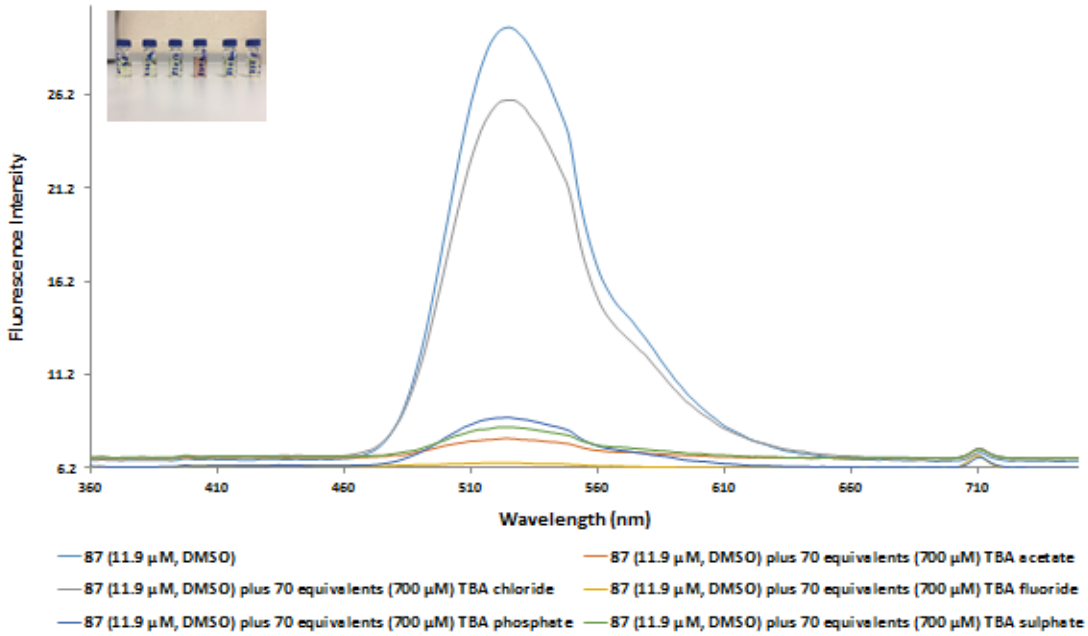

***2A 96**: Changes in the fluoresence emmission spectrum of **87** (11.9 µM, DMSO) at λ_{ex} 355 nm with 70 equivalents (700 µM) of different solution of anions as TBA salts in DMSO (AcO^-, Cl^-, F^-, PO_4^{3-} and SO_4^{2-})*

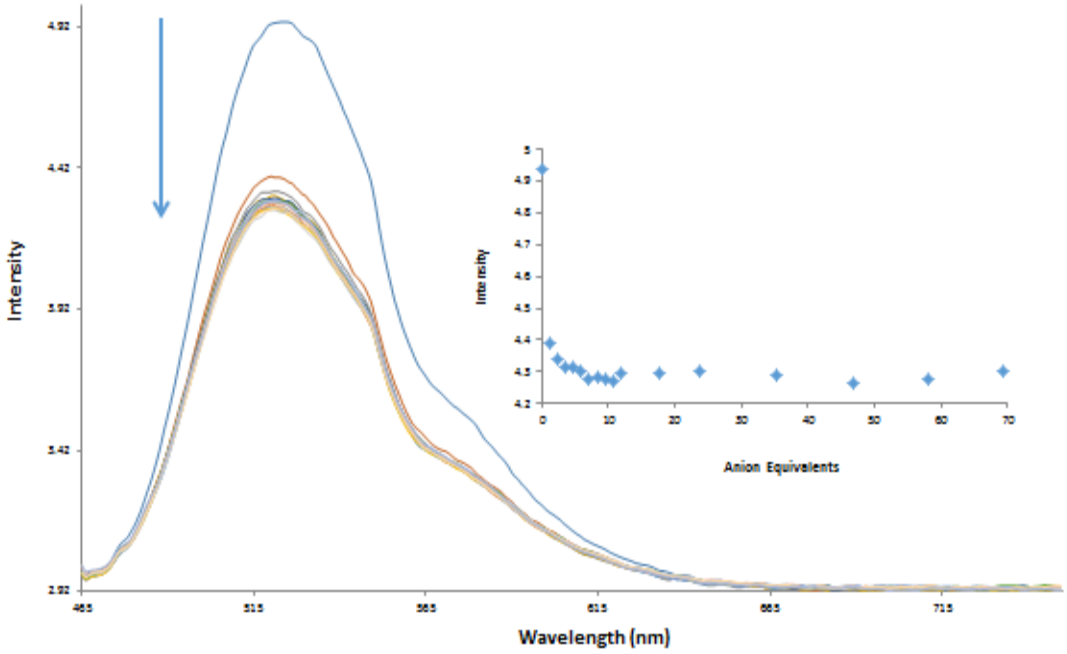

***2A 97**: Changes in the fluoresence emmission spectrum of **88** (11.9 µM) at λ_{ex} 460 nm with increasing TBA acetate equivalents in DMSO (0 – 70 eqs). **Inset:** Plot of the change in emmission intensity at 522 nm as a function of TBA acetate equivalents.*

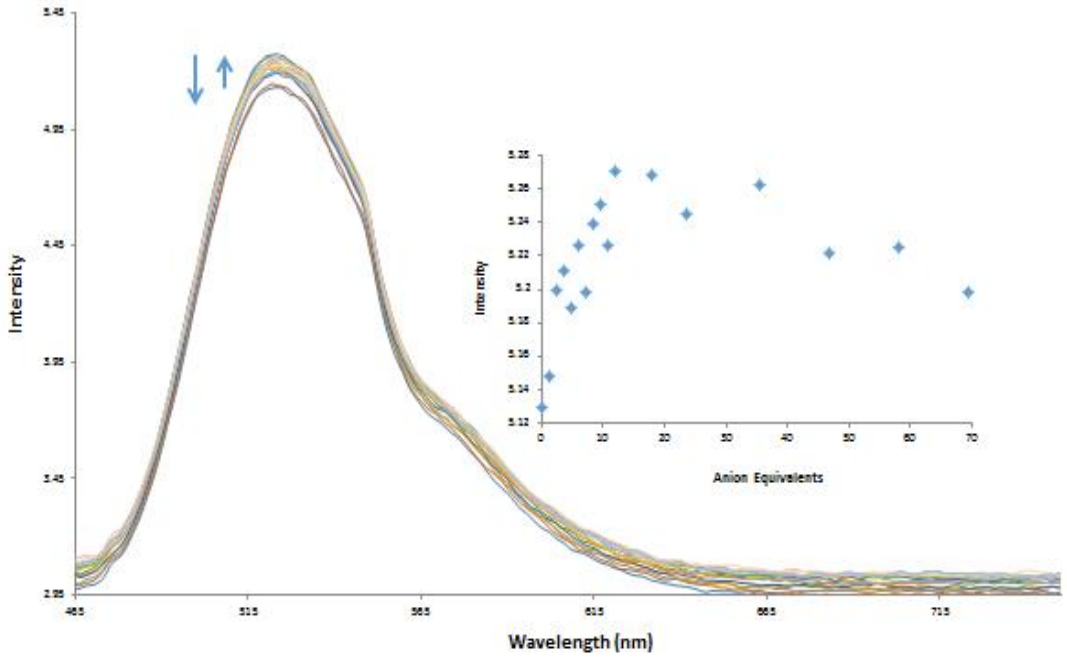

***2A 98**: Changes in the fluoresence emmission spectrum of **88** (11.9 µM) at λ_{ex} 460 nm with increasing TBA acetate eqivalents in DMSO (0 – 70 eqs). **Inset:** Plot of the change in emmission intensity at 522 nm as a function of TBA acetate eqivalents.*

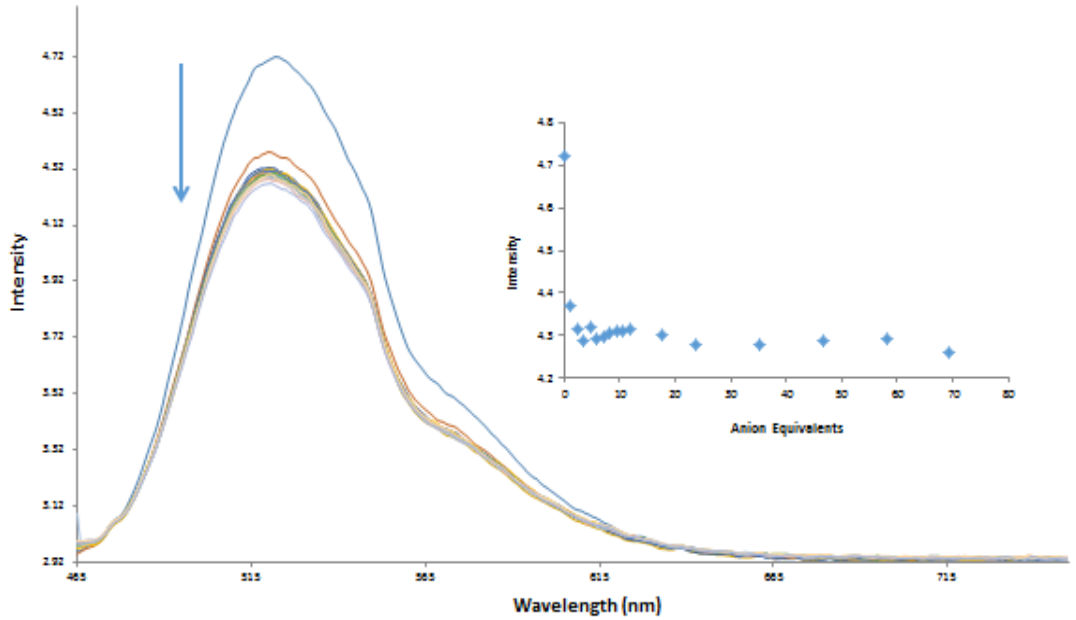

***2A 99**: Changes in the fluoresence emmission spectrum of **88** (11.9 μM) at λ_{ex} 460 nm with increasing TBA fluoride equivalents in DMSO (0 – 70 eqs). **Inset:** Plot of the change in emmission intensity at 522 nm as a function of TBA fluoride equivalents.*

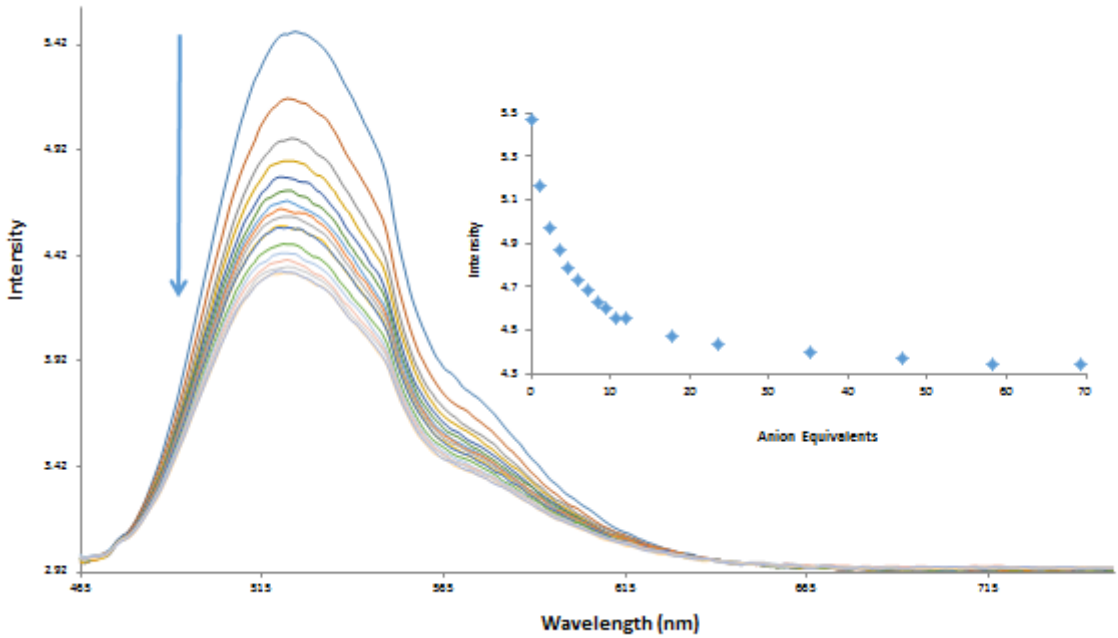

***2A 100**: Changes in the fluoresence emmission spectrum of **88** (11.9 μM) at λ_{ex} 460 nm with increasing TBA phosphate equivalents in DMSO (0 – 70 eqs). **Inset:** Plot of the change in emmission intensity at 522 nm as a function of TBA phosphate equivalents.*

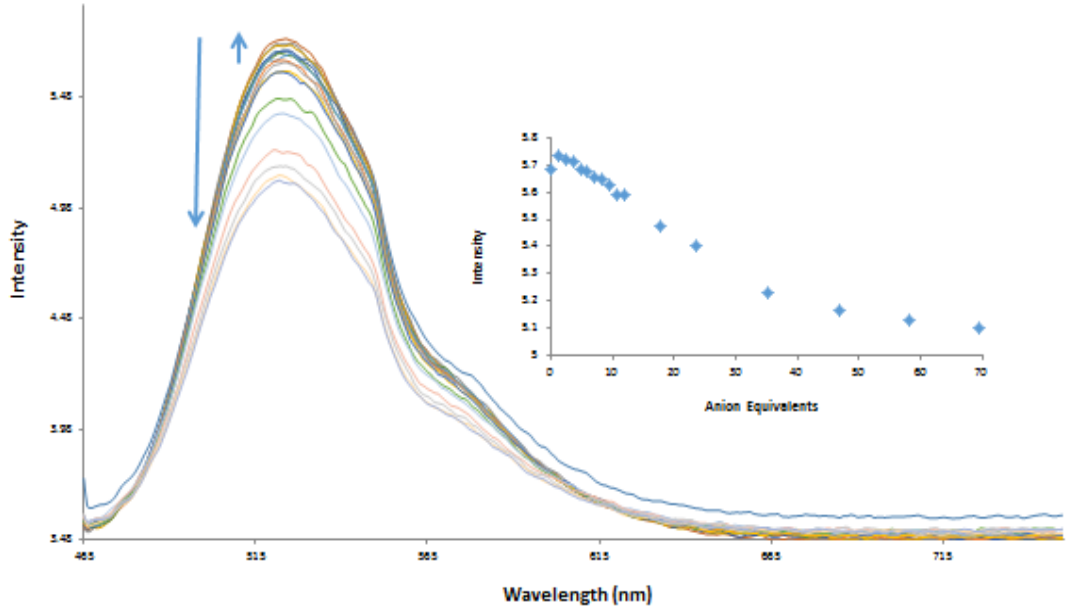

***2A 101**: Changes in the fluoresence emmission spectrum of **88** (11.9 µM) at λ_{ex} 460 nm with increasing TBA sulphate phosphate equivalents in DMSO (0 – 70 eqs). **Inset:** Plot of the change in emmission intensity at 522 nm as a function of TBA sulphate equivalents.*

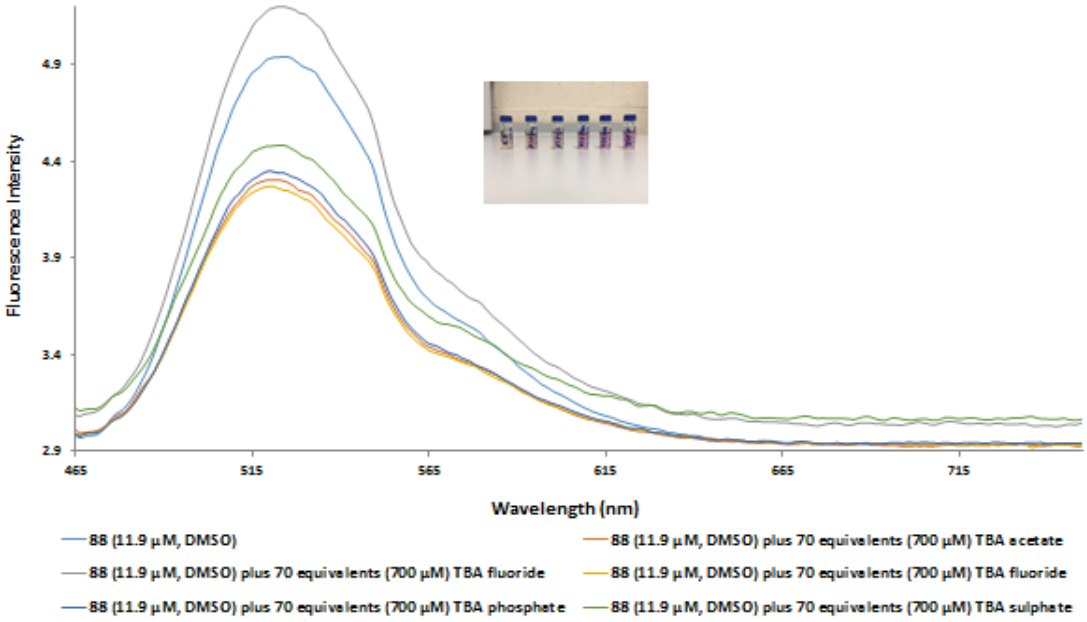

***2A 102**: Changes in the fluoresence emmission spectrum of **88** (11.9 µM, DMSO) at λ_{ex} 460 nm with 70 equivalents (700 µM) of different solution of anions as TBA salts in DMSO (AcO^-, Cl^-, F^-, PO_4^{3-} and SO_4^{2-})*

(a)

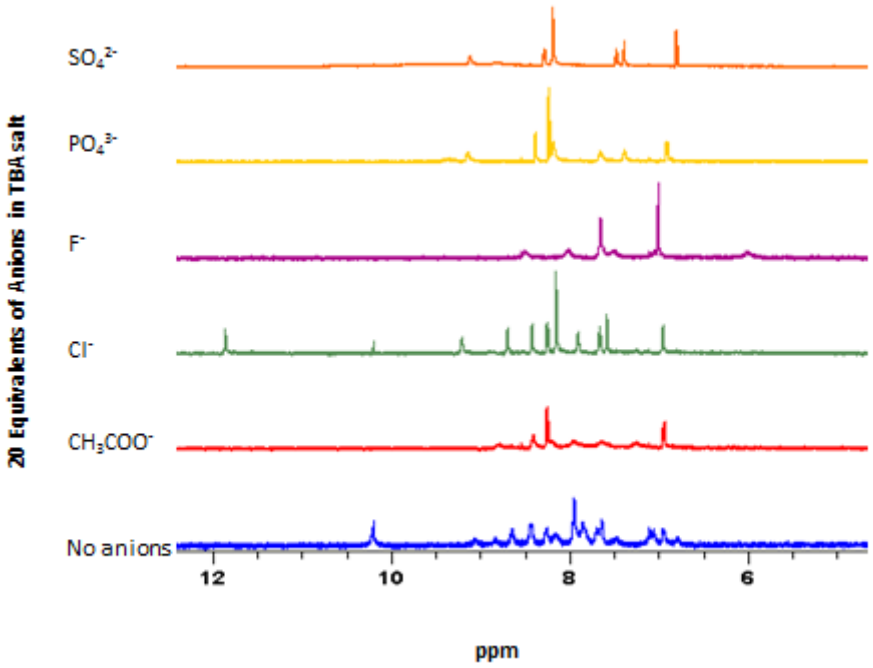
20 Equivalents of Anions in TBA salt
SO_4^{2-}
PO_4^{3-}
F^-
Cl^-
CH_3COO^-
No anions
12
10
8
6
ppm

(b)

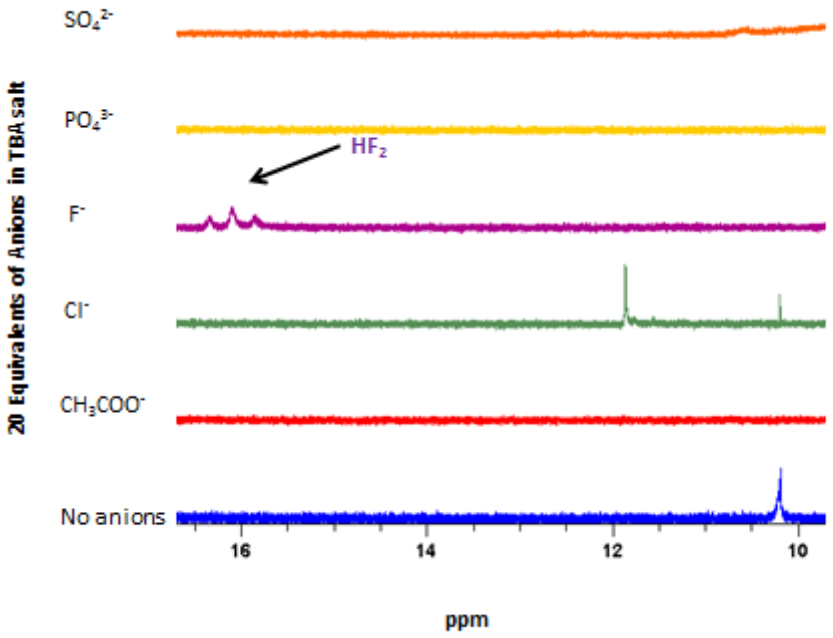
20 Equivalents of Anions in TBA salt
SO_4^{2-}
PO_4^{3-}
HF_2
F^-
Cl^-
CH_3COO^-
No anions
16
14
12
10
ppm

(c)

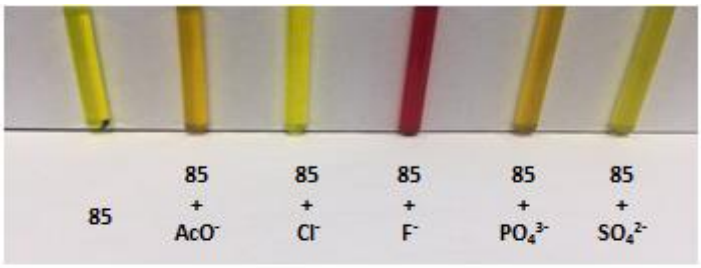

(d)

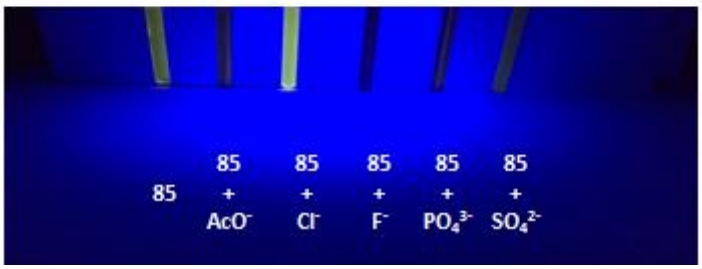

***2A 103**: Changes in the ^{1}H NMR spectrum of **85** (2.5×10^{-3} M) upon the addition of 20 eqvivalents of anions as TBA salts in DMSO-$_{d6}$ (AcO^-, Cl^-, F^-, PO_4^{3-} and SO_4^{2-}). **(a)**: Aromatic region of **85**. **(b)**: Formation of HF_2 upon the addition of 20 equivalents TBA fluoride to **85** in DMSO-$_{d6}$.[121, 122] The differing spectroscopic response of compound **85** upon the addition of 20 eqvivalents of anions as TBA salts in DMSO-$_{d6}$ (AcO^-, Cl^-, F^-, PO_4^{3-} and SO_4^{2-}). Changes in the appearance of a sample of **85** (2.5×10^{-3} M) upon the addition 20 equivalents of anions as TBA salts in DMSO-$_{d6}$ (AcO^-, Cl^-, F^-, PO_4^{3-} and SO_4^{2-}). **(c)** With the naked eye and **(d)** Under UV illumination.*

(a)

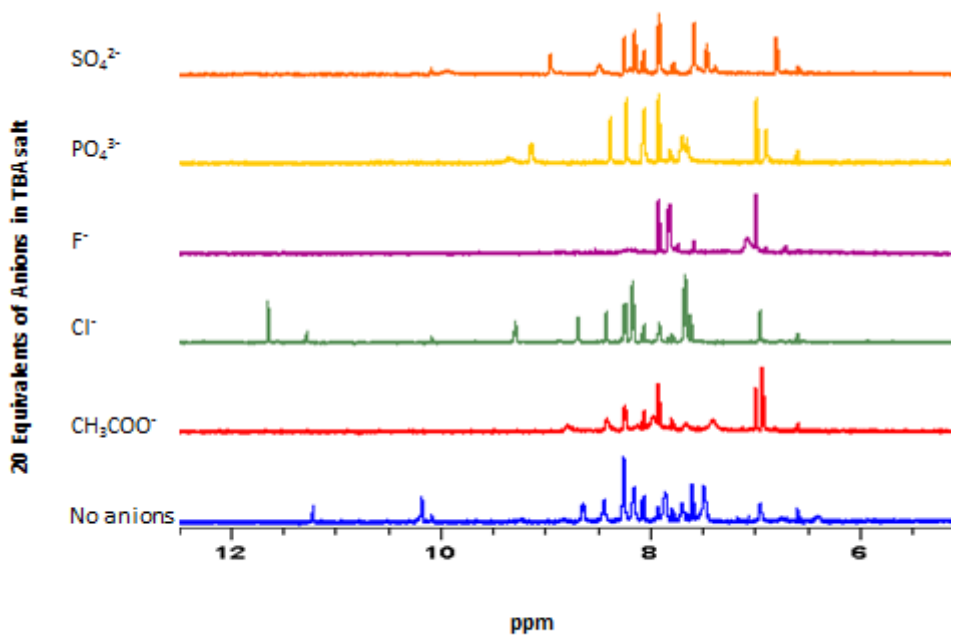

(b)

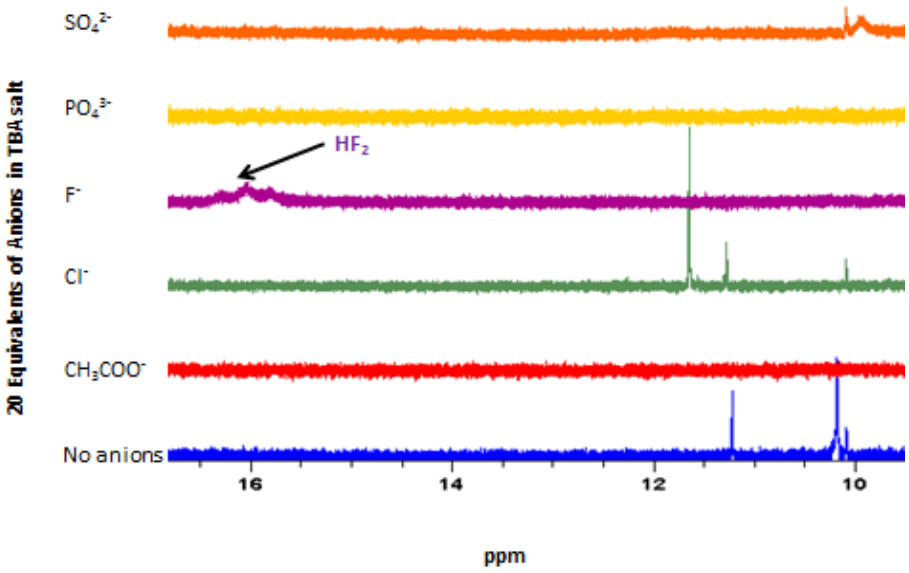

(c)

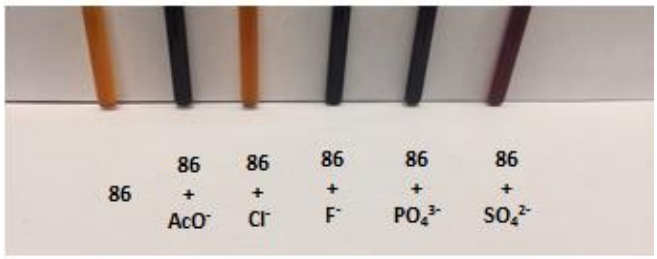

(d)

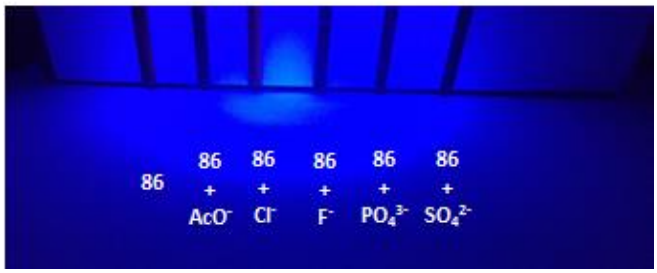

***2A 104**: Changes in the ^1H NMR spectrum of **86** (2.5×10^{-3} M) upon the addition of 20 eqvivalents of anions as TBA salts in DMSO-$_{d6}$ (AcO^-, Cl^-, F^-, PO_4^{3-} and SO_4^{2-}). **(a)**: Aromatic region of **86**. **(b)**: Formation of HF_2 upon the addition of 20 equivalents TBA fluoride to **86** in DMSO-$_{d6}$.[121, 122] The differing spectroscopic response of compound **86** upon the addition of 20 eqvivalents of anions as TBA salts in DMSO-$_{d6}$ (AcO^-, Cl^-, F^-, PO_4^{3-} and SO_4^{2-}). Changes in the appearance of a sample of **86** (2.5×10^{-3} M) upon the addition 20 equivalents of anions as TBA salts in DMSO-$_{d6}$ (AcO^-, Cl^-, F^-, PO_4^{3-} and SO_4^{2-}). **(c)** With the naked eye and **(d)** Under UV illumination.*

(a)

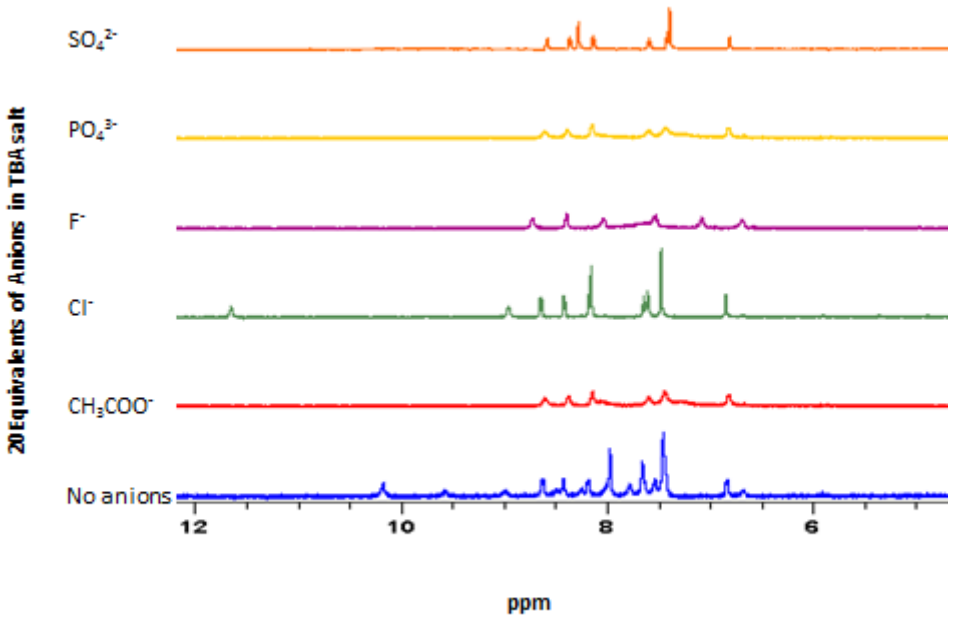
20 Equivalents of Anions in TBA salt
SO_4^{2-}
PO_4^{3-}
F^-
Cl^-
CH_3COO^-
No anions
12
10
8
6
ppm

(b)

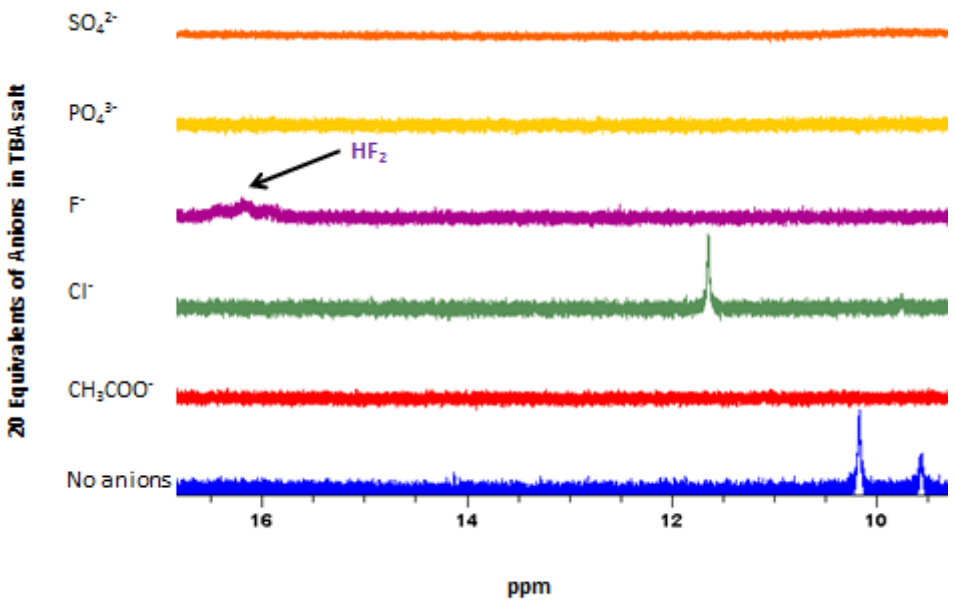
20 Equivalents of Anions in TBA salt
SO_4^{2-}
PO_4^{3-}
HF_2
F^-
Cl^-
CH_3COO^-
No anions
16
14
12
10
ppm

(c)

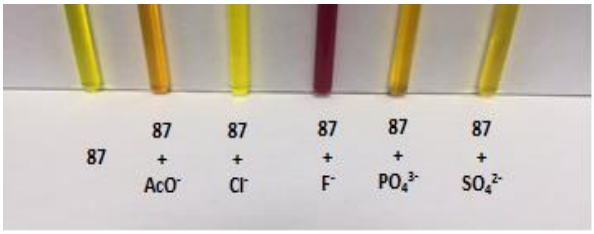

(d)

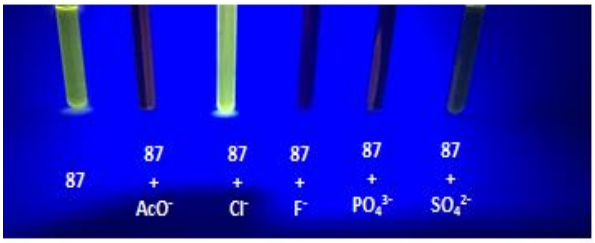

***2A 105**: Changes in the ^{1}H NMR spectrum of **87** (2.5×10^{-3} M) upon the addition of 20 eqvivalents of anions as TBA salts in DMSO-$_{d6}$ (AcO^-, Cl^-, F^-, PO_4^{3-} and SO_4^{2-}). **(a)**: Aromatic region of **87**. **(b)**: Formation of HF_2 upon the addition of 20 equivalents TBA fluoride to **87** in DMSO-$_{d6}$.[121, 122] The differing spectroscopic response of compound **87** upon the addition of 20 eqvivalents of anions as TBA salts in DMSO-$_{d6}$ (AcO^-, Cl^-, F^-, PO_4^{3-} and SO_4^{2-}). Changes in the appearance of a sample of **87** (2.5×10^{-3} M) upon the addition 20 equivalents of anions as TBA salts in DMSO-$_{d6}$ (AcO^-, Cl^-, F^-, PO_4^{3-} and SO_4^{2-}). **(c)** With the naked eye and **(d)** Under UV illumination.*

(a)

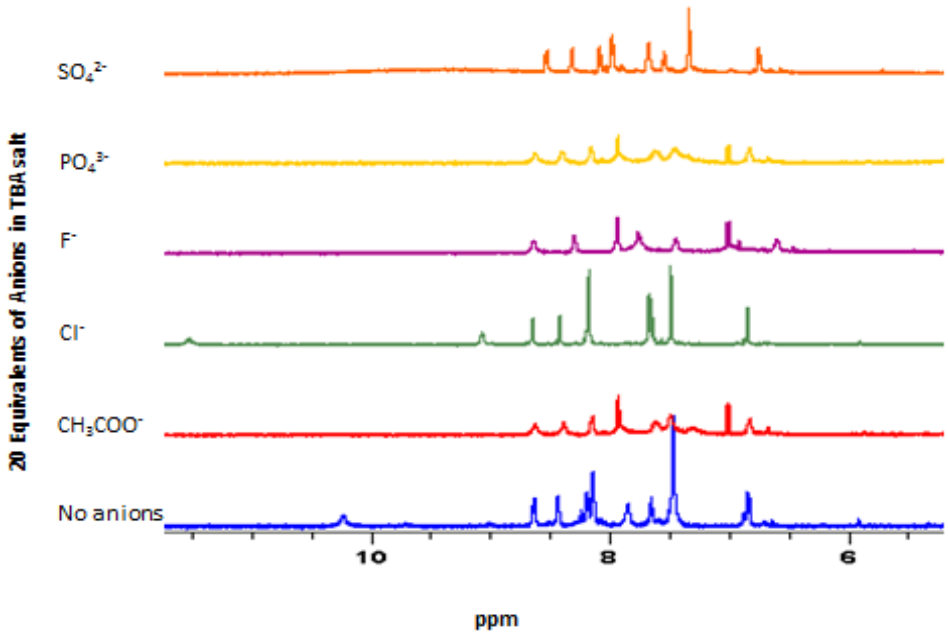

(b)

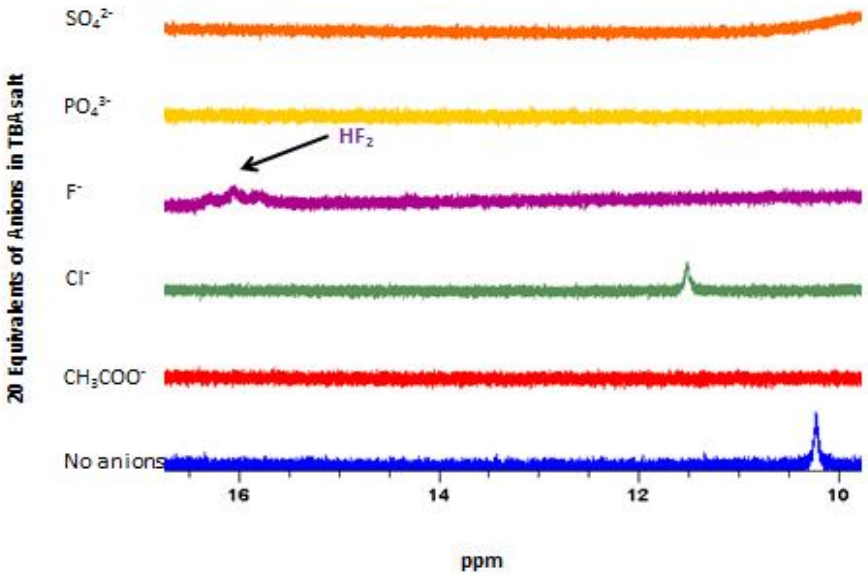

(c)

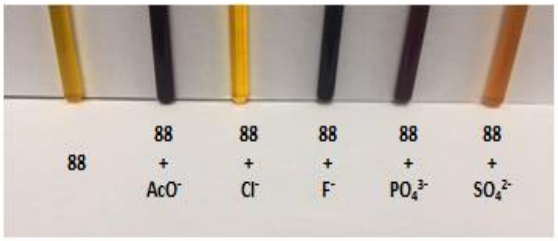

(d)

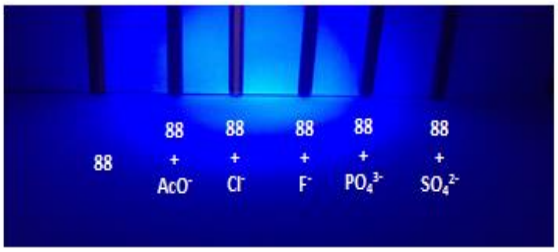

***2A 106**: Changes in the ^1H NMR spectrum of **88** (2.5 × 10^{-3} M) upon the addition of 20 eqvivalents of anions as TBA salts in DMSO-$_{d6}$ (AcO^-, Cl^-, F^-, PO_4^{3-} and SO_4^{2-}). **(a)**: Aromatic region of **88**. **(b)**: Formation of HF_2 upon the addition of 20 equivalents TBA fluoride to **88** in DMSO-$_{d6}$.[121, 122] The differing spectroscopic response of compound **88** upon the addition of 20 eqvivalents of anions as TBA salts in DMSO-$_{d6}$ (AcO^-, Cl^-, F^-, PO_4^{3-} and SO_4^{2-}). Changes in the appearance of a sample of **88** (2.5 × 10^{-3} M) upon the addition 20 equivalents of anions as TBA salts in DMSO-$_{d6}$ (AcO^-, Cl^-, F^-, PO_4^{3-} and SO_4^{2-}). **(c)** With the naked eye and **(d)** Under UV illumination.*

(a)

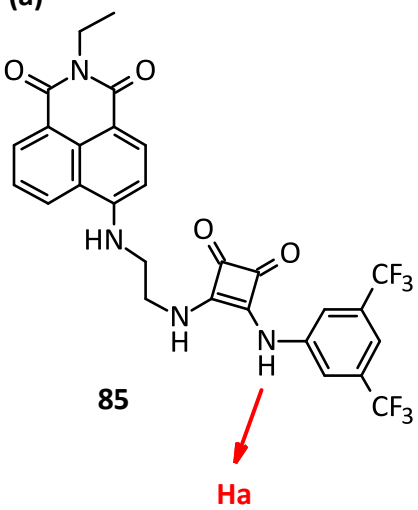

85

(b)

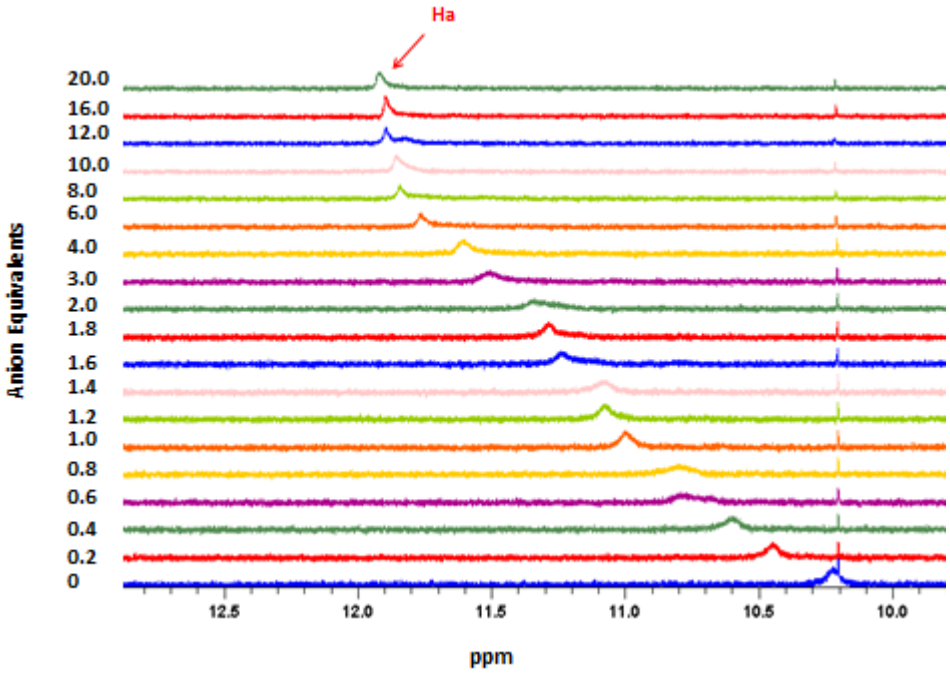

2A 107: ***(a)***: *Structure of* ***85*** *showing the NH proton as Ha.* ***(b)***: *Changes in the* ^{1}H *NMR spectrum (Ha proton) of* ***85*** *(2.5 × 10^{-3} M) upon the addition 0 - 20 eqvivalents of anions as TBA chloride in DMSO-$_{d6}$.*

(a)

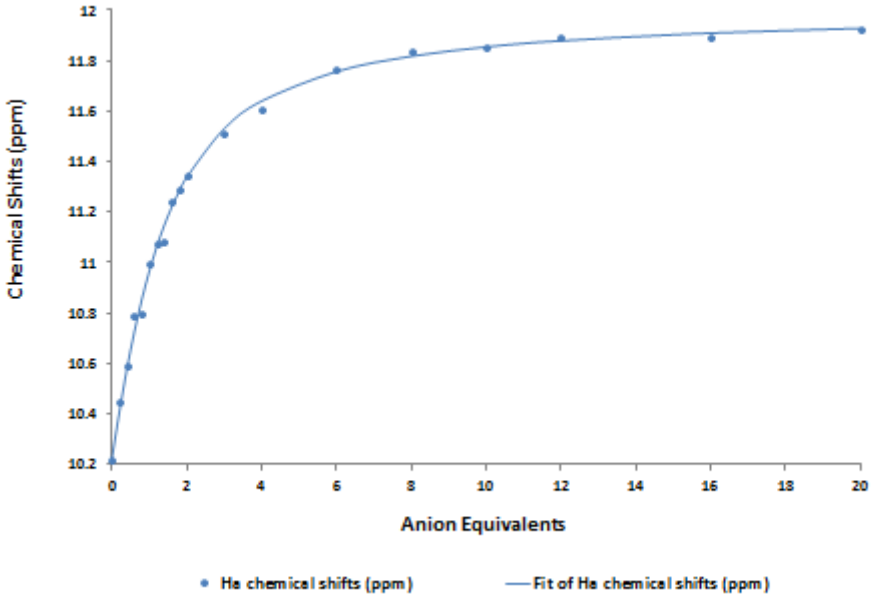

(b)

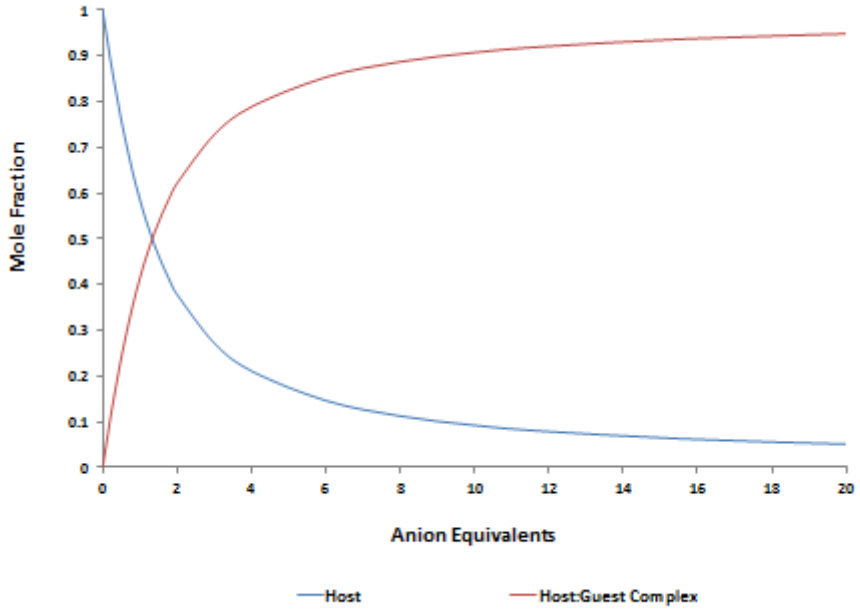

***2A 108**: **(a)**: Bind fit graph of the chemical shift of Ha proton (ppm) of **85** (2.5 × 10^{-3} M, DMSO-$_{d6}$) with increasing TBA chloride equivalents in DMSO-$_{d6}$ (0 - 70 eqs). **(b)**: Speciation graph of the chemical shift of Ha proton (ppm) of **85** (2.5 × 10^{-3} M, DMSO-$_{d6}$) with increasing TBA chloride equivalents in DMSO-$_{d6}$.*

(a)

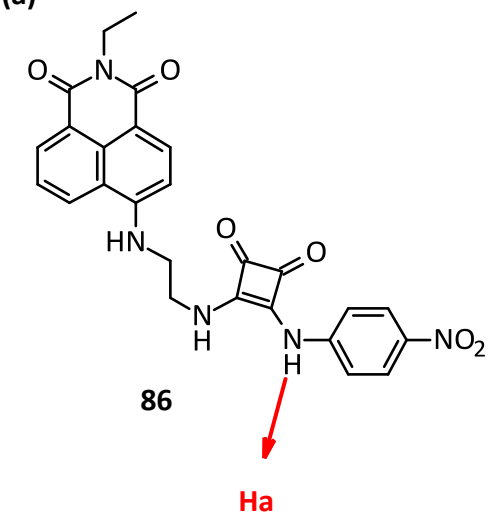

86

(b)

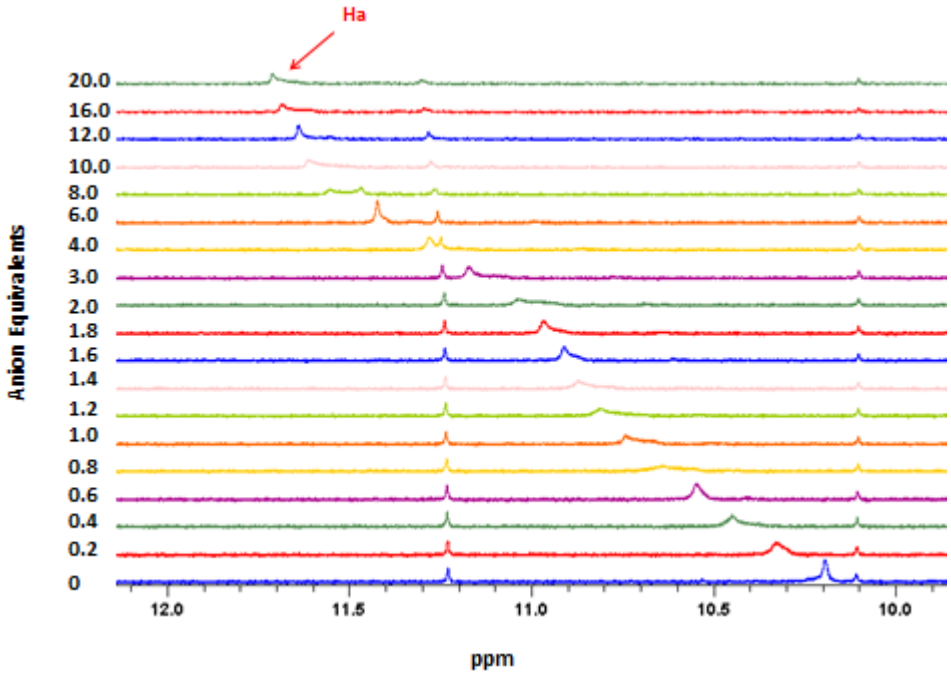

2A 109: ***(a)***: *Structure of* ***86*** *showing the NH proton as Ha.* ***(b)***: *Changes in the* ^{1}H *NMR spectrum (Ha proton) of* ***86*** *(2.5 × 10*$^{-3}$ *M) upon the addition 0 - 20 eqvivalents of anions as TBA chloride in DMSO-*$_{d6}$.

(a)

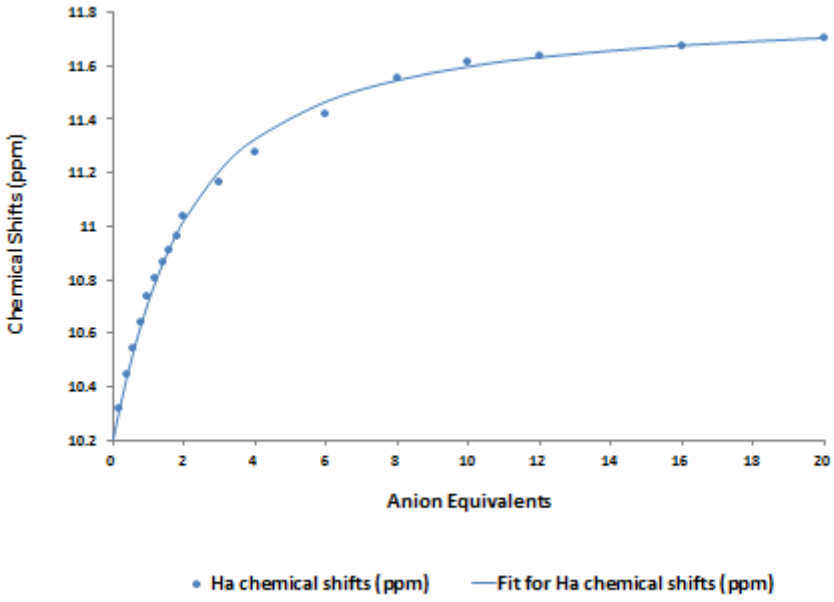

(b)

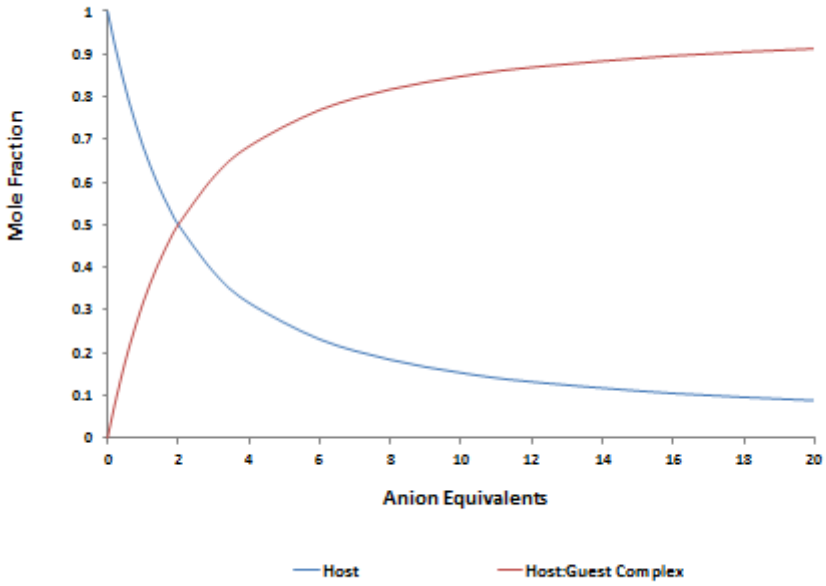

***2A 110**: **(a)**: Bind fit graph of the chemical shift of Ha proton (ppm) of **86** (2.5 × 10^{-3} M, DMSO-$_{d6}$) with increasing TBA chloride equivalents in DMSO-$_{d6}$ (0 - 70 eqs). **(b)**: Speciation graph of the chemical shift of Ha proton (ppm) of **86** (2.5 × 10^{-3} M, DMSO-$_{d6}$) with increasing TBA chloride equivalents in DMSO-$_{d6}$.*

(a)

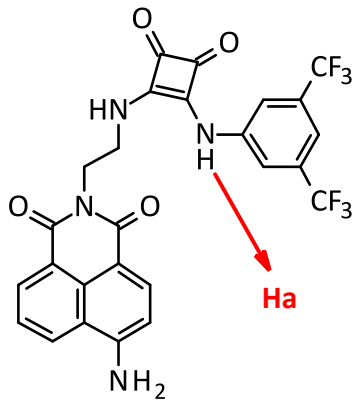

87

(b)

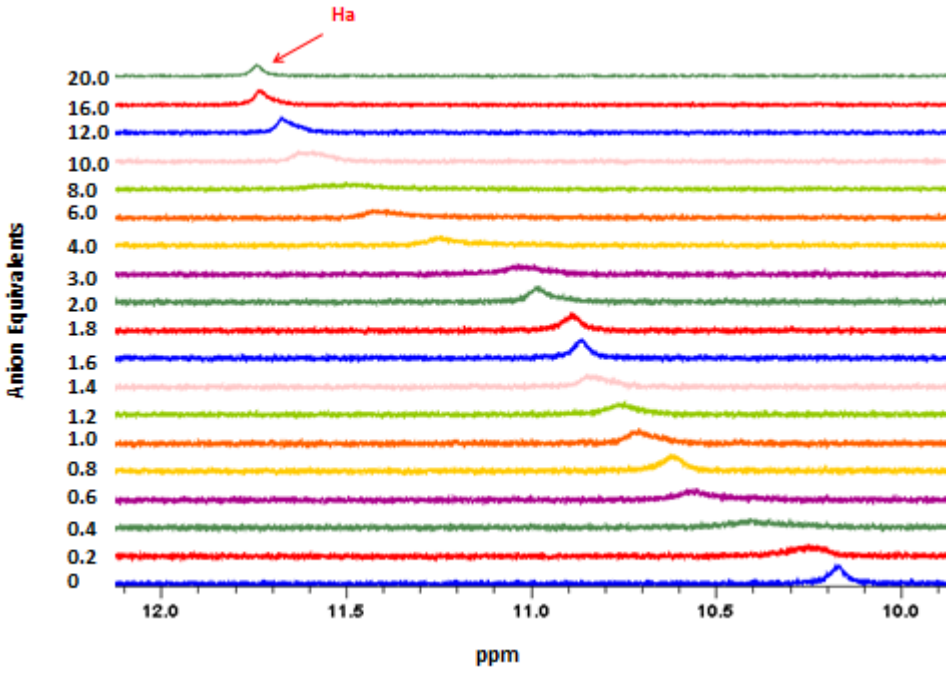

***2A 111**: **(a)**: Structure of **87** showing the NH proton as Ha. **(b)**: Changes in the ^{1}H NMR spectrum (Ha proton) of **87** (2.5×10^{-3} M) upon the addition 0 - 20 eqvivalents of anions as TBA chloride in DMSO-$_{d6}$.*

(a)

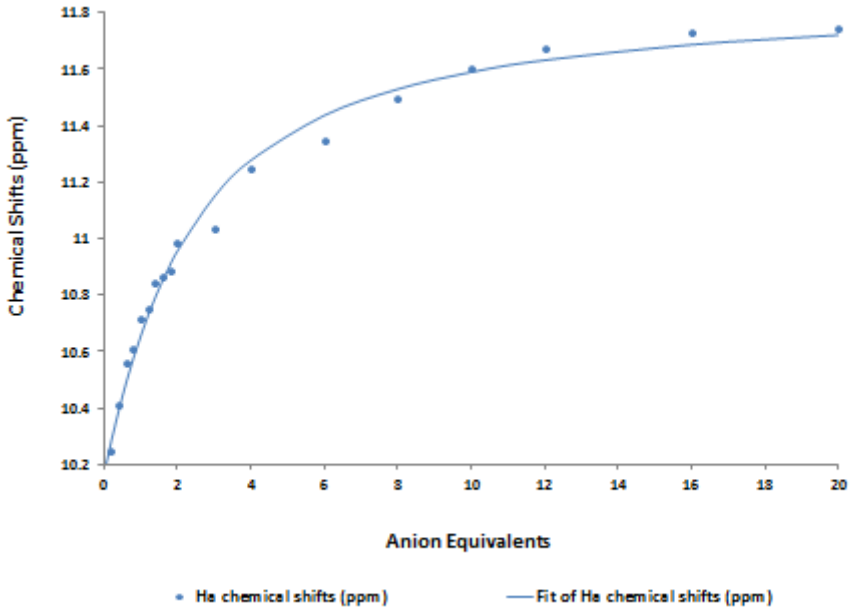

(b)

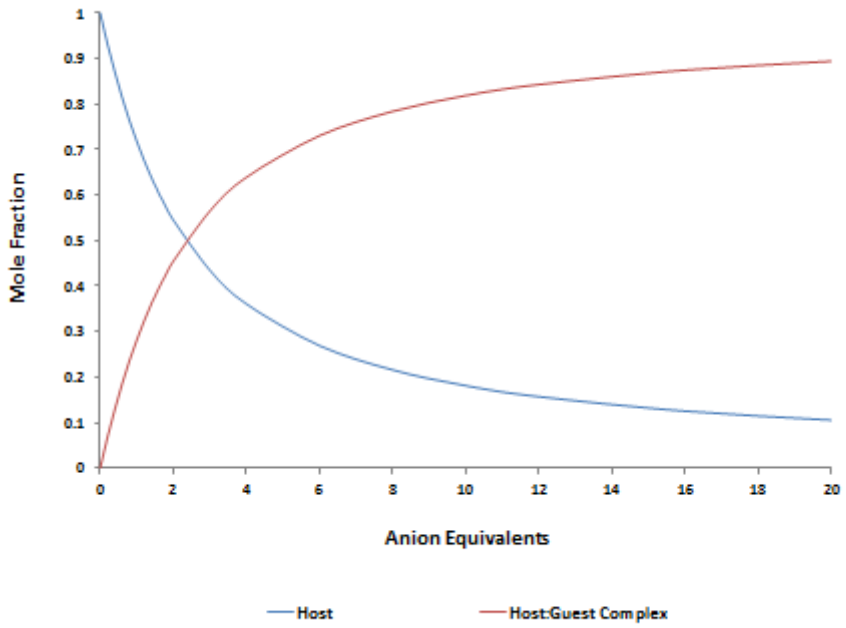

***2A 112**: **(a)**: Bind fit graph of the chemical shift of Ha proton (ppm) of **87** (2.5 × 10^{-3} M, DMSO-$_{d6}$) with increasing TBA chloride equivalents in DMSO-$_{d6}$ (0 - 70 eqs). **(b)**: Speciation graph of the chemical shift of Ha proton (ppm) of **87** (2.5 × 10^{-3} M, DMSO-$_{d6}$) with increasing TBA chloride equivalents in DMSO-$_{d6}$.*

(a)

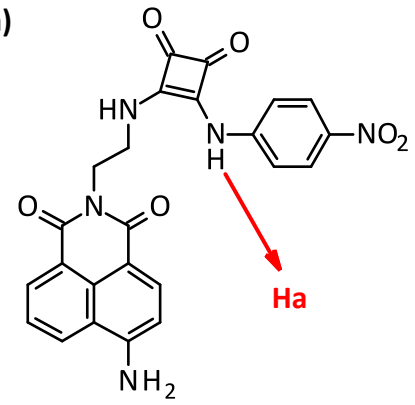

88

(b)

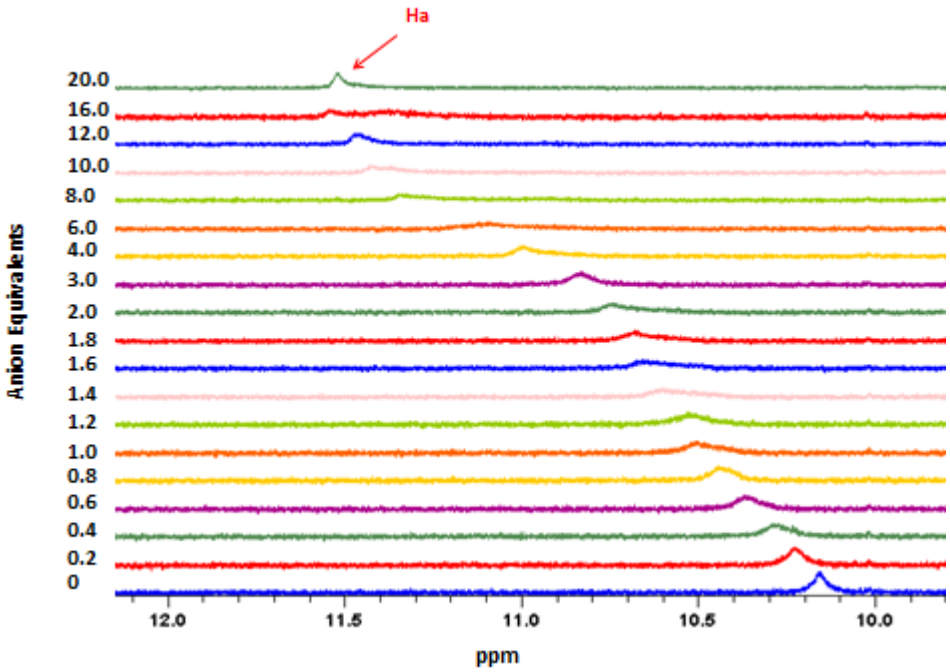

2A 113: ***(a)***: *Structure of* ***88*** *showing the NH proton as Ha.* ***(b)***: *Changes in the* ^{1}H *NMR spectrum (Ha proton) of* ***88*** *(2.5 × 10^{-3} M) upon the addition 0 - 20 eqvivalents of anions as TBA chloride in DMSO-$_{d6}$.*

(a)

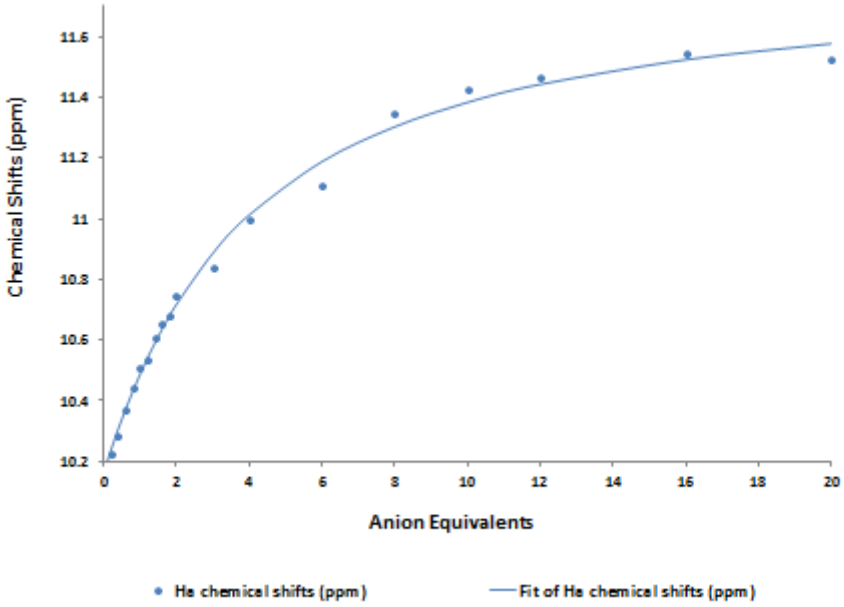

(b)

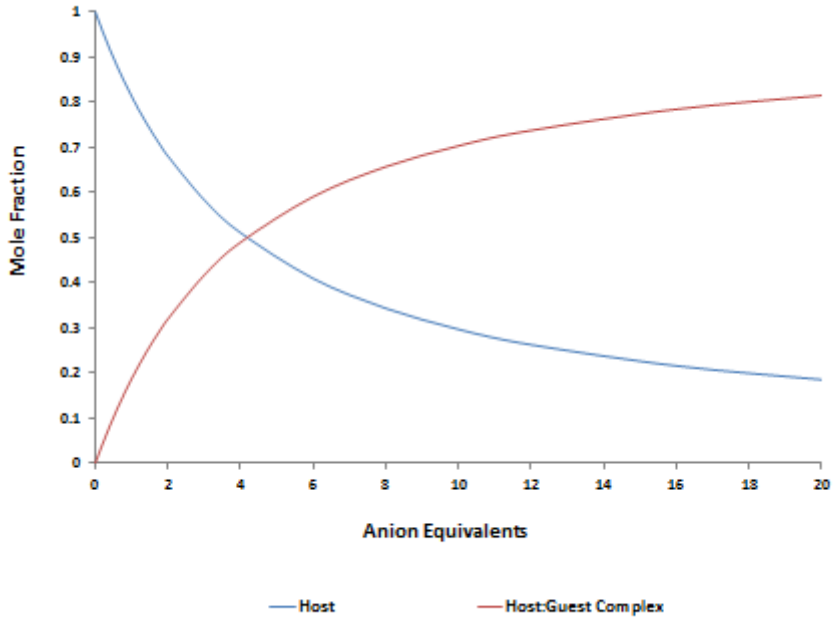

***2A 114**: **(a)**: Bind fit graph of the chemical shift of Ha proton (ppm) of **88** (2.5 × 10^{-3} M, DMSO-$_{d6}$) with increasing TBA chloride equivalents in DMSO-$_{d6}$ (0 - 70 eqs). **(b)**: Speciation graph of the chemical shift of Ha proton (ppm) of **88** (2.5 × 10^{-3} M, DMSO-$_{d6}$) with increasing TBA chloride equivalents in DMSO-$_{d6}$.*

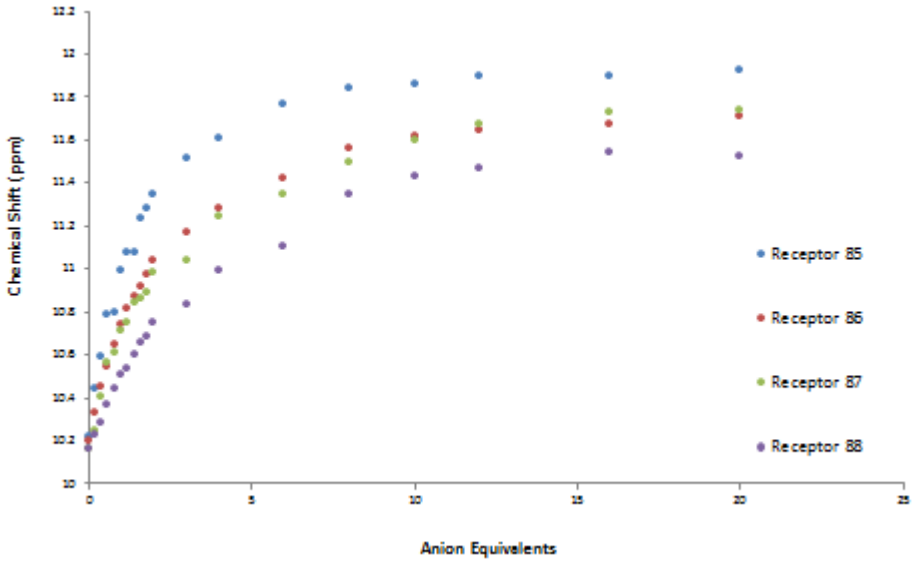

***2A 115**: **(a)**: Combination of bind fit graph of the ^{1}H NMR spectrum (chemical shift of Ha proton (ppm)) of **85, 86, 87** and **88** (2.5×10^{-3} M, DMSO-$_{d6}$) with increasing TBA chloride equivalents in DMSO-$_{d6}$.*

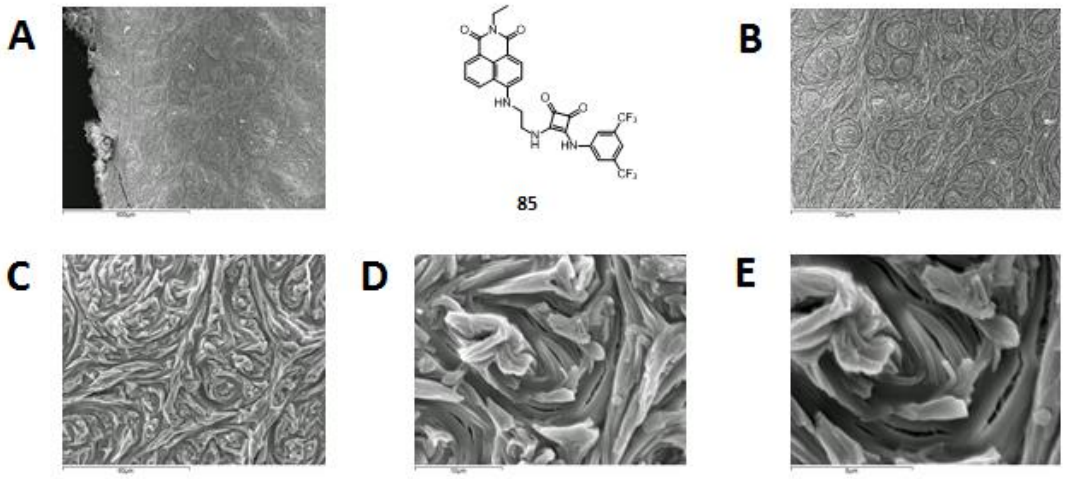

***2A 116**: Scanning electron microscopy (SEM) images of compound **85** spotted with Au, **(A):** Mag x 100; **(B):** Mag x 200; **(C):** Mag x 1000; **(D):** Mag x 4000; **(E):** Mag x 7000.*

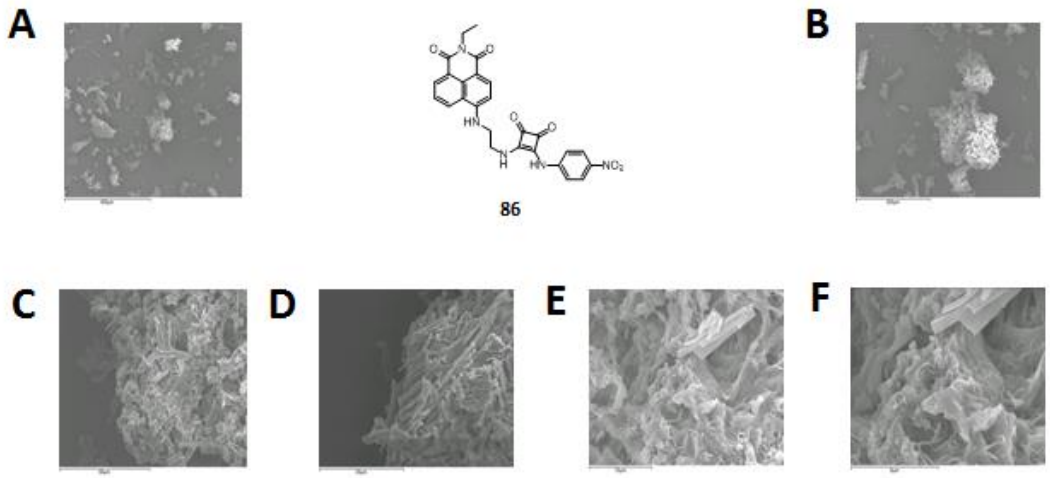

***2A 117**: Scanning electron microscopy (SEM) images of compound **86** spotted with Au, **(A):** Mag x 100; **(B):** Mag x 250; **(C):** Mag x 1000; **(D):** Mag x 1800; **(E):** Mag x 4000; **(F):** Mag x 7000.*

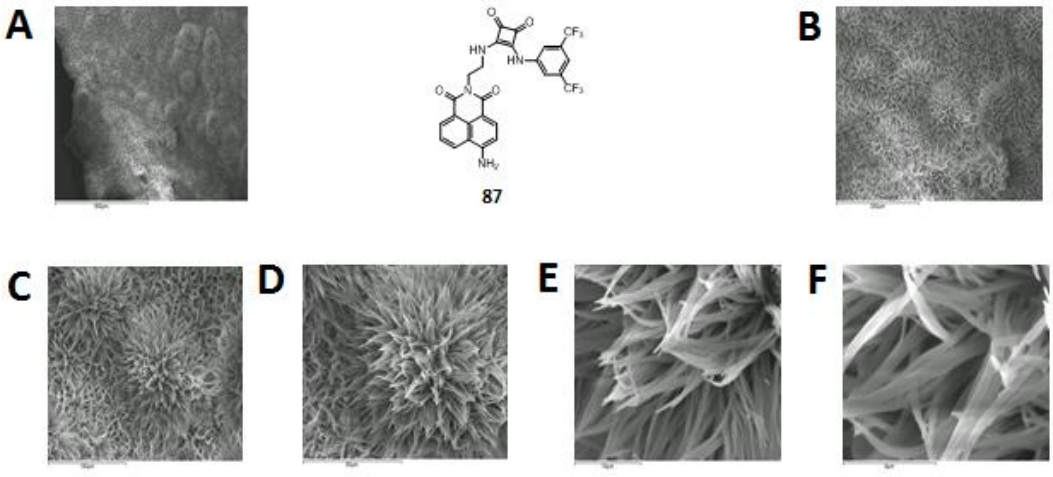

***2A 118**: Scanning electron microscopy (SEM) images of compound **87** spotted with Au, **(A):** Mag x 100; **(B):** Mag x 250; **(C):** Mag x 500; **(D):** Mag x 1000; **(E):** Mag x 4000; **(F):** Mag x 7000.*

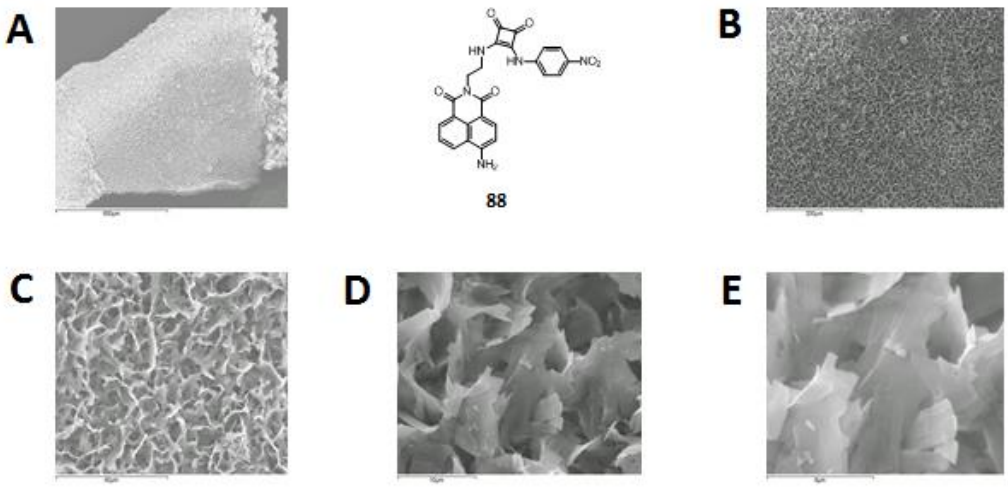

***2A 119**: Scanning electron microscopy (SEM) images of compound **88** spotted with Au, **(A):** Mag x 100; **(B):** Mag x 250; **(C):** Mag x 1000; **(D):** Mag x 4000; **(E):** Mag x 7000.*

Appendix 4:

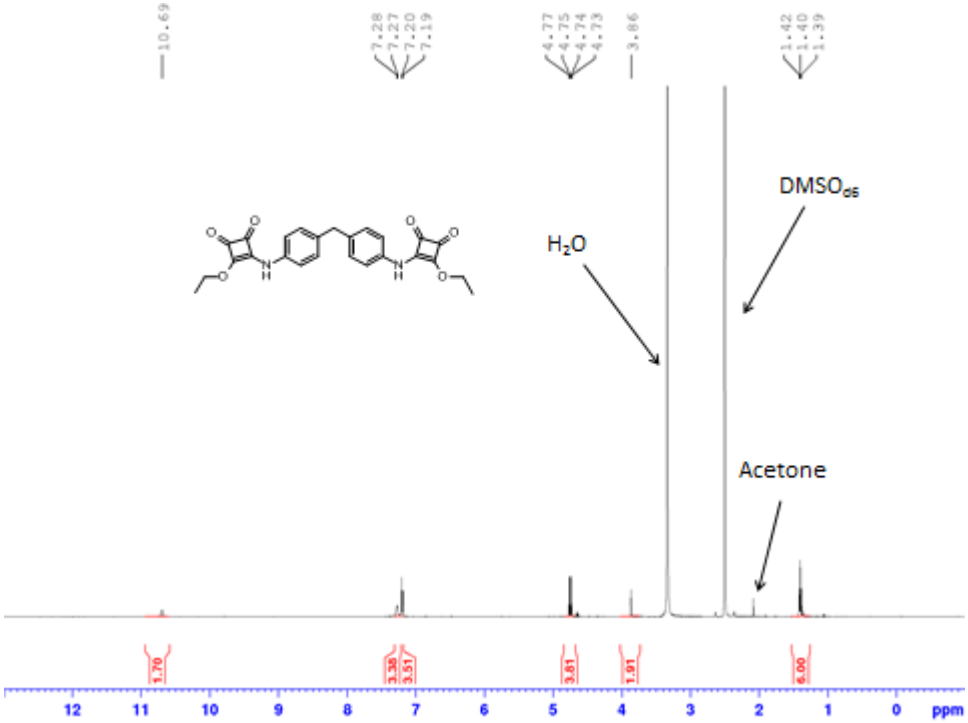

4A 1: *The ^{1}H NMR spectrum of* ***122*** *(500.13 MHz, DMSO-$_{d6}$)*

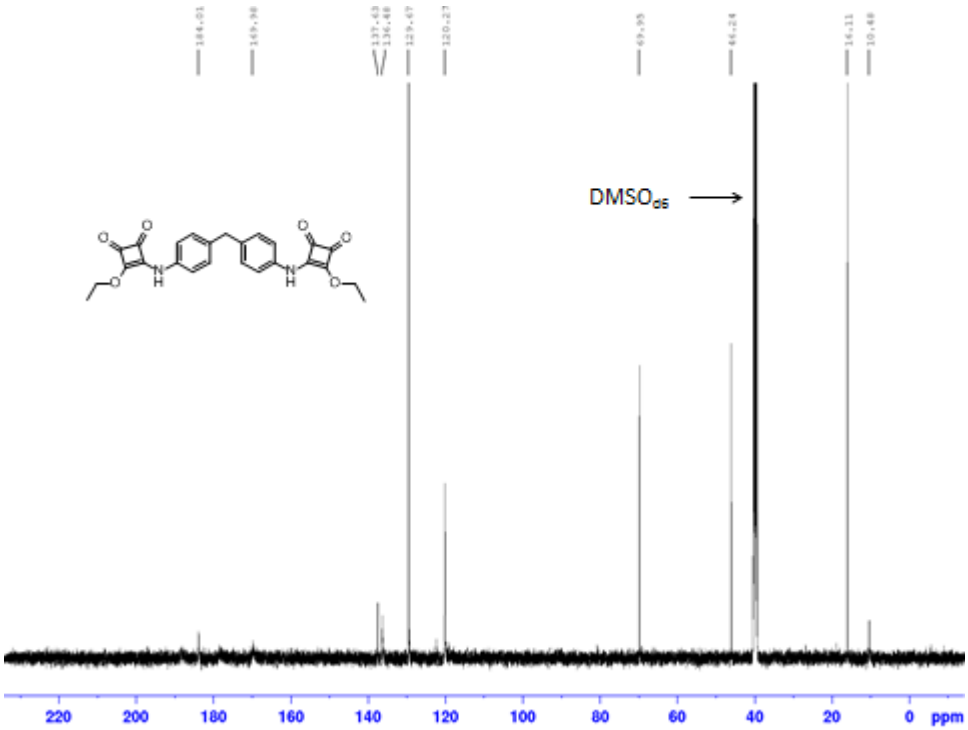

4A 2: *The ^{13}C NMR spectrum of* ***122*** *(125.76 MHz, DMSO-$_{d6}$)*

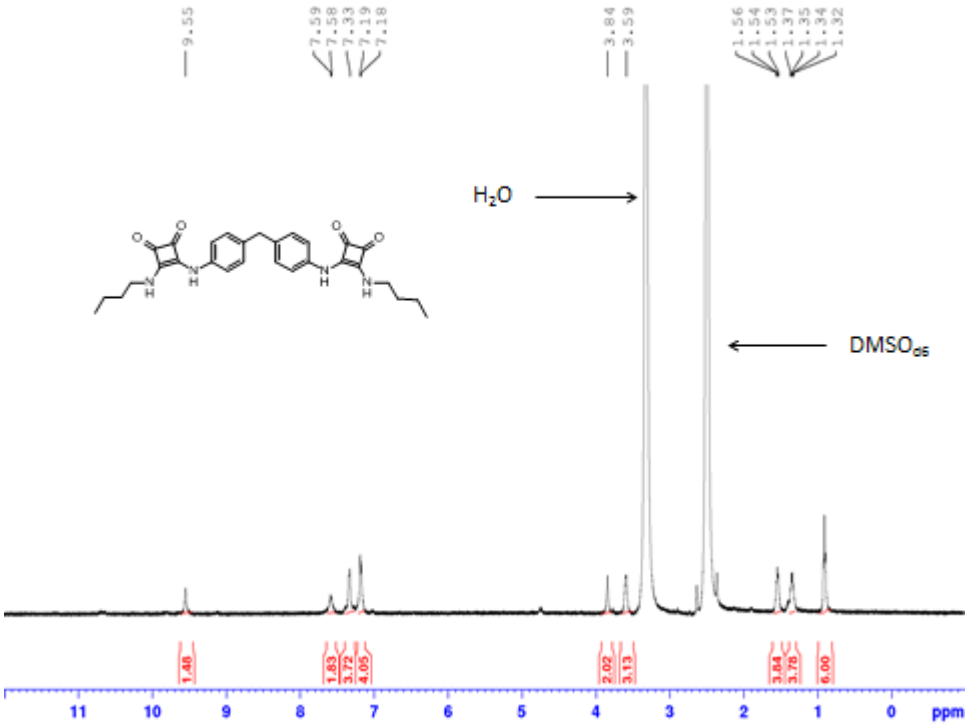

4A 3: *The ^{1}H NMR spectrum* ***132*** *(500.13 MHz, DMSO-$_{d6}$)*

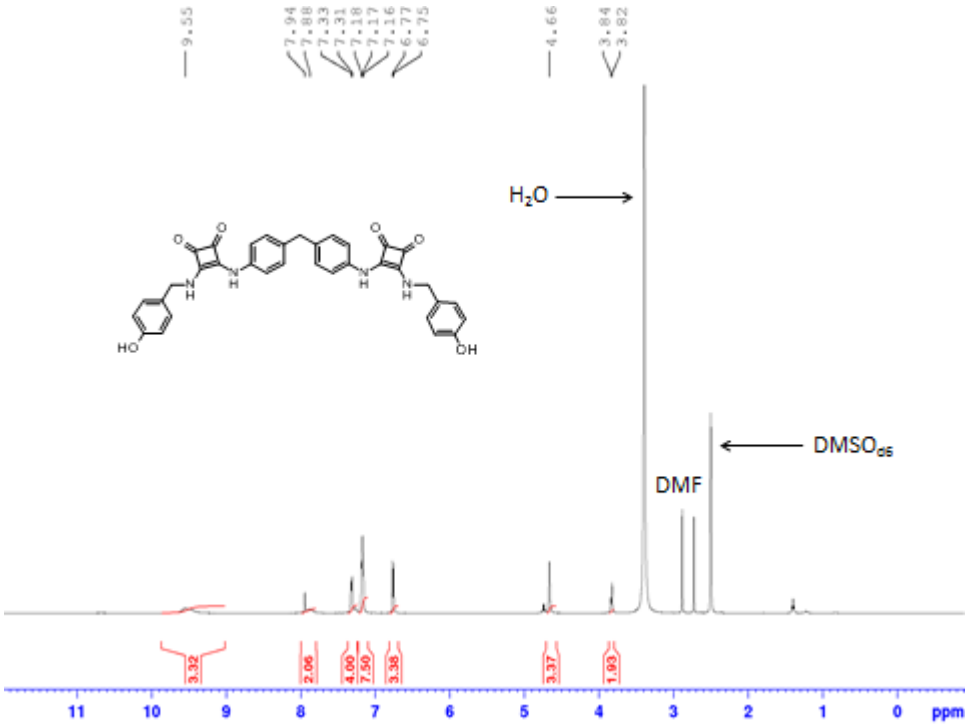

4A 4: *The ^{1}H NMR spectrum of* ***135*** *(500.13 MHz, DMSO-$_{d6}$)*

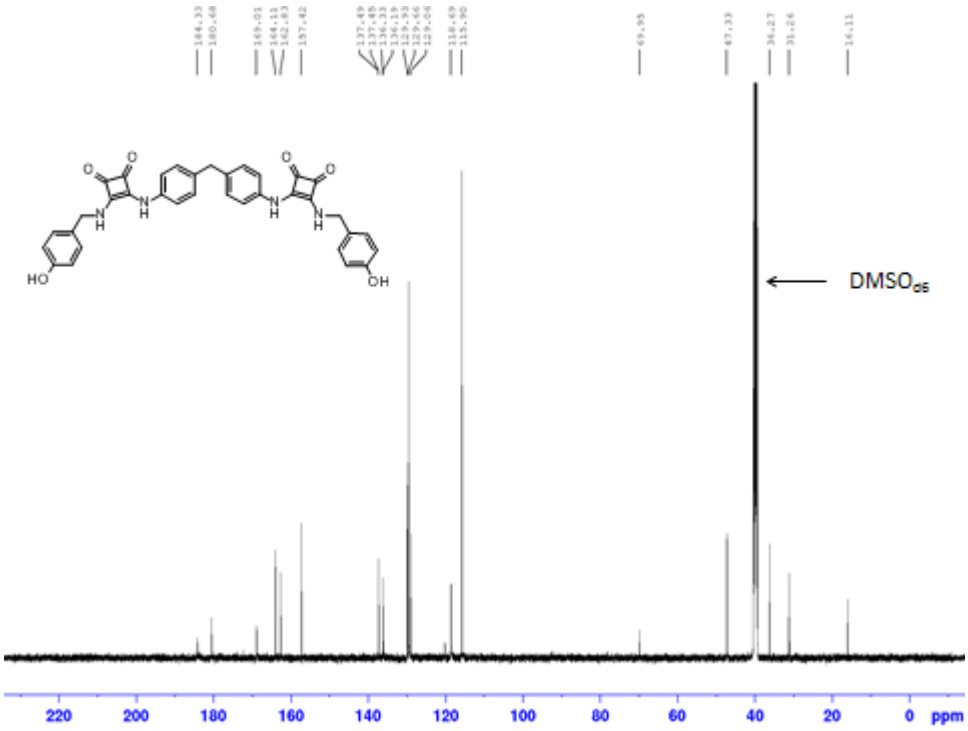

4A 5: *The ^{13}C NMR spectrum of* ***135*** *(125.76 MHz, DMSO-$_{d6}$)*

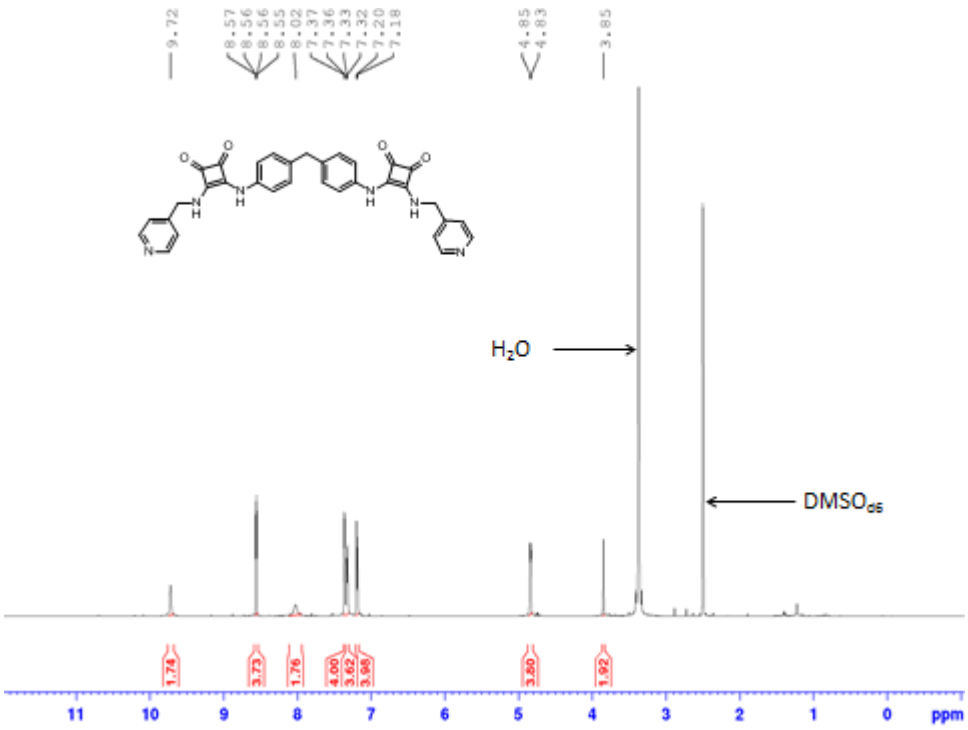

4A 6: *The ^{1}H NMR spectrum of* ***136*** *(500.13 MHz, DMSO-$_{d6}$)*

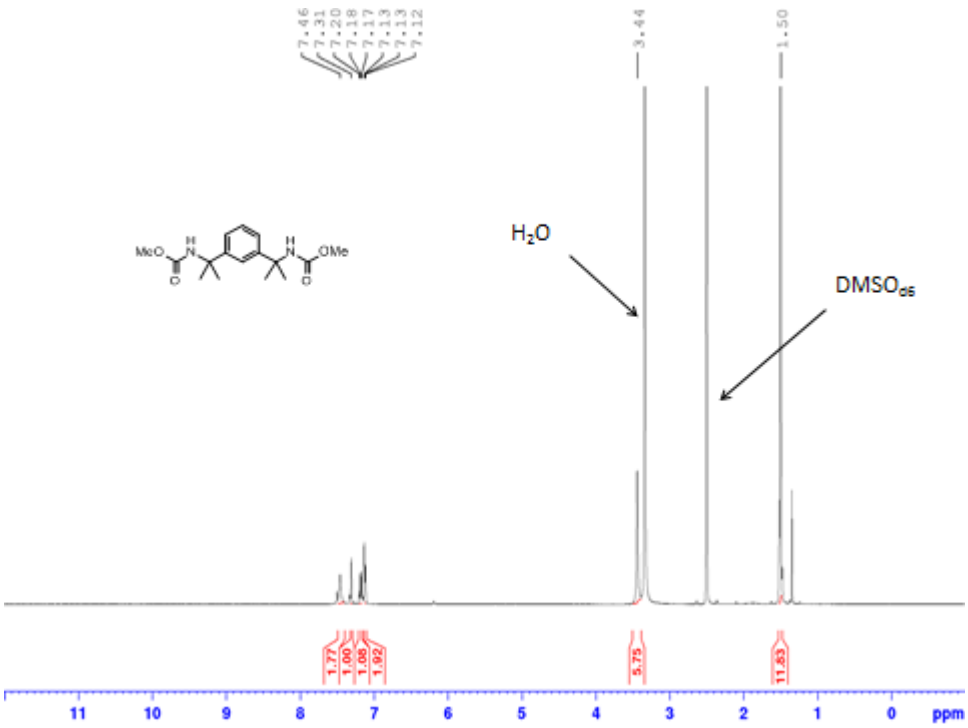

4A 7: *The [1]H NMR spectrum of* ***119*** *(500.13 MHz, DMSO-$_{d6}$)*

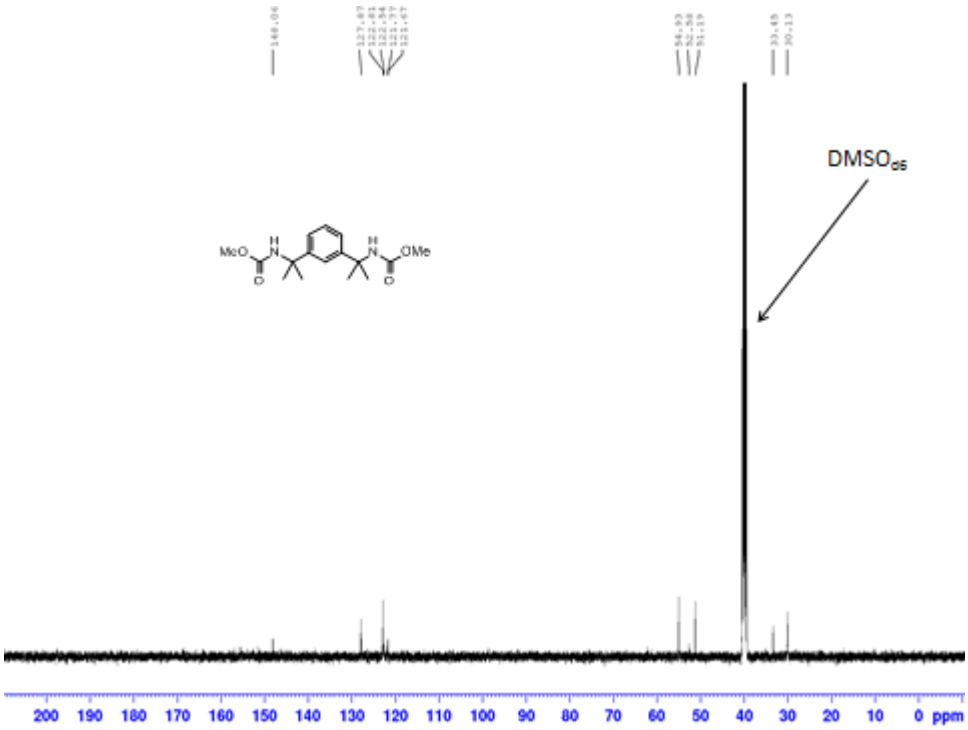

4A 8: *The [13]C NMR spectrum of* ***119*** *(125.76 MHz, DMSO-$_{d6}$)*

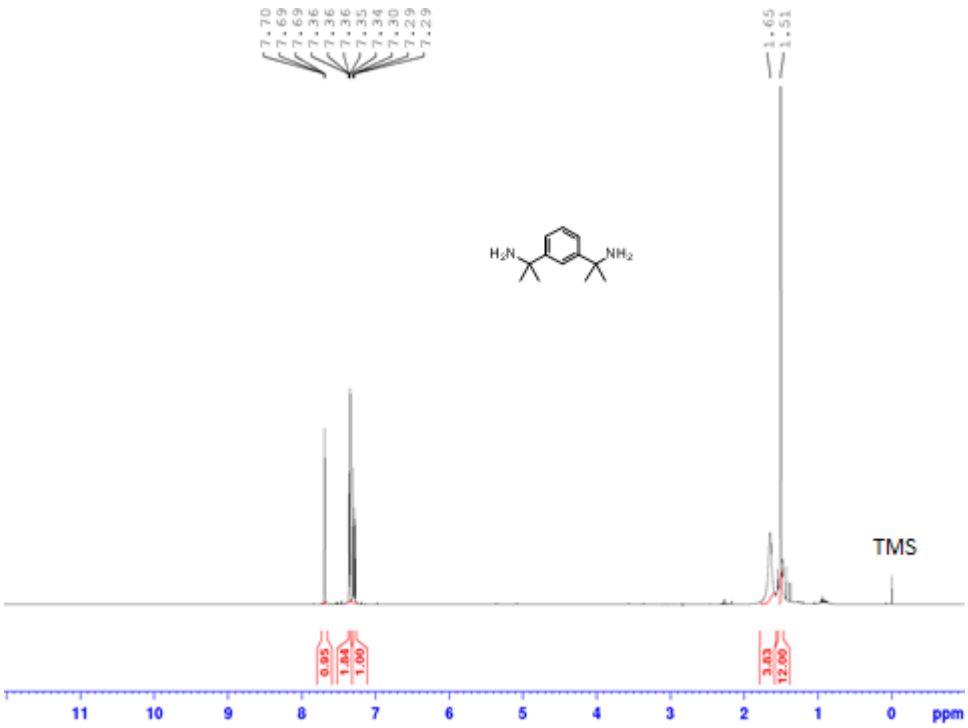

4A 9: *The ^{1}H NMR spectrum of* ***120*** *(500.13 MHz, $CDCl_3$)*

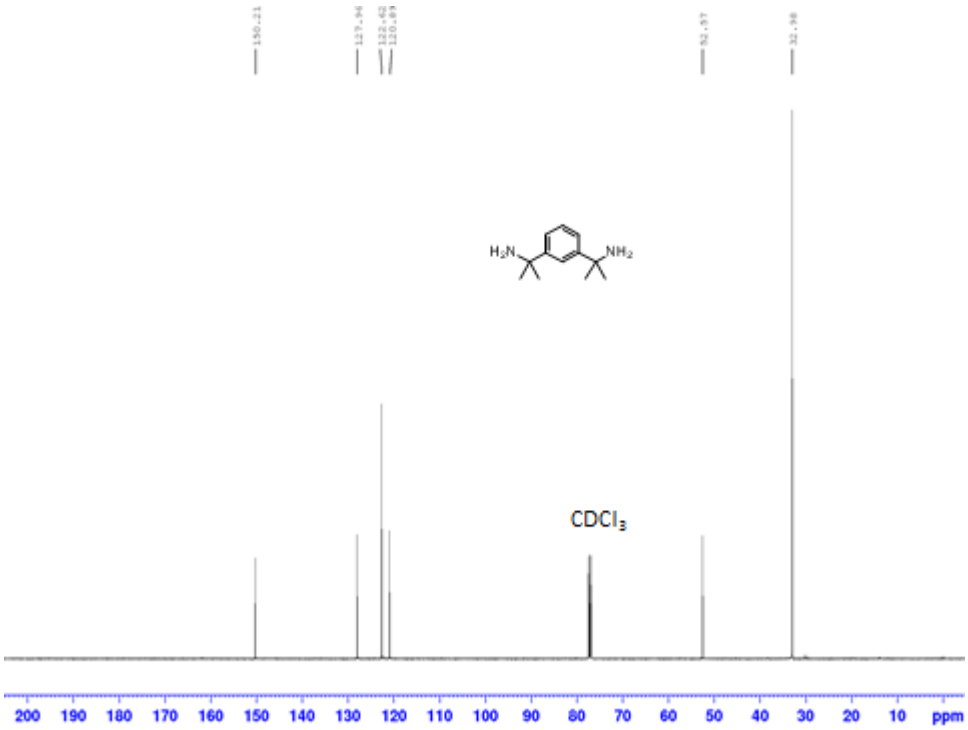

4A 10: *The ^{13}C NMR spectrum of* ***120*** *(125.76 MHz, $CDCl_3$)*

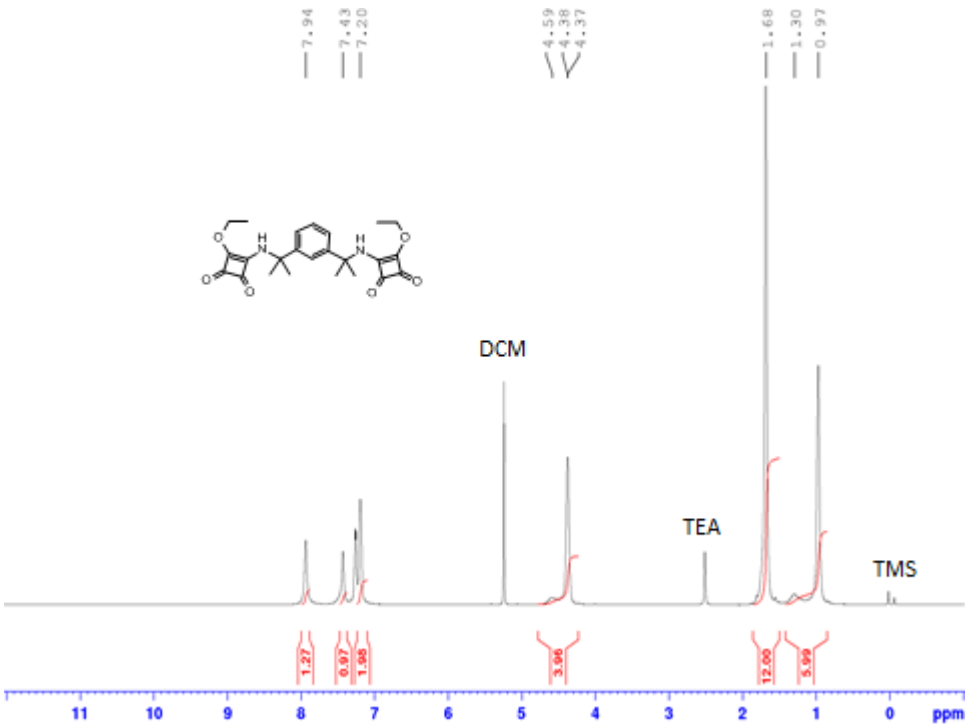

4A 11: *The ^{1}H NMR spectrum of* ***123*** *(500.13 MHz, $CDCl_3$)*

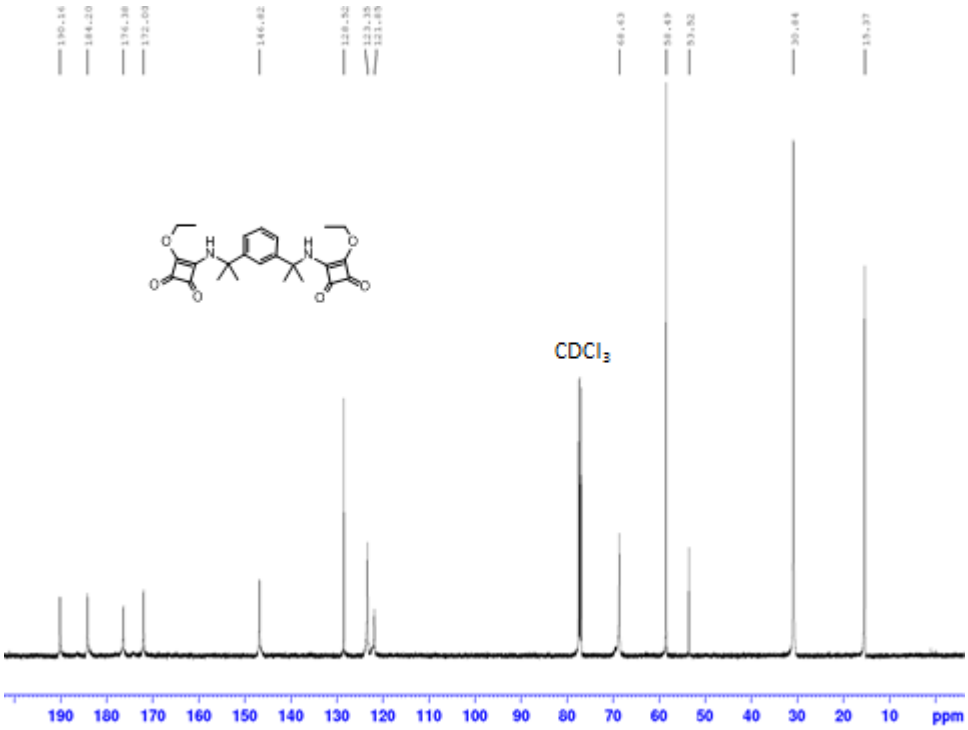

4A 12: *The ^{13}C NMR spectrum of* ***123*** *(125.76 MHz, $CDCl_3$)*

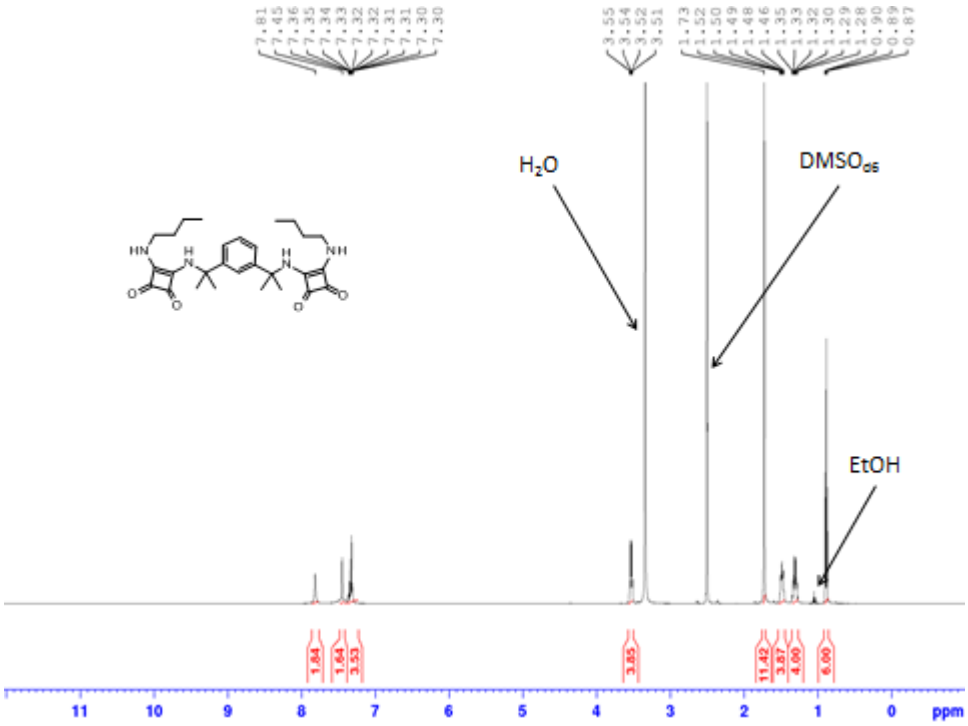

4A 13: *The ^{1}H NMR spectrum of **137** (500.13 MHz, DMSO-$_{d6}$)*

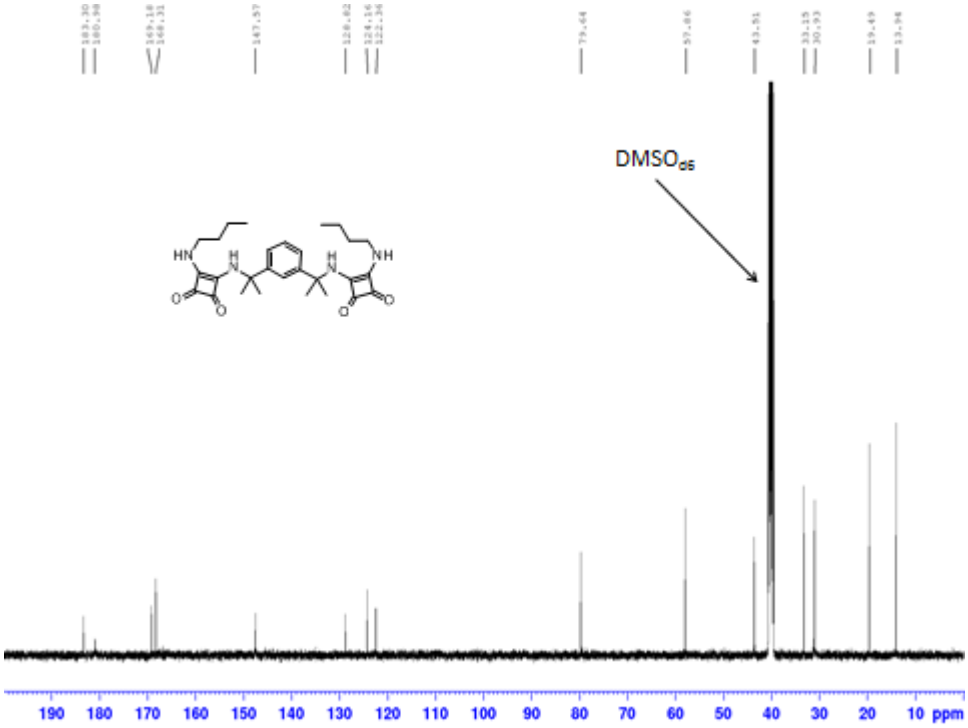

4A 14: *The ^{13}C NMR spectrum of **137** (125.76 MHz, DMSO-$_{d6}$)*

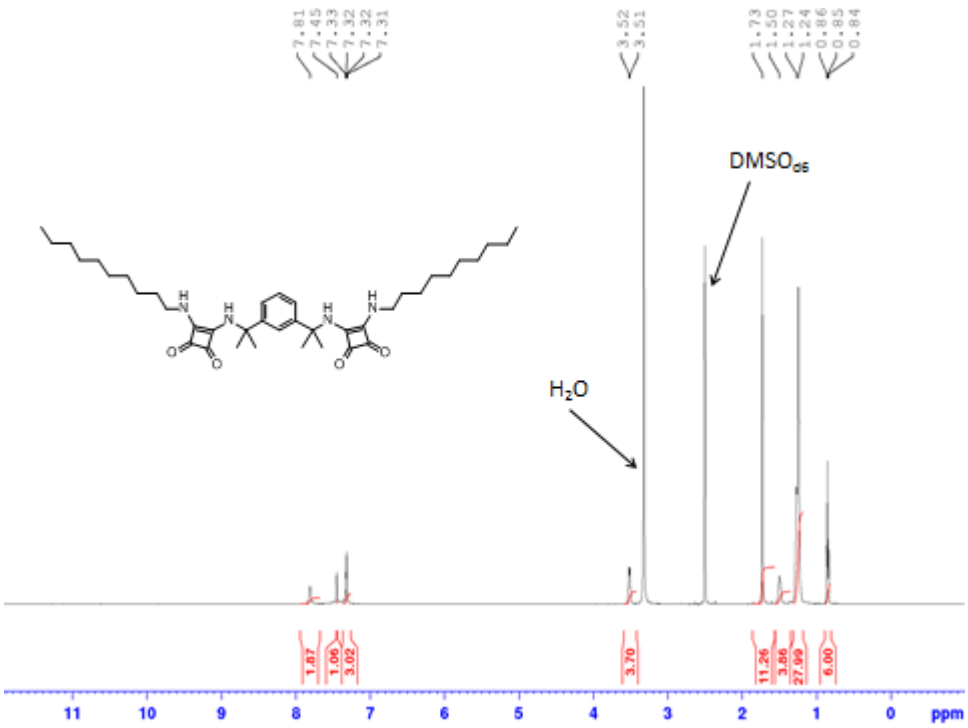

4A 15: *The ^{1}H NMR spectrum of* ***138*** *(500.13 MHz, DMSO-$_{d6}$)*

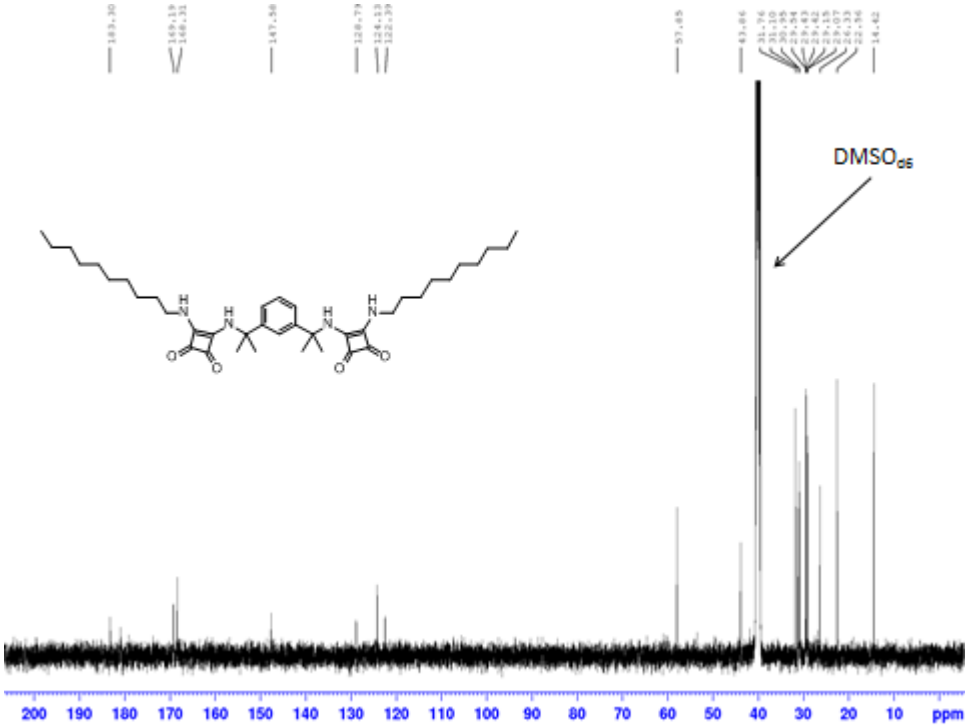

4A 16: *The ^{13}C NMR spectrum of* ***138*** *(125.76 MHz, DMSO-$_{d6}$)*

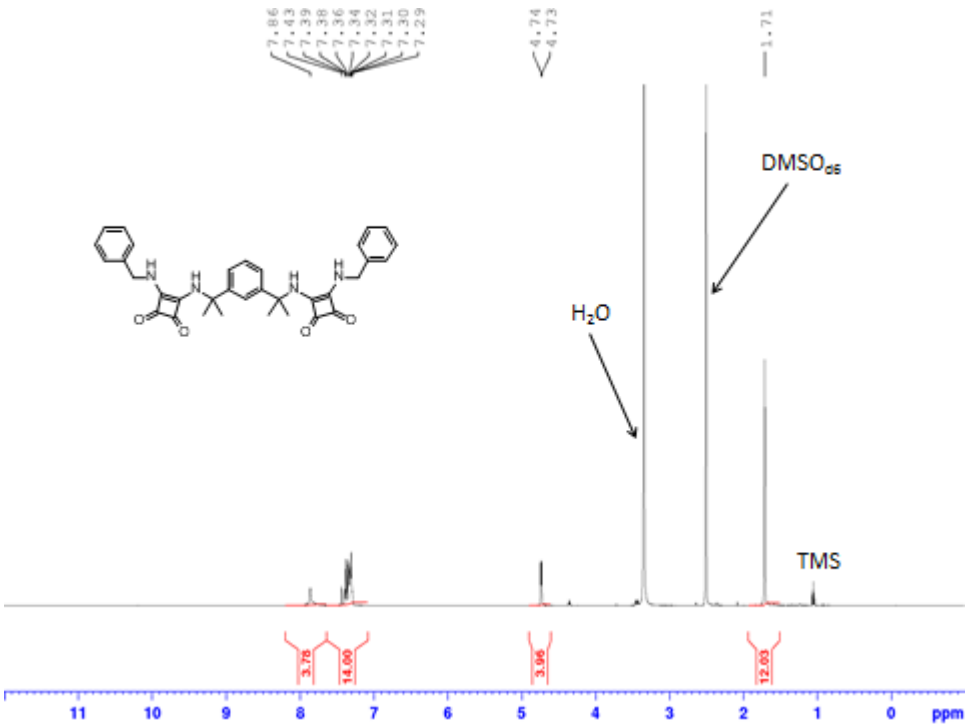

4A 17: *The ^{1}H NMR spectrum of **139** (500.13 MHz, DMSO-$_{d6}$)*

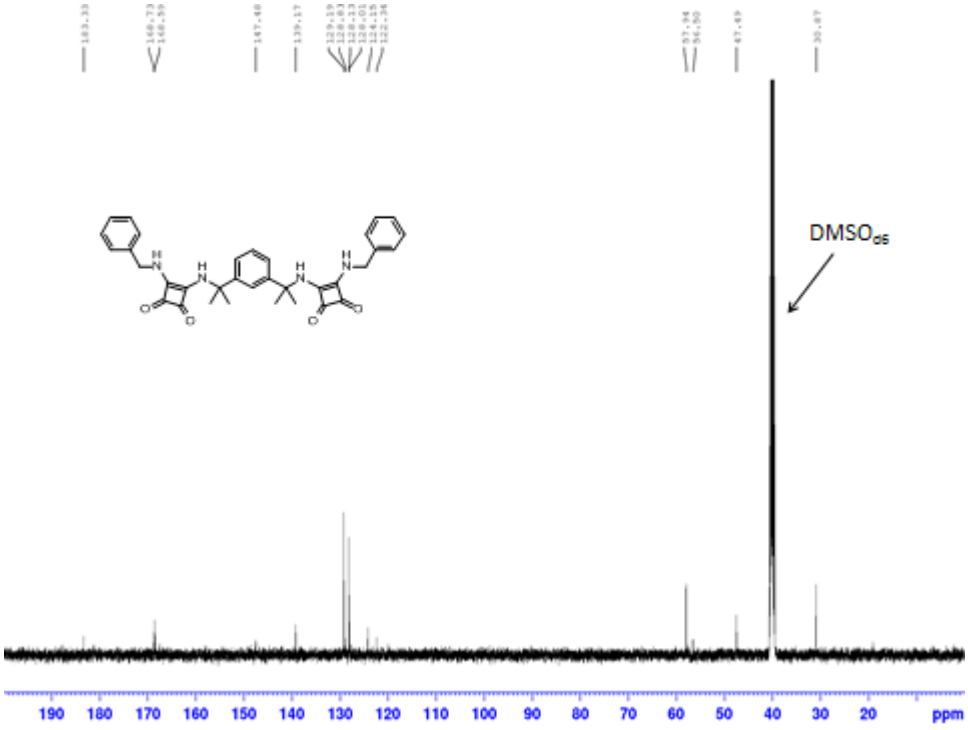

4A 18: *The ^{13}C NMR spectrum of **139** (125.76 MHz, DMSO-$_{d6}$)*

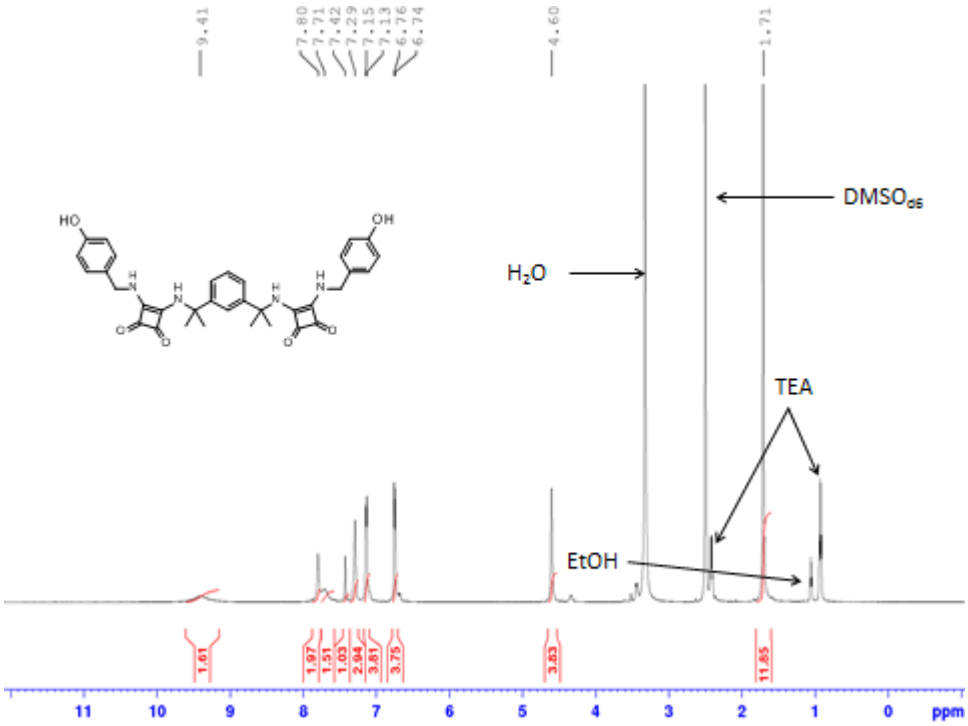

4A 19: *The ^{1}H NMR spectrum of* ***140*** *(500.13 MHz, DMSO-$_{d6}$)*

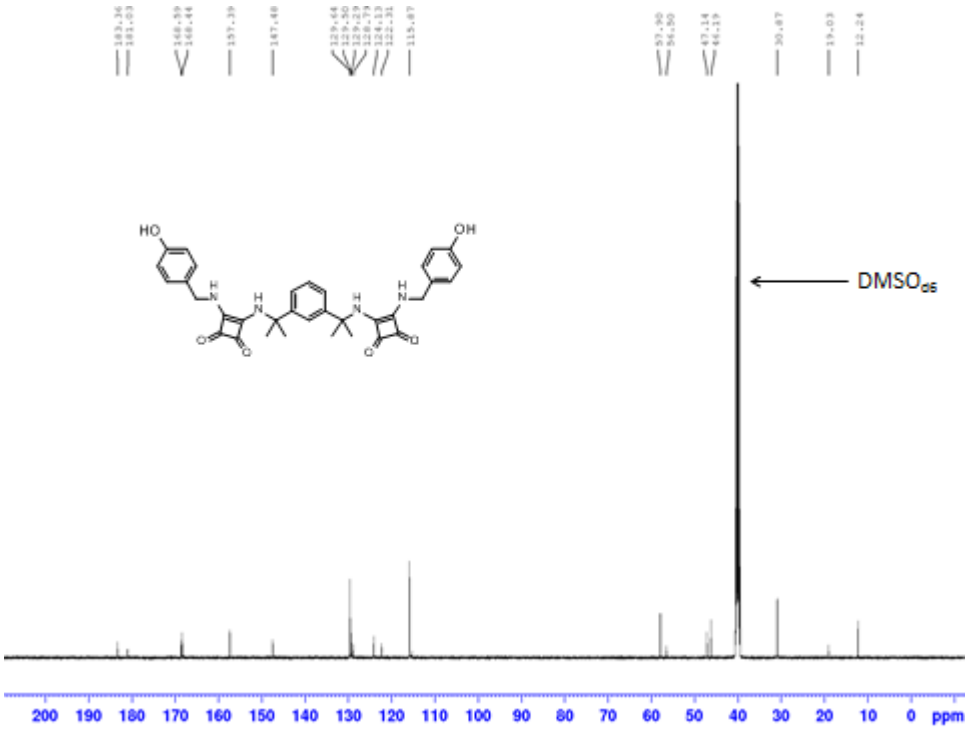

4A 20: *The ^{13}C NMR spectrum of* ***140*** *(125.76 MHz, DMSO-$_{d6}$)*

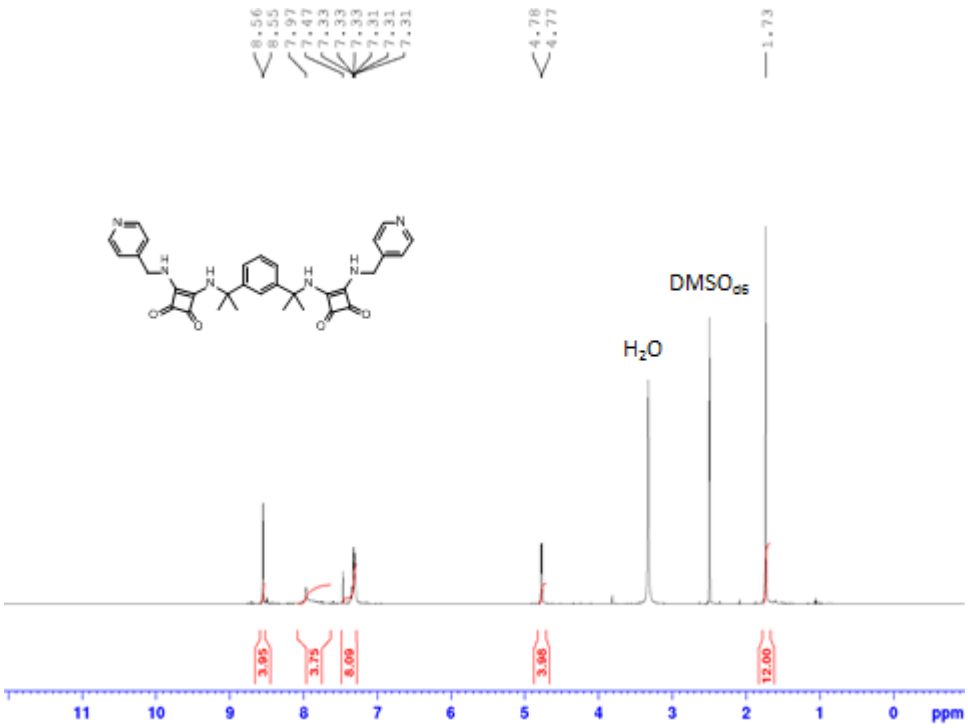

4A 21: *The ^{1}H NMR spectrum of* ***141*** *(500.13 MHz, DMSO-$_{d6}$)*

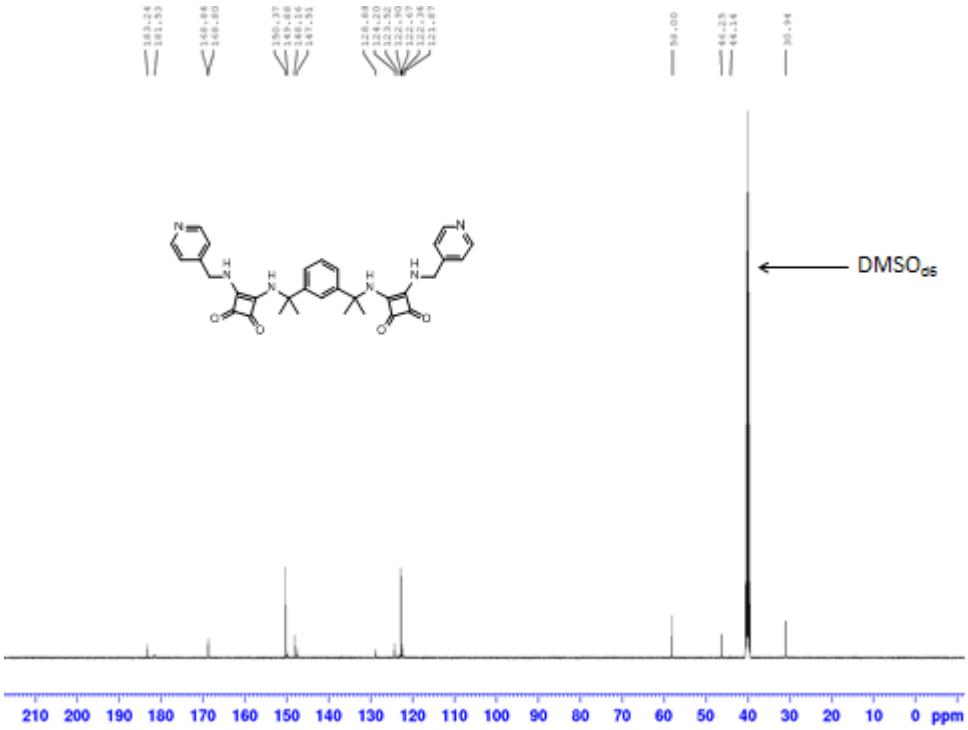

4A 22: *The ^{13}C NMR spectrum of* ***141*** *(125.76 MHz, DMSO-$_{d6}$)*

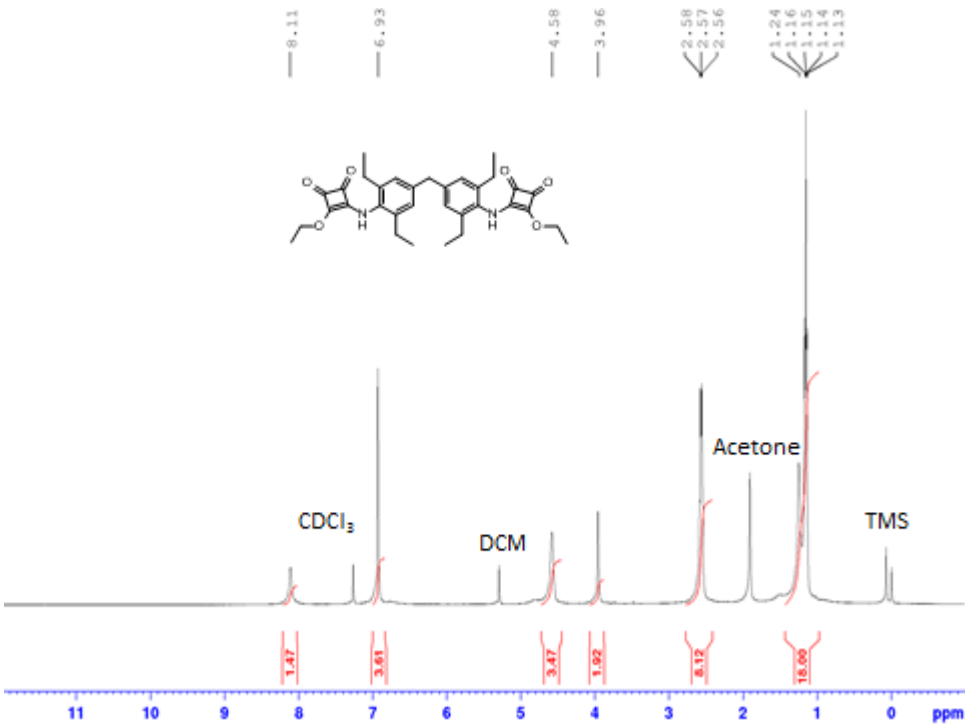

4A 23: *The ^{1}H NMR spectrum of* ***124*** *(500.13 MHz, $CDCl_3$)*

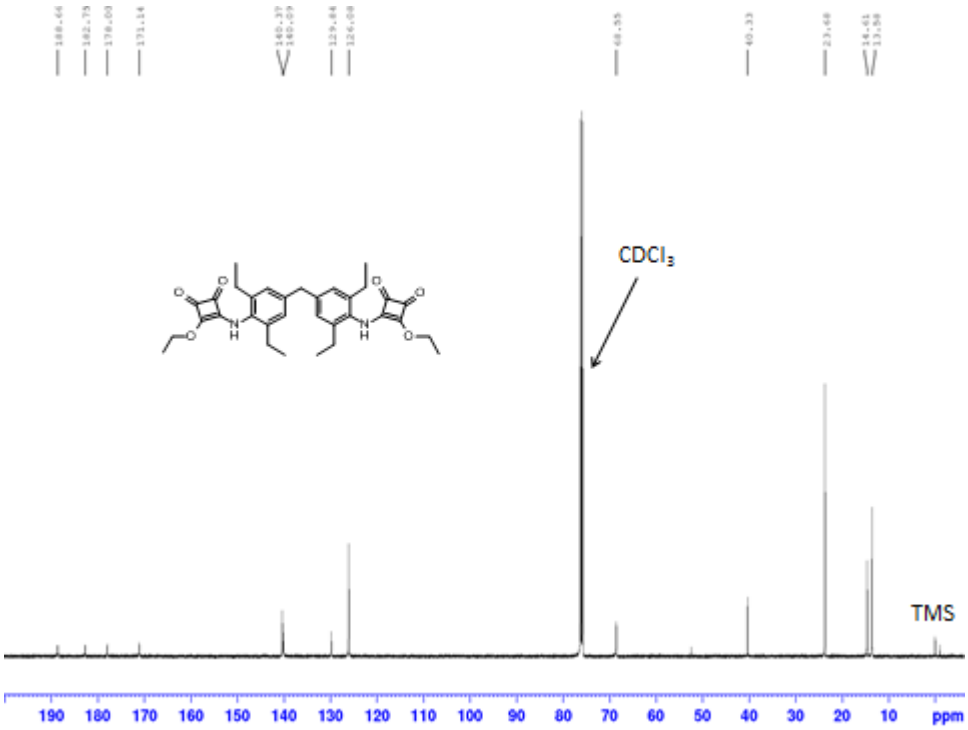

4A 24: *The ^{13}C NMR spectrum of* ***124*** *(125.76 MHz, $CDCl_3$)*

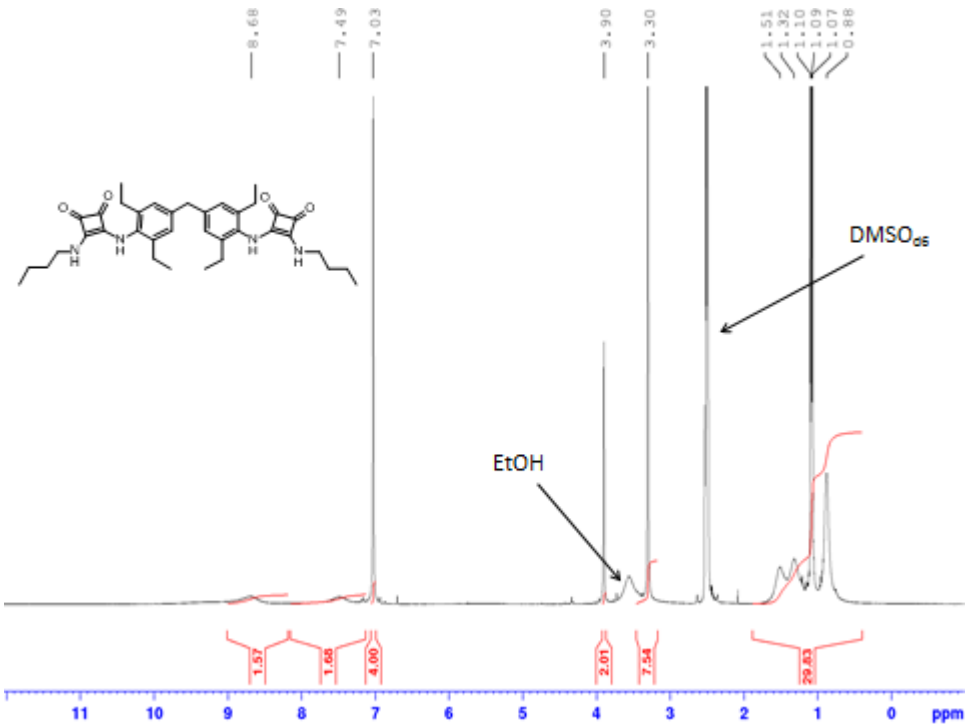

4A 25: *The ^{1}H NMR spectrum of* ***142*** *(500.13 MHz, DMSO-$_{d6}$)*

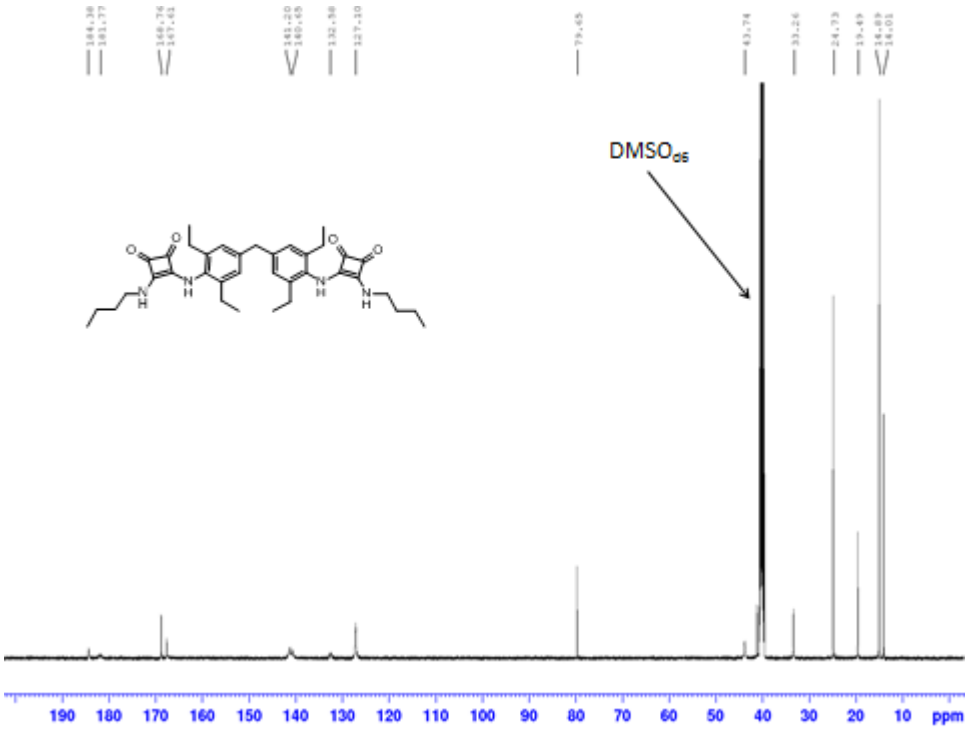

4A 26: *The ^{13}C NMR spectrum of* ***142*** *(125.76 MHz, DMSO-$_{d6}$)*

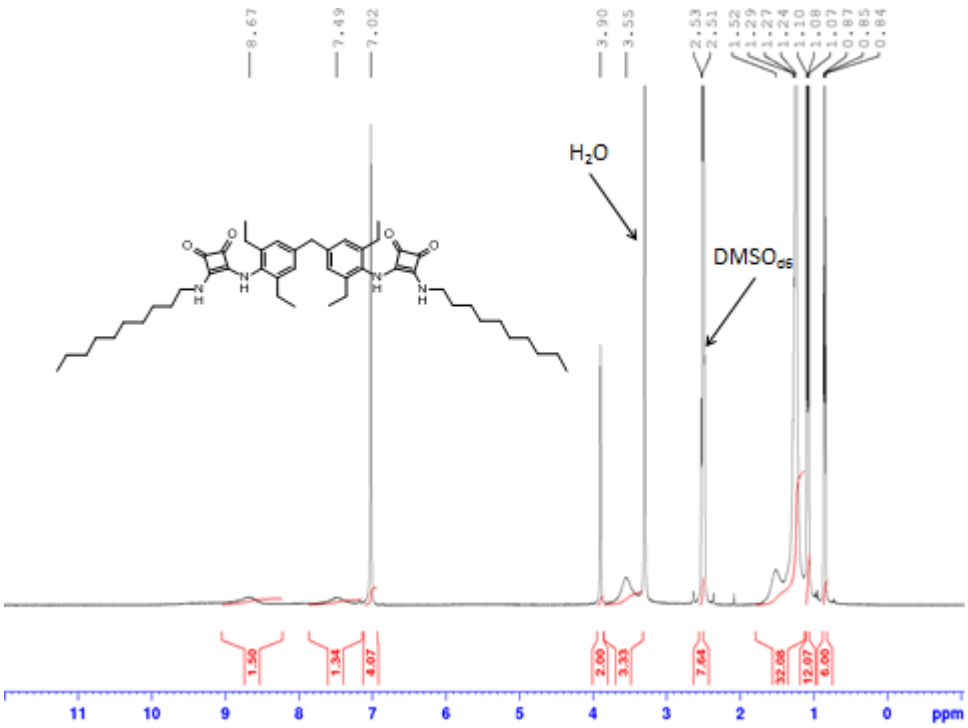

4A 27: *The ^{1}H NMR spectrum of* ***143*** *(500.13 MHz, DMSO-$_{d6}$)*

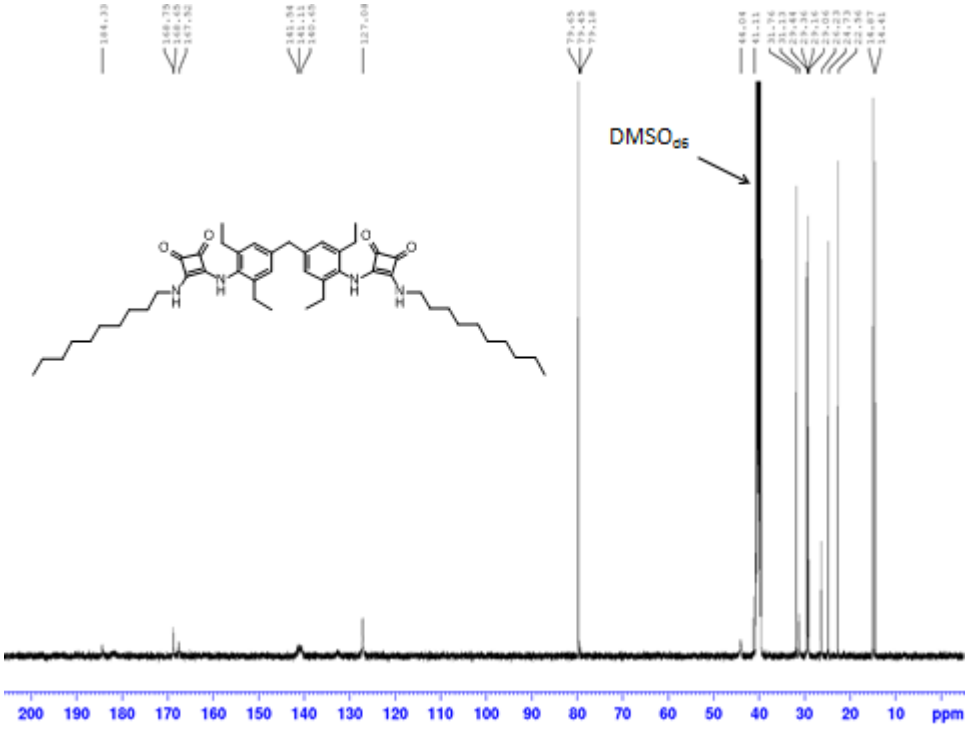

4A 28: *The ^{13}C NMR spectrum of* ***143*** *(125.76 MHz, DMSO-$_{d6}$)*

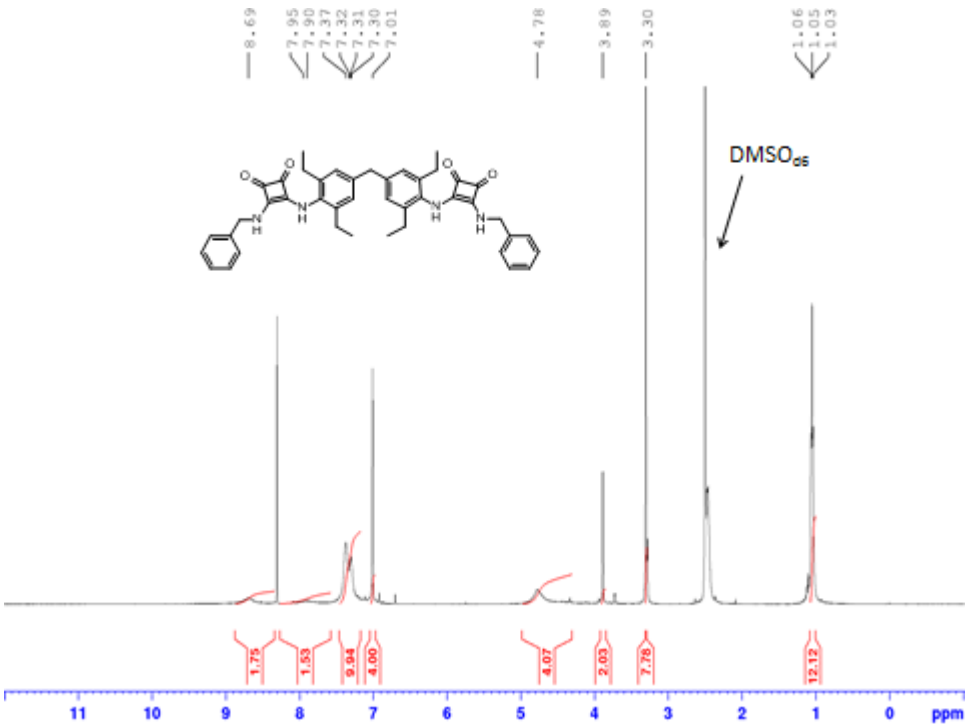

4A 29: *The ^{1}H NMR spectrum of* ***144*** *(500 .13 MHz, DMSO-$_{d6}$)*

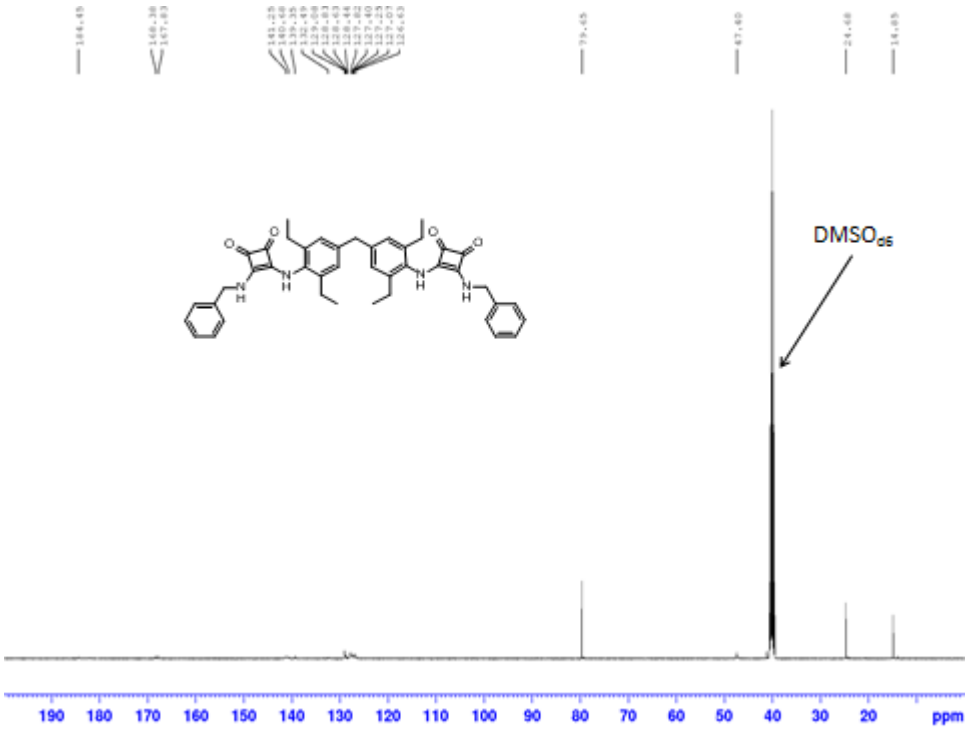

4A 30: *The ^{13}C NMR spectrum of* ***144*** *(125.76 MHz, DMSO-$_{d6}$)*

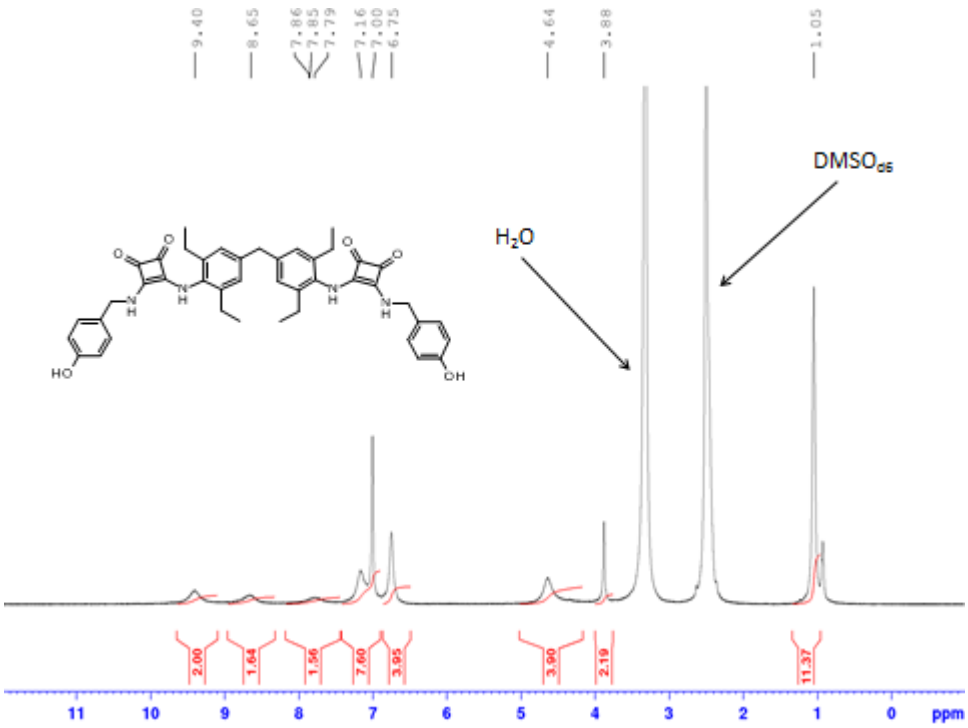

4A 31: *The ^{1}H NMR spectrum of* ***145*** *(500.13 MHz, DMSO-$_{d6}$)*

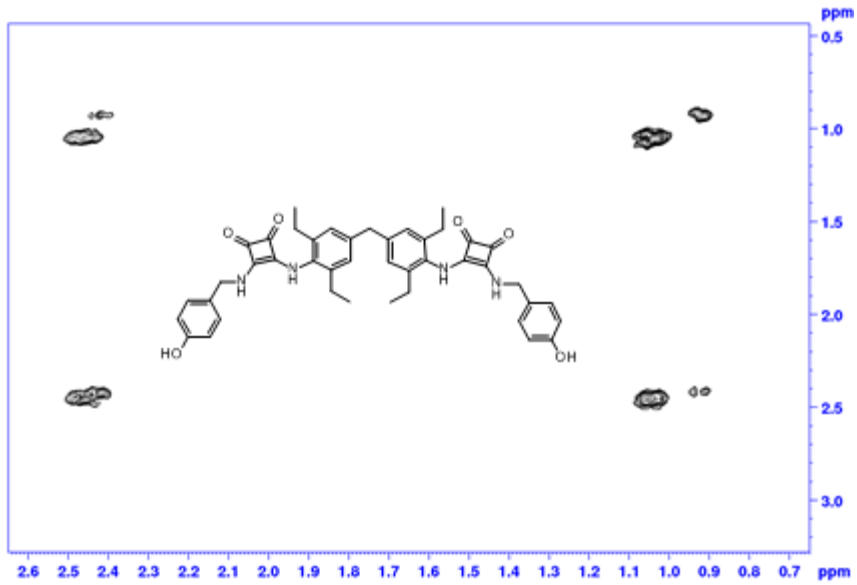

4A 32: *The COSY spectrum of* the aliphatic region of ***145*** *(125.76 MHz, DMSO-$_{d6}$)*

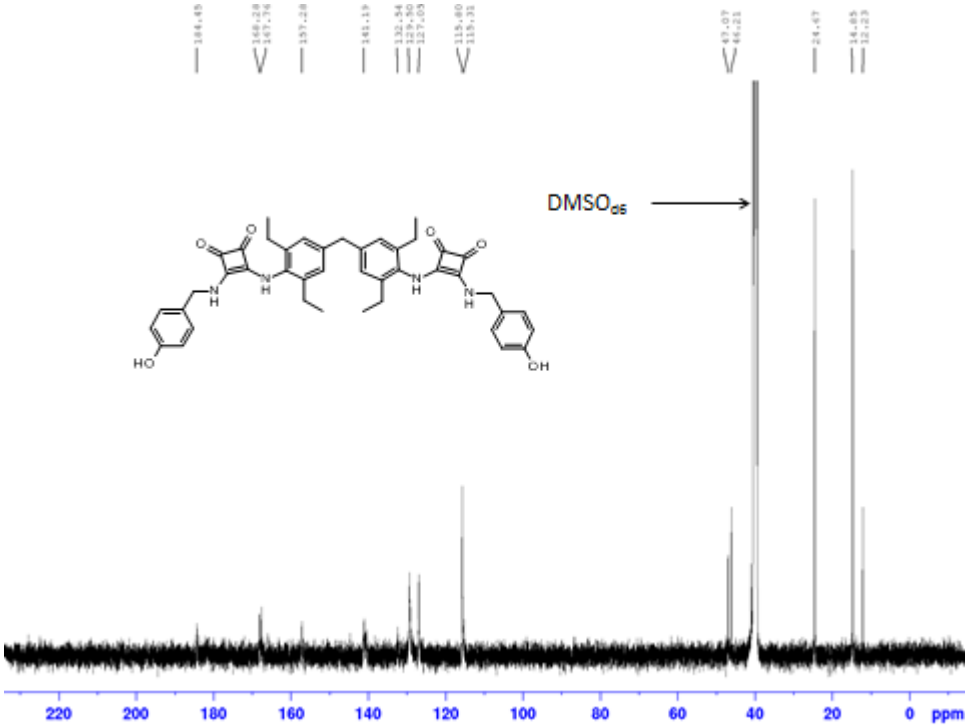

4A 33: *The ^{13}C NMR spectrum of* ***145*** *(125.76 MHz, DMSO-$_{d6}$)*

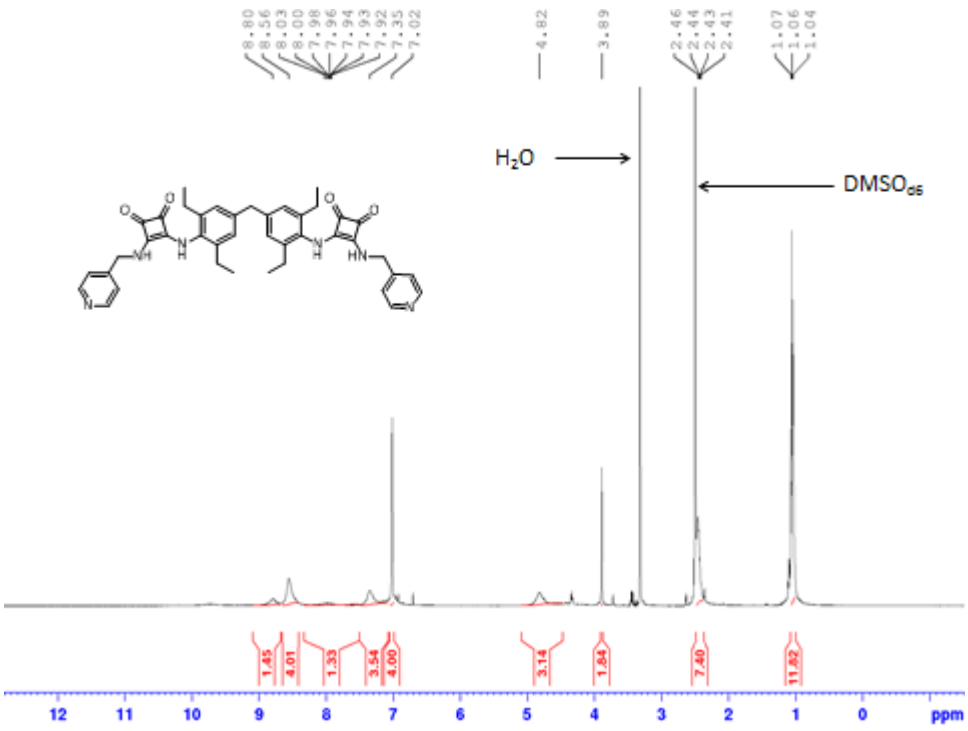

4A 34: *The ^{1}H NMR spectrum of* ***146*** *(500.13 MHz, DMSO-$_{d6}$)*

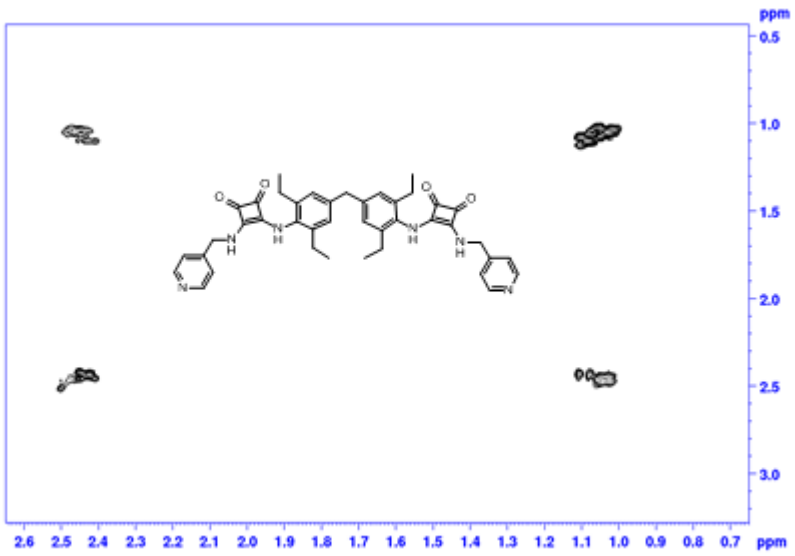

4A 35: *The COSY spectrum of* the aliphatic region of ***146*** *(125.76 MHz, DMSO-$_{d6}$)*

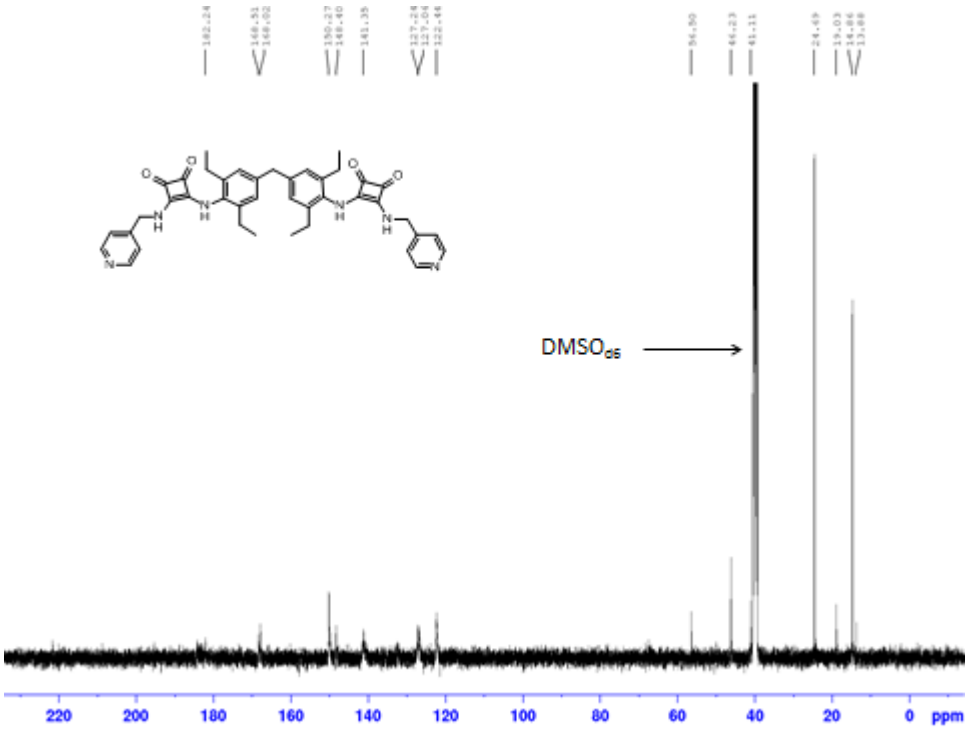

4A 36: *The ^{13}C NMR spectrum of* ***146*** *(125.76 MHz, DMSO-$_{d6}$)*

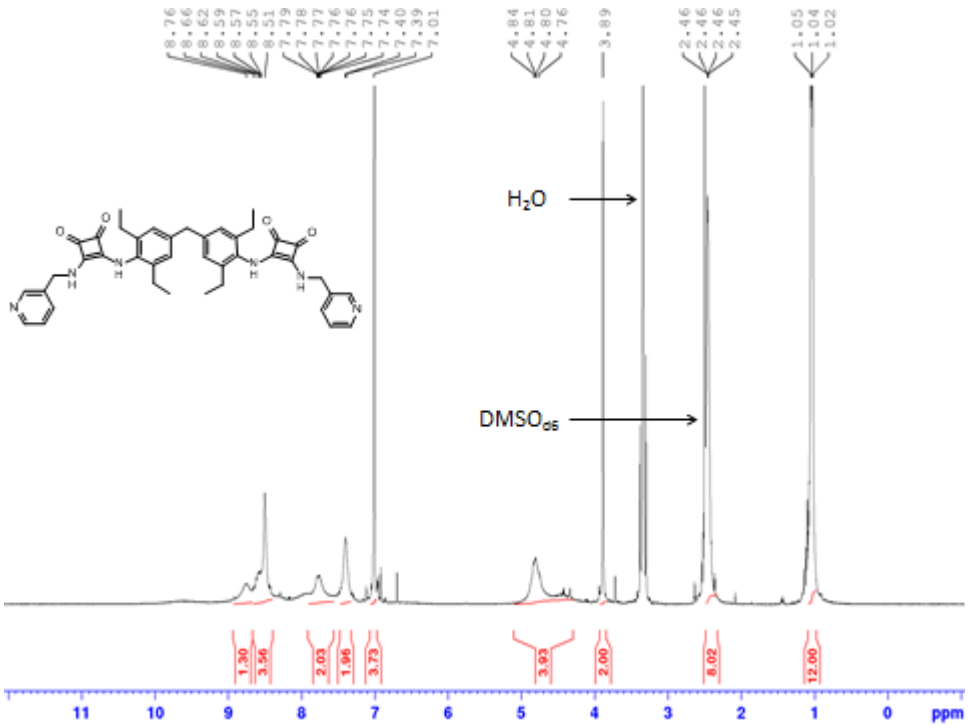

4A 37: *The ^{1}H NMR spectrum of* ***147*** *(500.13 MHz, DMSO-$_{d6}$)*

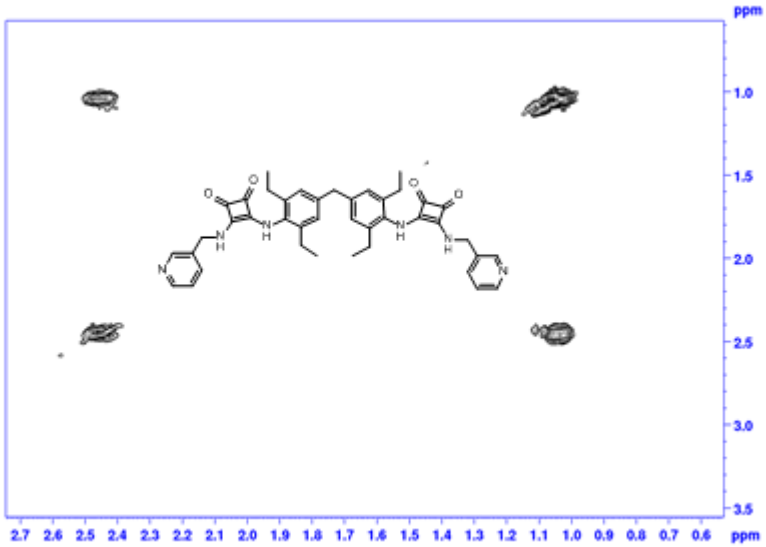

4A 38: *The COSY spectrum of* the aliphatic region of ***147*** *(125.76 MHz, DMSO-$_{d6}$)*

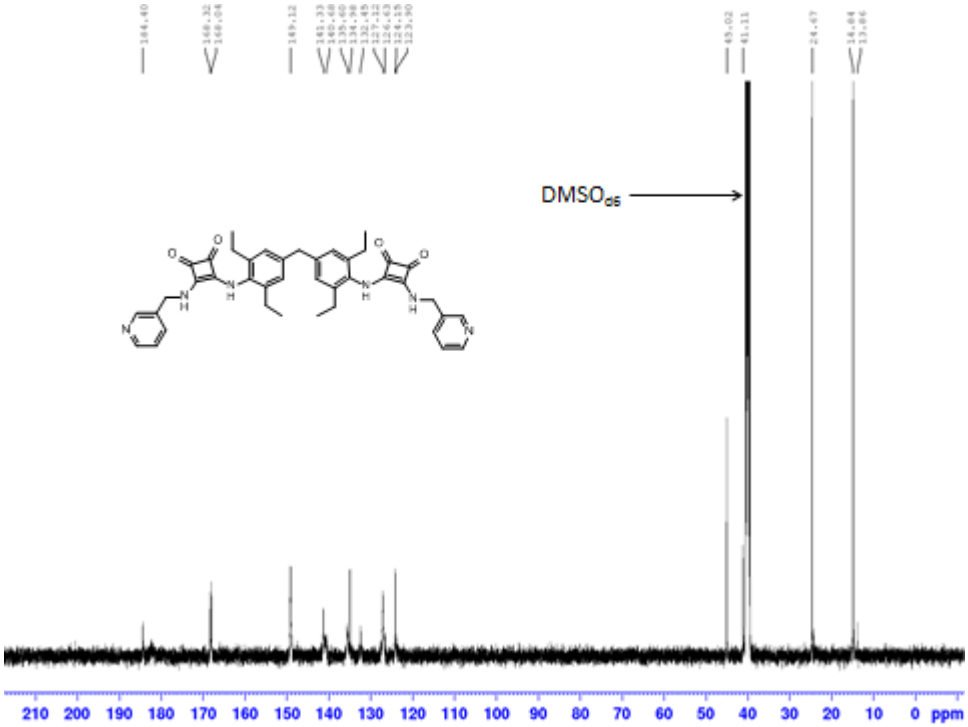

4A 39: *The ^{13}C NMR spectrum of **147** (125.76 MHz, DMSO-$_{d6}$)*

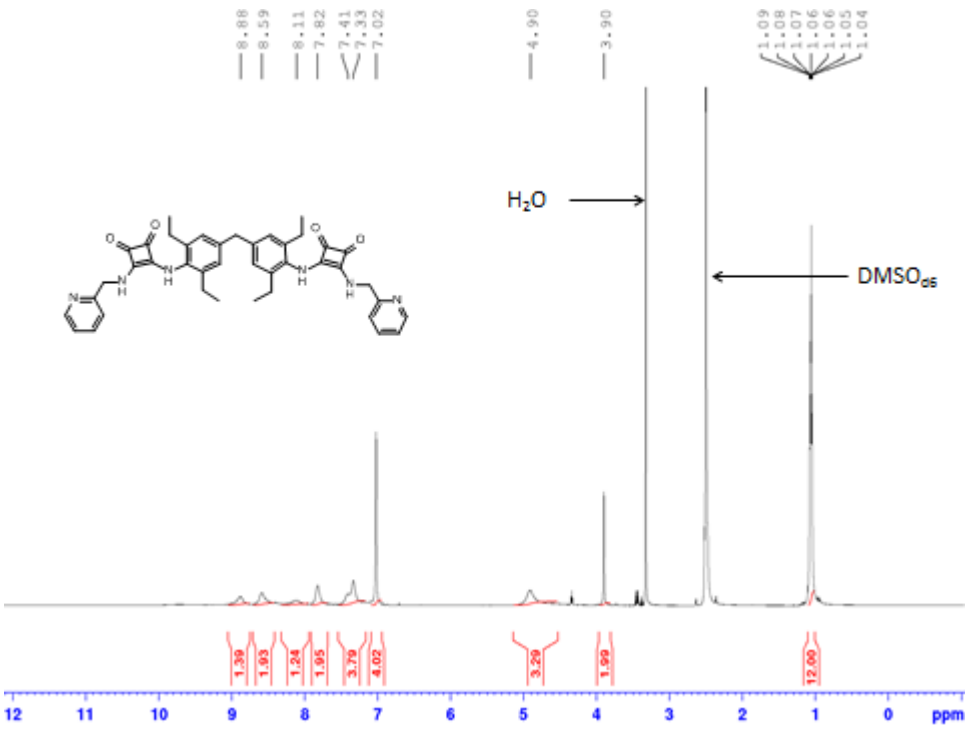

4A 40: *The ^{1}H NMR spectrum of **148** (500.13 MHz, DMSO-$_{d6}$)*

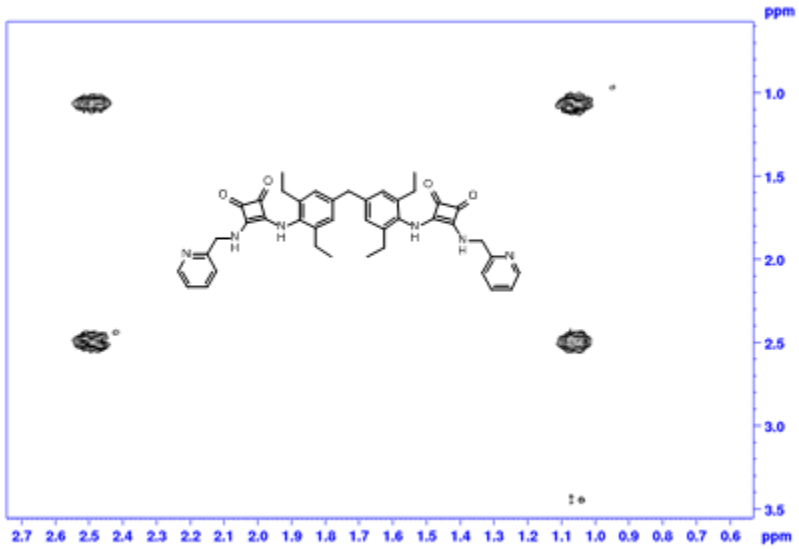

4A 41: *The COSY spectrum of* the aliphatic region of ***148*** *(125.76 MHz, DMSO-$_{d6}$)*

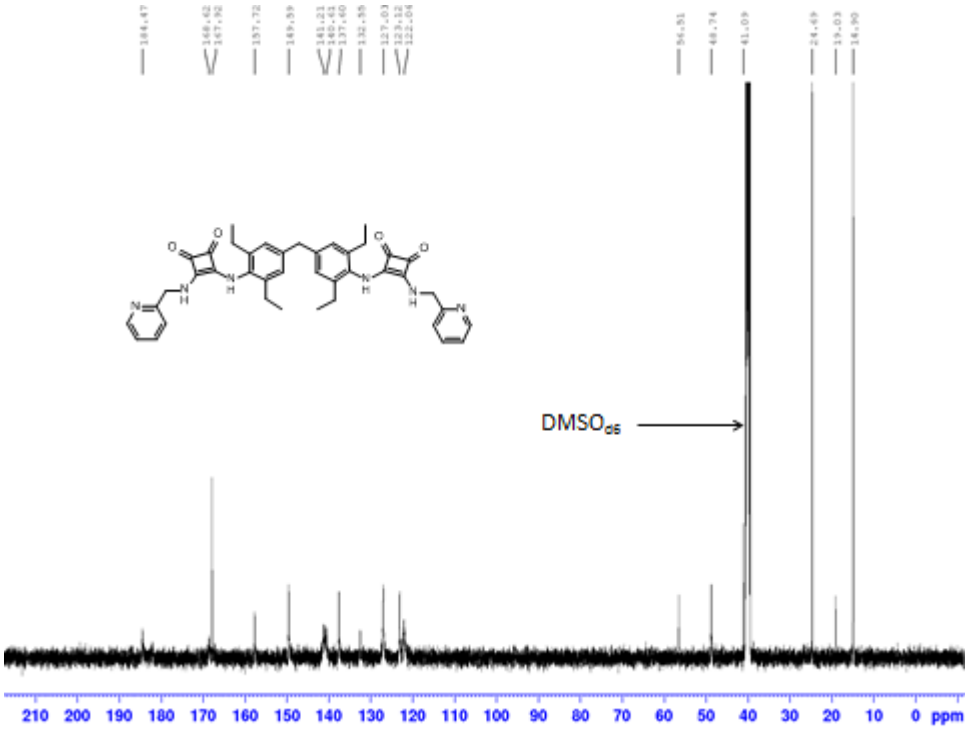

4A 42: *The ^{13}C NMR spectrum of* ***148*** *(125.76 MHz, DMSO-$_{d6}$)*

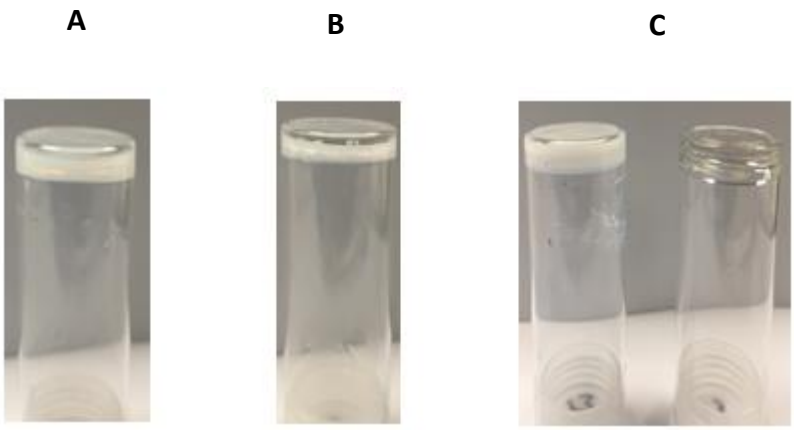

4A 43: *Representative photographs of up-side down vials containing LMWOGs prepared via heating-ultrasound (H-C) and heating-cooling (H-U).* ***(A)*** *Gelator* ***105*** *in DMSO.* ***(B)*** *Gelator* ***106*** *in DMF.* ***(C)*** *Gelator* ***113*** *in EtOH (left) and in toluene (right).*